MODELLING FORMER ICE SHEETS.

ANTONY JOHN PAYNE.

DOCTOR OF PHILOSOPHY

UNIVERSITY OF EDINBURGH

1988

I hereby declare that this thesis was composed by me and the work is my own research.

Antony J. Payne
November 1988.

ABSTRACT.

The aim of the project is to identify the critical factors determining ice sheet dynamics at regional scales. Numerical models are developed to simulate the behaviour of the former Loch Lomond and Antarctic Peninsula ice sheets. The models are based around the continuity equation for ice thickness and use a gridded topographic representation of the study area. They incorporate features such as ice flow (sliding and deformation), accumulation, calving, ablation, eustasy and isostasy. The models are tested by comparing their predictions with field reconstructions of former ice flow and extent.

The Loch Lomond case study is dominated by rapid phases of ice sheet growth and decay, separated by a fleeting maximum. The behaviour of the ice sheet is extremely sensitive to variations in accumulation and ablation, and to the distribution of bedrock topography. The Antarctic Peninsula case study predicts a complex sequence of ice dome and ice stream migration, and emphasizes the role of topography, climate and ice shelf basal melt in determining ice sheet dynamics.

ACKNOWLEDGEMENTS.

TABLE OF CONTENTS.

LIST OF TABLES.

Chapter 3.

Chapter 4.

Chapter 5.

LIST OF FIGURES.

Chapter 4.

Chapter 5.

PART ONE : INTRODUCTION AND BASIC CONSIDERATIONS.

CHAPTER ONE : AIMS AND MODELLING METHODOLOGY.

(1.1) OVERALL AIM.

The work reported here is concerned with the numerical modelling of former ice sheets. A number of specific case studies are undertaken with the aim of producing theoretical predictions of former ice sheet dynamics, which are then compared with field derived estimates. This procedure allows the theoretical model to be tested and sheds a glaciological perspective on geomorphological field interpretations.

This introductory chapter is sub-divided into four sections. The present section discusses the overall aim of the project and justifies both the scope of the research and the method of investigation used. The second section introduces the specific case studies undertaken in the project and gives the reasons for their selection. The third section describes the general modelling methodology used, and the final section outlines the structure of the rest of the thesis.

Earth surface systems are affected by key processes that have time scales in excess of a thousand years. One of the possible driving forces behind these processes is the variation of solar insolation produced by the earth's orbital anomalies. The size of these variations is,

however, small and if they are to explain the major climatic and glaciological oscillations known to have occurred during the last few million years then amplification of their signal must occur within the earth surface system. An appreciation of ice sheet mechanics and of the way in which ice sheets interact with climatic, geologic and oceanic processes is vital to the understanding of this amplification. One can seek to gain an insight into these interactions by studying the behaviour of the Quaternary ice masses, in particular those of the most recent Weichselian or Devensian glacial of c. 18,000 years before present (unless otherwise stated dates are given as ka BP, that is in thousands of years before present) which offers the most field evidence and the best opportunities for dating.

Two main methods of research exist in the area of Quaternary glacial studies, which can be termed 'field-led' and 'model-led' (Figure 1.1). The former approach is inductive in nature and proceeds from field evidence. This field evidence, and assumptions concerning ice mass behaviour, are used to reach conclusions concerning both the environment sustaining the ice mass and the dynamics of the ice mass itself. For instance, once former glacier extent has been mapped the use of accumulation area ratios, derived from present day glaciers, indicates the former firn line altitude and implies something of the

3

former climate. A good example is the work of Sissons and Sutherland (1976), who mapped the extent of the Scottish ice sheet during the Loch Lomond stadial of 10.0 ka BP and used this information to obtain estimates of climate, in particular precipitation, at that time. This approach is inductive because it seeks to derive explanations from previously gathered data.

The model-led approach is a recent alternative and is deductive in nature. It involves the use of a series of hypotheses involving glacial dynamics which, because of their relative complexity, are often formed into a numerical model. The predictions of the model can be tested, adding to or subtracting from the credibility of the initial hypotheses. One example is Sugden (1977), in which basal ice temperatures were modelled for the Laurentide ice sheet allowing various erosional domains to be predicted, which were then tested against geomorphic evidence. This approach is deductive because it seeks to test previously derived explanations/hypotheses using available field data.

Both model-led and field-led approaches have certain limitations. In the field-led approach the conclusions drawn from field data rely heavily on the interpretative assumptions used. These ought to be tested; however the available test data is limited because field data are

4

*used to draw palaeo-reconstructions. There are numerous
examples of the field-led approach to the study of
Quaternary ice mass fluctuations in the United Kingdom.
Although the area's glacial geomorphology has been the
subject of research for over a century there are still
large uncertainties concerning such fundamental points as
ice mass behaviour during phases of growth and retreat,
and the location and timing of maxima.*

*The field-led approach has no effective way of being
selective in the evidence collected from the present day
landscape. This landscape is a complex assemblage of
forms and contains elements created under the varying
process environments (subglacial, subaerial and
subaqueous) to which the location has been subjected to
in its past. Further complications exist in that some
process environments may leave no trace of their
existence, while others may obliterate evidence of pre-
existing environments.*

*The model-led approach in Quaternary glacial studies
uses numerical models to provide predictions of variables
such as ice extent and flow pattern. Field data
collection with a view to testing these specific
predictions is often more focused than that in field-led
research because the model predictions usually suggest
the locations and the types of field data necessary for*

5

their testing. The importance of testing is to substantiate the existing model and to cast a glaciological perspective on the field data already accumulated in an area. The more a prediction is based on known ice mass dynamics the greater is the relevance of this testing.

One associated difficulty with this approach is that the initial hypotheses very rarely boil down to the single 'if ... then ...' format appropriate to critical testing. This happens because input data are not unequivocal and numerical models inevitably rely on some parameterizations which involve the fitting of a simplistic relationship to what is in fact a far more complex process. Uncertainty in the relationships to be modelled implies that the exact form of the numerical model varies within a physically justifiable range. This may well lead to variation in the form of the model's predictions. This, in turn, ensures that initial hypotheses never have a one to one relationship with their consequent predictions and cannot therefore be tested conclusively. However model predictions can aid the interpretation and understanding of ice sheet behaviour at the large spatial and temporal scales typical of the system.

The present project adopts the model-led approach and uses numerical models to derive predictions of former ice sheet behaviour in Scotland and in the Antarctic Peninsula. These predictions are then compared to field evidence. As an abundance of field data already exists in the Quaternary literature for the areas, testing can be achieved through comparison with published data. The collection of new data would be helpful, but was incompatible with the time scale of the project. The project is a case study of the model-led approach to Quaternary studies and allows the effectiveness of this method to be compared with that of field-led methods.

The models used in this study are derived from the field of theoretical glaciology. Since the founding works of Nye (1959) and Glen (1955) the number of theoretical projects concerning the dynamics of ice masses has increased many fold. Common to the majority of these projects is the use of numerical modelling based on the partial differential equations thought to represent the behaviour of ice. There are two main approaches. One approach is to simplify the system of interest sufficiently to make an analytical solution possible. The disadvantage of this approach is that these solutions can only be tested if analogously simple real world examples are found. In the second approach, analytical techniques are used to break the problem down to a stage where the

7

partial differential equations involved can be approximated by the use of numerical techniques. This has the advantage that the degree of model complexity can be varied and may include many real world features. The disadvantage is that the numerical techniques only approximate the partial differential equations. This may lead to problems of approximation stability and accuracy. A vital factor in the shift of emphasis from the first to the second approach is the increased availability and speed of computers which provide the processing power necessary to employ numerical methods. The relative ease with which complex theoretical research can now be undertaken has lead to a rapid expansion in the number of variables and interactions thought to be important in determining the behaviour of ice sheets. Clearly if glaciology is to progress, the processes that are significant must be distinguished from those that are not. Field testing facilitates this selection procedure.

Within the profusion of glacial models a number of different families have developed. One particular scheme for dealing with continental ice sheet problems has been developed by Mahaffy (1976) and by Budd and Smith (1981). This is based on the continuity equation for ice thickness and allows ice sheet behaviour to be simulated through time over a horizontal grid. The present study builds on this inherited framework, although questioning

some of the details within the model, and applies it to a number of case studies. It is hoped to test this model against field data for these specific glacial events.

This particular family of ice sheet models was chosen for reasons of testability and flexibility. The models make spatial predictions of ice sheet form and behaviour that are appropriate to the type and scale of the available field evidence. They also make predictions about the nature of ice sheet changes through time which are compatible with the available test evidence. The flexibility of this type of model stems from the relative simplicity of its mathematical formulation. This eases the coupling of the ice sheet model to models of other earth surface systems, for instance atmospheric and lithospheric systems. The benefits inherent in the use of this type of model are further discussed in Chapter 2.

The efficient progress of both Quaternary geology and theoretical glaciology relies on the strength of the link between field measurement and theory. Here this link is provided by the use of field evidence to test the predictions of theoretical models. In this respect the use of former, as opposed to present day, ice masses is valuable. Current literature is increasingly focusing attention on interactions at the bed and their effects on large scale ice sheet behaviour (eg Boulton and Jones

9

1979). The beds of former ice masses are exposed and can therefore offer an efficient means of investigating these processes. In addition the bed contains information on a variety of ice sheet variables such as extent, thickness, flow direction and thermal regime. The data also reflect ice behaviour over several phases of the ice sheet's history. This is very important because the ice sheet's behaviour is likely to change significantly through time. In contrast present day ice masses allow a very restricted glimpse of behaviour at the bed and, with the exception of ice cores, offer information from a short time span.

(1.2) SPECIFIC AIMS.

The project aims to produce an ice sheet model which can be used to study the dynamics of former ice masses. From this initial aim it follows that the model should be linked to test events at specific geographical locations. These case studies are now introduced. The reasons why these specific case studies offer particularly good opportunities for the testing of ice sheet models are discussed, and the type of questions that can be addressed by the use of models are illustrated. Figure 1.2 illustrates the connection between the case studies described below and the thesis layout.

The Loch Lomond stadial (12.5 to 9.5 ka BP) in Scotland represents the most recent large scale glaciation in an area whose glacial geology is one of the most well researched in the world. It is therefore one of the most tightly constrained test cases for an ice sheet model. However the field data is not unequivocal and a number of uncertainties still remain. Examples include the likelihood of the ice mass reaching a steady state configuration, the extent of ice inheritance from previous glaciations and the nature of the climate at that time (in particular wind directions, precipitation rates and air temperatures). A major aim in the Loch Lomond stadial case study is to test hypotheses concerning the conditions required for steady state and to investigate whether the ice sheet form was predominantly a function of climatic factors or factors associated with ice flow. The climate of Scotland and the majority of North-West Europe is presently under the influence of the North Atlantic drift, which brings warm water north from the Caribbean. During the Loch Lomond stadial this current was deflected by a southerly extension of the oceanic North Atlantic polar front (Boyle and Keigwin 1987), which robbed North-West Europe of a major source of heat. The transition between the climate of the present and that of the Loch Lomond was both extremely rapid and severe, with July air temperature fluctuations of the order of 8 ^{O}C in 500

years (Coope 1975) and drastic changes in the continentality of the climate (Williams 1975). This extreme climatic instability makes the area interesting in relation to rates of ice sheet growth and decay. The case study addresses questions relating to these climatic changes, such as whether an ice sheet could influence its regional climate sufficiently to a make steady state likely despite the rapid air temperature fluctuations, and the effects of Polar Front migration on wind directions, atmospheric moisture contents and precipitation distributions.

The event was relatively simple from a glaciological stand point because the ice mass was solely land based. Thus its modelling need not be concerned with the more complicated mechanics of ice stream and ice shelf motion. In addition mass loss via calving and marine basal melt can be presumed to have been minimal. The only mass fluxes that require estimation are therefore surface ice melt (ablation) and snow accumulation. The behaviour of the model is determined by two driving variables (air temperature and precipitation changes), thus its response should be simpler and more easily understood than that of a partially marine based ice sheet.

The other case study concentrates on a predominantly marine ice sheet, which suffered very little surface

*ablation, this is the Antarctic Peninsula ice sheet of
the last glacial maximum (the Weichselian or Devensian,
18.0 ka BP). Again the model is driven by two forcing
functions (sea level and marine basal melt changes)
which are oceanic rather than climatic in nature. Here
the marine section of a general ice sheet model is
developed and tested. The Antarctic Peninsula is often
quoted as being similar to the U.K. during a glaciation
because it has a 'highlands and islands' type topography,
and a maritime climate dominated by warm, moist
Westerlies. Field interpretations in this area are fairly
scarce, and the modelling is therefore of a more
exploratory nature, in contrast to the very field
constrained modelling of the previous case study. The
approach is more predictive and provides a useful
contrast in the use of model output. As a consequence of
this, less emphasis is placed on testing against ice
maximum extent and more on the identification of ice
domes and streams and their changing positions. Problems
that are addressed involve the mechanisms that could lead
to ice advance in the area; whether reduction in marine
basal melt, decreased calving or increased surface
accumulation rates were dominant. In addition the effects
of isostasy, eustasy and ice flow are assessed.*

*It is now important to introduce the general modelling
methodology used. This is done with particular reference*

*to the problems associated with the modelling of former
ice masses and to the implications that the use of
modelling brings to field data collection in this
discipline.*

(1.3) OVERALL PROJECT METHODOLOGY.

*The flow diagram shown in Figure 1.3 illustrates a
typical modelling strategy. It is based on a deductive
approach to research. An initial set of hypotheses (a
word model) are used to make predictions. If these
predictions survive testing against real world evidence
then the initial hypotheses can be said to have some
explanatory capacity. In many cases this initial set of
hypotheses is too complex to yield predictions directly.
The hypotheses therefore have to be formed into a
mathematical model before predictions can be made.*

Variable selection.

*In order to move from a word model to a more
mathematical representation it is necessary to isolate
the system's components and relate them to each other.
First a boundary must be drawn around the system of
interest, both by determining the geographical and
temporal extent of the model and by selecting the
variables which are considered important in the problem.
These tasks are often interrelated in that different
variables are important at different spatial and temporal*

14

scales; once spatial and temporal scales have been
identified variable selection becomes easier. For
instance, features such as avalanches and cloud cover are
important when determining the monthly mass balances of
valley glaciers, but are insignificant when modelling
Quaternary ice sheet behaviour.

Second, the types of inter-relationships within the
system must be determined. In particular some of the
identified variables will be driving or external, in that
their behaviour determines system behaviour without being
affected in return. Other variables will be internal to
the system, being affected by its behaviour and, in turn,
affecting the system's behaviour.

The basic hypotheses within the word model constrain
variable selection and the determination of the links
between variables. Variables and relationships are
included within the structure of the model only if they
are believed to be important. It is not necessary to
include all possible variables and relationships because
the model's output can be used to test the assumption
that the omitted variables are unimportant in determining
the behaviour of the real world system. As an example one
might relate an ice sheet's stress field solely to simple
shear and assume the effects of longitudinal stress to be
minimal. If the model was subsequently unable to

reproduce flow patterns then this hypothesis would have *Not*
to be revised and extended. *necessity*

Parameterization.

Once the model structure has been determined the inter-relationships within the structure need to be quantified. This can be done in a number of ways. First, two variables can be related in a purely empirical manner and a simple mathematical relationship constructed from the correlation between real measurements of the two variables. An example is the use of environmental lapse rates to relate air temperature to surface elevation, which can be calculated from field measurements. This approach has the advantage that mechanisms of great complexity may be approximated simply. However the use of lapse rates glosses over the complex variation of energy budgets with elevation: the relationship derived is in no way causal but relies on the assumption that the actual physical mechanism underlying it does not vary. For these reasons the parameterization procedure is best employed when the relationship being dealt with is perceived as being both peripheral to the overall system and too complex to model in a more realistic fashion. Thus a parameterization of the fraction of precipitation falling as snow related to altitude could be employed. In such a case the parameterization is a simplification of the complex physics of snow formation but is justified

because the exact amount of snow is not expected to be crucial in determining overall model behaviour.

Inter-relationships can also be derived from the results of previous theoretical work on specific areas of the system. Thus a detailed study on a particular relationship within the system may have been able to determine the important factors involved. This reduces the complexity of the relationship sufficiently to allow its incorporation into the simulation as a whole. For instance theoretical work on the distribution of stress within ice masses and its effect on ice strain rates indicates that, over large distances, these complex phenomena can be approximated by fairly simple physics. Example!

It may be impossible to quantify a relationship to the desired level of accuracy. The form and values associated with a relationship are therefore likely to be imprecise, and each relationship will have a number of possible forms. A relationship predicting ablation from air temperature, for instance, may well take on different forms at different places and times depending on the underlying complex process of energy partition at the ice sheet surface. A unique model description does not therefore lead to an unique numerical model; rather many equally justifiable numerical models are possible. This feature is important in that one unique word model is

17

likely to vary in its predictions as different parameter values are employed. This is an undesirable feature in terms of model testing. It may be minimised either by using simpler models, in that fewer parameters are needed, or by ensuring that the model only requires parameters that are known to have a low variance in nature. For example, a model dealing with parameters such as ice density has a smaller range of possible numerical forms than a model which empirically relates sliding velocity to basal shear stress. Both simplification and the reliance on parameters of low variance are strategies that limit the number of possible numerical forms arising from a single initial word model. This reduces variation in output predictions, making the resultant models more testable.

Tuning.

The uncertainty concerning the values that are attached to model parameters has serious implications for the testing of the model. At this stage a model may be rejected if it cannot be made to approximate the real world without employing parameter values that are in excess of their known natural range. However the fact that a model can be tuned to mimic reality is no indication of its validity: it is relatively simple to replicate the real world without correctly modelling it, especially if loose parameterization has led to a highly

variable output.   The modelling of Quaternary ice sheet
behaviour has the additional problem that glaciations are
essentially unique events. Unlike other disciplines,
where a large data set is available both to tune and then
independently test the   model, the field of ice sheet
modelling is poor in available data. One solution is to
tune individual sections of the model using present day
data or to use parameters that have been tuned in studies
of other geographical areas. However, the underlying
mechanism, which the parameter is supposed to reflect,
may vary in degree between different places and at
different times. Using a previous example, a
parameterization of ablation as a function of air
temperature derived in one area may not be applicable in
another because the complex partitioning of energy at. a
snow surface (which determines both ablation and air
temperature) may very well alter between regions.

Testing.

The testing of the best fit model produced by tuning
is essential if one is to have confidence in its
explanatory powers.   Without adequate testing it is
impossible to determine whether the processes that the
model is depicting are ones that could have happened or
are ones that actually did happen. The model should,
therefore, be constructed so as to be testable and
predictions should be comparable to data derived in the

field. Further, different types of field evidence are liable to vary in the amount of confidence that can be attached to them. Models should therefore be built to predict test variables that have strong lines of equivalent field evidence.

Deficiencies in the data sets available to test ice sheet models (in many instances consisting of a mapping of a single variable at a single time) mean that the fit between model output and test data cannot be assessed using statistical techniques and often relies on purely qualitative comparison. The implication that testing is only possible at the qualitative level is not as serious as it may appear. From the foregoing discussion on model sensitivity it is clear that the types of model being used give predictions of low accuracy. It is unrealistic to expect these models to predict glacial conditions exactly. Rather the models can be used as tools to investigate ice mass behaviour and to isolate important factors within the ice sheet system. Field testing is used to maintain a link to the real world phenomena.

The paucity of field data means that there is a danger of circular argument. The same data could be used both as input and as a test. An example is ice sheet extent, which is often used to reconstruct ice sheets and also to test the validity of models. A solution is to ensure that

the initial word model uses unrelated variables as input
and output. Where possible a model should provide a link
between strong field data sets. For instance, one section
of the present study links a *fairly well constrained
record of July air temperatures* to an independently
derived estimate of ice sheet extent.

The fact that a model survives testing should not be
taken as proof that the real system is being correctly
modelled; rather it demonstrates that the model is able
to reproduce that particular data set. It is possible
that models derived from different sets of initial
hypotheses (word models) may be able to reproduce one
particular piece of field evidence. This problem of
equifinality occurs in many modelling applications.
However, it is particularly important in the field of ice
sheet modelling for the reasons identified earlier,
namely that the lack of field evidence leads to
inadequate model testing. In addition the range of the
predictions arising from an initially distinct word model
may be great; in fact the ranges of several distinct word
models may well overlap. A great danger therefore exists
of spurious correlations developing between predictions
and test evidence. That a model can survive a single test
is not particularly significant; only after several
different tests is a model worthy of confidence. A model
that can predict known ice sheet extent is not

noteworthy; it is possible that many models could do this. The number of models that could also predict thicknesses and flow patterns accurately would, however, be smaller. One therefore has increased confidence in a model that has survived a large number of different tests. Thus the only way to reduce the number of models potentially capable of explaining ice sheet behaviour is through repeated comparison with separate sets of field evidence.

These arguments have two implications for the modelled research approach defined in Section (1.1). First, if field work is to be orientated towards model testing then the more independent tests that can be made the greater the probability will be of reducing the number of rival explanatory models. It can also been argued that high resolution mapping of Quaternary geological evidence does not aid the testing of models significantly, since the models are unlikely to have a similarly high accuracy in their predictions. The most efficient method of field data collection would therefore be to collect approximate data on a series of glacial variables rather than high resolution data on a single variable. Emphasis on the precise mapping of maximum glacial extent is thus inefficient when viewed from a model testing perspective. A more economic approach is to combine studies of particular ice extent with those of ice thickness, flow

patterns and thermal regimes.

A second implication is that, given the essential dynamism of ice sheets, the concentration on glacial maxima can also be seen as inefficient. Although information concerning maxima is easily obtained, from the point of view of testing a dynamic system model the maximum is no more or less important than any other stage in the system's evolution. Thus a modeller would prefer less precise data in a time series to precise data from a single date, because the time series offers a greater number of tests. The collection of data from times other than glacial maxima can also be used to test the common assumption that maxima represent long term equilibrium states rather than times of rapid transition between advance and retreat.

Experimentation and Sensitivity Analysis.

It is necessary to consider the status of a model that has survived all the tests which the available field data can offer. Although the model is unlikely to be definitive, the fact that it has shown itself capable of correctly predicting field data indicates that the dynamics of the model itself are worthy of investigation. This can be done using the techniques of Sensitivity Analysis and Experimentation. In the former the values of model parameters are varied in a systematic way. Thus a

particular model is run repeatedly with parameter values varied in a range corresponding to the real or estimated range of the parameter. The aim is to isolate areas of the model that are particularly dominant in determining overall behaviour, thereby gaining an insight into the strength of the various inter-relationships within the model and the relative stability of the model's predictions.

The important areas identified by this analysis may represent key real world processes or they may be no more than artefacts of the particular model used. An understanding as to which of these explanations is the more likely can be gained by expanding the dominant section of the model, so that the processes in this section are modelled in greater detail. Thus in the stress field example quoted above, if ice is assumed to flow solely via simple shear and the model is found to be particularly sensitive to flow parameterizations, then the stress determination section of the model should be expanded. If the more complex model shows markedly different behaviour to that of the original then it is likely that the initial word model was inadequate. However, if more complex modelling does not radically alter the behaviour of the model then the particular section's dominance, as identified by sensitivity analysis, may well be a real feature.

A tested model may also be used to perform experiments. Quaternary ice sheets are unique phenomena. An understanding of ice sheet behaviour can be developed by modelling one of these unique events and the dynamics associated with it; however this is but one facet of the ice sheet system's overall behaviour. It is useful to have an insight into the range of ice sheet behaviour possible. A model may therefore be used to answer 'what if?' questions or, more explicitly, to explore the system's response to different forcing or to different imposed boundary conditions. The results of such experiments offer greater insight into the ice sheet system than the initial, tested runs. For instance, the tested model run may not give an indication of the likelihood of a steady state form developing because the model driving function varies too rapidly. The time required to reach equilibrium and the nature of that equilibrium may, however, be of interest. These features could be investigated by performing experiments with a constant driving function. However, these results should be treated with care for they represent extrapolated behaviour outside the tested range of the model. There is no guarantee that the real ice sheet system would behave in a similar manner; some unmodelled mechanism may be triggered that leads to drastically different behaviour. For this reason experiments should be taken as indications of real behaviour, all else being equal, but

no more.

To complete the discussion of the general modelling strategy we must investigate the implications of a mismatch between model predictions and field derived estimates. The likely inaccuracies mentioned above imply that it is difficult to impose a strict rationale for the rejection of initial hypotheses through model testing. Before a model can be rejected we have to answer questions concerning the likely accuracy of field estimates, because the interpretation of geomorphological features is often ambiguous. Thus a mismatch between predicted ice thicknesses and field estimates derived from trimlines raises questions relating to the quality of field interpretation. In addition, it is difficult to quantify the degree by which predictions and test data must differ before rejection is necessary. When it becomes possible to reject the initial set of hypotheses (word model) then the manner of model-field mismatch often indicates which of the original hypotheses were incorrect or, more likely, what crucial omissions were made from this original set.

(1.4) THESIS OUTLINE.

The thesis is divided into three parts. The first, consisting of Chapters 1 and 2 (Introduction and Basic Considerations), forms a background to the work presented

in Part II (the case studies). Following the methodology outlined in Section (1.3), Chapter 2 deals with selection and justification of initial hypotheses and with the construction of the numerical model.

The two case studies presented in Part II are designed so as to follow from model construction to tuning, testing and experimentation. As indicated in Section (1.2) their choice reflects the need to test different sections of the overall model in isolation (Figure 1.2). Thus the first case study (the Antarctic Peninsula ice sheet during the last 40,000 years) is concerned with the mechanisms by which oceanic change can affect ice sheet behaviour (via sea level and marine basal melt changes). The second case study covers two chapters. The first chapter (the Loch Lomond stadial ice sheet in Scotland) concentrates on the way in which climatic change affects ice sheets (via air temperature and precipitation changes), while the second chapter (the climate of the Loch Lomond stadial in Scotland) attempts to quantify the types of climatic change occurring during the stadial more precisely. Further information on these case studies is given in Section (1.2).

Where possible a strict format is adhered to in each case study. Each chapter starts with a statement of the aim of the particular case study, followed by a

discussion of the amendments made to the general model given in Chapter 2 and a description of the model's input data. Model predictions are then compared to field estimates and a sensitivity analysis is performed on the model in addition to any required experiments. Each case study then concludes with an implications section, relating back to the case study aim and drawing on results from model testing and experimentation.

Part III (Chapter 6) concludes the thesis. It contains a discussion of the implications generated by the case studies and an assessment of the usefulness of the modelling approach to Quaternary ice sheet studies.

field
observations

present day
correlations

initial
hypotheses

numerical
model

interpretative
assumptions

predictions

mismatch

palaeo-estimate

field
test
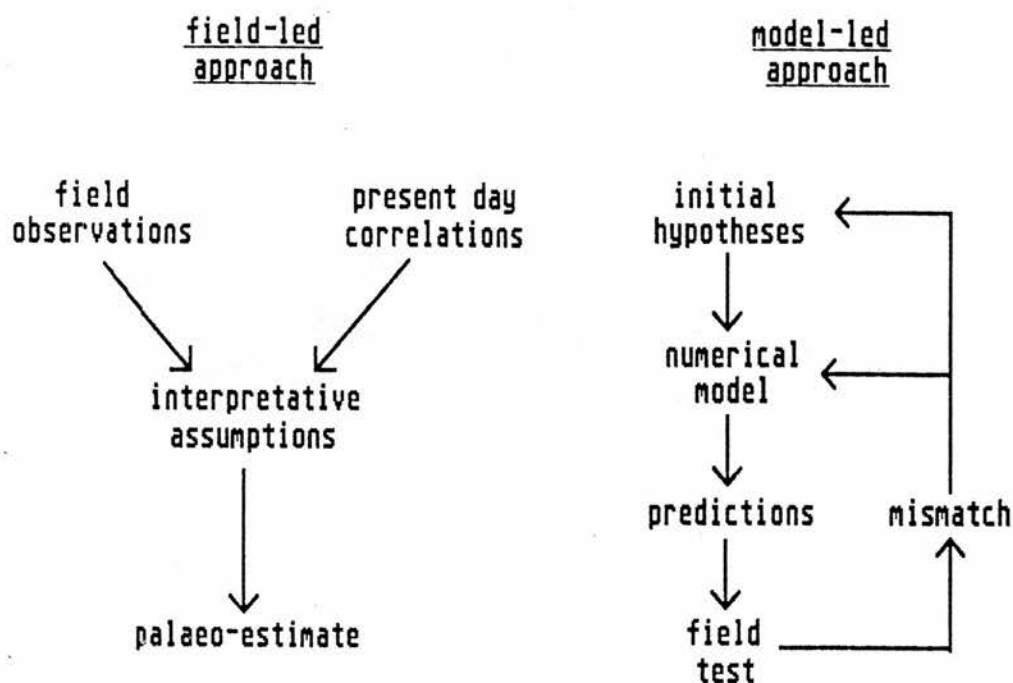
Figure 1.1 Two contrasting approaches used in the study of former ice masses.

Chapter 2.
Model construction
and input data.

Chapter 3.

The Antarctic Peninsula
ice sheet during the
last 40,000 years.
*eustatic sea level
and marine basal melt*

Chapter 4.

The Loch Lomond
stadial
ice sheet
in Scotland.
*air temperature
and precipitation*

Chapter 5.

The climate
of the Loch Lomond
stadial in Scotland.
*air temperature
moisture supply,
and precipitation*
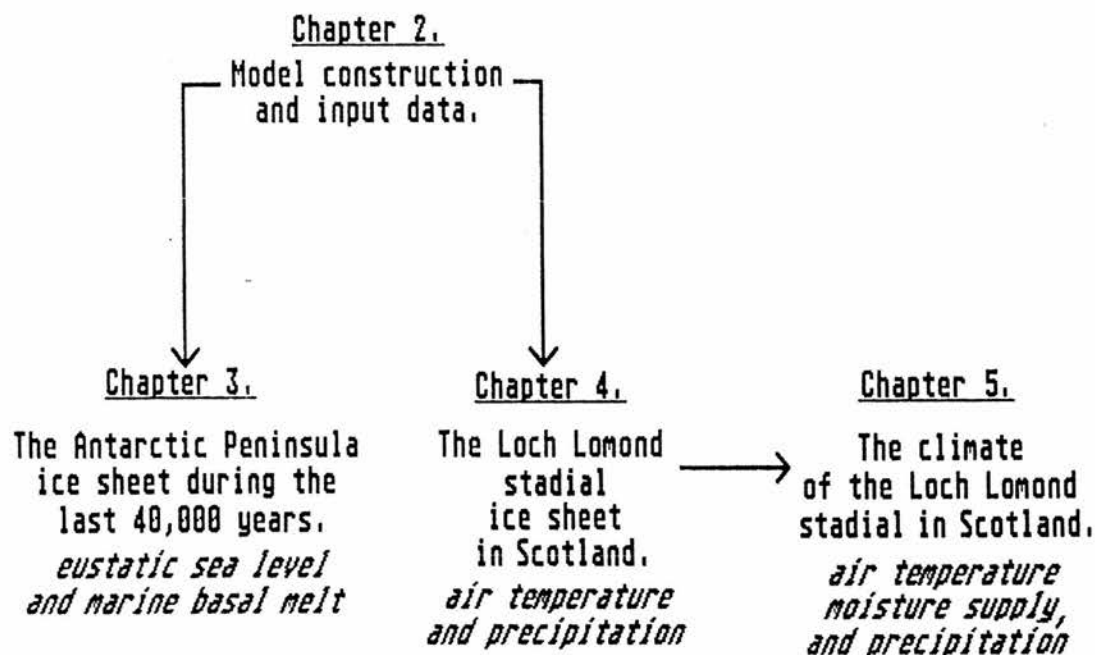
Figure 1.2 The case study structure of the thesis.
Model design is outlined in Chapter 2,
the remaining chapters are case studies
with driving variables in italics.

initial hypotheses ⟵──────────────────────────┐
    (word model)   │
        ↓   │
variables selected   │
        and   │
relationships determined   │
        ↓   │
parameterization   │
    ╱ ╱ ↓ ╲ ╲   │
  ↙ ↙ ↓ ↘ ↘   │
set of possible numerical models ⟵──────────┐   │
                ↓   │   │
            tuning ──────────────────────→ field│
                ↓   estimates
            testing ────────────────────────→ ↑
        ↙   ↘
sensitivity   experimentation
analysis
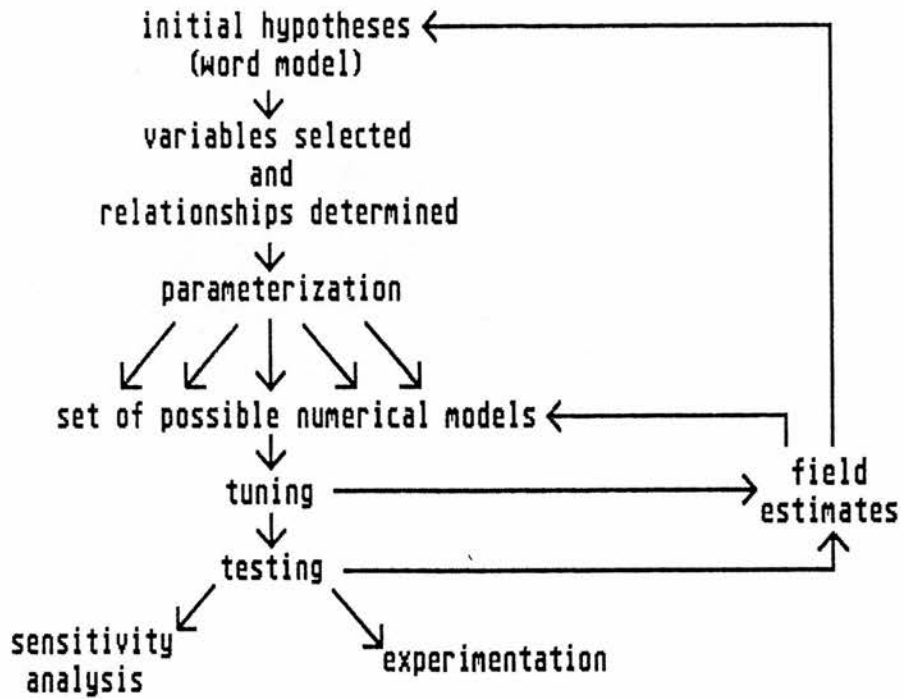
Figure 1.3 Flow diagram of the modelling procedure
used in the thesis.

CHAPTER TWO : MODEL CONSTRUCTION AND INPUT DATA.

The aim of this chapter is to describe the construction of the general ice sheet model used in the case studies. The chapter is sub-divided into five sections. The first section outlines the reasons for selecting the particular ice sheet model used, and also introduces this model. The second section describes the derivation of the three forcing functions used to drive the model in the individual case studies. The third and fourth sections describe and justify the individual components and relationships within the model. The former concentrates on interactions between an ice sheet and its environment, and the latter is concerned with the modelling of an ice sheet's internal flow dynamics. The fifth and final section considers some of the numerical problems associated with the construction of the model.

(2.1) BASIC CONSIDERATIONS.

(2.1.1) INITIAL MODEL REQUIREMENTS.

The purpose of this chapter is to introduce the core model used in the case studies. The model meets four basic requirements: it is

(i)   process orientated;

(ii)   capable of tracing ice sheet evolution through time;

(iii) capable of dealing with both horizontal dimensions (ie it is at least two dimensional); and

31

(iv) as simple as the above requirements allow it to be.

The need for these requirements is now discussed. The need for the model to be process orientated follows from the arguments of Chapter 1. If the processes acting within an ice sheet system can be simulated then predictions of form can be produced. This is necessary because the available field evidence provides estimates of form rather than process. The concentration on process allows glaciological theory to be used to construct the model, and means that there is no need to use assumptions concerning former ice sheet form. The palaeoclimatological data needed as model input are non-glacial in nature (often palaeoecological), thus field evidence (in the form glacial geomorphology) can be devoted to the tuning and testing of the model. A process model is therefore a link between palaeoclimatological and glacial geological estimates, the former are used as model input and the latter are compared to model output.

The processes operating within an ice sheet system vary through time. If this variation is small over long periods then time can be ignored as an independent variable and modelling can rely on steady state assumptions. A first impression of the likelihood of time dependence can be gained by comparing the time scale over which the quantities which determine ice sheet behaviour

32

vary with the ice sheet's likely response time. Response time is defined as the time required for a system to switch from one equilibrium (time independent) state to another in response to an instantaneous change in forcing. Continental ice sheet response times are estimated to be in excess of 20.0 ka (Oerlemans and van der Veen 1984). Variables that affect ice mass behaviour at continental scales include insolation, sea surface temperature and sea level. They exhibit variation with a period (the time between a maximum and the following minimum) of between 10.0 and 20.0 ka (Ruddiman et al 1977, Kellogg T. B. 1975, Bloom et al 1974 and Berger 1978). The time scale of variation in ice sheet forcing is therefore similar to the time an ice sheet requires to respond to these changes. An ice sheet system is thus unlikely to achieve equilibrium, and its form is therefore not a function of the forcing alone but also depends on time. This implies that it is extremely important for an ice sheet model to be able to trace ice sheet response to external forcing through time.

The realization that ice sheet behaviour is dynamic prompts a third requirement, namely that the model should be spatial. As an ice sheet responds to changing conditions features such as ice divides, domes and streams are liable to shift their positions. A one-dimensional model following a flow-line is not sufficient

33

to follow this type of ice sheet evolution. A minimal requirement is that the model should have two horizontal dimensions, allowing the changing importance of ice sheet features in different areas at different times to be assessed. Another important reason for this requirement is that much of the field evidence available for comparison with the model output is areal in nature. Thus a two-dimensional horizontal model is more testable than a flow-line model because it allows areal estimates of former extent and flow patterns to be used as test evidence.

The final requirement mentioned, that of minimal possible complexity, is the most contentious because it relates directly to the overall methodology used and to the question of what is expected of a model. There are two approaches to the question of the complexity desirable in a model, both of which have advantages as well as disadvantages. One approach is to produce a complex model, incorporating all known processes operating within the system of interest. Alternatively, modelling can proceed from a basic skeleton and recognize the very minimum of processes. The choice of the complexity of the initial model is subjective and relies on the modeller's personal view of the importance of varying processes.

The justification for producing complex initial models is that their predictions are based on the most realistic physics available. A large number of processes are incorporated into such models, thus a comparison can be made of the relative dominance of these processes in determining overall model and ice mass behaviour. This 'top-down' approach starts with a high degree of complexity and narrows the number of important processes down. A model of this type is likely to require less of the loose parameterization described in Section (1.3), and relies on more physically justifiable parameters. This type of model is therefore intrinsically more testable than simpler, more parameterized models because its predictions are less subject to variation. An example is the modelling of basal sliding. Simple models, such as those empirically relating sliding velocity to basal shear stress and normal load on the bed, are highly sensitive to the precise method of parameterization. They predict a wider range of sliding velocities, and are less testable, than the more complex physically-based models.

The opposite, initially simple, approach is used in this study. This approach is chosen for both practical and methodological reasons. It is extremely difficult to define an upper limit to the complexity of a model because there are always other processes and factors that could be included in the model. Thus it is

impossible to produce the complete model of a given system because it is always possible that important processes have been omitted. The use of an initially complex model to identify all of the important processes affecting a system's behaviour is therefore unrealistic.

The choice of complexity is scale related. An example is the Glen flow law, which is central to virtually all ice sheet models but would seem a gross empiricism to a materials scientist. This implies that, given an unlimited scale of investigation, there is no upward limit to the desirable level of complexity within a model. To take an extreme example the most realistic model of the late Quaternary Scottish ice mass would occupy an area of 70,000 km^2 and take thousands of years to run.

Given the unbounded nature of model complexity a sensible approach is to consider how simple a model can be made rather than how complex a model needs to be. From this perspective it is more reasonable to build up from a basic framework. If an initially simple model is found to be deficient (in that it cannot predict real world observations) then it can be expanded. This process of increasing model complexity should prove more economic than the production of an initially complex model. The effort needed to produce a simple model is obviously less

than that required to produce a complex one. The expansion of the simple model requires extra effort, depending on the amount of complexity found necessary, but the total effort expended is still likely to be less than that required to produce an initially complex model.

Whether a complex or a simple model is chosen, modelling often relies on the same input data. The accuracy of a model's predictions depend on the accuracy of this input data. The input data used in the modelling of ice sheets is often of poor quality. For example, the calculation of the mass budgets of present day continental ice sheets is hampered by inadequate knowledge of their accumulation distributions (eg Budd and Smith 1985, and Reeh 1985). This is equally true of the climate which nurtured the late Quaternary ice sheets. The input data's inaccuracy, and its effect on model predictions, implies that it is uneconomical to select too complex an initial model. The complexity of a model should be commensurate with the accuracy of the model's input data, and, in the case of former ice sheets, simpler models should therefore be chosen.

Three practical features also favour the use of simple models. First, there is the ease of output interpretation. Simpler models contain fewer components and interactions, and are capable of a narrower range of

behaviour. Their output is therefore more easily interpreted than the output of complex models. There is a danger that the understanding of complex model output will, in itself, become the subject of research. This must detract from the ability of a model to explain real events.

Second, there is the ease with which additional elements can be built into the structure of the model. This need may arise if certain sections of the initial model have to be expanded, or if the ice sheet model is to be coupled with models of other earth surface systems, such as the atmospheric, oceanic or lithospheric systems. In either case the task of amending the initial model is easier if the initial model is simple rather than complex.

No

Third, the use of the most concise model available is essential from a purely logistical point of view. The requirements of time dependence and areal perspective lead to models that involve many calculations. The degree of complexity is therefore somewhat restricted if computer processing time is to be kept within reasonable bounds.

Shouldn't be a problem.

(2.1.2) THE BUDD MODEL.

The model of Budd and Smith (1981) fulfils the four

basic requirements outlined above. It builds on the work of Mahaffy (1976) who generalized, to three dimensions *No* and to a non-steady state, methods previously used to analyse the steady state flow-line problem (Nye 1952, 1959). The model has been used to investigate the behaviour of several ice sheets. For instance Mahaffy (1976) used it to study the Barnes ice cap, Baffin Island. It has also been used to study the inception of the Laurentide (Andrews and Mahaffy 1976) and the Scandinavian (Oerlemans 1981) ice sheets. More recently, an expanded model has been used to study the evolution of the Laurentide and Antarctic ice sheets through a full glacial-interglacial cycle (Budd and Smith 1981, 1982).

These latter models represent a major advance over the initial Mahaffy papers because the model is extended to include many ice sheet-environment interactions. For instance, the original Mahaffy model was driven by changing Equilibrium Line Altitude, while the Budd models include separate dynamic representations of ablation, accumulation and isostasy. The Budd models have fundamentally recast the way in which ice sheets are modelled. Previous modelling had concentrated on the internal physics of an ice sheet and drew a boundary at the ice sheet surface. The work of Budd redefined the system of interest to include environmental interactions and has therefore gained a more holistic insight into ice

age glacial problems.

The key paper of Budd and Smith (1981) was described
by Hughes (1984) as 'epochal'. It combined two previously
isolated strands of Quaternary research, and linked the
continental ice sheet model to insolation variations
derived from Vernekar (1972). This allowed the
Milankovitch hypothesis to be tested. Previous work on
the Milankovitch forcing of Quaternary cycles used a one-
dimensional ice sheet model, which only dealt with
latitudinal bands (eg Birchfield et al 1981, Pollard 1978
and Oerlemans 1980). These models sought to reproduce the
global ice volume estimates obtained from the oxygen
isotope ratios of deep sea sediments (eg Imbrie and
Imbrie 1980). The Budd and Smith model represented an
advance on these models because it allowed both deep sea
core and terrestrial geomorphological data to be used as
model constraints.

The Mahaffy-type models are based on the continuity
equation for ice thickness:

$$\frac{\partial Z}{\partial t} = b - \nabla(\overline{U} \cdot Z) \qquad (2.1)$$

The coordinate system used is given in Figure 2.1.
Equation (2.1) relates the rate of change of ice
thickness (Z) at a specific point (x,y) and time (t) to a
net mass balance term (b, which can vary with time and

position) and to the flow convergence/divergence of ice within the ice sheet at that point. The evolution of an ice thickness distribution can be reconstructed by integrating (2.1) forward through time. All estimates of horizontal ice flux are obtained from the product of the vertically-averaged horizontal velocity (U_x and U_y) and ice thickness. The model does not therefore explicitly include the vertical dimension (z), and is thus called a two dimensional model.

In order for this equation to be used, net mass balance must be specified over x,y and t. This rate consists of calving, ablation and ice accumulation terms. The latter term is further sub-divided into the total annual precipitation and the fraction of precipitation falling as snow (the effectiveness). The determination of these quantities is given in Section (2.3). The flux divergence terms in equation (2.1) must also be determined and this is outlined in Section (2.4).

Variations in the net mass balance drive the system outlined by equation (2.1) because they represent net additions to and losses from the ice sheet, while the flux terms represent ice redistribution within the ice sheet. The models used in the case studies employ three different methods of changing the net mass balance term and driving the ice sheet system. These methods are

41

discussed in Section (2.2) and use air temperature (in the Loch Lomond case studies), eustatic sea level and marine basal melt (both used in the Antarctic Peninsula case study). In addition to external eustasy, there is an internal locally-produced component of sea level change (isostasy) which can affect ice sheet behaviour. The internal calculation of isostasy is discussed in Section (2.3).

The model can be summarized using a system diagram (Figure 2.2). This diagram indicates the chosen system boundary, and identifies important variables and their inter-relationships. Variables within the diagram's stippled area are internal to the model system, while those outside the model area are either driving variables or provide boundary conditions. The driving variables are marine basal melt, eustatic sea level and imposed regional air cooling, while latitude, initial surface topography and initial precipitation represent boundary conditions.

Within the model three sub-models can be identified: isostasy, ice flow and net mass balance. The three sub-models overlap because ice thickness is a vital component of each. The isostasy section has a relationship between ice thickness, bedrock depression and reduced ice surface elevations. There is a large time lag within this loop,

and periods in excess of 5.0 ka are needed for the bedrock to reach an equilibrium depression (Walcott 1970a). A second section within the model relates to ice flow. Increased ice thicknesses are associated with greater ice flow which then has the effect of decreasing ice thickness. This mechanism is controlled by the influence of surface slope. Finally the model contains a net mass balance section. Mass balance increases with surface elevation, and changes in ice thickness are therefore accentuated by positive feedback.

For an ice sheet to reach equilibrium the effects of the various loops described above must balance one another, and at any point on the ice sheet surface net mass balance must equal ice flow divergence/convergence.

(2.2) DERIVATION OF THE FORCING FUNCTIONS USED TO DRIVE THE MODEL.

This section introduces the three forcing functions used in the case studies. The Loch Lomond stadial case studies use a regional air temperature forcing function, which partially determines the ablation and accumulation rates predicted in the model. The Antarctic Peninsula case study uses two forcing functions, which are eustatic sea level and marine basal melt rate. The latter represents the rate of ice melt from the underside of marine ice shelves, while the former partial controls features such as calving and grounding line migration.

(2.2.1) REGIONAL AIR TEMPERATURES DURING THE LOCH LOMOND STADIAL IN SCOTLAND.

Both ablation and precipitation effectiveness (the fraction of precipitation falling as snow) are strongly dependent on air temperature. The variation of air temperature with latitude and altitude allows both ablation and effectiveness to be empirically linked to these variables. However the modelling of climatic variation during the Quaternary requires a regional air temperature change to be superimposed on this altitude/latitude pattern. The origins of this regional change for a particular area are complex and depend on both regional energy balances and global circulation systems (oceanic and atmospheric).

At the global scale air temperature changes can be related to changes in insolation. The work of Budd and Smith (1981) drives a continental ice sheet model using this insolation variation empirically converted to an equivalent regional air temperature change. The very much smaller size of the ice sheets modelled in this study (the United Kingdom has an area of 0.24 million km^2 compared to an area of 19.42 million km^2 for continental North America) means that different mechanisms are likely to drive the ice sheet-climate systems in the study. This is an example of the importance of spatial scale in determining model boundaries. At a continental scale

44

global insolation can be considered external while processes affecting surface energy balances, circulation systems and regional temperatures can be considered internal. For instance, the regional chilling of air temperatures produced by the high albedo of extensive ice and snow surfaces is internal to the system (Kellogg W. W. 1975). However, at a regional scale, air temperatures are dominated by processes such as albedo chill rather than by the original insolation signal.

Insolation variation is not used to drive the ice sheet model in this study because of these scale related problems. In addition it is not possible to use the regional air temperature predictions of a continental ice sheet model. These temperature predictions contain information on both insolation and albedo chill factors, however they do not reflect the influences of other continental scale processes. This point is illustrated in Figure 2.3, which compares a palaeoecological estimate of British July air temperature with mean summer air temperature output from the Budd and Smith (1981) model for 70 ^{o}N. The magnitude of air temperature variation is similar in both cases and the gross shape of both curves agrees from 50.0 ka BP to the present. Palaeoecological estimates before 40.0 ka BP suffer from large errors in radiocarbon dating (Lowe and Walker 1984) and should not be trusted. A more important point is that the

palaeoecological estimate shows variation over smaller time scales than the model output curve. In particular the event at 10.0 ka BP (the Loch Lomond stadial) is shown in the palaeoecological data as a rapid cooling from temperatures similar to those of the present day to those characteristic of glacial conditions (a 8.0 ^{o}C temperature depression). This brief cooling does not appear in the ice sheet model's output. Clearly this major event in the United Kingdom's climatic history cannot be predicted by an albedo-insolation mechanism and alternative explanations must be sought.

Ruddiman and McIntyre (1981a) have correlated the Loch Lomond stadial with a dramatic southward advance of the boundary separating subpolar and polar Atlantic surface waters (the North Atlantic polar front). This front can be identified from deep sea core data by the down-core variation of biogenic sediment types, which can be correlated with the changes in the palaeoecology and sea surface temperature of the overlying water mass. The use of a geographical distribution of cores and the dating of down-core sediment changes allows the evolving distribution of surface water types to be traced. Broecker et al (1988) have postulated that this advance was caused by meltwater released during the decay of the Laurentide ice sheet. The exact process leading to this cooling is not important here, however it is clear that

United Kingdom's Quaternary climate is controlled by many different mechanisms operating at a variety of scales.

Models of the former United Kingdom ice sheets need to exclude continental scale processes. The record of former regional air temperatures that is fed into the model must therefore incorporate the temperature signals arising from albedo feedback, oceanic front migration and insolation variation. In the absence of any global model capable of predicting such a record, an alternative is to use a palaeoecological index of climate. The air temperature index used in this study is based on the ecology of dated Coleoptera (beetle) assemblages.

To derive air temperature estimates from beetle assemblages the assemblage must be dated and the individual species occurring within the assemblage identified. The present day geographical distribution of these species can be used to derive an empirical estimate of the species' tolerance to climate, using meteorological station data. The most significant climatic parameters in determining a species' distribution are continentality (the difference between mean July and mean January temperatures) and mean July air temperature (Coope 1977). These air temperature correlations rely on present day observations, however there is good reason to assume that present day and late

Quaternary Coleoptera are physiologically identical and responded to temperature change in similar ways (Coope 1979).

The identified species within a fossil Coleoptera assemblage therefore carry decipherable information relating to the air temperature at their time of death. By comparing the derived thermal tolerances of each species within the assemblage a July temperature/continentality envelope can be constructed. This envelope then constrains the former temperature regime in which the Coleoptera assemblage lived (eg Atkinson et al 1985).

Palaeotemperature estimates based on Coleoptera are preferable to those based on pollen for three main reasons. First, climatic changes during the late Quaternary are thought to have been rapid, it is therefore important to use species that are known to colonize newly suitable territory rapidly. In this respect beetles are useful because they are highly mobile and, in the case of omniverous species, do not require the presence of specific ecological habitats (Buckland and Coope 1985). In contrast pollen producing plants are often slow to colonize because many species require specific habitats which only become available through the slow process of ecological succession. The absence of a

plant species may therefore be misinterpretated because a region may be climatically suitable for a species yet remain ecologically unsuitable.

A second advantage is that the Coleoptera assemblages found in freshwater deposits reflect the different species that lived throughout the whole of a catchment. Coleoptera assemblages therefore represent a spatially integrated record of conditions in several microclimates. This catchment scale resolution overcomes the problems of sampling specific microclimates, while still containing data from a distinct spatial location. Pollen data suffers from a spatial resolution problem because contaminating pollen may arrive from distant and ecologically dissimilar sources. A third advantage is that Coleoptera are readily identifiable at the species level. This allows palaeotemperature estimates to be more tightly constrained than is often the case with pollen based estimates.

The use of this type of data does run the risk of introducing some errors. The accuracy of the radiocarbon dating needed to put temperature estimates into a chronology is sometimes doubtful. These doubts mainly arise from of the risk of sample contamination with carbon of a different age (Lowe and Walker 1980). There are also limitations in the degree to which a given

Coleoptera assemblage can constrain the possible number of thermal environments in which it could have existed. The error of Coleopteran temperature estimates is typically 2 ^{O}C for average July temperature and 8 ^{O}C for continentality (Atkinson et al 1985). Even with these errors, the use of regional ecological indices as a model forcing function is preferable to an attempt to incorporate the type of global mechanisms discussed earlier.

The specific palaeotemperature estimate used in the Loch Lomond stadial case studies is shown in Figures 2.4, which is taken from Coope (1975). More recent work (Atkinson et al 1985) alters the shape of these curves slightly and also gives an estimate of changing continentality. The Loch Lomond stadial time series begins at 12.5 ka BP (the Lateglacial Interstadial), when July air temperatures were similar to present. This period is followed by a gradual, two-stepped temperature reduction, during which rates of cooling vary from 0.009 ^{O}C a^{-1} to 0.001 ^{O}C a^{-1}. A minimum July temperature of 9.0 ^{O}C is reached at 10.0 ka BP. This minimum is followed by an extremely rapid warming and present day temperatures are reached after only 300 a (representing a 0.025 ^{O}C a^{-1} average rate of warming). Temperatures then remain constant up to 7.5 ka BP.

The late Quaternary climate of the United Kingdom experienced severe changes in continentality as well in July temperature. This is illustrated in Figure 2.5, which is based on periglacial evidence and is taken from Williams (1975). This reconstruction agrees well with estimates of continentality derived from Coleoptera assemblages. The temperature curves of Figure 2.5 indicate that Britain suffered an exaggerated annual temperature cycle during the late Quaternary cold periods. Annual temperature range increased from the present 13.0 ^{O}C (for central, lowland England) to a value in excess of 30.0 ^{O}C (Coope et al 1971 and Williams 1975). These changes in continentality affect the air temperature estimates fed into the ice sheet model. A method of deriving these continentality estimates from July temperatures must therefore be incorporated into the model.

Regional air temperature directly affects the ablation and precipitation effectiveness components of the ice sheet model. The July air temperature time series shown in Figure 2.4 therefore has to be converted into a form suitable for use in the equations calculating ablation and effectiveness. The flow diagram in Figure 2.6 illustrates the procedure used.

July air temperatures are firstly converted to

51

differences relative to the present day value (17.0 ^{O}C) producing regional air temperature depressions. The ablation relationship of Budd and Allison (1975) requires air temperature depression to be expressed as an imposed shift in the altitude of July isotherms. This is achieved by using a constant lapse rate (6.5 ^{O}C km^{-1}). The majority of ablation occurs during the summer, it is therefore valid to use an air temperature depression based on July temperatures in the ablation calculation.

An estimate of annual temperature depression is, however, required for the effectiveness calculation because snow accumulation can occur all year round. Increased continentality leads to annual temperature experiencing a greater depression than July temperature. In the model mean annual temperature depression is estimated from July air temperature depression using the twin assumptions of a sinusoidal annual temperature cycle and a linear relationship between July air temperature depression and continentality. This procedure is outlined in Appendix I. Finally, annual temperature depression is converted to the imposed shift in annual isotherms required in the effectiveness calculation.

(2.2.2) EUSTATIC SEA LEVEL CHANGE.

Global sea level changes affect model behaviour in four ways. First, sea level, in conjunction with ice

thicknesses and isostasy, determines the ice sheet grounding line. Beyond this line the ice sheet suffers increased ice loss because of melting from the underside of floating ice shelves (marine basal melt). Second, ice sheet margins that impinge on the sea suffer a calving loss which is partially controlled by eustatic sea level change. Third, ice sheet interaction with sea level affects the flow dynamics of the ice sheet. Thus the sections of an ice sheet that are grounded below sea level may experience an enhanced sliding velocity because the friction produced by the normal stress of ice against bed is reduced via buoyancy. In addition the type of strain within the ice mass is partially determined by whether or not the ice is floating. Grounded ice deforms predominantly by shearing, which is controlled by the horizontal differences in pressure produced by a sloping ice sheet surface. In contrast floating ice deforms by normal strain.

A fourth way in which global sea level affects ice sheet behaviour is in the accumulation and ablation terms. A fall in sea level is equivalent to a rise in surface elevation. Thus, as sea level falls, land surfaces (which are at a constant distance from the earth's centre but at an increased distance from the current sea level) suffer relatively less ablation and relatively more snowfall because they are at a relatively

greater altitude. The rationale is that land surfaces, especially those in maritime locations, are further away from their main heat source, the sea. The effect is fairly minor, and a 120 m eustatic sea level fall causes an apparent cooling of 0.8 ^{O}C.

Eustatic sea level forcing is not introduced into the Loch Lomond case studies because this ice sheet is known to have been almost entirely land based. The only way in which eustatic sea level change could affect this ice sheet is via its apparent cooling effect. Sea level does, however, play an important role in the modelling of the marine Antarctic Peninsula ice sheet. The Antarctic Peninsula model is thus partly driven by a time series of global sea level change. In addition, the combination of externally imposed eustasy and modelled isostasy allows shoreline evidence to be used as another means of testing model predictions.

The process of eustatic sea level change is highly complex and contentious. Processes such as the tectonic enlargement and the sedimentary infilling of ocean basins, and ocean water density changes obscure the basic signal produced by global ice volume changes. A good estimate of this latter component can be obtained from deep sea cores and their record of down-core oxygen isotope ratios (eg Shackleton and Opdyke 1973). The ratio

of Oxygen-18 to Oxygen-16 provides an estimate of global ice volume. Relatively more of the lighter isotope evaporates from the oceans and is stored in continental ice sheets. Thus the growth of continental ice sheets reduces the concentration of Oxygen-16 in ocean water, which is recorded as a Oxygen-16 deficient layer in deep sea cores.

Three further complications arise when the oxygen isotope record in deep sea cores is used to estimate global eustasy. First, isotopic ratio is affected by water mass' temperature so that the down-core record is a composite of ice volume and ocean temperature signals (eg Emiliani 1955). Second, the sediment within a core will have suffered a certain amount of bioturbation resulting in the down-core record being a smoothed version of the actual isotopic changes. Third, Mix and Ruddiman (1984) argue that the oxygen isotope record in deep sea cores lags behind the actual ice volume changes. This happens because the isotopic ratio of snow accumulated on ice sheet surfaces depends on the altitude of these surfaces, this altitude changes during ice sheet growth and snowfall therefore becomes isotopically lighter through time. Thus growing ice sheets are isotopically heavier than steady state ice sheets of the same size.

Budd (1981) uses several empirical sea level curves,

derived from dated shoreline features, to produce a simulation of the oxygen isotope record which is in gross agreement with the actual isotope curve of Duplessy (1978). This agreement implies that the oxygen isotope record accurately records global ice volumes and glacial eustasy. The above sources of inaccuracy may therefore be minimal in their effects.

The Antarctic Peninsula case study investigates the period around the last glacial maximum of 18.0 ka BP. The eustatic sea level time series used in this case study is derived from Shackleton (1987), who gives two estimates of eustatic sea level over the past 160.0 ka. One is derived from New Guinea marine terraces (Bloom et al 1974) and the other from oxygen isotope measurements corrected for changes in ocean temperature. Both data sets agree closely from 20.0 ka BP to the present. They both have a maximum depression of 120 m, which occurs at 18.0 ka BP. This is followed by a rapid rise to present day values at 7.0 ka BP. During the period 40.0 to 20.0 ka BP both curves show oscillations of $\pm$ 10 m around a central value. This central value is 50 m in the case of the New Guinea data and 70 m in the case of the oxygen isotope data.

The actual sea level time series used in the Antarctic Peninsula case study is shown in Figure 2.7, and

represents an idealized time series drawn using both of the above data sets for the period 40.0 ka BP to the present. The inaccuracy introduced by using a smoothed, idealized function for sea level is within the range of error involved in the estimation of bathymetry for the case study area.

(2.2.3) THE VARIATION OF BASAL MARINE MELT AROUND THE ANTARCTIC PENINSULA DURING THE LAST 40.0 KA.

A second forcing function that affects the behaviour of marine ice sheets is the variation of basal melt rates through time. A time series of basal melt rate changes around the Antarctic Peninsula is therefore needed. Basal melt rate is the annual rate of melting from the underside of ice shelves. It is related in a complex way to the oceanic circulation under an ice shelf (Bentley 1983, MacAyeal 1984), however a simplified estimate is possible because basal melt rate is also related to the type of water mass adjacent to an ice shelf.

Areas that are adjacent to a polar water mass have basal melt rates that are typically below 0.5 m a^{-1}, for instance Bentley and Jezek (1981) and Doake (1985) cite values of 0.2 and 0.3 m a^{-1} respectively for the Ross ice shelf, and Budd (1966) cites a value of 0.5 m a^{-1} for the Amery ice shelf. In contrast areas that are adjacent to a sub-polar water mass have higher melt rates, thus the George VI ice shelf experiences an annual melt rate

of 2.0 m a^{-1} (Bishop and Walton 1981). In the following discussion the term polar water mass is used for an area that is perennially covered by pack ice, while the term sub-polar water mass is used for an area which is only covered by pack ice during the winter. The Weddell Sea is an example of the former and the Bellinghausen Sea an example of the latter (Schwerdtfeger 1970).

Deep sea core evidence indicates that the presently sub-polar water mass to the West of the Antarctic Peninsula was replaced by a polar water mass during most of the last 40.0 ka. The movement of the oceanic polar front that separates these two types of water mass can be traced in time and space by the down-core variation of radiolarian assemblages (Hays 1978). A geographical distribution of these core analyses around the Antarctic continent indicates that the position of the front was formerly further North than at present, and that polar water masses occupied roughly ten times their present day area of 2.6 x 10^6 km^2 (Cooke and Hays 1978).

The recent southerly movement of the front to its present position started at approximately the same time (18.0 ka BP) as the disappearance of the northern hemisphere ice sheets and the consequent rise of eustatic sea level (Hays 1978). The area West of the Antarctic Peninsula, during the period 40.0 ka BP to 18.0 ka BP, is

*therefore associated with a polar water mass and with
low basal melt rates. In this study a value of 0.5 m a^{-1}
is taken as being typical for this period. Between 18.0
ka BP and the present this polar water mass was replaced
by a sub-polar water mass, with a consequent rise in
basal melt rate to the present value of 2.0 m a^{-1}. There
is no available data indicating the rate at which the
polar water mass was replaced by the sub-polar water
mass, nor is there any information about the rate of
increase of the basal melt rate. A simple linear increase
from 18.0 ka BP to the present is therefore assumed.
Figure 2.8 shows the time series of basal melt rates used
in the model as a second forcing function.*

*This temporal variation of basal melt rate only
happens in the area West of the Antarctic Peninsula. At
the present day the Peninsula forms a distinct oceanic
divide between sub-polar water to the West and polar
water to the East (Doake 1985). Thus the basal melt rate
increases discussed above only apply to the West of the
Peninsula. To the East basal melt rates always remain at
the low (0.5 m a^{-1}) rate. This contrast is captured in
the model by assigning a time dependent melt rate to the
area that is both North of 75 ^{O}S and West of 67 ^{O}W, and a
constant minimum melt rate to the rest of the area.*

(2.3) PROCESSES LINKING AN ICE SHEET TO ITS ENVIRONMENT.

The environment of an ice sheet includes the atmospheric, lithospheric and oceanic earth surface systems. An ice sheet is linked to its environment via a number of processes. In this section the model's representation of four of these processes is discussed. The estimation of net mass balance in the model links the ice sheet with its atmospheric environment, this link also involves the representation of topography in the model. The link between an ice sheet and the oceanic system determines the representation of calving and basal melt rate in the model. And finally, the influence of the lithospheric system on ice sheet behaviour is manifested via isostasy.

(2.3.1) NET MASS BALANCE TERMS.

The calculation of net mass balance (b) involves the determination of three quantities; ablation (Ab), precipitation (P) and the fraction of precipitation falling as snow (effectiveness, Eff). They are linked in the following way:

$$b = P \cdot Eff - Ab$$

(2.2)

All the equations used in this section refer to mass balance rates in m a^{-1}. Both effectiveness and ablation are associated with air temperature, which in turn is related to surface elevation, latitude and imposed

regional temperature change. The model uses correlations against these three independent variables to predict changes in effectiveness and ablation.

The relationship between ablation and air temperature is not directly causal because the rate of melt at a snow/ice surface actually depends on the partitioning of energy at the snow/ice surface. The energy budget of such a surface is dominated by short wave incoming radiation, which provides most of the energy used in ice melt (Braithwaite 1981). Increased incoming radiation is balanced in the surface energy budget by an increase in both latent and sensible heat fluxes. The former flux determines the rate of ablation, while the latter creates variation in air temperature. This produces a strong, but coincidental, correlation between air temperature and ablation.

Despite the above argument, statistical techniques show a stronger association between ablation and air temperature than between ablation and incoming radiation. This happens because incoming radiation is negatively correlated with the other energy fluxes occurring at the ice surface, such as long wave emission. Its effect in determining ablation is therefore smoothed. Sensible heat flux is, in contrast, positively correlated to the majority of the energy fluxes at the surface (Braithwaite

and Olesen 1984) and is therefore strongly correlated with ablation.

Any relationship using air temperature, surface elevation and latitude to predict ablation is purely empirical. However the method is popular because it is both simple and reasonably accurate. A major attempt to specify ablation patterns from energy budget considerations is that of Williams (1979) for the potential glaciation of arctic Canada. This method is not incorporated into the present model because of the problems associated with the parameterization of former climatic variables, such as cloud cover and cloud type. The uncertainty introduced in parameterizing these quantities counters any increase in accuracy produced by the use of energy balance calculations. The correlation of ablation with altitude and latitude captures the essential dynamics of the process at a level sufficient for the project.

Budd and Allison (1975) investigate the relationship of ablation to altitude and latitude for a world wide distribution of 32 glaciers. This information, and data from Meier et al (1971), allowed Budd and Smith (1981) to derive the following relationship:

$$Ab = 10^{(E_o - E)/1.2}$$

(2.3)

where E is surface elevation and E_0 is the elevation of the 1 m a^{-1} ablation isopleth (both in km). This latter is determined from latitude (ϕ) and imposed July isotherm shift ($\triangle E_J$ km, derivation given in section 2.2.1):

$$E_0 = 6{\cdot}85 - 0{\cdot}085\phi + \Delta E_J \qquad (2.4)$$

The approach taken in determining effectiveness is similar to that used for ablation. A link to both surface altitude and latitude is possible via air temperature. The Corps of Engineers (1956) indicate that precipitation falls as snow if surface temperature is below 1.5 ^{o}C. This type of relationship operates over periods of hours, however effectiveness estimates are needed for yearly intervals. To produce these estimates a regression analysis was performed on meteorological data from the United Kingdom and Scandinavia. The sources for this data were Chandler and Gregory (1976), Manley (1970) and Johannssen (1970).

The annual fraction of precipitation falling as snow is not a commonly measured quantity, an estimated precipitation effectiveness was therefore based on the recorded number of days with snowfall. This estimate was then regressed against surface altitude and latitude. The details of this analysis and the procedure used to estimate effectiveness from the number of days with

observed snowfall are given in Appendix II. A good linear regression was obtained for the 21 sites used, with a R^2 value of 98.6 %:

$$Eff = -0.698 + 0.014\phi + 0.224(E - \Delta E_A) \qquad (2.4)$$

where $\triangle E_A$ is imposed annual isotherm shift in km (section 2.2.1).

Both of these calculations incorporate the forcing of net mass balance by imposed temperature changes in the form of altitudinal shifts in isotherms. In the case of ablation, these shifts are for July, while in the case of effectiveness mean annual shifts are used. Both ablation and effectiveness vary strongly with surface elevation so that overall net mass balance is far greater at higher altitudes. The relationship to latitude is weaker in both cases. Figures 2.9 and 2.10 illustrate the variation in these quantities for regional air temperature depressions, surface elevations and latitudes typical of Scotland during the Loch Lomond stadial.

Finally an estimate of total annual precipitation is needed. Budd and Smith (1981) use the present day distribution. Initially this study follows the same approach. The use of a present day precipitation distribution has several advantages relating to the ease of modelling, but it also carries several implicit

64

assumptions that should be tested. The advantages stem from the fact that a real distribution has many features that would otherwise be time consuming to incorporate. An example is seen in the present day distribution of precipitation over the United Kingdom. A regression analysis of precipitation as a function of altitude produces a relationship:

$$P_0 = 0.8 + 1.8E \qquad (2.6)$$

where P_0 is present day precipitation.

The areas with the greatest deviation from this regression equation are:

> *+0.8 m South-West Grampians, Lake District, North Wales and Kerry, Connermara and Donegal in Eire.*

< *-0.8 m The Cairngorms.*

This distribution of residuals implies westerly airflow, with considerable orographic enhancement in the West and a precipitation shadow in the East. The use of present day precipitation as a model input therefore implies that airflow was also westerly in the past. In addition it implies that that the effect of orographic enhancement on precipitation was the same as today, and that regional air temperature depressions had no effect on atmospheric moisture and precipitation. The latter two effects are partially included in the Budd and Smith (1981) model by the use of an 'elevation desert effect',

whereby air masses over the interior of an ice sheet are associated with reduced precipitation rates (Sugden 1977). This happens because of the great distances separating ice sheet interiors from oceanic moisture sources. In addition low air temperature over the ice sheet interior leads to a reduction in the atmosphere's ability to carry moisture. This effect is parameterized using:

$$P = \begin{cases} P_0 & \text{if } E \leq 2 \\ P_0/2^{(E-2)} & \text{if } E > 2 \text{ and } B \leq 2 \\ P_0/2^Z & \text{if } E > 2 \text{ and } B > 2 \end{cases} \qquad (2.7)$$

(2.3.2) TOPOGRAPHIC REPRESENTATION.

The model used in this study simulates ice sheet behaviour on a gridded bedrock topography. A realistic representation of bedrock topography is important for two main reasons. First, high altitude areas are vital during ice sheet initiation because of the strong dependence of net mass balance on surface altitude. As ice sheets expand, the changing geographical positions of features such as ice domes, divides and streams are dependent on the locations of these initial seeding areas. Since the migration of these features is an important element in model testing, it is essential to capture the positions of the initial ice sheet seeding areas accurately. Second, bedrock topography, even when inundated by ice, determines the position and dynamics of both ice streams

66

and grounding lines.

*Equations (2.2) to (2.5) incorporate a strong
dependence of net mass balance on altitude. This fact
carries important implications for the representation of
bedrock topography in the model. In the model ice sheet
evolution is traced over a horizontal rectangular grid,
and the specified surface altitude of each grid cell
partly determines the cell's net mass balance. The model
uses a single estimate of altitude in each grid cell.
This estimate is a summary of the highly varied real
world topography within the cell. Usually a mean is
taken. However, the non-linearity of the net mass
balance/altitude relationship implies that a prediction
based on mean surface altitude under-estimates the true
net mass balance of the cell. This is because of the
importance of the high altitude areas within a cell in
determining whether the cell has a positive or a negative
overall net mass balance. The estimate of topography
should therefore be biased towards the higher surface
altitudes within the grid cell.*

*A similar problem has been encountered by global
circulation modellers in their parameterization of the
effect of orographic barriers on air flow (Tibaldi 1986).
Their solution is to represent topography by the mean
elevation within a grid cell plus some fraction of the*

standard deviation of topography within the cell (an
envelope topography). The exact fraction used in the
parameterization is determined by tuning. The topography
data sets used in this study are not large enough to
allow the estimation of a standard deviation for each
grid cell, a simpler procedure is therefore used:

$$B = B_{mean} + a(B_{max} - B_{mean})$$
(2.8)

The topographic representation of bedrock (B in km) is
equal to the mean elevation within the grid cell (B_{mean})
plus some fraction of the difference between the mean and
maximum (B_{max}) values within the cell. The value of the
constant a is determined by tuning. The use of envelope
topography is illustrated in Figure 2.11. It has little
effect in plateau areas but simulates the accentuated net
mass balances in areas of varied altitude.

The contribution of ice growth to surface elevation is
now incorporated into the procedure. Unlike bedrock
altitude, the variation of ice thickness at the sub-
grid level is minor, a single mean value is therefore an
adequate representation. Ice surface altitude can be
calculated either by adding the accumulated ice thickness
to the mean or to the upwardly biased bedrock
representation. Valley glacier flow and avalanching lead
to the movement of ice into lower altitudinal positions.
In the model ice thickness is therefore added to the mean

estimate of topography, which simulates the effect of ice redistribution within a grid cell from higher to lower altitudes. The surface altitude of a grid cell (E) is defined as:

$$E = \max\left(B, B_{mean} + Z\right)$$ *(2.9)*

The surface altitude of a grid cell (and its net mass balance) remain constant until ice thickness in the grid cell is greater than the difference between the mean and biased bedrock altitude. Surface altitude then equals the mean bedrock elevation plus the ice thickness, and net mass balance rates can begin to increase. This procedure simulates the effect of non-glaciated peaks within an area and is illustrated in Figure 2.11. Peaks have a greater accumulation rate than adjacent, lower, ice-covered areas. This extra accumulation is transferred down to the adjacent ice-covered areas, leading to enhanced ice growth in these areas.

An advantage of this technique is that the topographies needed to determine net mass balance and ice flow can be kept separate. The latter is often artificially smoothed to ensure the numerical stability of a model. The separation of topographies ensures that this has little effect on the sensitive net mass balance behaviour of the model.

69

Another important issue is the selection of the grid size used in the model. There are several opposing influences on grid size selection. First, models that use larger grid cells are faster to run because a given area can be covered by fewer individual cells. Second, the maximum stable time step used in a model is dependent on grid size (Budd and Jenssen 1975). Larger grids therefore allow larger time steps and faster rates of computation.

Opposing these arguments in favour of larger grid cell sizes is a third point, which is that smaller grid sizes produce more testable model predictions because their resolution is greater and more precise predictions are possible. This increase in testability with decreasing grid size is constrained by the need to incorporate an increasing number of small scale processes. For instance, Budd (1970a and 1970b) shows that the stress environment that drives ice sheet motion changes with horizontal scale. In particular, only shear stresses are important over large horizontal distances, while, at smaller distances, longitudinal stresses become significant. A model using only shear stresses therefore has a minimum grid size limit, below which increased grid resolution does not result in output that is more testable.

A small grid cell size of 5 km is used in the Loch Lomond stadial case study because a larger grid size

would flatten much of the topography of the area. In addition the field evidence used in this case study is fairly precise in nature and therefore warrants a high resolution model. In contrast, the Antarctic Peninsula case study uses a 25 km grid size. Field evidence in this area is not as precise as that of the Loch Lomond case study because it relates to ice flow directions and isostatic deflection, and not to ice limits. A lower resolution model can therefore be used without a significant loss in test potential.

(2.3.3) MARINE ICE LOSS TERMS.

Two mechanisms of ice loss arise through the interaction of an ice sheet with the ocean, they are marine basal melt and ice berg calving. Marine basal melt occurs from the underside of floating ice shelves. The point at which ice ceases to be grounded and starts to float can be determined using simple physics. The relation between ice thickness and water depth (which is equivalent to negative bedrock altitude, -B) at this point is:

$$ Z > \frac{\rho_w}{\rho_i}(-B) \qquad (2.10) $$

The pressure exerted at the base of ice thickness Z, of density ρ_i (870 kg m^{-3}) must be greater than that exerted by sea water depth B of density ρ_w (1080 kg m^{-3}). When the ice is thinner, or the water deeper, an ice

shelf is formed and a basal melt rate is applied. The exact value of this melt rate depends on the melt rate forcing function (discussed in sub-section 2.2.3).

A second consequence of ice shelf formation is that ice surface elevations are no longer the sum of ice thickness and bedrock elevation (see sub-section 2.3.2). Ice shelf surface elevations are found using the grounding line physics discussed above:

$$E = \left(1.0 - \frac{\rho_i}{\rho_w}\right)Z \qquad\qquad (2.11)$$

This surface elevation is used to determine net mass balance rates on the ice shelves.

The second process involving the marine loss of ice is the calving of ice bergs. Any ice sheet margin that impinges on the open sea suffers calving. The physics of this process are poorly understood. Reeh (1968) determines a theoretical failure zone from considerations of the stress distribution within a floating ice tongue, however his analysis does not predict calving velocity. A more recent treatment of the calving problem is that of Fastook and Schmidt (1982), who used a finite element analysis but were unable to produce a calving law from theoretical principles. Calving is also attributable to tidal flexure, the effect of storm surges (Reeh 1968) and the release of englacial meltwater (Brown et al 1982).

72

The poor understanding of the calving process forces the adoption of a purely empirical approach. The study of Brown et al (1982) uses 17 Alaskan tidewater glaciers to relate width-averaged calving velocity (V_c, km a^{-1}) to average water depth at the glacier terminus (in km). Brown et al defined calving velocity as the difference between forward ice flow and the rate of change of the glacier snout's position. The relationship produced was:

$$V_c = 27.1 \left(-B \right)$$

(2.12)

This equation is incorporated into the overall ice sheet model by converting calving velocity to an equivalent ice thickness reduction rate (C). The calving velocity given by equation (2.12) is equivalent to a rate of grid width reduction ($\triangle x$, km). This rate of width reduction is, in turn, converted to a rate of ice thickness reduction by using the rectangular geometry of grid width and ice thickness.

Calving flux also depends on the geometry of the ice margin, for example exposed ice peninsulas experience more calving than areas sheltered within an embayment. This feature is incorporated by an multiplication factor (m), which depends on the number of adjacent grid cells that are both marine and ice free. The final relationship is:

$$C = \frac{mZ}{\triangle x} \min \left(V_c, V_{c\,max} \right)$$

(2.13)

73

A maximum calving velocity (C_{max}) is imposed to avoid the excessive velocities that are predicted when ice extends to the edge of the continental shelf. Kollmeyer (1980) cites a maximum observed velocity of 7.5 km a^{-1} at Jakobshavn Isbrae, Greenland.

The calving ice flux is essentially different to the ice fluxes involved in net mass balance and marine basal melt because it represents a line loss rather than a loss of mass over an area. This means that the behaviour of marine ice sheets and non-marine ice sheets is likely to be widely contrasted.

(2.3.4) ISOSTASY.

Bedrock elevation is central to the dynamics of the ice sheet model. Changes in bedrock elevation are brought about by imposed eustatic sea level change and by internal isostasy. This latter mechanism is produced by the effect of changing ice and water loads on the underlying bedrock. The essential feature of isostatic depression is its delayed nature, and response times in excess of 5.0 ka are often needed for bedrock to reach an equilibrium depression (Walcott 1972).

Isostasy has three main effects on the overall ice sheet system. First, the depression of bedrock and ice surfaces counteracts the positive feedback between net

74

mass balance and ice thickness. Second, isostasy affects ice loss via marine melt and calving. Thus thicker ice sheets cause greater isostatic depression and so are more susceptible to marine ice loss. Third, isostasy influences the ice flow dynamics of the model by changing ice surface slopes (which affect deformation velocities) and by altering bedrock depth below sea level (which affects ice sheet grounding and sliding).

Budd and Smith (1981 and 1982) approximate isostatic depression (B^*, km) by relating it to current ice thickness and to former ice thickness 5.0 and 10.0 ka ago (Z_5 and Z_{10}):

$$B^* = \frac{1}{16}\left(Z_{10} + 2Z_5 + Z\right)$$

(2.14)

This relationship produces the desired time lag and the correct equilibrium depression of approximately one quarter of the ice thickness. However, the use of the equation (2.14) in this project lead to a predicted isostatic response that was too abrupt. An alternative method of incorporating isostasy is therefore required. The method chosen is based on the diffusion equation approach of Brotchie and Silvester (1969).

The growth of an ice sheet imposes an additional load on the local bedrock. This causes compensation deep within the underlying viscous asthenosphere, which

75

gradually flows away from the area of increased load. This process leads to an equilibrium depression equal to the overlying ice sheet's equivalent thickness in rock. This equilibrium depression (L) is given by:

$$L = Z \frac{\rho_i}{\rho_m} \qquad (2.15)$$

where ρ_m is mantle density (3300 kg m^{-3}).

An additional load is imposed by changing depths of ocean water. These changing water depths are principally caused by eustasy, however areas depressed by a subsequently decayed ice sheet also support an increased ocean water load. If grounded ice is not locally present then the equilibrium depression is:

$$L = (B - B_0) \frac{\rho_w}{\rho_m} \qquad (2.16)$$

where B_0 is the initial bedrock elevation and is B the current bedrock elevation (which is influenced by isostasy and eustasy).

Oerlemans and van der Veen (1984) give the rate of change of bedrock elevation as:

$$\frac{\partial B}{\partial t} = D_a \nabla^2 (B_0 - B + L) \qquad (2.17)$$

where D_a is a diffusion constant whose value controls the rate of isostatic response and the time needed to establish an equilibrium depression. The value of D_a depends on the thickness and viscosity of the

asthenosphere and lies in the range 35 to 50 km^2 a^{-1}
(Walcott 1972).

The other terms in equation (2.17) are: the
equilibrium depression L, given by equations (2.15) and
(2.16); the current bedrock elevation B, given relative
to initial sea level so that the apparent changes
produced by eustasy are ignored; and initial bedrock
elevation B_0. The difference between the initial and the
current bedrock elevation represents the equivalent
'load' produced by previous bedrock movements. This is
upward and buoyant if current bedrock is below the
initial bedrock surface, and is downward if current
bedrock is above the initial bedrock surface.

The isostasy model outlined above assumes that all of
the bedrock underlying an ice/water load is viscous.
However, the upper layers of the earth (the crust and the
lithosphere) are not warm enough for viscous flow and
behave as elastic solids. An imposed load is, therefore,
not solely supported by the bedrock directly beneath the
load (as assumed in the above model), because the
rigidity of the lithosphere allows the imposed load to be
partially supported by the surrounding lithosphere. This
means that deflection directly under the load is less
than assumed above. In addition, the areas adjacent to
the load are deflected upward in forebulges.

Oerlemans and van der Veen (1984) indicate that the reduction of the deflection directly under the load is minimal and the forebulges produced by the lithospheric rigidity mechanism are small in comparison to those produced by the dynamic extrusion of the asthenosphere (whose typical size is 80 m, Walcott 1970b). The latter type of forebulge are incorporated into the initial asthenospheric flow model. Lithospheric rigidity is omitted from the isostasy model because the majority of the important features of isostasy (the presence of forebulges, the delayed response and the size of equilibrium depression) are included in the simpler asthenospheric flow model.

(2.4) INTERNAL ICE SHEET FLOW DYNAMICS.

This section describes the incorporation of ice flow into the model. Ice can flow either by the internal deformation of ice within the body of an ice sheet or by the sliding of the ice sheet over its bed.

(2.4.1) ICE SHEET FLOW BY DEFORMATION.

The stresses set up within an ice sheet cause ice to deform. The flow of ice by deformation can be found by first estimating the stress distribution within the ice sheet, and then calculating the strain rate arising from these stresses. The following discussion defines stress as the force per unit area experienced in any direction

within the ice mass, while strain rate is the defined as the deformation per unit time expressed as a fraction of the original dimensions.

The physics used to achieve the twin aims of stress estimation and stress-strain coupling are readily available (eg Paterson 1981). This section discusses the assumptions used to simplify the complex physics of ice behaviour and gives the flow relationships used in the model.

The type of deformation that occurs in grounded ice masses is distinctly different from that which occurs in floating ice masses. The stress fields of grounded ice masses are dominated by shear stresses, while those of floating ice masses are dominated by normal stresses. These two types of stress differ in that normal stresses are perpendicular to surfaces, while shear stresses are tangential to surfaces (Turcotte and Schubert 1982). The coupling of these two distinct modes of deformation within a continuous medium is a major ice flow modelling problem (Muszinski and Birchfield 1987). This coupling is most important where the dominant mode of deformation changes at the complex transition between ice streams and ice shelves. The case studies presented here concentrate on the behaviour of grounded ice masses because the majority of the available field evidence

relates to the behaviour of former ice masses on dry land. The full complexity of the transition between grounded and floating ice is not, therefore, investigated.

The deformation of grounded ice.

The ice velocity produced by deformation depends on the stress distribution within an ice mass and on the relationship between stress and strain. The first step needed to determine a relationship between ice sheet form and deformational velocity is the estimation of the stress field. Mahaffy (1976, following Nye 1952) makes several simplifying assumptions about this stress environment:

(i) shear stress variation in the horizontal x-y plane is minimal;

(ii) a glaciostatic state of stress exists, thus all normal stresses are equal to the hydrostatic pressure; and

(iii) the variation of hydrostatic pressure with ice depth far exceeds the variation of vertical shear stress with horizontal distance.

The very slow flow in ice sheets means that acceleration can be ignored and the orthogonal stress components can therefore be equated as follows:

$$\frac{\partial \sigma_{xx}}{\partial x} + \frac{\partial \tau_{xy}}{\partial y} + \frac{\partial \tau_{xz}}{\partial z} = 0 \qquad (2.18)$$

$$\frac{\partial \sigma_{yy}}{\partial y} + \frac{\partial \tau_{yx}}{\partial x} + \frac{\partial \tau_{yz}}{\partial z} = 0$$

$$\frac{\partial \sigma_{zz}}{\partial z} + \frac{\partial \tau_{xz}}{\partial x} + \frac{\partial \tau_{zy}}{\partial y} = -\rho_i g$$

where σ are normal stresses, τ are shear stresses and g is the gravitational constant ($9.81\ m\ s^{-2}$). Figure 2.12 illustrates this stress system and indicates the relevance of the subscripts used in equation (2.18).

Assumptions (i), (ii) and (iii) simplify this system so that an analytical solution is possible. The mathematics involved is not given here because it is commonly available from other sources. The only

Which?

significant stresses are shear stress in the x-z plane and shear stress in the y-z plane. These stresses are given by:

$$\tau_{xz} = \rho_i g \alpha_x (E - z)$$

$$\tau_{yz} = \rho_i g \alpha_y (E - z)$$

(2.19)

where and are ice surface slopes in the x and y directions. These slopes are found as the first derivative of surface elevation in the appropriate direction. The surface elevation used in these calculations is the sum of ice thickness and mean bedrock altitude.

Shear stress at the base of the ice sheet (τ_b) is:

$$\tau_b = \rho_i g Z \alpha$$

(2.20)

where α is the overall ice surface slope:

$$\alpha^2 = \alpha_x^2 + \alpha_y^2 \qquad (2.21)$$

The three assumptions used to derive equations (2.19) and (2.20) from equation (2.18) identify insignificant stresses. Assumption (i) states that shear in the horizontal plane is insignificant. This assumption does not hold where shearing occurs in response to a horizontal velocity gradient, which happens where ice masses of different velocities impinge on one another and where ice flows past a stationary bedrock wall. These situations only occur near ice sheet margins, near the flanks of ice streams and where outlet glaciers and their valley walls have similar depths.

Assumptions (ii) and (iii) state that shear stress variation is greater than normal stress variation, and that the normal stresses in the x, y and z directions are identical. Normal stresses are important only where shear stresses are low, examples include ice divides (where surface slopes are low) and areas near the ice margin (where ice thicknesses are small).

These two assumptions are tested by Budd (1970a and 1970b) in a theoretical work on ice flow over bedrock undulations. He relates the importance of longitudinal stresses (stresses in the x and y directions) to

horizontal scale. A more complicated expression is obtained for basal shear stress (compared to equation 2.20):

$$\tau_b = \rho_i g Z \alpha + 2G - T \qquad (2.22)$$

The second term is determined from the horizontal variation of longitudinal stress, and the third term is related to variation in shear stress. The importance of these additional terms depends on scale. At horizontal distances less than four times ice thickness G becomes important, while at horizontal distances equivalent to ice thickness both additional terms need to be considered. Morland and Johnson (1980) and Hutter (1981) proved these relationships using a more complete analysis.

The horizontal grid scales used in the case studies are 5 km (in the Loch Lomond case studies) and 25 km (in the Antarctic Peninsula case study). They fall above the range requiring the determination of G. The original formulation for basal shear stress is therefore used (equation 2.20).

The second stage in the estimation of deformation velocity from ice sheet form is the definition of a relationship between stress and strain rate, which is done using a flow law. The Glen (1955) and Nye (1957)

flow law is the most commonly used:

$$\dot{\epsilon}_{xz} = A\tau^{n-1}\tau_{xz}$$

$$(2.23)$$

$$\dot{\epsilon}_{yz} = A\tau^{n-1}\tau_{yz}$$

where A and n are flow constants, $\dot{\epsilon}$ is the shear strain rate (in the subscripted plane), and τ is the effective shear stress. The effective shear stress is a measure of the overall stress environment. In the situation outlined above, the effective shear stress depends on the shear stresses τ_{xz} and τ_{yz} alone.

Shear strain rate is also related to ice velocity:

$$\dot{\epsilon}_{xz} = \frac{1}{2}\left(\frac{\partial U_y}{\partial z} + \frac{\partial U_z}{\partial y}\right)$$

$$(2.24)$$

$$\dot{\epsilon}_{yz} = \frac{1}{2}\left(\frac{\partial U_x}{\partial z} + \frac{\partial U_z}{\partial x}\right)$$

where U is ice velocity in the subscripted direction.

Horizontal ice velocities can now be calculated using equations (2.19) to (2.24). A certain amount of manipulation allows these equations to be combined, which produces a single relationship for the vertically-averaged horizontal velocity ($\overline{U}_x$ and $\overline{U}_y$) as a function of ice thickness and surface slope:

$$\overline{U}_x = \frac{2A(\rho_i g)^n}{n+2}|\alpha|^{n-1}\alpha_x Z^{n+1}$$

$$(2.25)$$

$$\overline{U}_y = \frac{2A(\rho_i g)^n}{n+2}|\alpha|^{n-1}\alpha_y Z^{n+1}$$

These estimates of the vertically-averaged horizontal

velocity are added to estimated sliding velocity (Section 2.4.2) and the sums are then used in the ice continuity equation (equation 2.1).

The flow law used in equation (2.23) is empirical. The exact values of the two flow law constants (A and n) are determined by ice temperature, impurity content, crystal size and crystal orientation. The power law constant (n) is shown by Weertman (1973) to vary between 1.5 and 4.2. The constant's mean value (3.0) is used in the present study.

The flow law multiplication factor (A, known as the Arrhenius constant) is extremely variable and has a range of at least two orders of magnitude. Ice temperature is the major influence on the value of the Arrhenius constant, which increases from $1.8 \times 10^{-16} \text{ s}^{-1} \text{ kPa}^{-3}$ at $-20 \,^{o}C$ to 5.3×10^{-15} at $0 \,^{o}C$ (for n equal to 3, Paterson 1981). In this study constant values of 5.3×10^{-15} and $2.6 \times 10^{-15} \text{ s}^{-1} \text{ kPa}^{-3}$ are used. This implies that the modelled ice sheets are isothermal and that the areas of greatest strain (the basal layers) are at pressure melting point. The assumption that the modelled ice sheets are isothermal means that the complex procedure needed to explicitly model the temperature distribution within an ice sheet is avoided.

One of the primary aims of this study is to use a two-dimensional, dynamic model. At present the only work to combine ice flow and temperature calculations in this type of model is Jenssen (1977). Problems involving numerical stability mean that this model can only be run using very coarse grids and it is therefore unsuitable for use in the present study.

Other attempts to model ice flow and temperature simultaneously are limited either to two-dimensional, steady state reconstructions to one-dimensional, time dependent models. Budd et al (1971) and Sugden (1977) are examples of the former approach, while Oerlemans (1982) is example of the latter approach. These pre-existing models imply that the present study can use one of two approaches. These are either to adopt an isothermal model which is both spatial and time dependent, or to use an ice flow/temperature model which is either steady state or flowline. The isothermal model is adopted because adequate testing relies on the spatial and time dependent nature of a model rather than on the inclusion of temperature calculations.

The deformation of floating ice.

A different procedure is needed to estimate deformation flow when the grounding criteria (equation 2.10) indicates that floating, rather than grounded, ice

86

is present. The deformation of grounded ice is controlled by shear stresses. Floating ice does not shear to the same extent because the base of the ice sheet is no longer in contact with a stationary bedrock boundary. Normal stresses and strains are therefore dominant.

The analysis of Weertman (1957) indicates that the normal strain rate of an unconfined ice shelf depends on ice thickness and ice flow properties. An analogously simple approach is used in the West Antarctic ice stream models of McInnes and Budd (1984), who approximate ice shelf deformation using a constant strain rate. This study uses the same approach and assumes a constant strain rate of 0.005 a^{-1}. The velocity of floating ice is estimated as:

$$\overline{U}_X = \overline{U}_{X0} + \triangle X \cdot \epsilon_S \qquad (2.26)$$

where $\overline{U}_{x0}$ is the velocity of ice flowing into the particular grid cell. A similar expression is used for flow in the y-direction. These estimates of the vertically-averaged horizontal velocity are used in the ice continuity equation (equation 2.1).

The above scheme simplifies the flow of ice shelves and its effect on the behaviour of ice streams. Marine ice streams are intimately linked to ice shelves. Ice flowing along an ice stream becomes progressively less well grounded, until it reaches the grounding line and

becomes part of an ice shelf. This progression is accompanied by accelerated sliding velocities (McIntyre 1985). Hughes (1987) and Young (1981) believe that the longitudinal stresses produced by this acceleration actually pull grounded ice (from the surrounding ice sheet) into the ice stream. The present model does not determine longitudinal stresses and so cannot incorporate this effect.

The omission of longitudinal stresses from the ice flow model also means that the buttressing effect of ice shelves upon ice streams is not incorporated. This effect relies on the back-pressure that is developed when the flow of an ice shelf is retarded by marine bedrock rises and fjord side walls (Fastook 1985). This back-pressure is transmitted through the ice shelf to the adjoining ice stream. It thus counters down-slope shear stresses within adjoining ice streams and reduces ice stream velocities.

The simple stress model used here cannot reproduce this buttressing effect. When back-pressures are constant, this defect can be overcome by the correct parameterization of sliding. However, good parameterization is not sufficient when back-pressures vary. The degree of ice shelf grounding determines both the amount of back-pressure imposed on adjoining ice streams and flow dynamics of these ice streams. Variation

in the degree of ice shelf grounding becomes important
when eustatic sea level varies. Thus a rise in sea level
reduces the amount of ice shelf/bedrock contact, and
results in the acceleration of ice stream flow (Thomas
1985).

Both the buttressing effect of ice shelves and the
pulling effect of ice streams operate at relatively local
scales. The marine ice sheet studied in this project (the
Antarctic Peninsula case study) is likely to exhibit
changes over large distances. The incorporation of the
effects of ice streams and ice shelves discussed above
may not therefore be critical.

(2.4.2) ICE SHEET FLOW BY SLIDING.

Ice flows either by deformation within the body of the
ice mass or by the sliding of the ice mass over its bed.
Several different media interact at the ice sheet bed to
produce sliding, these media include ice, water, bedrock
and unconsolidated sediment. The physics of sliding is
therefore more complex than that of internal deformation.
Many different sliding mechanisms have been proposed. For
instance Weertman (1957) and Morland and Smith (1984)
suggest a mechanism of regelation and enhanced plastic
flow, and Weertman (1964) and Lliboutry (1968) indicate
the importance of both water at the bed and normal load
on the bed. More recently Boulton and Jones (1979) have

*emphasized the contribution of deformation in basal
sediments.*

*This broad range of possible mechanisms and the
likelihood that the dominant mechanism varies between
locations necessitates the use of an empirical approach.
This study does not attempt to understand the process of
basal sliding, but incorporates sliding as one component
of an ice sheet model and attempts to assess its
importance in determining overall ice sheet behaviour.*

*Budd et al (1979) produced a general sliding law using
basal shear stress and normal load as independent
variables. This laboratory work was extended by the West
Antarctic ice stream modelling work of Budd et al (1984
and 1985). These latter studies produced a predictive
equation for sliding. The work assumes that the present
day West Antarctic ice thickness distribution is in
steady state. The distributions of both deformation
velocity and balance velocity can be estimated from this
distribution. Sliding velocities can then be found as the
difference between these two calculated velocities.*

*These estimated sliding velocities are then related to
the independent variables of basal shear stress and
normal load. The justification behind the choice of these
two independent variables is that the former represents*

the driving stress behind sliding, and the latter opposes sliding via friction. Normal load is predominantly determined by the thickness of ice unsupported by buoyancy. Effective ice thickness (Z^*) is therefore a good surrogate for normal load:

$$Z^* = Z - \frac{\rho_w}{\rho_i}(-B)$$ (2.27)

The calculation of basal shear stress has already been outlined (equation 2.20). The final equation for sliding velocity (U_S) is:

$$U_S = K_2 \frac{\tau_b}{Z^{*2}}$$ (2.28)

where K_2 is a constant equal to 5 x 10^6 m^3 bar^{-1} a^{-1}. This represents the best-fit form obtained by Budd et al (1984). Total velocity is found as the sum of its deformation (equation 2.25) and sliding (equation 2.28) components and then used in the continuity equation for ice (equation 2.1).

This sliding formulation is valid only for marine ice streams, where accelerated flow is controlled by changes in ice buoyancy. The sliding velocities of land-based ice sheets may vary in response to two related mechanisms. Both of these mechanisms rely on the meltwater released when ice sheet basal temperatures reach pressure melting point. The first effect of this released meltwater is to enhance basal sliding by lubricating the interface

between the ice sheet and its bed. Oerlemans (1982) investigated this process using a one-dimensional model, and found that it was significantly in determining overall ice sheet behaviour at continental scales. A second effect of meltwater release was investigated by Boulton and Jones (1979). Who suggested that an ice sheet underlain by unconsolidated sediment would experience an apparent sliding motion as the sediment deformed in response to shear stress.

The current model assumes that ice sheets are isothermal and does not explicitly calculate ice temperatures. The modelling of the above mechanisms requires the determination of the basal temperature regime in order to predict basal melting. The model used in this project cannot, therefore, reproduce this type of behaviour. However, Budd et al (1985) showed that the use of a coupled ice flow/temperature model lead to little improvement in the prediction of marine ice stream sliding, when compared to an isothermal model (Budd et al 1984). The omission of the effects of meltwater release from the present model may not therefore be critical.

(2.5) SUMMARY AND NUMERICAL DETAILS OF THE MODEL.

The model described in the preceding sections forms the basis of the case studies discussed in the second part of this thesis. The equations given in the preceding

text are summarized in Appendix III, while the variables used in the model, with their symbols, are listed in Appendix IV. Some of the equations used in the model involve partial differentials, referring to rates of change with respect to time or to horizontal distance. In particular the continuity equation for ice thickness (equation 2.1) involves the horizontal derivatives of ice flux and the rate of change of ice thickness with time. Also the calculation of both sliding and deformation velocities (equations 2.25 and 2.28) use ice surface slope, which is the first horizontal derivative of surface elevation. Finally the model determines isostasy using a diffusion equation (2.17) which involves the rate of change of bedrock elevation with time and the second horizontal derivatives of isostatic load.

The model runs on a rectangular grid consisting of a regular array of square elements. At each node in this array the equations of the model are used to calculate ice thickness and velocity. In order to do this the derivatives mentioned above are approximated using the the value of the appropriate variable at the particular node and at the adjacent nodes.

A centred difference scheme is used to approximate the horizontal derivatives. The arrow in the following equations means 'is approximated by'. Node coordinates

are subscripted using i,j notation, where i refers to the x direction and j to the y direction.

The first horizontal derivative:

$$\frac{\partial F}{\partial x} \implies \frac{F_{i+1} - F_{i-1}}{\triangle X} \qquad (2.29)$$

where F represents ice surface elevations.

The second horizontal derivative:

$$\frac{\partial^2 F}{\partial x^2} \implies \frac{F_{i+1} - F_i + F_{i-2}}{(\triangle X)^2} \qquad (2.30)$$

where F represents isostatic loads (equations 2.15 and 2.16).

The above equations approximate derivatives in the x direction, analogous equations are used for the y direction.

Derivatives in time are approximated by forward differences:

$$\frac{\partial F}{\partial t} = G \implies F_{t+1} = F_t + \triangle t.G \qquad (2.31)$$

where T is the time step used, F represents ice thickness or bedrock elevation, and G represents horizontal variation in ice flux or in isostatic load (equations 2.1 and 2.17 respectively).

The finite difference scheme approximates the continuous variation of differential equations using

differences between adjacent points. There are two
problems with this approximation. First, finite
differences become inaccurate if they are used to model
rapid continuous fluctuations. The horizontal grid size
used in the model determines the maximum possible time
step which can be used before the approximation becomes
unstable. If this maximum is exceeded then linear
instability occurs and the model suffers an
unrealistically explosive expansion of ice thickness.
Budd and Jenssen (1975) relate maximum stable time step
($\triangle t_{max}$) to grid size:

$$\triangle t_{max} = \frac{(\triangle X)^2 |\alpha'|}{2U'Z'n} \qquad (2.32)$$

where α', U' and Z' are estimates of maximum ice surface
slope, deformation velocity and thickness.

The second problem involved in the use of finite
differences is non-linear instability and manifests
itself as a series of high frequency waves within the ice
thickness distribution. This feature is removed
artificially by the application of a smoothing function
on the ice thickness distribution. The smoothing function
has the form:

$$Z_{i,j}^+ = \frac{1}{16}\left(Z_{i+2,j} + Z_{i-2,j} + 10Z_{i,j} - 4\left(Z_{i+1,j} + Z_{i-1,j}\right)\right)$$

$$(2.33)$$

$$Z_{i,j} = \frac{1}{16}\left(Z_{i,j+2}^+ + Z_{i,j-2}^+ + 10Z_{i,j}^+ - 4\left(Z_{i,j+1}^+ + Z_{i,j-1}^+\right)\right)$$

This scheme is applied on 1 to 5 % of the model's iterations through time. A major disadvantage with the use of this scheme is that it produces an artificial ice thickness loss at the margins of the modelled ice sheet because points on the ice sheet margin (where ice thickness is greater than zero) are smoothed using the adjacent ice-free points (where ice thickness is zero). This problem is overcome by estimating the total volume of ice lost during each smoothing and redistributing equal portions of this volume to all of the points along the ice sheet's margin.

The incorporation of smoothing and finite difference schemes completes the construction of the model.
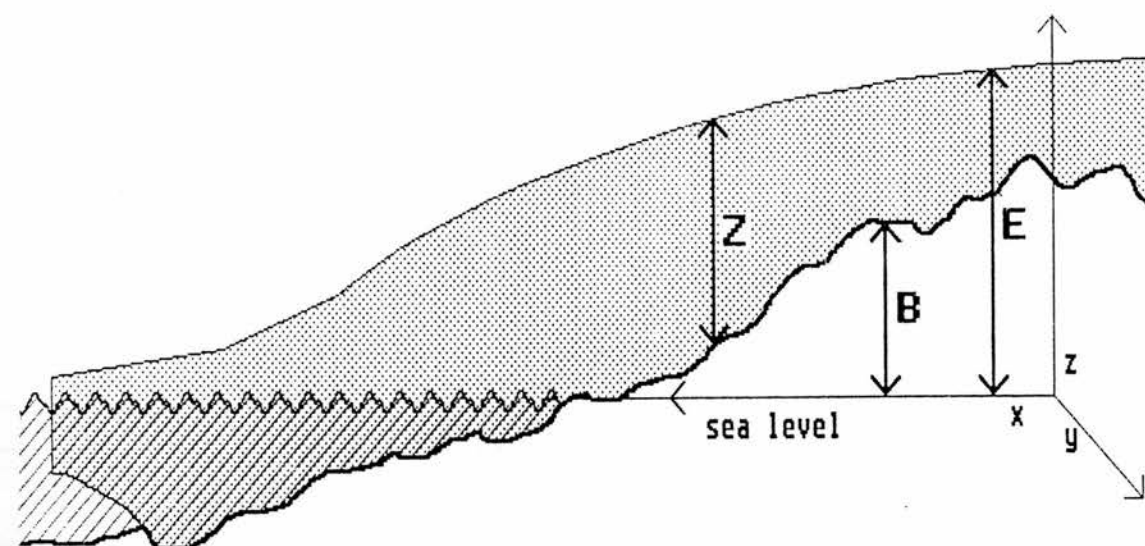
Figure 2.1 The coordinate system used in the model.
Z is ice thickness, B bedrock elevation
and E ice surface elevation.
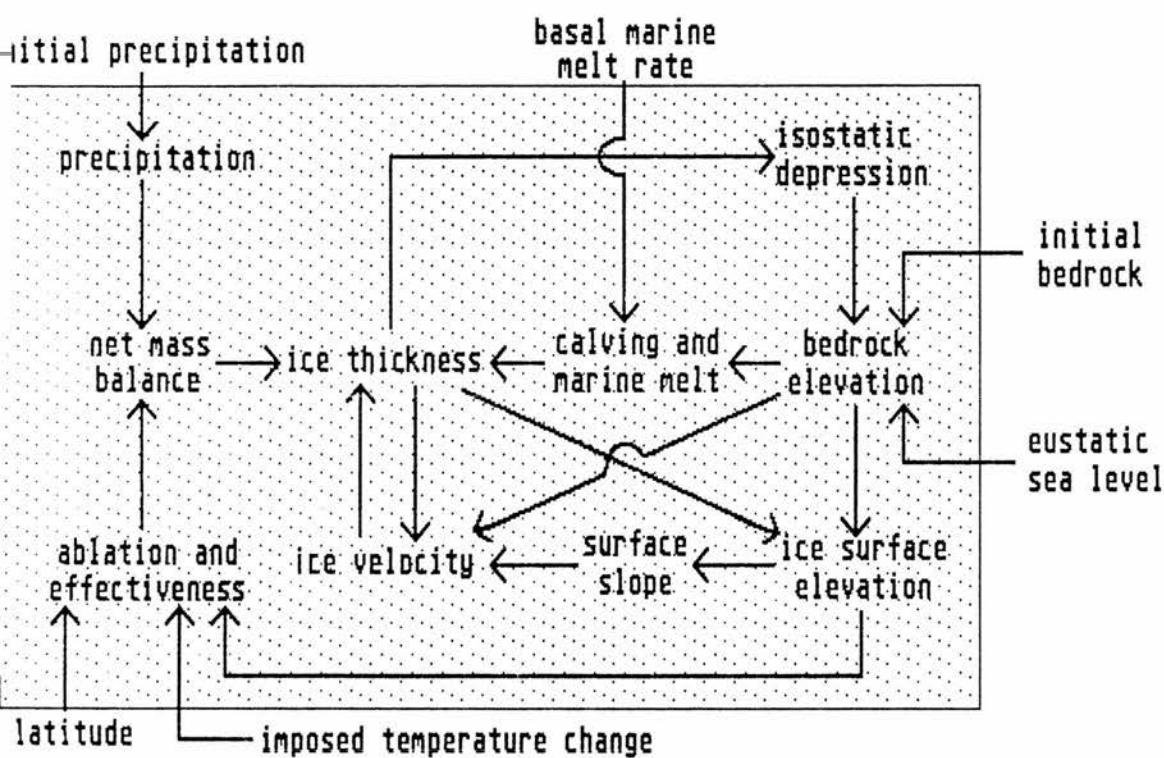
Figure 2.2 A diagrammatic representation of an ice sheet system.

2.3 Summer temperatures during the last 120.0 ka: a comparison of a palaeoecological estimate (Coope 1975) and the output of a continental ice sheet model (Budd and Smith 1981).
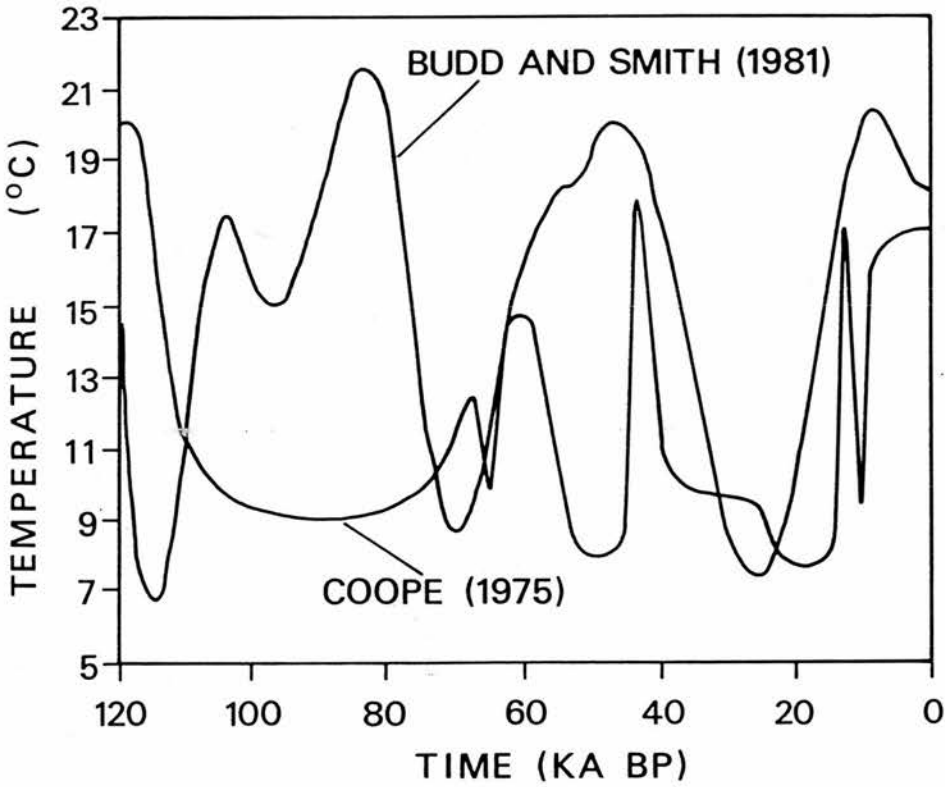
FIGURE 2.4 THE JULY AIR TEMEPERATURE FORCING FUNCTION USED IN THE MODEL,
WHICH WAS DERIVED FROM COOPE (1975).
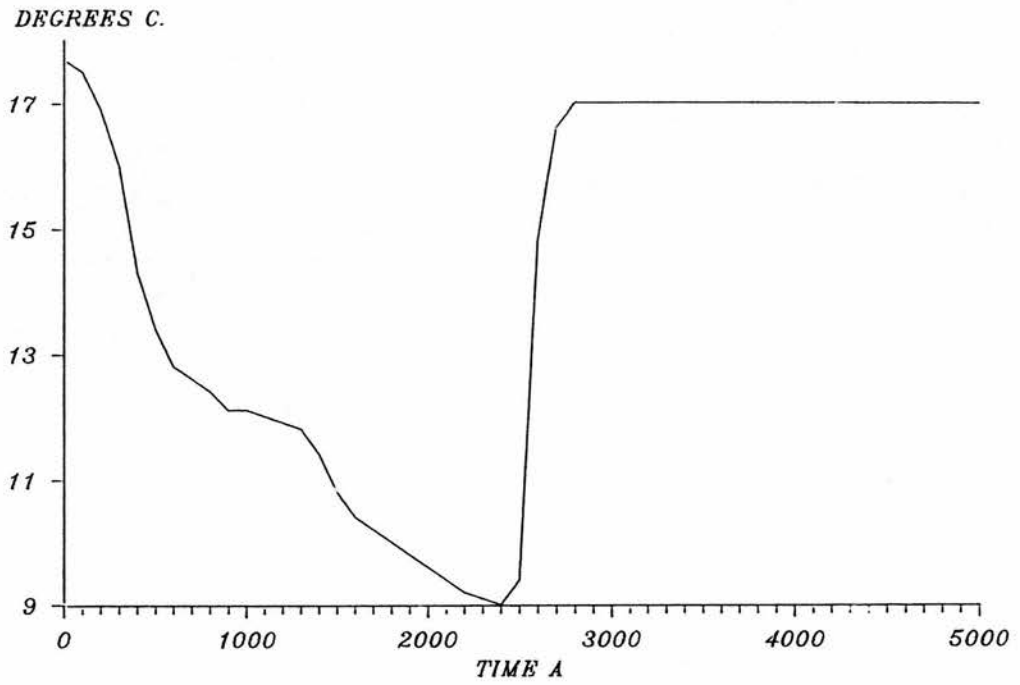
2.5 The annual air temperature curve for lowland Britain at the present day (A) and during a glacial (B), indicating the increased continentality associated with glacials. After Williams (1975).

mean July
temperature

J

↓

July cooling

$\Delta J = J - J_0$

present July temperature: $J_0 = 17.0$ °C
lapse rate: lapse = 6.5 °C/km
conversion from July to
annual cooling[+]: $f = 2.571$

imposed July
isotherm shift

$\Delta E_j = \Delta J / \text{lapse}$

annual cooling

$\Delta A = f * \Delta J$

↓

imposed annual
isotherm shift

$\Delta E_a = \Delta A / \text{lapse}$

↓

Ablation
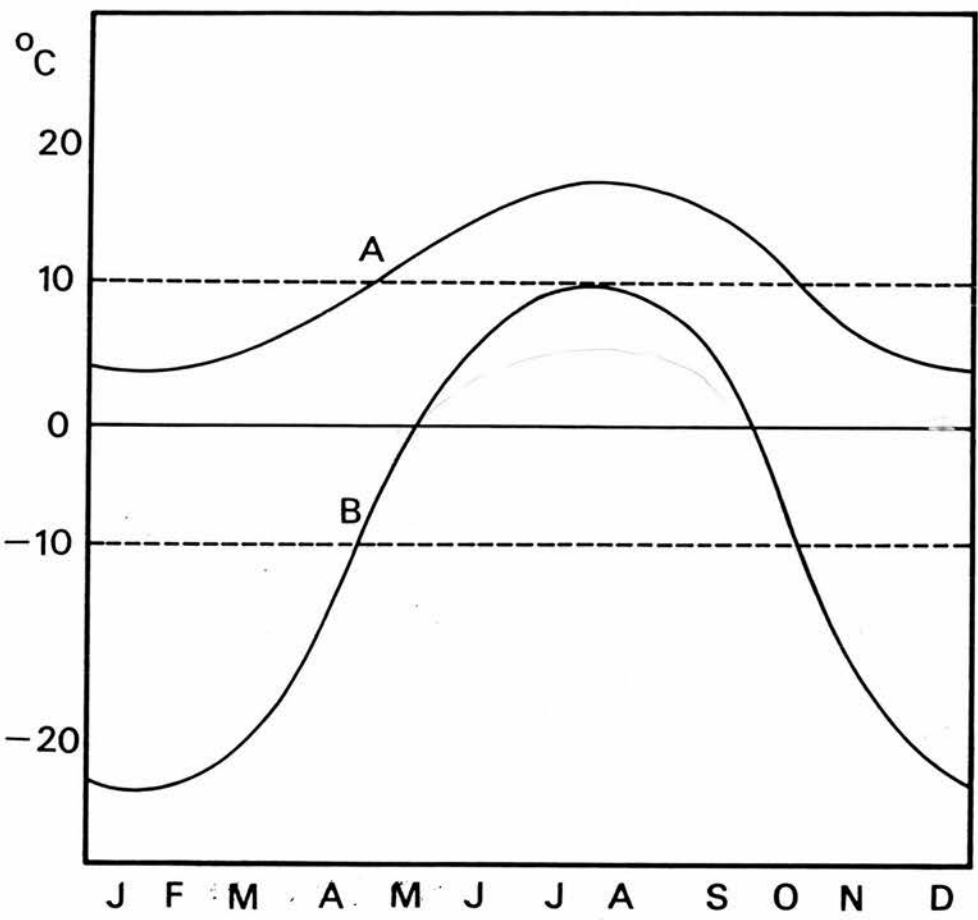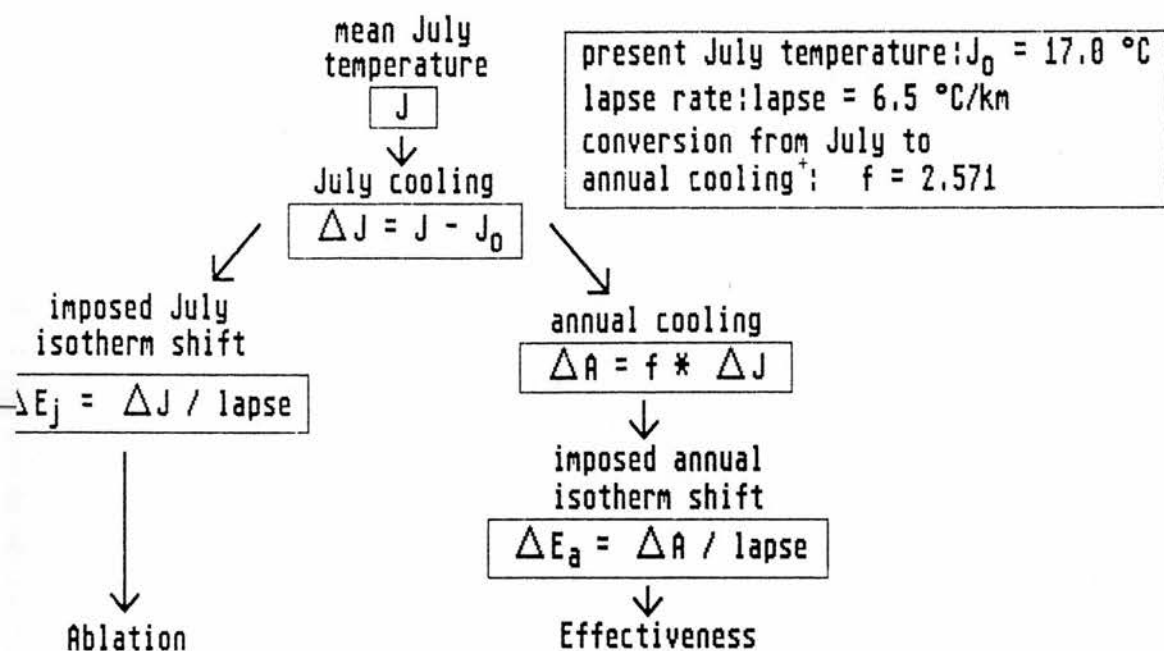
Effectiveness

Figure 2.6 The procedure used to relate the July temperature data
of Figure 2.4 to ablation and effectiveness.

+ for derivation of f see Appendix I.

FIGURE 2.7 THE EUSTATIC SEA LEVEL FORCING FUNCTION USED IN THE MODEL,
WHICH WAS DERIVED FROM SHACKLETON (1987).
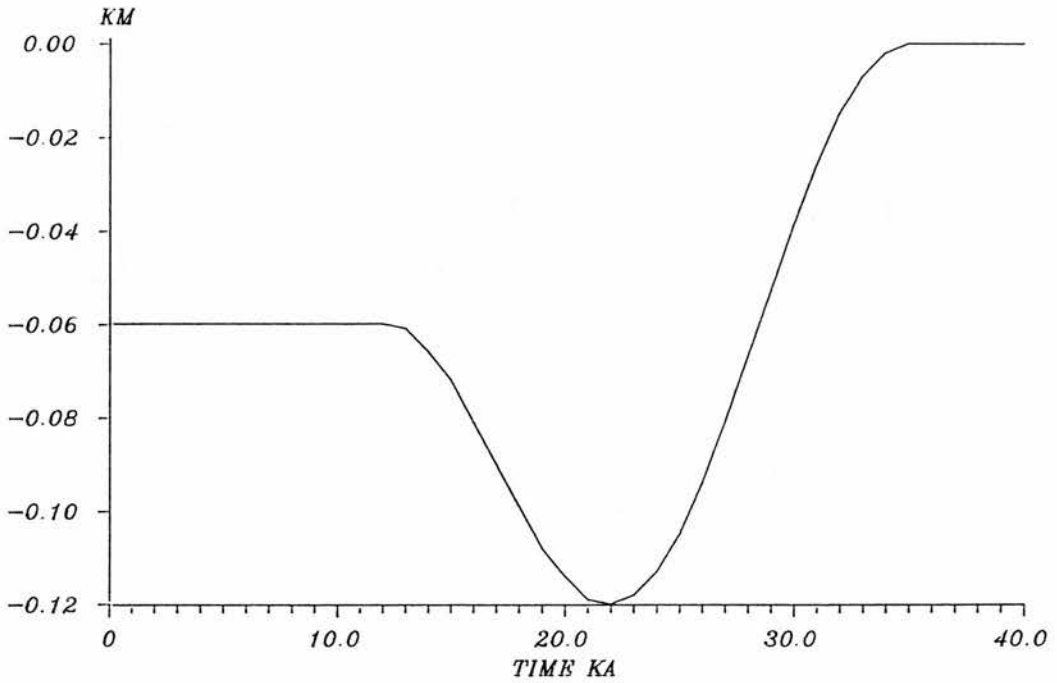
FIGURE 2.8 THE MARINE BASAL MELT FORCING FUNCTION USED IN THE MODEL,
WHICH REPRESENTS THE IMPOSED RATE OF MELTING BENEATH ICE
SHELVES AND IS USED FOR AREAS TO THE WEST OF THE PENINSULA.
MELT RATES TO THE EAST OF THE PENINSULA ARE MAINTAINED AT
0.5 M/A THROUGHOUT THE MODEL RUNS.

102
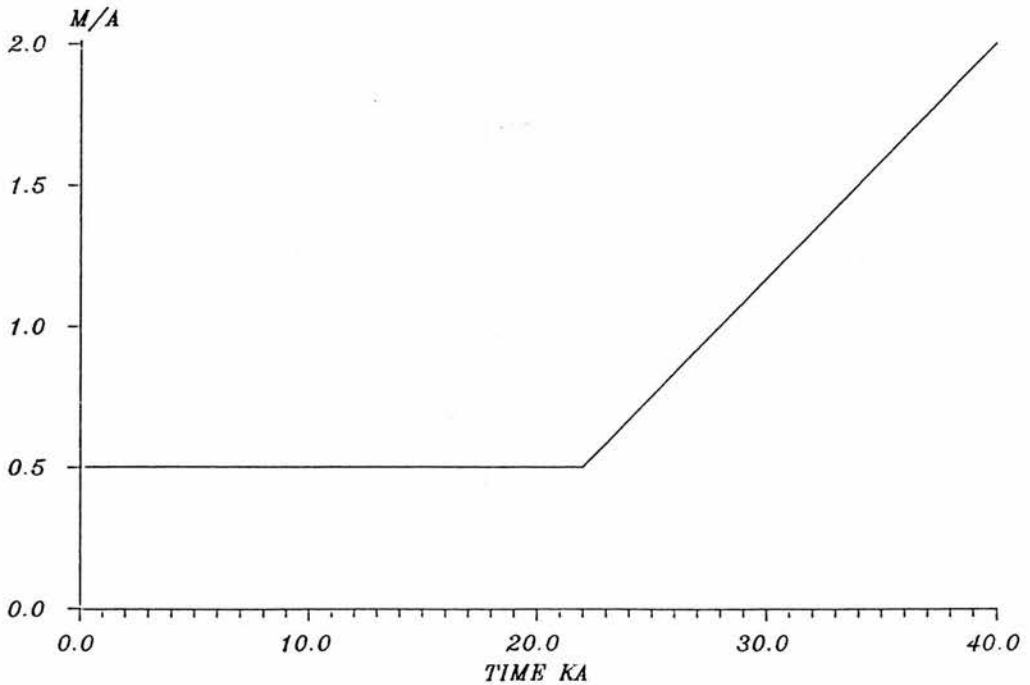
FIGURE 2.9 LINES OF EQUAL ABLATION PLOTTED AS A FUNCTION OF SURFACE
ELEVATION AND IMPOSED JULY TEMPERATURE DEPRESSION. ABLATION
IS SHOWN FROM 0.5 TO 6.0 M/A IN STEPS OF 0.5.
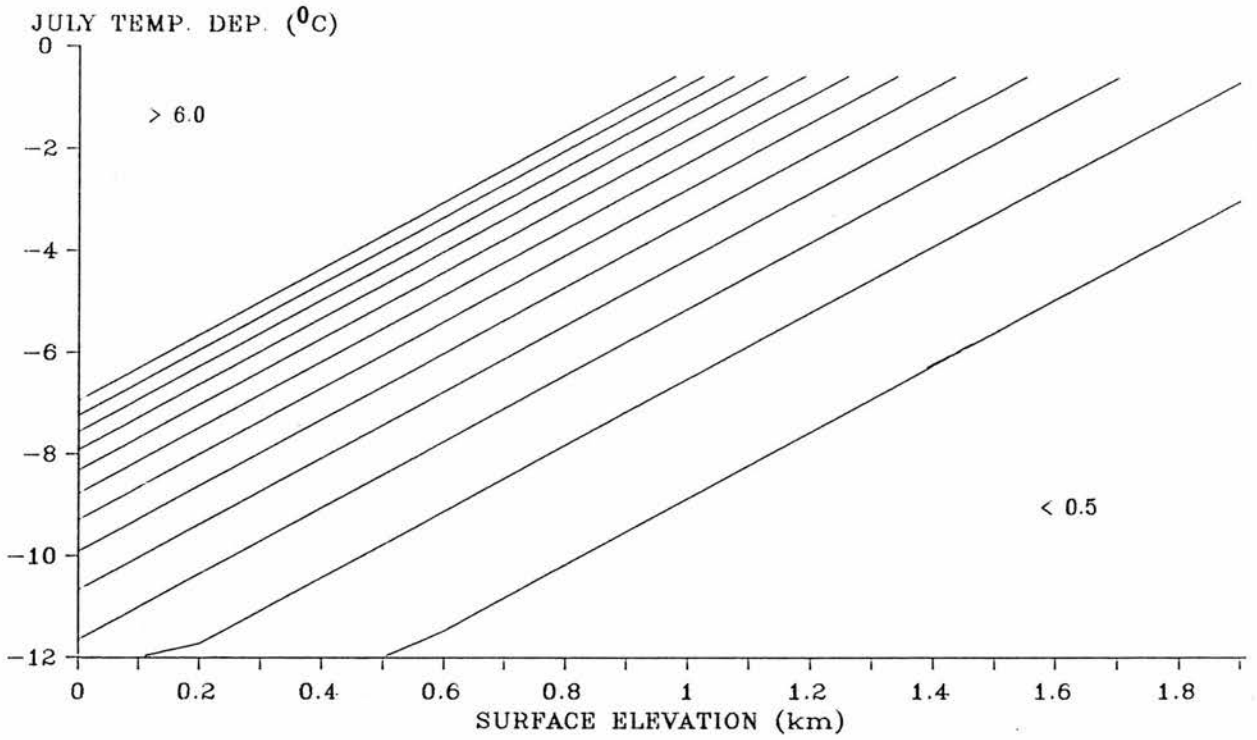
FIGURE 2.10 LINES OF EQUAL EFFECTIVENESS AS A FUNCTION OF SURFACE
ELEVATION AND IMPOSED JULY TEMPERATURE DEPRESSION.
EFFECTIVENESS IS SHOWN FROM 0.2 TO 1.0 IN STEPS OF 0.1.

peak type
topography

plateau type
topography
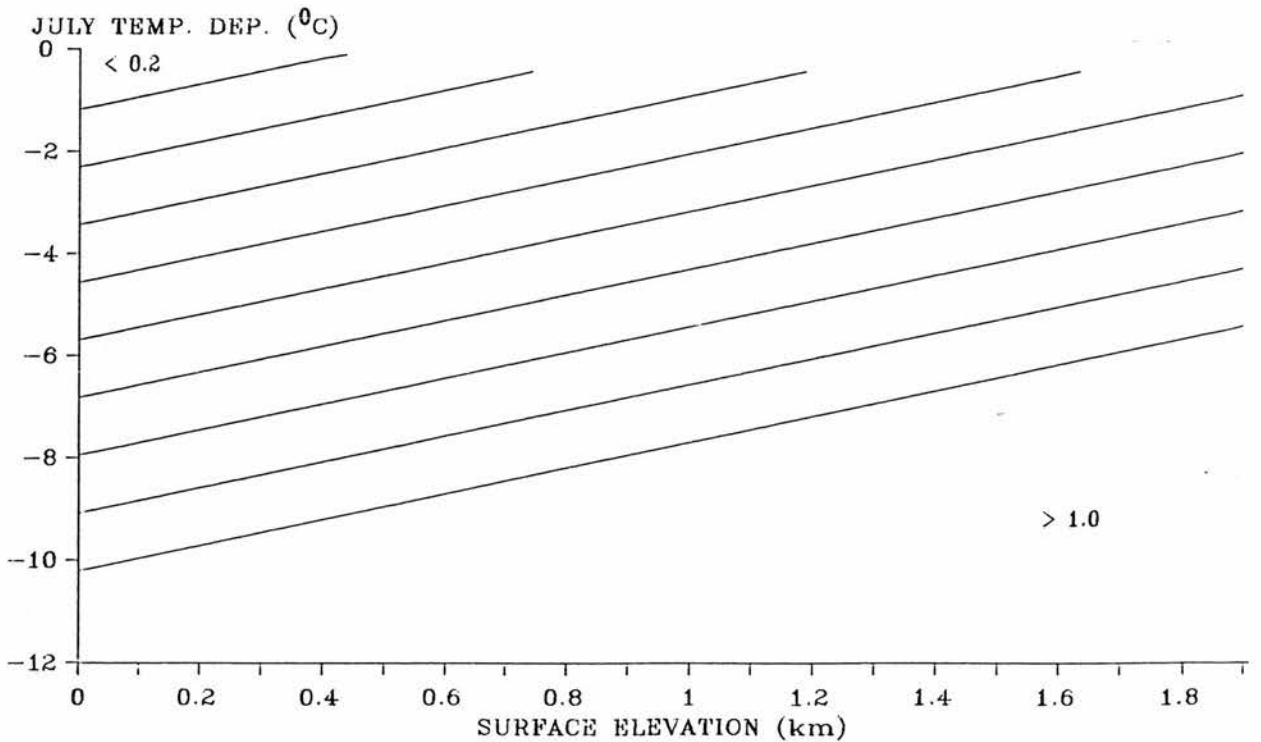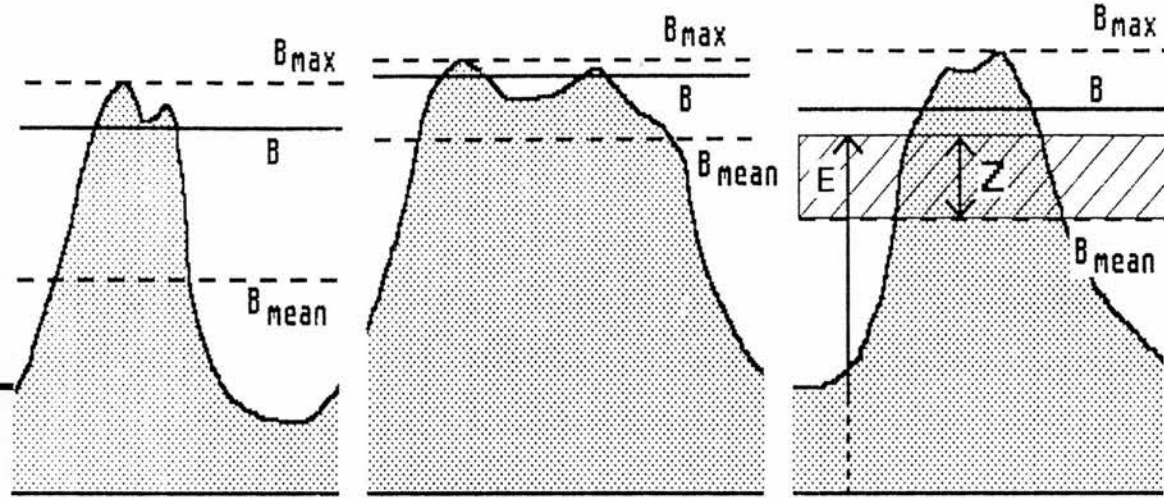
Figure 2.11 The determination of bedrock and ice sheet surface altitudes
using the mean and maximum topographic representations.

Symbols: Z ice thickness, E ice surface altitude, B bedrock altitude,
B_{max} maximum and B_{mean} mean bedrock representations.
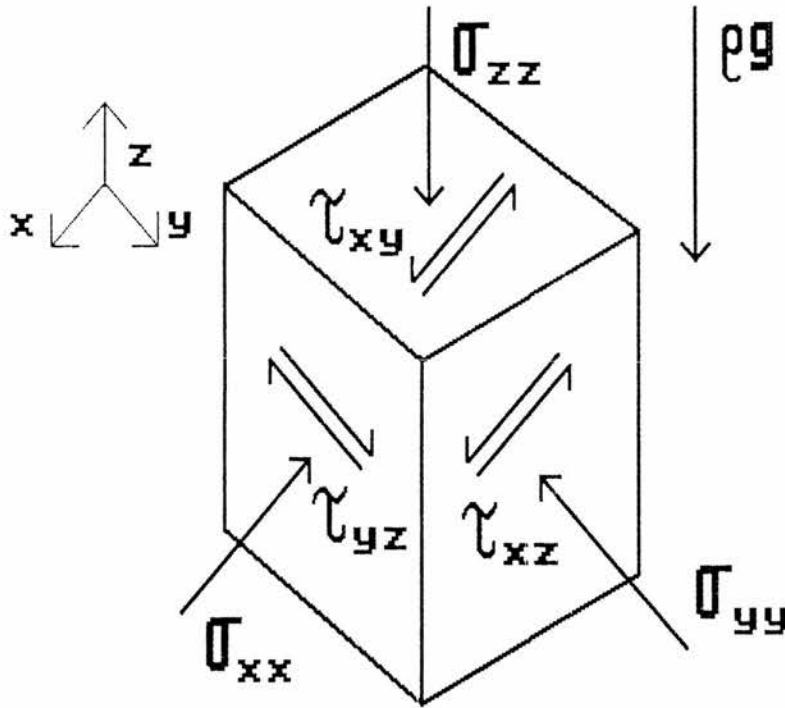
**Figure 2.12 The orthogonal stress system used
in equation (2.18).**

PART TWO : THE CASE STUDIES.

CHAPTER THREE : THE ANTARCTIC PENINSULA ICE SHEET DURING THE LAST 40,000 YEARS.

(3.1) THE AIMS OF THE CASE STUDY.

The late Quaternary Antarctic Peninsula ice sheet forms an interesting case study for two main reasons. First, the ice sheet was predominantly controlled by changes in the surrounding oceans rather than by atmospheric changes. This is because ablation, the major cause of variation in the atmosphere/ice sheet water budget, is minimal in the area at present (Reynolds 1981). It is also likely to have been minimal throughout the last 40.0 ka because air temperatures were always cooler than those of the present day.

A second major reason for studying the ice sheet's late Quaternary growth and decay is that the topography, size and climate of the area is similar to that of the U.K. during a glacial period. In both areas there is a close association between mountain massifs and relatively deep oceanic trenches. For instance, in the Antarctic Peninsula, the 400 m deep trough of George VI Sound lies only 300 km away from the 2000 m peaks of Palmer Land; while, in the U.K., an altitude difference of 1500 m exists over the 200 km between the South-West Grampians and the North Channel of the Irish Sea. In addition, both areas have a similar latitudinal extent (around 1300 km) and have westerly, maritime climates with high annual

106

precipitation totals of 1000 mm (Antarctic Peninsula) and
2400 mm (U.K). This latter similarity is in sharp
contrast to much of continental Antarctica, where annual
precipitation totals are less than 100 mm (Budd et al
1971). Climate, topography and size all significantly
affect ice sheet dynamics; the Antarctic Peninsula is
therefore a good analogue of the marine sections of the
former late Devensian U.K. ice sheet.

Given these reasons for studying the late Quaternary
behaviour of the Antarctic Peninsula ice sheet, the aims
of this case study are:

(i)   to test a numerical model of a marine based ice
*   sheet by comparing field evidence from the area*
*   with predictions from the model;*

(ii) to produce a general model of the dynamics
*   associated with ice sheet decay in the area, which*
*   can then be used to identify useful areas for the*
*   further testing of the model; and*

(iii) to identify the relative importance of the
*   processes affecting the growth and decay of a*
*   marine ice sheet, including factors such as*
*   eustasy, isostasy, initial topography, ice flow,*
*   basal marine melt and calving.*

(3.2) MODEL MODIFICATION AND INPUT DATA.

Net mass balance in the model.

The model described in Chapter 2 was used with the
following amendments to the net mass balance section.
Ablation is thought to have had minimal influence on the
behaviour of the Antarctic Peninsula ice sheet. Present
day net mass balance measurements indicate that ice loss

107

via ablation is minimal (Reynolds 1981). However the area's climate is warmer than at any other time in the last 40.0 ka, it is therefore likely that ablation was insignificant throughout the whole of this period. Since ablation is the major cause of variation in the atmosphere/ice sheet water budget, it can be assumed that the effects of climatic change on the ice sheet were minimal and that present day accumulation rate is the only net mass balance component that needs to be estimated.

Present day measurements of annual accumulation rate (the product of effectiveness and annual precipitation rate) are scarce, however Potter et al (1984) summarize measurements from 26 sites on Palmer Land, Alexander Island and the George VI ice shelf. The present model calculates net mass balance using a linear regression equation based on these measurements:

$$b = 1.24 + 0.21E - 0.12\theta + 0.10\phi \qquad (3.1)$$

where b is net mass balance in m a^{-1} and is constrained to lie between 0.0 and 1.2 (the observed maximum), E is surface elevation in km, ϕ is latitude in $^{\circ}$S and θ is longitude in $^{\circ}$W.

This equation is used throughout the whole of a model run. An individual point's net mass balance increases

with increasing surface elevation, increasing distance North and increasing distance West. The relationship to surface elevation allows a positive feedback loop to develop between ice thickness, surface elevation and net mass balance. The relationships between net mass balance, latitude and longitude reflect the maritime nature of the area's climate. In particular, the longitudinal net mass balance gradient emphasizes the role of the Antarctic Peninsula as a climatic divide with maritime, moist conditions to the West and continental, dry conditions to the East (Schwerdtfeger 1970). The use of this equation to directly predict accumulation rates frees the model of the need for a separate precipitation distribution input.

A secondary modification of the net mass balance section of the model is the omission of the envelope topographic representation. The principal use of the envelope scheme is in the Loch Lomond stadial case studies, where it simulates the effects of nunataks on net mass balance during the initial phases of ice sheet growth. The present case study uses a present day ice thickness distribution as an initial condition. This distribution covers the vast majority of the bedrock above sea level and leaves little need for the simulation of nunataks.

Topography in the model.

The area covered by the model forms a square on the polar stereographic projection and has a latitudinal extent of 66 to 78 ^{O}S, and a longitudinal extent of 50 to 80 ^{O}W. The projection used gives a true representation of shape, however it exaggerates distance. This exaggeration is not particularly significant and amounts to a 2.5 % distortion of the area's North-South extent and a 5.6 % distortion of the area's East-West extent (distortions derived using the equations of Kellaway 1949). The area to be modelled is divided into 50 by 50, 25 x 25 km grid elements.

In this case study it is assumed that both bedrock and ice cover at 40.0 ka BP (the start of the model run) were similar to their present day distributions. Alternatively it could be assumed that the difference in model behaviour arising from the use of present day initial conditions is minimal. These assumptions are discussed further in the results section of the case study.

The mean bedrock elevation and ice thickness in each of the 2500 grid elements was derived from the Scott Polar Research Institute Antarctic Glaciological and Geophysical Folio, Sheets 2 to 4 (the surface of the Antarctic ice sheet, the bedrock surface of Antarctica and Antarctic ice sheet thickness and volume). The

British Antarctic Survey ice thickness maps of Alexander Island (Series BAS 500R 1/1) and Palmer Land (unpublished sketch), and the Canadian Hydrographic Service GEBCO charts were also used. A contoured representation of mean bedrock elevation is shown in Figure 3.1. This bedrock distribution is used with the distribution of present day ice cover (Figure 3.2) as initial conditions in the model.

The initial bedrock is altered during a model run by isostasy, which is modelled using a diffusion equation based on both the bedrock-equivalent loads of water and ice, and the bedrock's deflection away from an initially relaxed bedrock distribution (Section 2.3.4). This initially relaxed bedrock distribution represents a third boundary condition that must be specified. The present day topography does not represent a relaxed distribution because the existing ice cover exerts a load on the bedrock and deflects it. In addition uplift may presently be occurring in response to the removal of the load imposed by the expanded late Quaternary ice sheet. This latter component is likely to be minimal because the Peninsula has had a reduced ice cover for at least 6.5 ka (Clapperton and Sugden 1983), which is an ample time period for the majority of uplift to have occurred (Oerlemans and van der Veen 1984). An estimate of the relaxed topography can be obtained by assuming an

111

equilibrium depression under the present day ice load. This depression can then be used to determine the initially relaxed topography from the present day topography:

$$B_0 = Z \frac{\rho_i}{\rho_m} + B \qquad (3.2)$$

The Antarctic Peninsula place names used in Chapter 3 are shown in Figure 3.3. Initial topography, initial ice thickness, relaxed topography and the area's latitude/longitude all represent boundary conditions used in the model. In addition, time series of eustatic sea level and marine basal melt conditions are needed to drive the model. The derivations of the eustatic sea level and the marine basal melt time series are discussed in Sections (2.2.2) and (2.2.3) respectively. These forcing functions are shown in Figures 3.4 and 3.5.

The introduction of isostasy, eustasy, calving and ice shelf formation considerably increases the complexity of the overall ice sheet model compared to the model used in the land-based Loch Lomond stadial case studies. The model's response to the twin driving variables of eustatic sea level change and marine basal melt is consequently more complex. An increased number of possible feedback loops exist within the model structure. The Loch Lomond model incorporates net mass balance/ice thickness/surface elevation and ice thickness/ice flow

feedback loops. While the Antarctic Peninsula model includes additional loops, such as the negative ice thickness/isostatic depression/bedrock elevation/surface elevation loop and the positive sliding velocity/ice thickness/ice depth above buoyancy loop.

(3.3) RESULTS : THE STANDARD MODEL AND ITS TESTING.

Unless otherwise stated the results discussed in this section were obtained using the parameter values given in Table 3.1. The standard model run is for the period 40.0 ka BP to the present. The discussion uses a chronology of elapsed time relative to the model starting time (40.0 ka BP), so that an elapsed time of 30.0 ka is equivalent to 10.0 ka BP. The model produces output distributions of ice thickness, bedrock topography (relative to current model sea level, thus omitting the altitudinal differences arising from eustasy) and the magnitude of ice velocities. In addition, the output includes time series of total ice volume, volume added to the ice sheet via surface accumulation (net mass balance), volume lost from the ice sheet via calving and basal melt, and mean bedrock elevation.

This section discusses the standard model run and is divided into four sub-sections. First, the gross response of the ice sheet model to changes in sea level and marine basal melt is described in terms of total ice volumes

and fluxes. Second, the detailed spatial dynamics of ice
sheet growth and decay are discussed with reference to
the spatial distributions of ice thickness, velocity and
isostasy. Third, specific model predictions are compared
with the available field evidence from the area and an
attempt is made to test the model. Fourth, the
predictions of the model are used to identify useful
areas for future fieldwork.

(3.3.1) THE GROSS DYNAMICS OF THE STANDARD MODEL.

The time series of total ice sheet volume produced by
the standard model run is shown in Figure 3.6. At the
start of the model run ice volumes increase rapidly until
a steady state volume of 800×10^3 km^3 is reached at 8.0
ka. Subsequently ice volumes remain stable until 17.0 ka
into the model run, when volumes rise more slowly to a
second steady state value of 929×10^3 km^3. Ice volumes
start to fall at 25.0 ka, and a rapid retreat is
initiated at 29.0 ka. A final steady state volume of 235
$\times 10^3$ km^3 is reached at 36.0 ka. The ice sheet can
therefore maintain three steady state volumes, depending
on the particular values of the model's driving
variables.

The presence of these steady state ice volumes
supports the assumption stated in Section (3.2) that the
initial ice sheet and bedrock conditions do not

significantly affect the behaviour of the ice sheet during the model run. Further runs using a variety of initial ice and bedrock conditions showed similar behaviour, with an initial phase of rapid growth leading to a steady state ice volume in excess of 800×10^3 km^3.

The early ice volume expansion occurs while sea level is 60 m below present day levels and basal melt rate is 0.5 m a^{-1}. Eustatic sea level begins to fall at 14.0 ka, however the ice sheet does not respond to this change in forcing until sea level is 90 m below its present day level. The rate of sea level fall is at a maximum during this period, and the ice sheet is therefore being affected by large changes in forcing. Rapid sea level fall reduces calving rates because of the dependence of calving on water depth at the ice sheet perimeter. The volume variation produced by this sea level fall is relatively minor and amounts to only 14 % of the maximum volume.

Both sea level and basal melt rate begin to rise at 23.0 ka. However ice sheet volume does not respond until 25.0 ka, when there is a minor phase of volume loss which slows as volume returns to its initial steady state value. At 29.0 ka increasing basal melt rates and sea levels trigger an instability and ice volumes start to decrease at a rapid, continuous rate. This retreat

reduces ice sheet volume to 25 % of the maximum volume and ceases at 36.0 ka, at which time a small, steady state ice sheet is maintained despite further increases in basal melt rate.

The response of the ice sheet has two characteristic features. First, transitions between steady state ice sheet volumes are rapid and occupy relatively brief periods in comparison with the time spent in steady state. Three steady state forms are present, which include two large marine based forms and a small predominantly land based form. Second, the ice sheet response to changes in forcing is not direct but occurs in short, distinct phases. Changes in forcing appear to produce a potential instability in the ice sheet that is only triggered when further changes exceed a threshold value.

The isostatic response produced by these ice sheet volume changes is shown in Figure 3.7. This time series represents the mean bedrock elevation as a fraction of the mean elevation of the relaxed bedrock and omits the elevation changes produced by eustatic sea level change. The curve is a dampened, inverse form of the ice volume curve.

116

The fluxes of ice entering (net mass balance) and leaving (calving and marine basal melt) the ice sheet are shown in Figures 3.8 and 3.9 respectively. The input flux remains fairly constant throughout the majority of the run. It increases by only 17 % during the first 23.0 ka of the model run and reaches a maximum rate 19.5 of km^3 a^{-1}. It then falls rapidly during the phase of ice sheet retreat to reach 53 % of the maximum value by the end of the run.

The initial and final ice sheet volumes are similar (Figure 3.6), however the final input flux is only 63 % of the initial value. This is because initial and final ice sheets have a dissimilar areal extent. The initial input distribution (Figure 3.2) covers a wide area but is relatively thin and has many extensive ice shelves. In contrast the modelled ice sheet at 40.0 ka BP (Figure 3.10) covers a reduced area but is thicker, especially in the George VI Sound area. The initial ice sheet therefore has a larger input flux because it has a larger area over which ice can accumulate. The following section on model testing contains a more detailed comparison of these two distributions.

The output flux from the ice sheet (Figure 3.9) varies irregularly through time, and has fluctuations with wavelengths of 1.0 ka around a stable trend. These

117

fluctuations are caused by the sensitivity of calving rate to water depth and the irregularity of the bedrock topography used in the model. Thus the ice sheet perimeter suffers minor phases of expansion and retreat which result in fluctuations in overall ice loss rate. The particularly large peaks during the first 2.0 ka of the model run are produced by the calving of the initially extensive ice shelves mentioned above. The majority of the Filchner ice shelf is lost early on because it is not supplied by ice discharge from West Antarctica (to the South-West of the study area). This is a limitation of the model, which arises because the model is limited to the Antarctic Peninsula and does not include the rest of West Antarctica. An extended model would not suffer from these difficulties.

The growth and decay of overall ice sheet volume is related to output flux variation rather than to input flux variation. Thus the ice sheet initially grows while output flux is low and reaches a steady state when input and output fluxes are equal. The slight expansion at 17.0 ka is related to a subtle drop in output flux while input flux remains constant. A new steady state is reached as output flux rises. The final decay of the ice sheet at 29.0 ka is led by an output increase, with peaks reaching 159 % of the previous steady state values. It is only after the areal extent of the ice sheet has been

*significantly reduced, 4.0 ka after the start of rapid
retreat, that the input flux begins to fall.*

*The very irregular rate of output during deglaciation
is a result of the sensitivity of the ice sheet's marine
margin, in particular both calving and grounding are
extremely sensitive to water depths. Initially the ice
sheet perimeter is able to maintain a constant position
on bedrock rises. However, with increasing melt rates and
rising sea levels, this perimeter eventually becomes
unstable and a phase of rapid retreat (increased output
flux) is initiated. This retreat continues until the
perimeter stabilizes on another bedrock rise, which leads
to a temporary fall in output flux.*

(3.3.2) THE SPATIAL DYNAMICS OF THE STANDARD MODEL.

*The sequences of ice surface elevations and ice
velocities produced during ice sheet growth and decay are
very similar. The decay data is discussed here because it
can be compared to geomorphological estimates from the
area, which record only the most recent phases of ice
sheet behaviour.   Figures 3.11 to 3.18 show the paired
distributions of ice surface elevation and ice velocity
for 26.0 ka (14.0 ka BP), 30.0 ka (10.0 ka BP), 33.0 ka
(7.0 ka BP) and 36.0 ka (4.0 ka BP). These times reflect
four important phases; the ice sheet maximum, the end of
the phase of gradual ice sheet retreat, the mid-point of*

the phase of rapid decay and the establishment of a new steady state ice sheet.

In the following discussion variations in the positions of ice streams are traced using the distribution of velocity magnitudes and estimates of ice flow direction based on the ice sheet surface form. It is assumed that ice flow is down slope and perpendicular to the ice surface contours.

At 26.0 ka the ice sheet surface form (Figure 3.11) is relatively simple, with a single ice dome lying over the East Bellinghausen Sea. Concavities in the surface form of the ice sheet reveal the locations of three major ice streams; at the North of George VI Sound, to the West of Alexander Island and towards the edge of the continental shelf in the Bellinghausen Sea. The ice velocity distribution (Figure 3.12) confirms the presence of these ice streams and indicates the presence of several minor ice streams to the East of Palmer Land.

At 26.0 ka the position of the ice streams is determined by the presence of bedrock trenches near the ice sheet perimeter. Over the next 4.0 ka ice sheet volume decreases at a relatively slow rate. The ice sheet surface form at 30.0 ka (Figure 3.13) shows a general lowering by several hundred meters. This is partly a

consequence of continued isostatic depression under the ice dome. Ice velocities (Figure 3.14) show an intensification of ice stream flow. This is a result both of eustatic sea level rise and of continued isostatic depression. Both factors increase the bedrock's depth below sea level and increase sliding velocities. This faster flow contributes to the reduction in surface elevation because it reduces ice thickness in the ice sheet interior.

These increased ice stream velocities do not lead to an increase in the areal extent of the ice sheet because increased basal melt rates impede any advance. Increased marine ice losses also produce a minor retreat to the West of Alexander Island. Ice volume loss between 26.0 and 30.0 ka is therefore partly a consequence of ice sheet thinning and partly a consequence of the shrinkage of the ice sheet's areal extent.

At 33.0 ka the ice sheet is mid-way through its phase of rapid retreat (Figures 3.15 and 3.16). Between 30.0 and 33.0 ka, 45 % of ice sheet volume is lost but ice sheet area is only reduced by 22 %. These percentages indicate that volume is lost not only by ice sheet retreat but also by progressive ice sheet thinning (Figures 3.13 and 3.15). The time series of marine loss (Figure 3.9) indicates that this volume reduction occurs

as several overlapping peaks, and in particular the remnants of the Filchner ice shelf are lost. The western flank of the ice sheet also retreats but with considerable spatial variation. The area of greatest retreat is along the Bellinghausen Sea trough, where there is a channel of deep water along which the ice sheet retreats continuously in the absence of bedrock rises. The ice sheet to the West of Alexander Island retreats at a far slower pace. This is because of both the shallow water depths in this area and the isostatic uplift of a bedrock rise (the Beethoven Peninsula), on which the ice sheet perimeter stabilizes. Ice sheet extent to the East of Palmer Land is far more stable and the convergence of ice flow from North Alexander Island and Palmer Land is sufficient to maintain a constant the ice front position at the North of George VI Sound.

The period of progressive ice sheet retreat between 30.0 and 33.0 ka alters both the magnitude and the direction of ice flow within the ice sheet (Figures 3.14 and 3.16). The main Bellinghausen Sea ice stream maintains its strength and retreats along its bedrock trench, but the intensity of the flow of the other ice streams is reduced. This reduction is mainly a result of the isostatic rebound initiated by the decay of the maximum ice sheet, which leads to reduced water depths and reduced sliding velocities. The continuous band of

high ice velocity to the West of Alexander Island at 30.0 ka becomes fragmented by 33.0 ka because of the isostatic emergence of both the Beethoven Peninsula and North Alexander Island.

At 26.0 ka ice flow predominantly radiates from the major Bellinghausen Sea ice dome with slight convergence into the three major ice streams described above. However at 33.0 ka the ice flow pattern is far more complex. The retreat of the Bellinghausen Sea ice stream and its increasing proximity to Palmer Land leads to the bifurcation of the single Bellinghausen Sea ice dome into two smaller domes centred over dry land. The presence of the ice stream also leads to accelerated flow which reduces ice dome thicknesses. The eastwards migration of the ice stream produces a shift in the direction of ice flow over South Alexander Island. At 30.0 ka, ice flow is towards the West, while at 33.0 ka convergence into the adjacent ice stream produces a more southerly flow. This is contrasted by the situation at the North of Alexander Island where ice flow is always towards the North.

A final, stable ice sheet form is reached at 36.0 ka. Between 33.0 and 36.0 ka there is a sharp peak in marine losses (Figure 3.9), after which both marine loss and surface accumulation rates reach reduced steady state values. The ice thickness distribution at 36.0 ka (Figure

3.17) indicates that this peak in marine losses represents the final decay of the Bellinghausen Sea ice dome. This final retreat is extremely rapid (lasting approximately 500 a) and leaves a predominantly land based ice sheet. This rapid retreat is explained by the lack of potentially stabilizing bedrock rises in the trench area. The rest of the ice sheet perimeter remains stable during this period.

Ice stream activity declines with this final retreat (Figure 3.18) because of continued isostatic uplift and the near-shore position of the majority of the ice sheet margin. Minor ice streams are still maintained along the East coast of Palmer Land and at either end of the George VI Sound. This final slowing of ice stream activity is accompanied by a dramatic switch in the direction of ice flow over Alexander Island. A separate ice dome has now formed over the Island, leading to radial flow from the centre of the Island. This replaces the dominant westward flow of Palmer Land ice over the Island. In the South of the Island this westward flow is replaced by southward or even south-eastward flow. However, in the North of the Island, flow is similar to that previously existing and shows a strong convergence into North George VI Sound.

(3.3.3) TESTING THE MODEL.

Geomorphological evidence in the area can be used to

test four specific predictions of the model. The first is related to the way in which the direction of ice flow changes spatially and through time. The second concerns the timing of the area's deglaciation, the third relates to the spatial nature of isostatic uplift during this deglaciation and the fourth compares actual and predicted present day ice sheet morphologies. The predictions of the model for former ice thicknesses, extent and flow magnitudes are untestable because no equivalent field data exist.

Testing the model's predictions of changing ice flow directions.

Geomorphological evidence can be used to test the model's predictions of changing ice flow directions around Alexander Island and the George VI Sound. The predictions of the model can be summarized as follows:

(i)   to the North ice flow always converges strongly into George VI Sound and flows northwards;

(ii) to the West ice flows initially in an ice stream directed towards the North-West, but, as the ice sheet margin retreats, flow both slows and becomes westward; and

(iii) to the South ice flow is initially from the mainland and is directed towards the West. As the Bellinghausen Sea ice dome decays flow gradually veers towards the South-West, the South and finally, in places, to the South-East.

The geomorphology of nunataks in the area has been used to estimate former flow directions (Clapperton and Sugden 1982). In particular indicators such as

125

striations, roche moutonne orientations and glacial erratics were used. Figure 3.19 shows the flow line reconstruction of Sugden and Clapperton (1982) for the Wisconsin maximum ice sheet (18.0 ka BP).

The strong northward flow of prediction (i) is evident, in addition the westward and north-westward flow of prediction (ii) is present. However the flow in the South is north-westward and westward, and is contrary to prediction (iii). This latter mismatch may reflect shortcomings in the field interpretation because the reconstruction of Figure 3.19 was principally based on evidence from areas adjacent to George VI Sound. Both the predictions of the model and the field interpretations of maximum ice sheet flow are, however, in general agreement.

The model can also furnish predictions about the persistence of ice sheet flow. The geomorphology of North Alexander Island and the areas immediately adjacent to George VI Sound is expected to yield a more readily decipherable signal of ice flow direction than the geomorphology of South and West Alexander Island. This is because flow in the North was persistently towards the North and occurred at high speeds, whereas flow in the South and West varied greatly both in direction and magnitude. Sugden (pers. com.) indicates that this

contrast did, in fact, exist in the field. The geomorphology of locations such as Ablation Point and Two Step Cliffs (Figure 3.3) gave an unequivocal picture of northward ice flow, whereas the geomorphology of the more southerly areas was confused and contained many cross-cutting flow indicators.

Testing the model's predictions of deglaciation chronology.

A second model prediction that can be tested is the timing of deglaciation. Sugden and Clapperton (1980) postulate a disappearance of George VI Sound ice at 6.5 ka BP (33.5 ka in the chronology used here). The model ice sheet suffers a period of rapid retreat during the period 33.0 to 33.5 ka (Figures 3.15 and 3.17), however at no time does George VI Sound become ice free. One possible explanation of this mismatch is the under-prediction of isostasy by the model. The clearing and subsequent refilling of George VI Sound may have been a consequence of greater isostatic depression than predicted by the model. This increased isostatic depression may have destabilized the ice sheet sufficiently to allow total decay. Subsequent isostatic rebound may then have initiated regrowth.

Testing the model's predictions of isostatic uplift.

The geomorphology of Alexander Island's nunataks offers a third means of testing the model, which uses

evidence of relative sea level change in the area. Clapperton and Sugden (1982) mention the presence of a series of Palmer Land erratics along the East coast of Alexander Island. These erratics are believed to have been transported across George VI Sound either by the ice shelf or (more likely) by ice rafting during the ice free period of 6.5 ka BP. Their positions are therefore likely to be controlled by former sea levels. The distribution of these erratics varies from around 80 m above current sea level (at Ablation Point, Figure 3.3) to 120 m above sea level (at Two Step Cliffs, Figure 3.3). This implies that the area has suffered differential isostatic uplift and that the South of George VI Sound has risen considerably more than the North.

The modelled effects of isostasy can be used to predict the pattern of uplift in the area. The field estimates of relative sea level mentioned above are undated and cannot be used to estimate rates of uplift. However they can be used to estimate the uplift trend, which is now used as a further test of the model.

The pattern of maximum ice sheet thickness (at 25.0 ka) is shown in Figure 3.20. The greatest depths of ice are over the Bellinghausen Sea and over the positions of the present day Larsen and Filchner ice shelves. The pattern of isostatic uplift consequent on the removal of

this ice sheet is shown in Figure 3.21. This pattern was
obtained by subtracting the glacial maximum topography
(at 25.0 ka) from the final (40.0 ka) bedrock topography.
Areas with positive values are predicted as having
rebounded during the last 15.0 ka, and larger amounts of
rebound are represented by increasingly more positive
values. The comparison of this distribution with that of
present day topography (Figure 3.1) indicates a strong
North-South gradient of uplift along George VI Sound.
This result agrees with the field estimates discussed
above, which imply the existence of a large ice dome to
the South of George VI Sound and support this element of
the model's predictions.

Testing the model's predictions of present day ice sheet morphology.

A final test of model performance is the comparison of
the actual present day ice surface form with the final
surface form predicted by the model at 40.0 ka. These two
ice sheet forms are shown in Figures 3.2 and 3.10
respectively. The present day is the only time at which
comparison of modelled and actual ice sheet morphologies
is possible because geomorphic estimates of former
thicknesses and extent are unavailable.

The agreement between predicted and actual ice sheet
forms is generally good, however there are two
discrepancies. The first of these is related to the ice

129

shelves of the area, in particular to the Filchner, Larsen and George VI ice shelves. Reasons for the modelled collapse of the Filchner ice shelf have already been discussed. These reasons are concerned with the westerly boundary of the model across Ellsworth Land and the modelled ice discharge from West Antarctica, which is insufficient to maintain the Filchner ice shelf.

The predicted southerly extent of the George VI ice shelf is under-estimated, perhaps indicating that the imposed basal melt rate of 2 m a^{-1} is too great in this southerly area. The predicted extent of the Larsen ice shelf is in agreement with the actual extent, but ice thicknesses in this area are over-estimated especially over Graham Land. The surface accumulation function used in the model may be the cause of this over-estimation because it is based on data from the George VI Sound area and incorporates a northward increase. The northward extrapolation of this equation may lead to excessive estimates of surface accumulation.

A second discrepancy between predicted and actual ice sheet form is the over-estimation of ice thicknesses in the George VI Sound area. The model predicts a 1.5 km thick grounded ice mass in the area, whereas the actual ice cover is a 0.2 km thick floating ice shelf. This over-prediction is related to the decay of the

Bellinghausen Sea ice dome discussed above. Sugden and Clapperton (1980) suggest that the collapse of the ice dome at 6.5 ka BP lead to the clearance of George VI Sound. The present George VI ice shelf then reformed during the continued isostatic uplift of the area. The modelled collapse of the ice dome stops short of the deglaciation of George VI Sound and leaves a large grounded ice mass. The reason for the over-prediction of ice in this area is therefore under-estimated ice sheet decay. Possible reasons for this under-estimate include the under-prediction of the area's isostatic depression (as discussed earlier) and the grid size of the model. The grid size of the present model is 25 km, this means that George VI Sound is represented by a single column of grid cells. This resolution may not be sufficient to capture the dynamics of the ice shelf/ice sheet transition and may thus lead to the prediction of an overly stable ice sheet.

(3.3.4) THE FUTURE TESTING OF THE MODEL.

The four tests discussed above partially support the predictions of the model. However two major discrepancies exist. These are concerned with the nature of ice sheet decay in George VI Sound and the effect of the disintegration of the Bellinghausen Sea ice dome on flow directions over Alexander Island. Field evidence related to both of these aspects of ice sheet decay is sparse and

the aim of this sub-section is therefore to indicate, using the predictions of the model, areas which are likely to provide this key evidence.

The results of the model and the quoted field work both indicate that the late Quaternary saw the decay of a large marine ice sheet in the Antarctic Peninsula. The area offers a key site for the investigation of the causes and effects of such a decay. Information concerning the changing extent and flow dynamics of the ice sheet can be obtained from the analysis of the area's offshore sediments and landforms.

An equally useful and far more economic approach is to gather information from the area's nunataks. One problem associated with this type of field work is the selection of the nunataks which contain useful data from the vast number of existing nunataks. The use of predictions from a numerical model can aid in this selection procedure.

Information on three elements of overall ice sheet dynamics can be obtained from nunataks, these are: isostasy and relative sea level changes; ice flow magnitudes and directions; and ice thickness and extent. This type of information can also be gathered as a time series.

Isostasy and relative sea level changes.

The distribution of the area's nunataks is shown in Figure 3.22. The following discussion identifies the positions of nunatak groups that are potentially useful in solving specific ice sheet decay problems. The nunataks labelled A in Figure 3.22 can be used to assess isostatic uplift in the area. In addition to their coastal position these nunataks should ideally be low lying. The identification and possible dating of shore line features on these nunataks can be used to determine rates and patterns of uplift. Which, in turn, give an estimate of the position and size of former ice domes in the area and can test the specific hypothesis of a former Bellinghausen Sea ice dome.

Ice flow magnitudes and directions.

The nunatak groups labelled B, C, D and E in Figure 3.22 can be used to investigate changing ice sheet flow directions. A more complete history of the time dependent behaviour of the ice sheet can be obtained if the nunataks selected for study have a large height of rock above the present day ice surface. In this way more than one sequence of ice flow is likely to be recorded. Geomorphology near the summit of these nunataks reflects ice flow during the maximum. While geomorphology near the present ice surface reflects more recent ice flows. A transect up the nunatak will therefore produce a time

133

dependent history of ice flow.

The results of the model predict that the nunataks of area B should reflect a progressive anti-clockwise rotation of ice flow direction, starting to the West and finishing towards the South or South-East. A similar, although not so dramatic, clockwise rotation should be found on the nunataks of area C. If these predictions are not confirmed then the existence and disintegration of the Bellinghausen Sea ice dome is unlikely. The nunataks of area D are discussed by Clapperton and Sugden (1982) and confirm the expected northward ice flow. Finally nunataks in area E can be used to investigate the late Quaternary dynamics of the Filchner ice shelf. Although no predictions are possible using the present model, it is likely that abrupt changes in ice flow direction occurred as the much thickened late Quaternary Ellsworth Land ice sheet decayed.

Ice thickness and extent.

The third aspect of ice sheet behaviour amenable to investigation via nunatak geomorphology is ice thickness and extent. Again a large height of rock above the present day ice surface is desirable. This increases the probability that the nunatak stood proud of former ice sheet surfaces and increases the likelihood of a trimline identifying these former surfaces being present.

Information about ice thickness is particularly important in two areas; on the East coast of Palmer Land and adjacent to George VI Sound. The model predicts that former ice sheet extent to the East of Palmer Land was not significantly greater than the present day extent. The reasons for this are discussed later. This specific prediction can be tested by the use of the group F nunataks as 'dip sticks' of former ice thickness. Finally the nunataks of groups A and B should provide information on the changing ice thicknesses in George VI Sound and improve our understanding of the Sound's deglaciation.

(3.4) RESULTS : EXPERIMENTS WITH THE MODEL.

The model agrees tolerably well with the available evidence from the area, and has provided a basis from which to predict sites for future field work. The fact that the model has survived testing against all available field evidence indicates that it simulates the behaviour of marine ice sheets well. It is interesting to experiment with the model in order to understand its dynamics because these dynamics may well be similar to the dynamics of actual marine ice sheets.

A series of 34 experiments were performed to isolate the roles and the importance of the various processes within the ice sheet model. These experiments are described in a series of sub-sections. The topics of

these various sub-sections are: the relative importance of model's two forcing functions; the role of isostasy in the model; the sensitivity of the model's net mass balance parameterization; the sensitivity of the model's the calving parameterization; the role of basal melt rate in the model; and the sensitivity of the model's velocity parameterization. A summary of these experiments is given in Table 3.2.

(3.4.1) THE RELATIVE IMPORTANCE OF THE MODEL'S TWO FORCING FUNCTIONS.

As discussed in Section (3.2) the model employs the twin forcing functions of eustatic sea level and marine basal melt (Figures 3.4 and 3.5). The exact role of each forcing function in determining ice sheet behaviour is unclear. Two experiments were therefore performed which employed, in turn, just one of the original forcing functions. The results for ice sheet volume are shown in Figure 3.23. Neither sea level nor marine basal melt variations can produce complete deglaciation alone.

The run using basal melt variation alone does not show the second steady state volume of the standard run at 20.0 ka. This implies that the expansion leading to this second steady state volume is solely a consequence of the sea level fall from -60 to -120 m during the period 12.0 to 22.0 ka. Rapid retreat is initiated in the basal melt run, however the ice sheet only reaches minimum

volume is 530 x 10^3 km^3.

The run using sea level variation alone produces an ice sheet that does not decay past the initial steady state volume of 800 x 10^3 km^3. The effect of sea level rise from -120 to 0 m during the period 22.0 to 40.0 ka is therefore minimal when not in accompanied by basal melt increase. These runs imply that complete ice sheet decay is only possible if both forcing functions are used in tandem, although the maximum ice sheet can be destabilized by basal melt increase alone.

(3.4.2) THE INFLUENCE OF ISOSTASY IN THE MODEL.

The discussion about ice sheet decay (sub-section 3.3.2) identified isostasy as an important factor in determining the behaviour of the model. A series of experiments were performed to assess the sensitivity of the overall model's behaviour to changes in the bedrock diffusivity (D_a). Oerlemans and van der Veen (1984) identify the range of this constant as $\pm$ 15 km^2 a^{-1}. Figure 3.24 shows the ice sheet volumes achieved in the standard run (D_a = 35); in runs with bedrock diffusivity equal to 20 and 50; and in a run with no isostasy.

The maximum ice sheet volume attained in these runs is not particularly sensitive to the variation of bedrock diffusivity. However the nature of ice sheet decay does

differ between runs using different diffusivity values. The complete retreat of the ice sheet appears to rely on smaller diffusivity values. Thus the run with diffusivity equal to 50 has a slower, more erratic retreat than the standard run. Greater bedrock diffusivity produces a faster bedrock response to ice sheet decay because it allows the bedrock to rise more rapidly. This reduces both calving and marine basal melt rates. In contrast the run with diffusivity equal to 20 produces a faster rate of ice sheet decay because the ice sheet perimeter is retreating into areas that have been over-deepened by isostasy and have not yet responded to the reduced ice overburden.

The decreased diffusivity run (Figure 3.24) shows oscillations of ice sheet volume between 4.0 and 14.0 ka, and between 32.0 and 40.0 ka. These oscillations are caused by the increased time lag between ice sheet evolution and isostatic response. The first oscillation is produced by extra growth during the initial expansion of the ice sheet, which is, in turn, caused by the reduced bedrock depression in this run compared to the standard run. Eventually the bedrock responds to the increased ice overburden and a minor instability occurs along the ice sheet margin. This leads to retreat back to the usual steady state volume of 800×10^3 km^3.

A less dramatic oscillation occurs immediately after ice sheet retreat. A minimum ice cover distribution is reached at 32.0 ka. This distribution is shown in Figure 3.25. Comparison between this ice sheet form and the ice cover after 40.0 ka in the standard run (Figure 3.10, similar to ice sheet form after 40.0 ka in the Da = 20 run) reveals that the additional volume loss is a consequence of increased ice sheet retreat along George VI Sound. However a considerable depth of ice still remains in the Sound at the end of the run.

As discussed above the deglaciation of George VI Sound is one area of mismatch between model predictions and field interpretation. One explanation advanced as a reason for this mismatch was the under-prediction of isostasy in the model. The results from the Da = 20 run indicate that ice volume oscillations can be produced by isostasy, however such oscillations are not large enough to explain the complete deglaciation of George VI Sound and the subsequent growth of the George VI ice shelf. Alternative explanations must therefore be sought to explain this mismatch.

The run without isostasy achieves a slightly greater maximum volume than the standard run but does not retreat fully. The larger maximum volume is caused by the absence of isostatic bedrock lowering and the consequent lack of

ice sheet surface lowering. This leads to additional ice sheet growth via the net mass balance/ice thickness/surface elevation mechanism. The incomplete decay of the ice sheet implies that decay in the standard run relies on the isostatic over-deepening of the bedrock beneath the ice sheet interior. This over-deepening allows retreat to progress further because the ice sheet perimeter is continually retreating into deeper water and thus becoming progressively more unstable.

The series of experiments discussed above indicate that the exact nature of modelled ice sheet retreat is fairly sensitive to isostasy. However, when isostasy is incorporated into the model, the basic pattern of growth and decay is unaltered by variation in the diffusivity parameter.

(3.4.3) *THE INFLUENCE OF THE NET MASS BALANCE PARAMETERIZATION IN THE MODEL*

Ice sheet growth in the standard model is predominantly towards the West and the greatest expansion occurs across the Bellinghausen Sea. In contrast there is little expansion of ice sheet extent to the East of Palmer Land. This asymmetry of growth may have two possible causes. First, the net mass balance function used in the model incorporates a steep increase in accumulation rate towards the West. Ice accumulation is greater on the ice sheet's western flank than on its

eastern flank, and the ice sheet therefore expands in towards the West.

A second possible cause of the asymmetry of growth is the layout of topography in the area. The topography to the West of Palmer Land forms a large basin into which ice can converge, while the area to the East has no such basin and forces ice flow to diverge. Convergent ice flow leads to faster ice sheet growth than divergent ice flow. This is because convergent flow increases the flux of ice into an area. This increased flux is more likely to overcome local calving and basal melt, and more likely to lead to ice sheet advance.

An experiment was performed with the aim of finding out which of these two factors is the more important in determining the asymmetry of ice sheet expansion. In this experiment the westward bias of the net mass balance function was removed. The equation therefore read:

$$b = 1.24 + 0.21E + 0.10\phi \qquad (3.3)$$

This alteration has two effects; to remove the westward bias of net mass balance and to generally increase net mass balance everywhere over the area (because the negative longitudinal term has been removed).

141

The ice sheet form at 25.0 ka in this run is shown in Figure 3.26 (compare to the standard run at 25.0 ka in Figure 3.20). The flattening of the net mass balance/longitude gradient does not reduce the westward bias of ice sheet growth around South Palmer Land, which is therefore a product of the area's topography. In the East the convex coastline of Palmer Land ensures that ice flow is divergent and ice advance is therefore unlikely. While to the West the concave coast surrounding the Bellinghausen Sea ensures convergent flow and makes advance more probable. This is not the case further North around Graham Land. Here the coastline is fairly straight on both the East and the West coasts, ice sheet growth is therefore unlikely to be controlled by topographic factors. In this area the westward bias of ice growth in the standard model is a function of the longitudinal net mass balance gradient. When this gradient is removed the ice sheet grows equally to the East and to the West of the mainland.

The link between general net mass balance magnitudes and maximum ice sheet size warrants closer investigation. It is caused by an increased flux of ice at the ice sheet margin. Which increases the probability that local calving and basal melt will be overcome, and increases the extent of the ice margin's advance. A series of experiments were performed to assess the sensitivity of

this relationship. These experiments were run for 10.0 ka only and involved the alteration of the intercept term in equation (3.1) to 0.63, 0.86, 1.05, 1.43 and 1.60. Which represent respectively 50, 68, 83, 117 and 133 % of the original value of 1.26 m a^{-1}. Other model parameter values, initial conditions and forcing functions were kept the same, and these experiments therefore simulate the ice sheet growth stage between 40.0 and 30.0 ka BP.

The volumes achieved in these runs are shown in Figure 3.27. The relationship between general net mass balance magnitude and ice sheet growth is both continuous and sensitive. Given a certain general net mass balance magnitude the ice sheet will expand until marine losses equal the input of ice via net mass balance. Larger net mass balance magnitudes produce larger ice sheets because they increase ice margin fluxes and allow the ice sheet to penetrate further into deeper water. The sensitivity of this relationship has two causes. First, the net mass balance/ice sheet thickness/surface elevation loop leads to positive feedback. Second, once a sufficiently large ice flux has developed to carry the margin through water of a given depth, then the ice sheet will continue to advance until water of a greater depth is encountered. In the case of the Bellinghausen Sea, deeper water is not encountered until the ice margin is far to the West and by the time the margin is in this position the volume of

the ice sheet has grown considerably.

The experiments described in this sub-section indicate that ice sheet growth is sensitive to general net mass balance conditions. Perturbations of the net mass balance parameterization can produce both significantly larger than standard ice sheets and smaller land-based ice sheets. The sub-section has also shown that the West-East asymmetry of ice sheet growth around southern Palmer Land is caused predominantly by the distribution of topography.

(3.4.4) THE INFLUENCE OF THE CALVING PARAMETERIZATION IN THE MODEL.

The previous sub-section gave an indication of the type of behaviour associated with perturbations to the ice sheet net mass balance. These perturbations are linked to the input side of the ice sheet's mass budget. A similar set of experiments are now described for perturbations to the output side of the mass budget, and in particular to the calving rate.

Calving is estimated in the model by the use of an empirical relationship to water depth. A best fit value of 28.75 a^{-1} is used for the constant in this relationship. This value compares well to the literature value of 27.1 a^{-1}, which has a range of $\pm$ 2.0 a^{-1} (Brown et al 1982). Four additional model runs were completed for

the first 10.0 ka of the simulation. These experiments used values of 25.0, 35.0, 40.0 and 45.0 a^{-1} for the calving parameter. The resultant ice volumes are shown in Figure 3.28.

The volume curves in Figure 3.28 indicate that model behaviour is not sensitive to the parameterization of calving. A parameter value of 3.75 a^{-1} lower than the standard value only produces a 11 % increase in maximum ice volume, while a parameter value of 16.25 a^{-1} greater than the standard value leads to a 21 % decrease in maximum ice volume. The calving parameter perturbations used in these runs are considerably in excess of the range quoted in the original paper (Brown et al 1982) but produce only small changes in maximum ice volume.

The relationship between calving and ice sheet growth is fairly regular. This supports the previous sub-section's suggestion of regularity between general net mass balance magnitude and ice sheet growth. However, the volume curves for parameter values of 40.0 and 45.0 are similar. This implies that they represent a minimum value, which may be related to a particular bedrock trough beyond which ice cannot extend if calving is too great. The 10.0 ka ice sheet for these runs is similar to that produced after 10.0 ka in the standard model run, although it is generally thinner and does not extend so

far West into the Bellinghausen Sea.

An ice sheet that extends towards the continental shelf can be grown with a calving parameter as high as 45 a^{-1}. This suggests that such an ice sheet may both grow and decay solely in response to sea level variation, and without the additional forcing of marine basal melt variation. Figure 3.29 shows the volume curve for such a run and compares it with the standard run. When a calving parameter of 45.0 a^{-1} is used it is possible for an ice sheet to both grow and decay in response to sea level forcing alone. This is possible because the calving parameter relates calving to water depth. As this parameter is increased calving becomes more sensitive to sea level variation and the potential for ice sheet growth and retreat is increased. The maximum volume of the ice sheet is, however, only 69 % of the standard run's maximum.

The runs described in this sub-section indicate that the behaviour of the model is not particularly sensitive to perturbations of the calving parameterization. In addition they show that both ice sheet growth and decay can be achieved using sea level forcing alone if the calving parameter is increased to 45.0 a^{-1}.

(3.4.5) THE INFLUENCE OF BASAL MELT VARIATION IN THE MODEL.

Basal marine melt is the other component of the output side of the ice sheet's mass budget. Variations in basal melt are also used to drive the model, in fact previous experiments have indicated that basal melt variation is the model's dominant forcing function. The purpose of this sub-section is to assess the sensitivity of modelled ice sheet growth and decay to basal melt rate perturbations.

Two sets of experiments are discussed. The first deals with the first 10.0 ka of the simulation (between 40.0 and 30.0 ka BP) and investigates the effect of basal melt conditions on ice sheet growth. The standard basal melt rate of 0.5 m a^{-1} is replaced by values of 0.750, 1.000, 1.188, 1.125, 1.250 and 1.500 m a^{-1}. In all cases these values are kept constant throughout the whole model run. The initial conditions, sea level input and model parameter values in these runs are the same as in the standard model run.

The second set of experiments deals with the period between 15.0 ka BP and the present, and investigates the link between increasing basal melt rates and the decay of the maximum ice sheet. The initial conditions for these runs are the distributions of ice thickness and bedrock

elevation from the standard run at 25.0 ka. The model parameter values and the sea level input (rising between 25.0 and 40.0 ka) are the same as those used in the standard model run. In the standard run basal melt rates begin to increase at 22.0 ka. The rate of increase is 8.83×10^{-5} m a^{-2} and basal melt reaches a maximum of 2.0 m a^{-1} at 40.0 ka. In these experiments the rate of this increase is varied and the final maximum rate therefore varies. The experiments used rates of increase that resulted in final basal melt rates of 0.50 (no increase), 1.00, 1.25, 1.50 and 1.75 m a^{-1}.

The results of the ice sheet growth experiments are shown in Figure 3.30. The type of clustering noticed in the calving experiments (Figure 3.28) is again evident. In the calving experiments several runs attained a steady state volume of 650×10^3 km^3 after 10.0 ka. In the present experiments a similar group of runs (those for melt rates of 1.000, 1.188 and 1.125 m a^{-1}) reach a steady state of 600×10^3 km^3 after 10.0 ka. This agrees with the hypothesis of a bedrock trough limiting ice sheet volume to around 600×10^3 km^3; ice sheet expansion cannot continue beyond this trough when marine losses (either by calving or by basal melt) are too great. The clustering around 250×10^3 km^3 represents instances where the ice sheet is almost entirely limited to dry land.

The ice sheet decay results are shown in Figure 3.31.
Again some clustering of the individual volume curves is
evident. In particular four values of ice sheet volume
are associated with either new steady state forms or with
reductions in the rate of ice sheet decay. These values
are 825 x 10^3, 625 x 10^3, 450 x 10^3 and 225 x 10^3 km^3.
The latter value is that associated with the final, land
based ice sheet of the standard run. All of the runs that
use melt rates which increase to final values in excess
of 1.25 m a^{-1} reach this stage of decay, albeit at
different speeds. The rate of basal melt increase in the
1.25 m a^{-1} run is half of the rate in the standard run,
however deglaciation in this run is still complete.
Deglaciation is therefore a stable feature of the model
provided basal melt rates are increased.

The second ice volume around which clustering occurs
is 450 x 10^3 km^3. This is reflected by a long standstill
during the 1.25 m a^{-1} run and by a slowing of the rate of
retreat in both the standard and the 1.75 m a^{-1} runs.
This volume is associated with an ice sheet form similar
to that in the standard run at 33.0 ka (Figure 3.15). At
this point the ice sheet is in a state of quasi-
stability. The marine margin of the ice sheet is grounded
on bedrock rises which reduce the degree of marine ice
loss via calving and basal melt. It is only in the face
of rising sea levels and increasing basal melt rates that

this position becomes unstable and further retreat is initiated. In the 1.25 m a^{-1} run marine basal melt increases at a slower rate than in the other runs mentioned, the period of temporary stability is therefore prolonged in this run.

A similar situation exists when ice volumes reach 625 x 10^3 km^3. In this case deglaciation in the 1.0 m a^{-1} run remains incomplete. The faster rate of marine basal melt increase in the other runs means that this potentially stable ice volume is reflected only as a brief reduction in the rate of decay.

The two sets of experiments in this sub-section reveal a complex relationship between ice sheet behaviour (both growth and decay) and basal melt rate variation. Ice sheet growth is sensitive to initial basal melt rate, and large ice volumes cannot grow when basal melt rate is much in excess of 0.5 m a^{-1}. The final ice sheet volumes achieved in these runs are related to basal melt rate in a non-linear fashion, and there are distinct threshold values about which the final volumes cluster. This type of behaviour is more pronounced in the ice sheet decay experiments and is related to the stability of the ice sheet margin. Ice sheet decay is not particularly sensitive to basal melt rate variations, and complete deglaciation is always possible when basal melt rate

increases to a value in excess of 1.25 m a^{-1}. However the exact nature of retreat and the role of various threshold volumes during retreat is sensitive to basal melt rate perturbation.

(3.4.6) THE INFLUENCE OF THE VELOCITY PARAMETERIZATION IN THE MODEL.

The model determines the sliding and deformational components of ice velocity separately. The calculation of deformational velocity relies on ice thicknesses and on surface slopes, and the relationship to both is positive. Sliding velocity is related positively to both surface slope and the bedrock's depth below sea level, and is negatively related to ice thickness. The response of the model to velocity parameter perturbations is expected to be complex because of the variety of independent feedback loops that either include or are influenced by deformational velocity, sliding velocity or both. For example, velocity variation can influence ice thicknesses, surface elevations and net mass balances. It can also alter the flux of ice at the ice sheet margin and hence influence the effects of calving and marine basal melt.

Two sets of experiments will be described; one set uses the 10.0 ka period of ice sheet growth and the other uses the 15.0 ka period of ice sheet decay. The former models the period between 40.0 and 30.0 ka BP, and uses

the forcing and initial conditions of the standard run.
Four individual experiments were performed. In each
experiment either the deformation parameter or the
sliding parameter was either increased or decreased,
while all other parameters were kept equal to their
values in the standard run. In both this set of
experiments and those associated with ice sheet decay the
following alterations were made: the deformation
parameter was increased to 5.3 x 10^{-24} (equivalent to an
ice temperature of 0 ^{O}C); the deformation parameter was
decreased to 5.2 x 10^{-25} (equivalent to an ice
temperature of -10 ^{O}C); the sliding parameter was
increased to 8 x 10^{-4} ; and the sliding parameter was
decreased to 5 x 10^{-5}. The tuned values used in the
standard run are 1.7 x 10^{-24} for the deformation
parameter (equivalent to an ice temperature of -5 ^{O}C) and
2 x 10^{-4} for the sliding parameter. The latter is a
four-fold increase on the original literature value for
this parameter (Budd et al 1984).

The ice sheet decay experiments model the period
between 15.0 ka BP and the present, and use the forcing
functions and parameter values of the standard run
during this period. As with the marine basal melt decay
runs, the distributions of ice thickness and bedrock
elevation from the standard run at 25.0 ka were used as
initial conditions. Four individual experiments were

performed, each using either a decreased or an increased value for one of the velocity parameters.

The results of the ice sheet growth experiments are shown in Figure 3.32. The runs in which the deformation parameter was altered show only small deviations from the standard run. The run in which deformation was increased has a final volume that is 95 % of the standard run's final volume, while the run in which deformation was decreased has a final volume that is 114 % of the standard. These deviations arise through the relationship between ice flow and ice thickness. Faster flowing ice is associated with reduced ice thicknesses and reduced surface elevations. These reductions lead, in turn, to reduced net mass balances because of the positive relationship between net mass balance and surface altitude. Faster flowing ice sheets therefore tend to have reduced net mass balances and reach smaller sizes. The reverse path of reasoning can be used to explain the fact that the run with decreased deformation produces a larger than standard ice sheet after 10.0 ka.

The alteration of the sliding parameter has different effects. Increased sliding has virtually no effect, and the run using an increased sliding parameter produces an ice sheet at 10.0 ka which has a volume that is 99.8 % of the standard 10.0 ka ice sheet's volume. However the run

in which sliding is reduced produces a 10.0 ka ice sheet whose volume is only 61 % of the standard volume. If the logic used to explain the results of the deformation runs were followed then one would expect reduced sliding to be associated with increased (rather than decreased) volumes. Clearly another process is dominant in determining the relationship between sliding and ice sheet growth. This process is linked to the flux of ice at the ice sheet margin. When sliding velocities at the ice margin are reduced the margin's ice flux is also likely to be reduced. This flux is then less able to contend with local marine losses. Calving and basal melt are therefore more likely to keep the ice sheet's growth in check if the sliding parameter is reduced.

Sliding velocities are a large component of total ice velocity in the offshore regions of the ice sheet, because increased water depths increase both buoyancy and sliding. However, deformation velocities are the more important component of total ice velocity in onshore areas. Thus the perturbation of the sliding parameter and of the deformation parameter affect different parts of the ice sheet. Perturbation of the deformation parameter predominantly affects land-based ice and produces changes via the process of net mass balance feedback. However perturbation of the sliding parameter predominantly affects marine ice and produces changes via the

alteration of the ice flux at the ice sheet margin. The same type of perturbation can therefore have different effects when it is applied to the sliding and to the deformation parameters.

The results of the ice sheet decay experiments are shown in Figure 3.33. The pattern of deglaciation in both of the deformation perturbation experiments is very similar to the pattern in the standard run, and the final ice sheet volumes produced in all three cases are almost identical. The run using an increased deformation parameter has a more evenly paced decay than the standard run, while deglaciation in the run using a decreased deformation parameter is more abrupt than deglaciation in the standard run. Both of these features can be related back to the influence of the deformation velocity on surface elevations and net mass balances. Thus an ice sheet produced in a run with increased deformation will suffer a lowering of interior surface elevations, leading to a reduction in net mass balance input. This input reduction and the increased marine losses (arising from sea level rise and basal melt increase) lead to an initially fast rate of decay compared to the standard run. As deglaciation continues a steady rate of volume reduction is maintained because the retreating calving front is encountering ice that has already been thinned by the effects of increased ice flux. The accelerating

rate of volume loss evident in the standard run is therefore not produced. A similar argument can be used to explain the comparatively abrupt deglaciation of the decreased deformation run.

In these decay runs the perturbation of the sliding parameter has a greater effect than the perturbation of the deformation parameter. This was also a feature of the ice sheet growth experiments. The effects of sliding perturbation during growth and during decay are contrasted in that a sliding decrease is the more important perturbation during growth but a sliding increase is the more important perturbation during decay. The run with decreased sliding has a pattern of decay that is similar to the standard pattern, however the run with increased sliding does not achieve complete deglaciation.

For deglaciation to be initiated the rate of marine loss at the ice sheet margin must exceed the ice flux towards the margin. If this condition is met then the ice margin will begin to retreat over isostatically deepened bedrock. This retreat leads to increased water depths at the ice margin, and to increased marine loss rates and an accelerated rate of decay. The run in which the sliding parameter was increased is able to resist complete deglaciation because ice margin velocities and

fluxes are larger than those in the standard run. The ice sheet is thus able to maintain a relatively constant ice margin position and the accelerated decay created by ice margin retreat is averted. This is achieved at the cost of increased ice fluxes and decreased interior ice surface elevations. Reductions of ice sheet volume are therefore partially a result of ice sheet thinning.

The two sets of experiments in this sub-section indicate that the relationship between ice sheet behaviour and the velocity parameterization is complex. Perturbations of the deformation parameter and of the sliding parameter have different consequences that are brought about by entirely different processes. The model is not sensitive to the variation of the deformation parameter but is fairly sensitive to the variation of the sliding parameter.

(3.5) CONCLUSIONS.

The general ice sheet model derived in Chapter 2 has been used to study the behaviour of the Antarctic Peninsula ice sheet. This formerly marine ice sheet responds predominantly to changes in the surrounding oceans, and in particular to changes in sea level and sea surface temperature (which affects basal melt rate). The model couples an ice sheet model to a model of the isostatic bedrock response. It produces predictions of

ice sheet extent, thickness, flow direction, flow speed and isostatic bedrock deflection.

Output from the model indicates that the ice sheet's response to oceanic changes was often rapid and delayed. States of relative stability are separated by brief phases of transition. The nature of these transitions is complex. It is associated with the interaction of thresholds within the ice sheet system and the gradual changes of the model's driving variables. An example is the effect of rising sea level on calving, which is influenced by the spatial distribution of bedrock rises.

The main predictions of the model are concerned with the growth and decay of a large marine ice dome in the Bellinghausen Sea area. Ice sheet growth is dominated by the offshore advance of this ice dome. While ice sheet retreat sees the rapid decay of the dome. This decay is initiated by rising sea levels and increasing basal melt rates, and it affects the positions and orientations of ice streams within the rest of the ice sheet. The predicted dynamics of these ice streams varies greatly through time and over space. For instance, the decay of the Bellinghausen Sea ice dome leads to a dramatic rotation of the ice flow direction over southern Alexander Island, while ice flow over northern Alexander Island is virtually unaffected by the decay of the ice

dome.

This degree of spatial variation implies that a model with two horizontal dimensions is needed to study marine ice sheet behaviour fully. In addition, the modelling of the ice sheet's behaviour through time as a series of steady states is unlikely to capture the complex behaviour of the ice sheet during transition periods. This omission is important because ice sheet behaviour during these transitions determines both the dynamics and the morphology of the steady states.

The testing of the model relies on four specific predictions. The first relates to ice flow directions and speeds; the second to the chronology of ice sheet decay; the third to the relative uplift subsequent to this decay; and the fourth to the present day ice sheet morphology. Field evidence agrees reasonably well with the predictions of the model.

The discrepancies that do exist between field evidence and predictions indicate the likely shortfalls of the model. Two of these discrepancies are of particular interest. The first is concerned with the effect of ice dome decay on the ice flow over Alexander Island. This mismatch may have occurred because of our inadequate knowledge of the area's geomorphology. The output of the

model suggests themes for future field research in the area, which would aim to resolve the conflict between model predictions and field estimates. This use of a numerical model to produce an initial scenario of ice sheet behaviour in an area is a new and efficient means of guiding field work, which may otherwise be unfocused.

The second discrepancy between the predictions of the model and field evidence is associated with the inability of the model to predict complete ice sheet decay. This leads to an over-estimate of the extent and thickness of grounded ice in George VI Sound. It is argued that this mismatch is caused by the inadequate spatial resolution of the model, which fails to capture both the depth of water in George VI Sound and its effect on the Sound's calving and grounding line dynamics.

The inadequacy of the model's spatial resolution emphasizes the importance of topography in determining modelled ice sheet behaviour. Two further results imply that topography is important. The first relates to the contrasting retreat rates of the ice sheet's western flank. In the southerly area around the Bellinghausen Sea retreat is rapid and continuous because the exposed calving front of the ice sheet retreats along a deep bedrock trench which has no potentially stabilizing bedrock rises. Ice sheet retreat in the North-West (West

of Alexander Island) is slow and erratic because the ice sheet is retreating through shallow water which is becoming shallower via isostatic uplift.

The second set of evidence that indicates the importance of topography in the model is related to an experiment in which the usual westward increase in net mass balance was removed. Ice sheet growth in this experiment was asymmetric and was predominantly towards the West. This implies that the geographical distribution of topography biased ice sheet growth, thus the concave coastline of West Palmer Land favoured ice sheet expansion, while the convex coastline of East Palmer Land did not.

Experiments were performed to assess the importance of different model sections in determining overall model behaviour. These experiments indicated that net mass balance conditions are extremely important in the growth of the ice sheet. A minimum mean accumulation rate of 0.34 m a^{-1} was identified, below which a marine ice sheet could not develop. This estimate is important because it constrains the late Quaternary precipitation climate of the area. A large marine ice sheet is known to have existed in the area during the late Quaternary, the mean accumulation rate over the area must therefore have been in excess of 0.34 m a^{-1} (compared to a present day mean

rate of 0.76 m a^{-1}).

Experiments also indicated that basal marine melt is more important than sea level in determining ice sheet behaviour. However both are required if the ice sheet is to decay completely. The speed of isostatic response, the calving rate and the velocity parameterization also influence the detailed pattern of ice sheet growth and decay. However the gross dynamics of the ice sheet's response to changing sea levels and marine basal melt rates is unaffected by any of these factors.

Table 3.1 Summary of the parameter values used in the standard run of the model. (relevant equation in brackets)

Parameter	Standard value	Units
Net mass balance (3.1)		
intercept	1.26	$m\ a^{-1}$
latitude multiplier	-0.12	$m\ a^{-1}\ {}^oS^{-1}$
longitude multiplier	0.10	$m\ a^{-1}\ {}^oE^{-1}$
elevation multiplier	0.21	$m\ a^{-1}\ km^{-1}$
maximum accumulation constraint	1.2	$m\ a^{-1}$
Marine ice losses (2.12) (2.13)		
calving		
-multiplier	28.75	a^{-1}
-maximum calving rate constraint U_c Max	20.0	$km\ a^{-1}$
Ice flow		
deformation (2.25)		
-flow law multiplier A	1.7×10^{-33}	$m^3 s^5 kg^{-3}$
-flow law power n	3.0	--
sliding (2.28)		
-sliding law multiplier K_2	2.0×10^5	$m^3 (bar\ a)^{-1}$
-minimum ice thickness at which sliding occurs	0.1	km
ice shelf strain rate (2.26) $\dot\varepsilon_s$	0.001	a^{-1}
maximum velocity constraint	2.0	$km\ a^{-1}$
gravitational acceleration g	9.81	$m\ s^{-2}$
density of ice ρ_i	870.0	$kg\ m^{-3}$
density of sea water ρ_w	1025.0	$kg\ m^{-3}$
Isostasy (2.15)-(2.17)		
density of asthenosphere ρ_M	3300.0	$kg\ m^{-3}$
diffusivity of asthenosphere D_a	35.0	$km^2\ a^{-1}$
General		
grid unit Δx	25.0	km
time step Δt	2.5	a
topographic representation	mean only	

163

<u>Table 3.2</u> <u>Summary of the experiments carried out using the</u>
<u>model, showing the relevant figures.</u>

<u>Description</u>   <u>Relevant Figures</u>

Relativeimportance   *3.23 (Volume 40 ka BP to present)*
of the two forcing
functions.

Influence of   *3.24 (Volume 40 ka BP to present)*
isostasy.   *3.25 (Ice surface at 40 ka)*

Parameterization of   *3.26 (Ice surface at 25 ka)*
net mass balance.   *3.27 (Volume 40 to 30 ka BP)*

Parameterization of   *3.28 (Volume 40 to 30 ka BP)*
calving.   *3.29 (Volume 40 ka BP to present)*

Influence of basal   *3.30 (Volume 40 to 30 ka BP)*
melt rate variation.   *3.31 (Volume 15 ka BP to present)*

Parameterization of   *3.32 (Volume 40 to 30 ka BP)*
velocity.   *3.33 (Volume 15 ka BP to present)*

164

FIGURE 3.1 A CONTOURED REPRESENTATION OF THE PRESENT DAY BEDROCK TOPOGRAPHY, WHICH IS USED AS THE INITIAL TOPOGRAPHY IN THE MODEL.
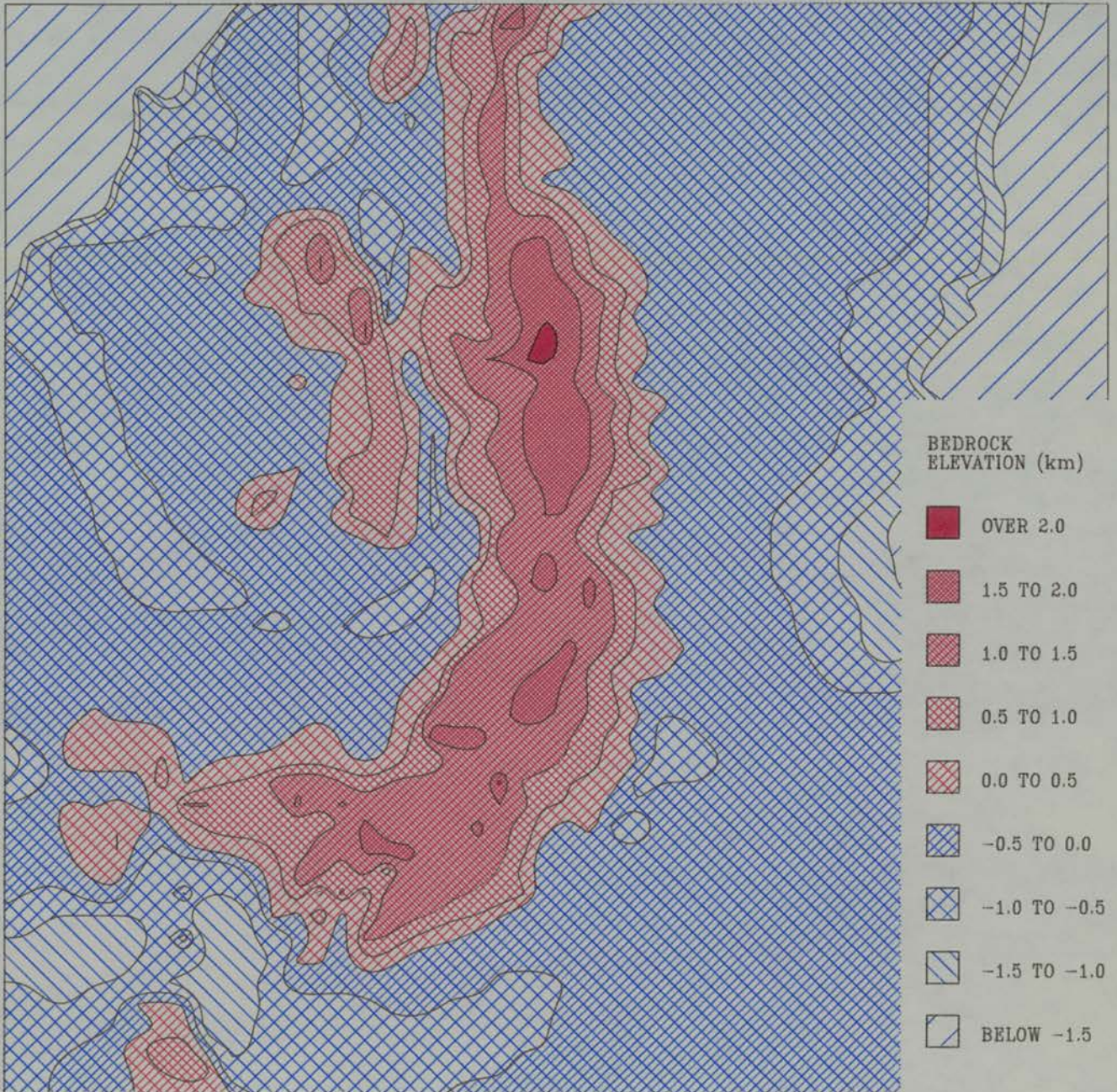
FIGURE 3.2 A CONTOURED REPRESENTATION OF THE PRESENT DAY ICE SHEET
MORPHOLOGY, WHICH IS USED AS THE INITIAL ICE SHEET IN THE
MODEL. THE RED LINE REPRESENTS SEA LEVEL AND THE GREEN LINE
REPRESENTS A WATER DEPTH OF 0.5 KM.

SURFACE
ELEVATION (km)

OVER 2.5

2.0 TO 2.5

1.5 TO 2.0

1.0 TO 1.5

0.5 TO 1.0

0.0 TO 0.5
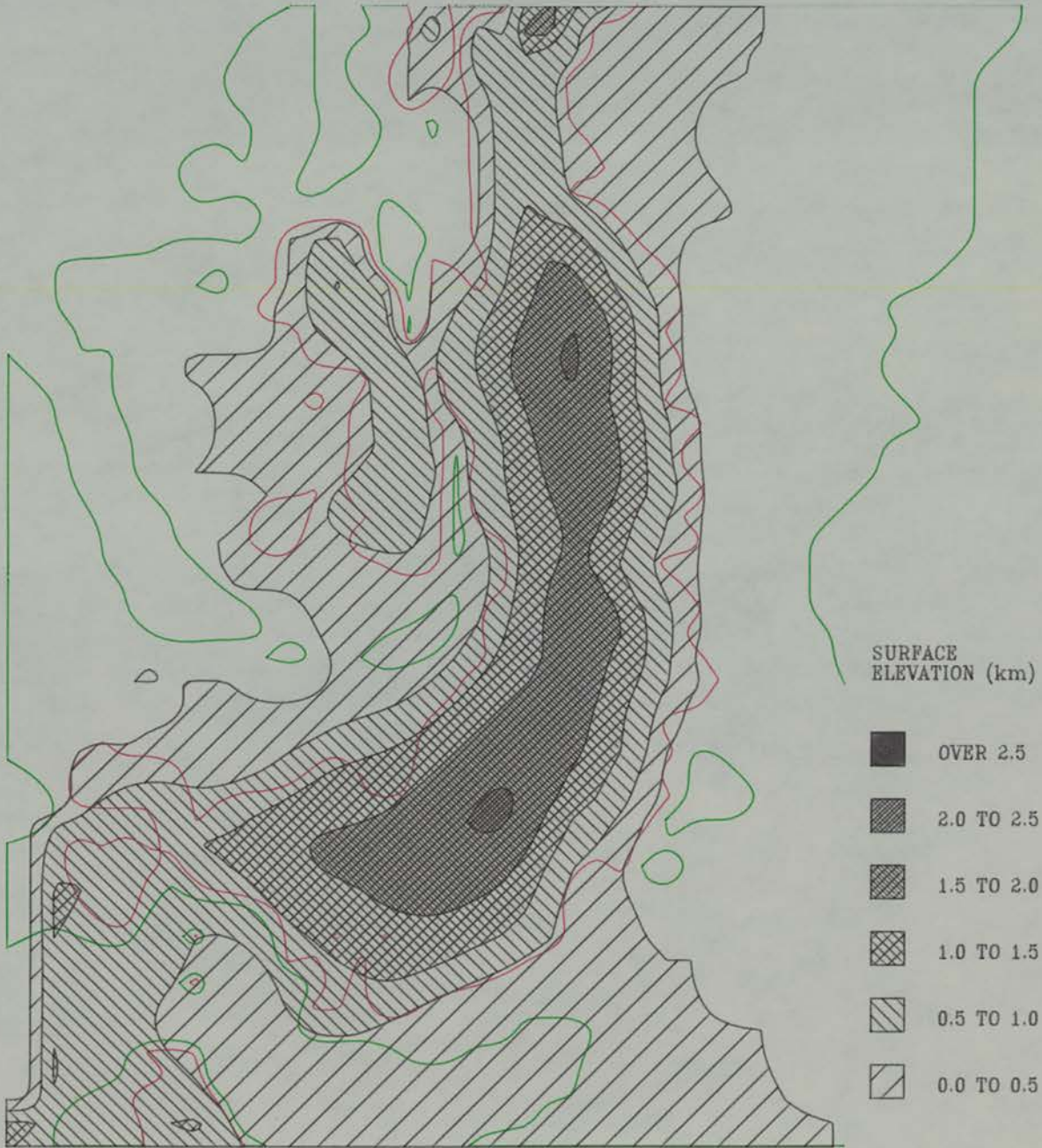
FIGURE 3.3 PLACE NAMES USED IN CHAPTER 3, WITH THE PRESENT DAY
BEDROCK TOPOGRAPHY.

BEDROCK
ELEVATION (km)

ABOVE 0.0

BELOW 0.0
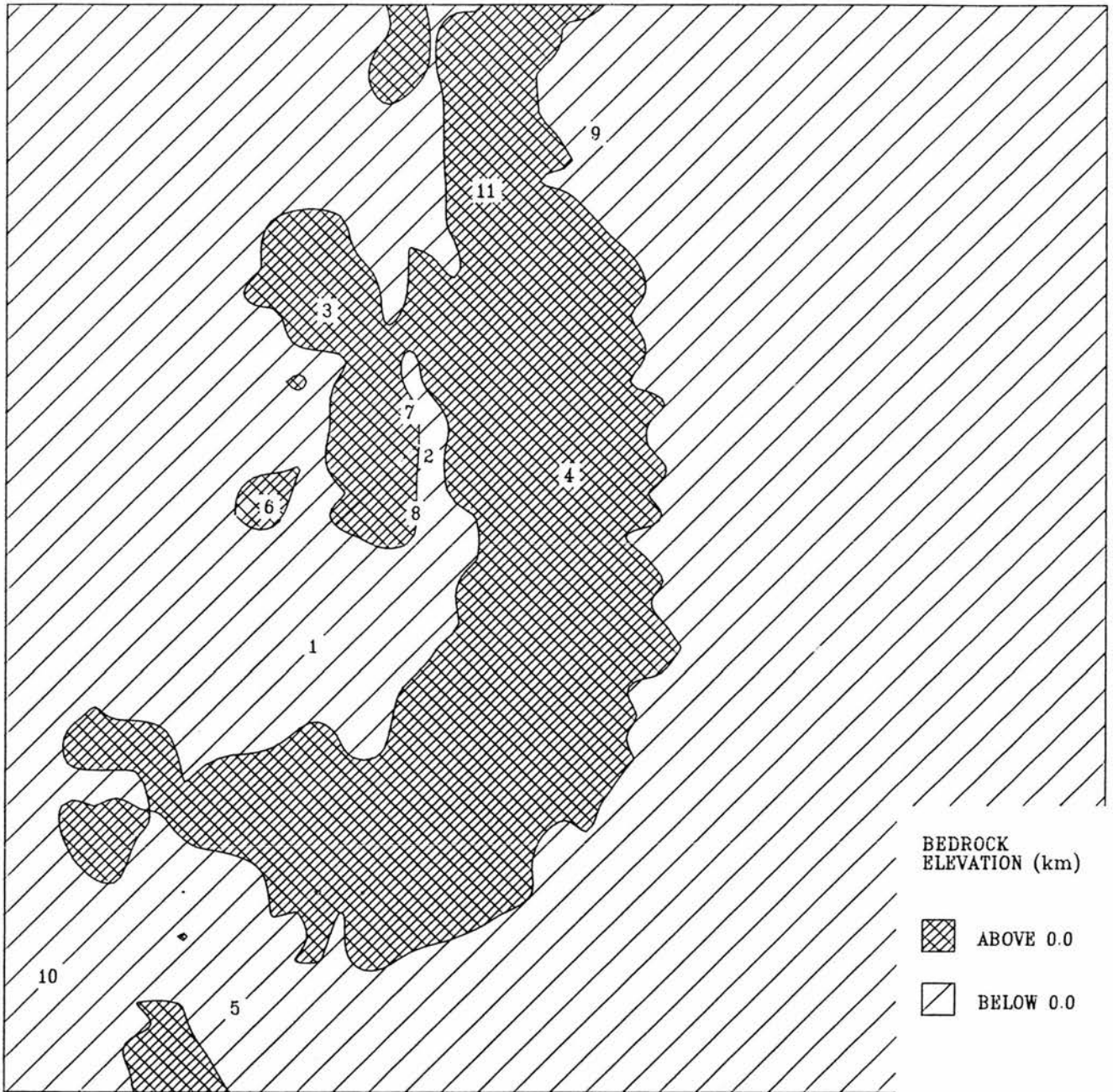
KEY:

(1) BELLINGHAUSEN SEA
(2) GEORGE VI SOUND
(3) ALEXANDER ISLAND
(4) PALMER LAND
(5) FILCHNER ICE SHELF
(6) BEETHOVEN PENINSULA

(7) ABLATION POINT
(8) TWO STEP CLIFFS
(9) LARSEN ICE SHELF
(10) ELLSWORTH LAND
(11) GRAHAM LAND

FIGURE 3.4 THE EUSTATIC SEA LEVEL FORCING FUNCTION USED IN THE MODEL,
WHICH WAS DERIVED FROM SHACKLETON (1987).
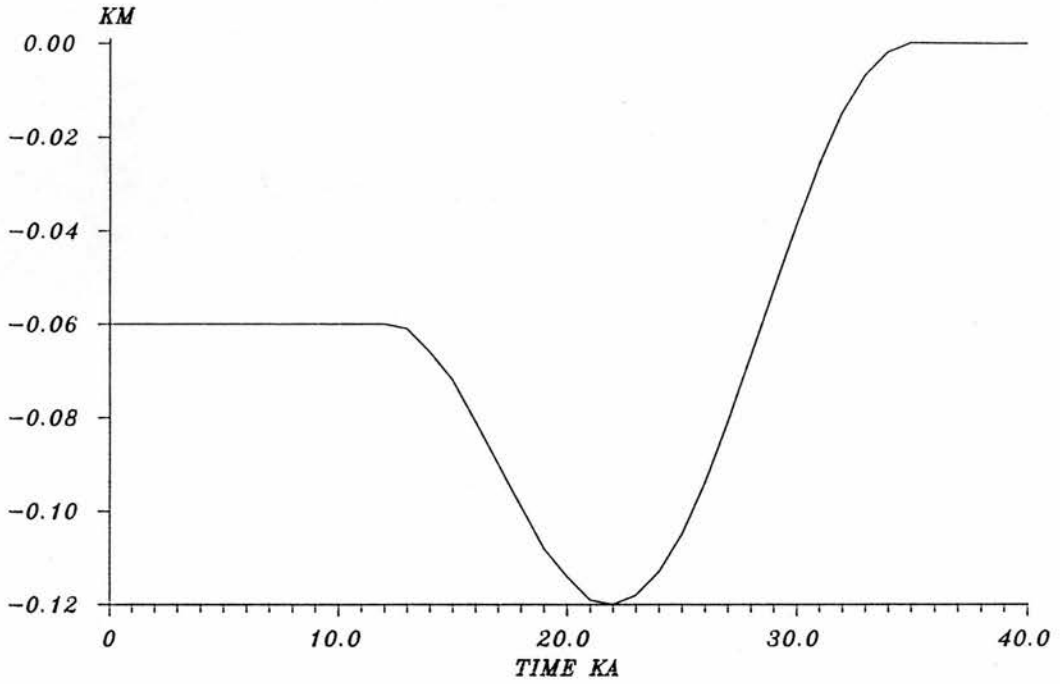
FIGURE 3.5 THE MARINE BASAL MELT FORCING FUNCTION USED IN THE MODEL,
WHICH REPRESENTS THE IMPOSED RATE OF MELTING BENEATH ICE
SHELVES AND IS USED FOR AREAS TO THE WEST OF THE PENINSULA.
MELT RATES TO THE EAST OF THE PENINSULA ARE MAINTAINED AT
0.5 M/A THROUGHOUT THE MODEL RUNS.
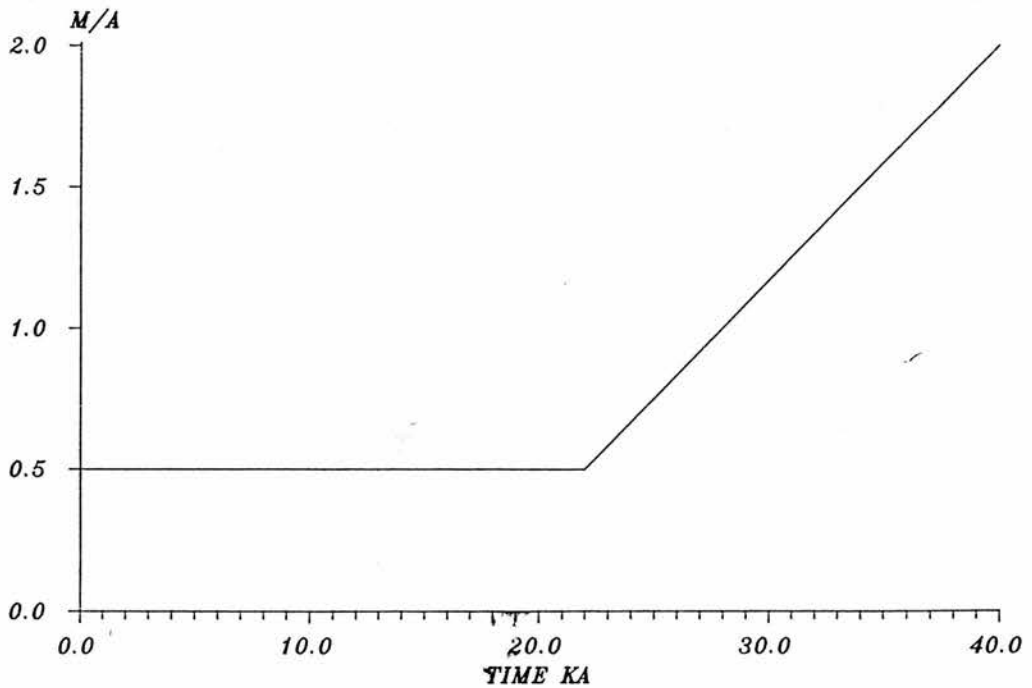
FIGURE 3.6 THE ICE SHEET VOLUME OUTPUT PRODUCED BY THE
STANDARD RUN.
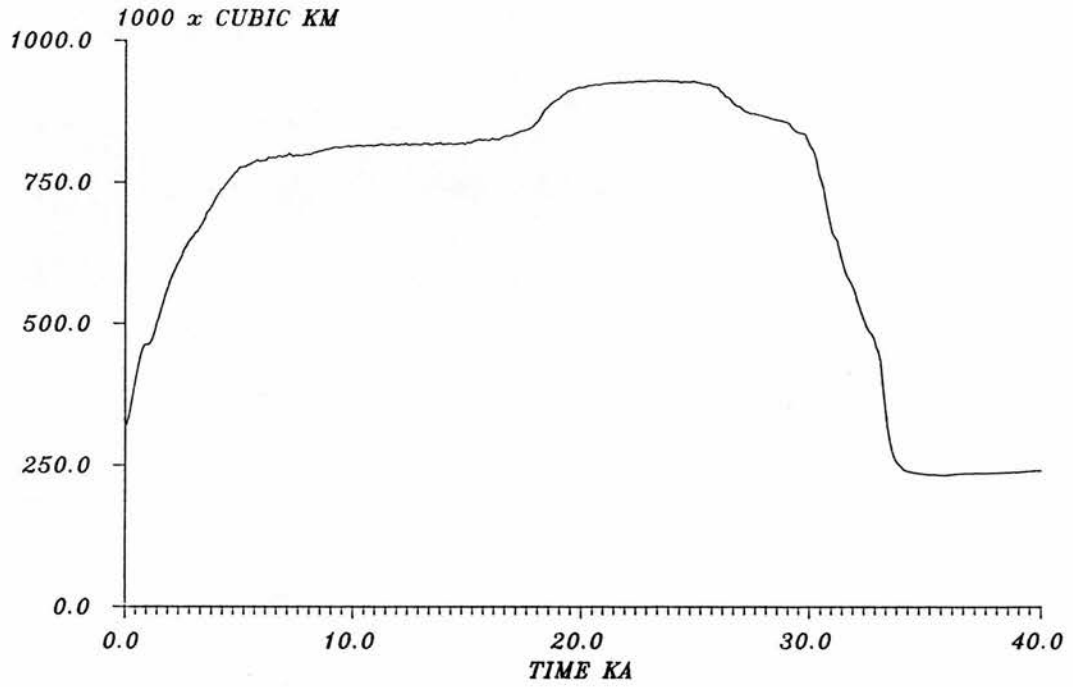
FIGURE 3.7 THE MEAN BEDROCK ELEVATION OUTPUT PRODUCED BY THE
STANDARD RUN AND EXPRESSED AS A FRACTION OF THE
MEAN ELEVATION OF THE RELAXED TOPOGRAPHY.
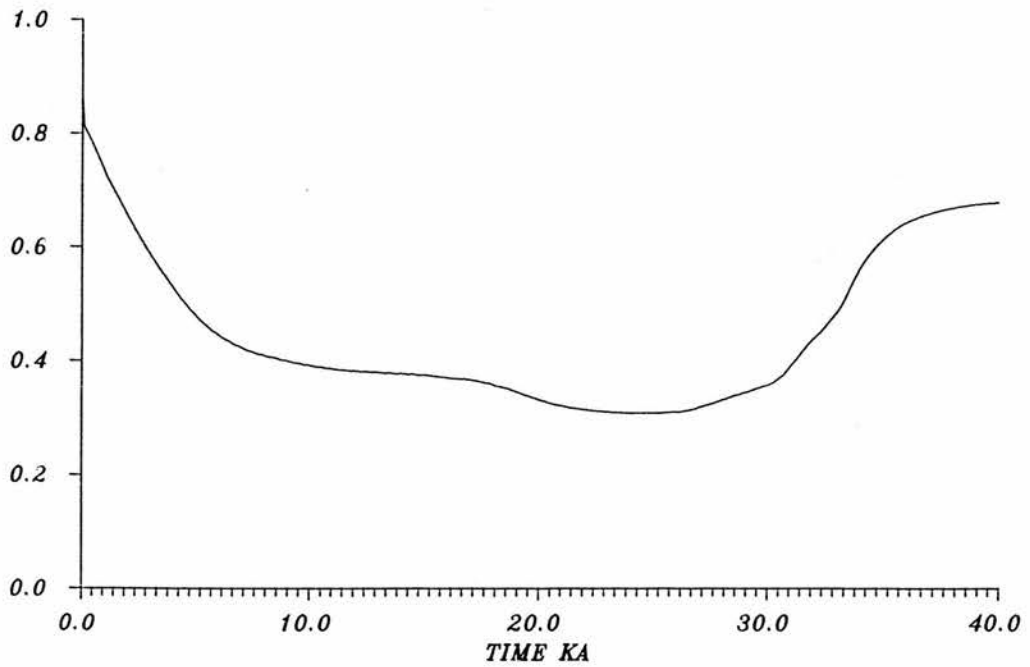
FIGURE 3.8 THE FLUX OF ICE ENTERING THE ICE SHEET VIA SURFACE
ACCUMULATION DURING THE STANDARD RUN.
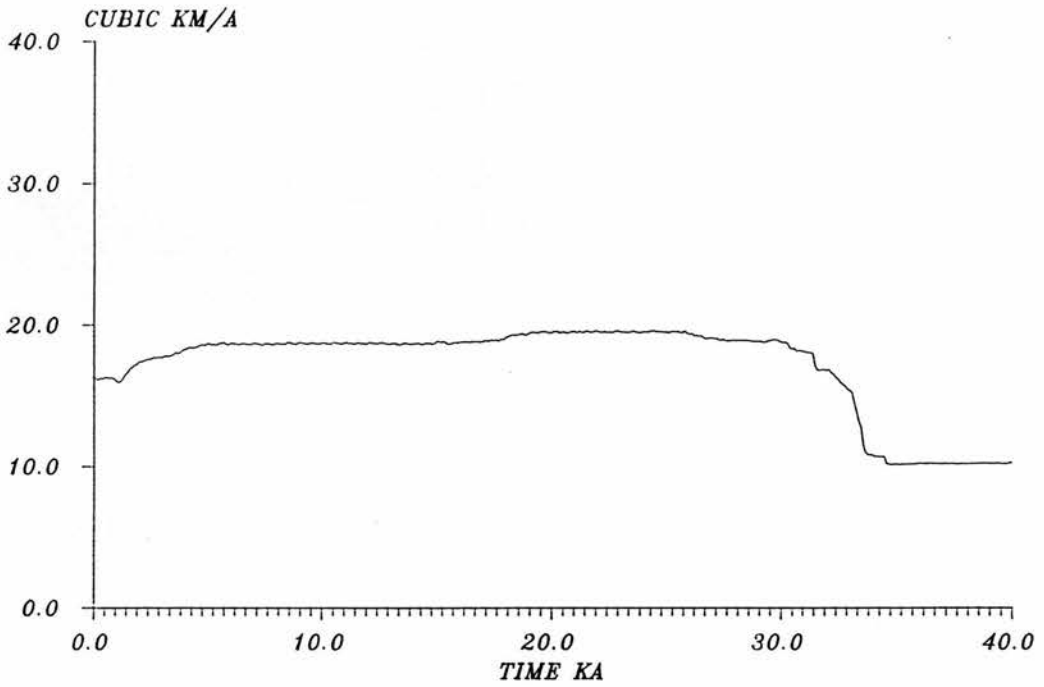
FIGURE 3.9 THE FLUX OF ICE LEAVING THE ICE SHEET VIA CALVING
AND MARINE BASAL MELT DURING THE STANDARD RUN.
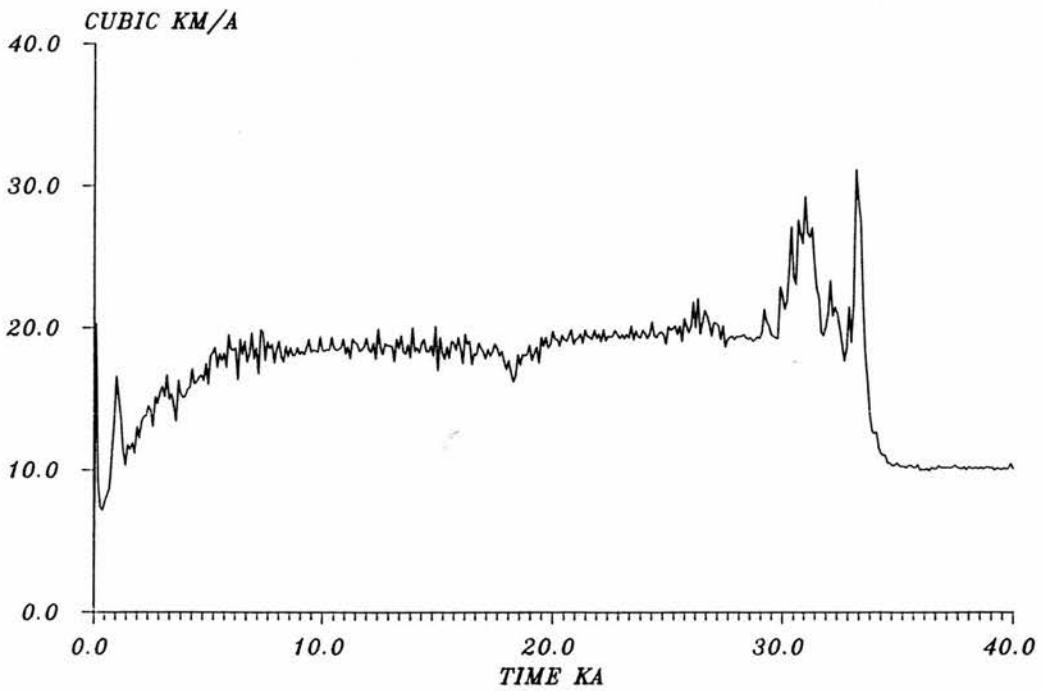
FIGURE 3.10 THE PREDICTION OF THE STANDARD RUN FOR ICE SHEET MORPHOLOGY AT 40.0 KA (THE PRESENT DAY). THE RED LINE REPRESENTS SEA LEVEL AND THE GREEN LINE REPRESENTS A WATER DEPTH OF 0.5 KM.

SURFACE ELEVATION (km)

OVER 2.5

2.0 TO 2.5

1.5 TO 2.0

1.0 TO 1.5

0.5 TO 1.0

0.0 TO 0.5
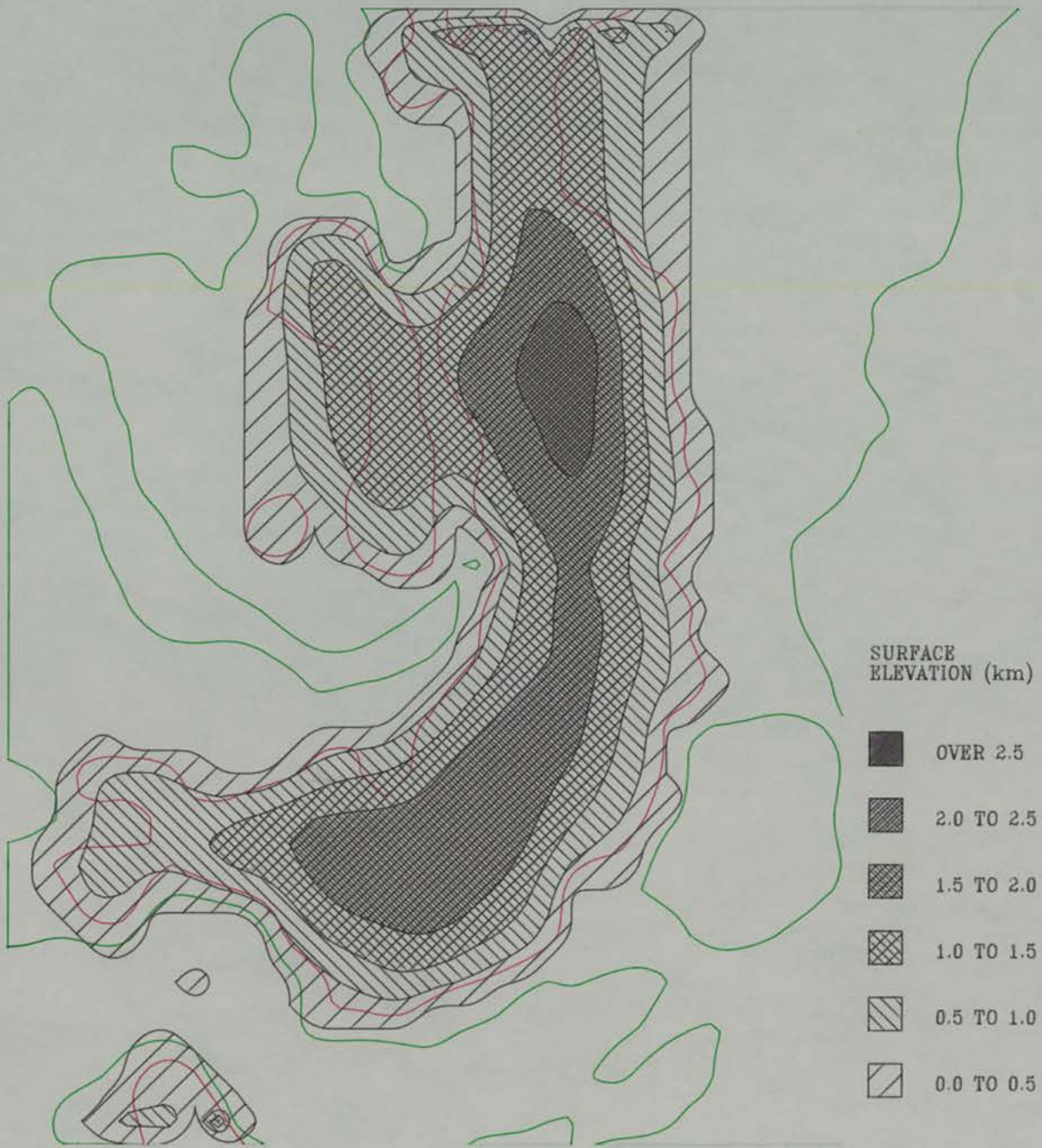
FIGURE 3.11 THE PREDICTION OF THE STANDARD RUN FOR ICE SHEET MORPHOLOGY AT 26.0 KA (14.0 KA BP). THE RED LINE REPRESENTS SEA LEVEL AND THE GREEN LINE REPRESENTS A WATER DEPTH OF 0.5 KM.

SURFACE
ELEVATION (km)

OVER 2.5

2.0 TO 2.5

1.5 TO 2.0

1.0 TO 1.5

0.5 TO 1.0

0.0 TO 0.5
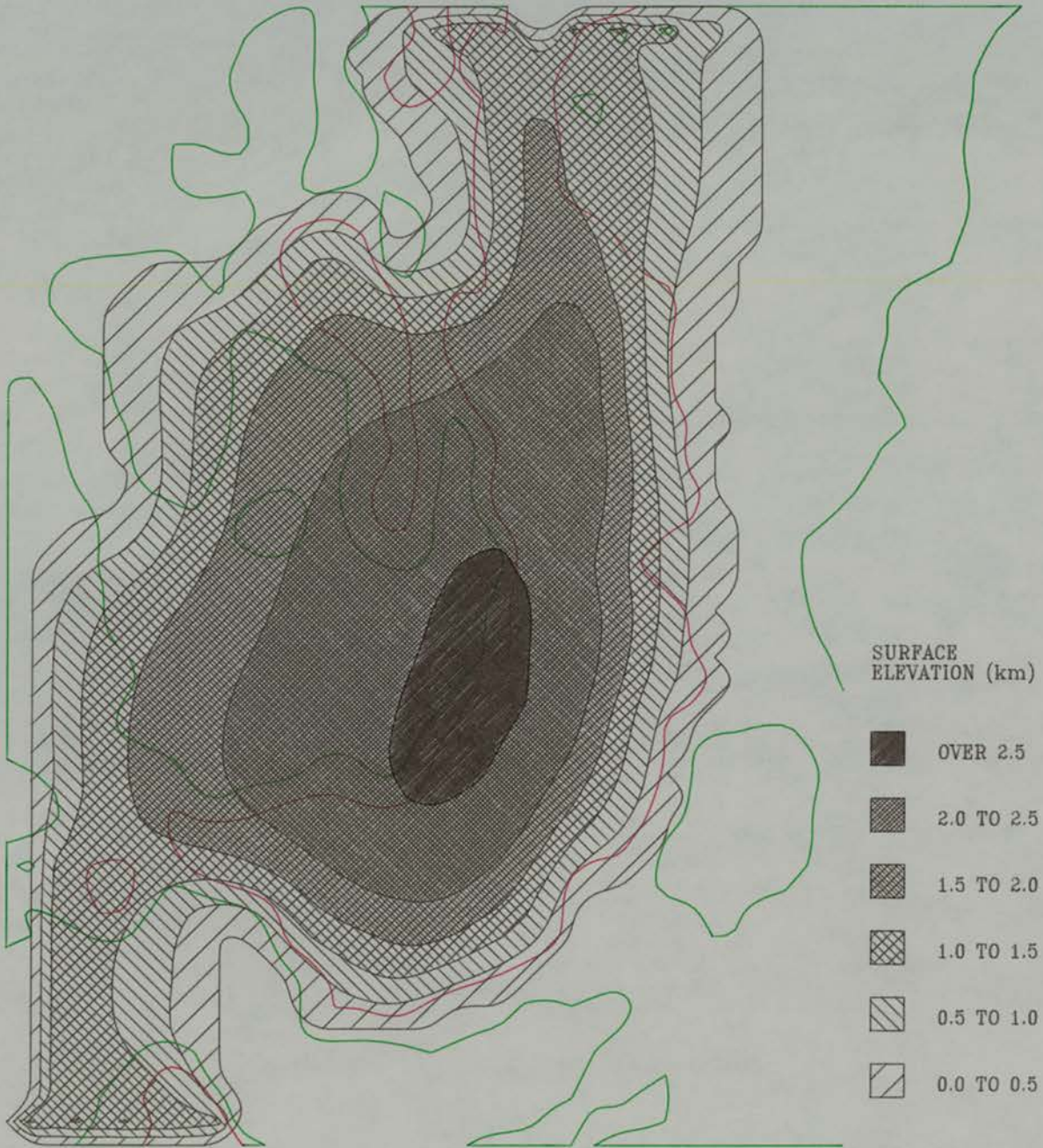
FIGURE 3.12 THE PREDICTION OF THE STANDARD RUN FOR ICE SHEET VELOCITIES AT 26.0 KA (14.0 KA BP). THE RED LINE REPRESENTS SEA LEVEL AND THE GREEN LINE REPRESENTS A WATER DEPTH OF 0.5 KM.

VELOCITY (km/a)

OVER 0.5

0.4 TO 0.5

0.3 TO 0.4

0.2 TO 0.4

0.1 TO 0.2

0.0 TO 0.1

FIGURE 3.13 THE PREDICTION OF THE STANDARD RUN FOR ICE SHEET MORPHOLOGY AT 30.0 KA (10.0 KA BP). THE RED LINE REPRESENTS SEA LEVEL AND THE GREEN LINE REPRESENTS A WATER DEPTH OF 0.5 KM.

SURFACE ELEVATION (km)

OVER 2.5

2.0 TO 2.5

1.5 TO 2.0

1.0 TO 1.5

0.5 TO 1.0

0.0 TO 0.5
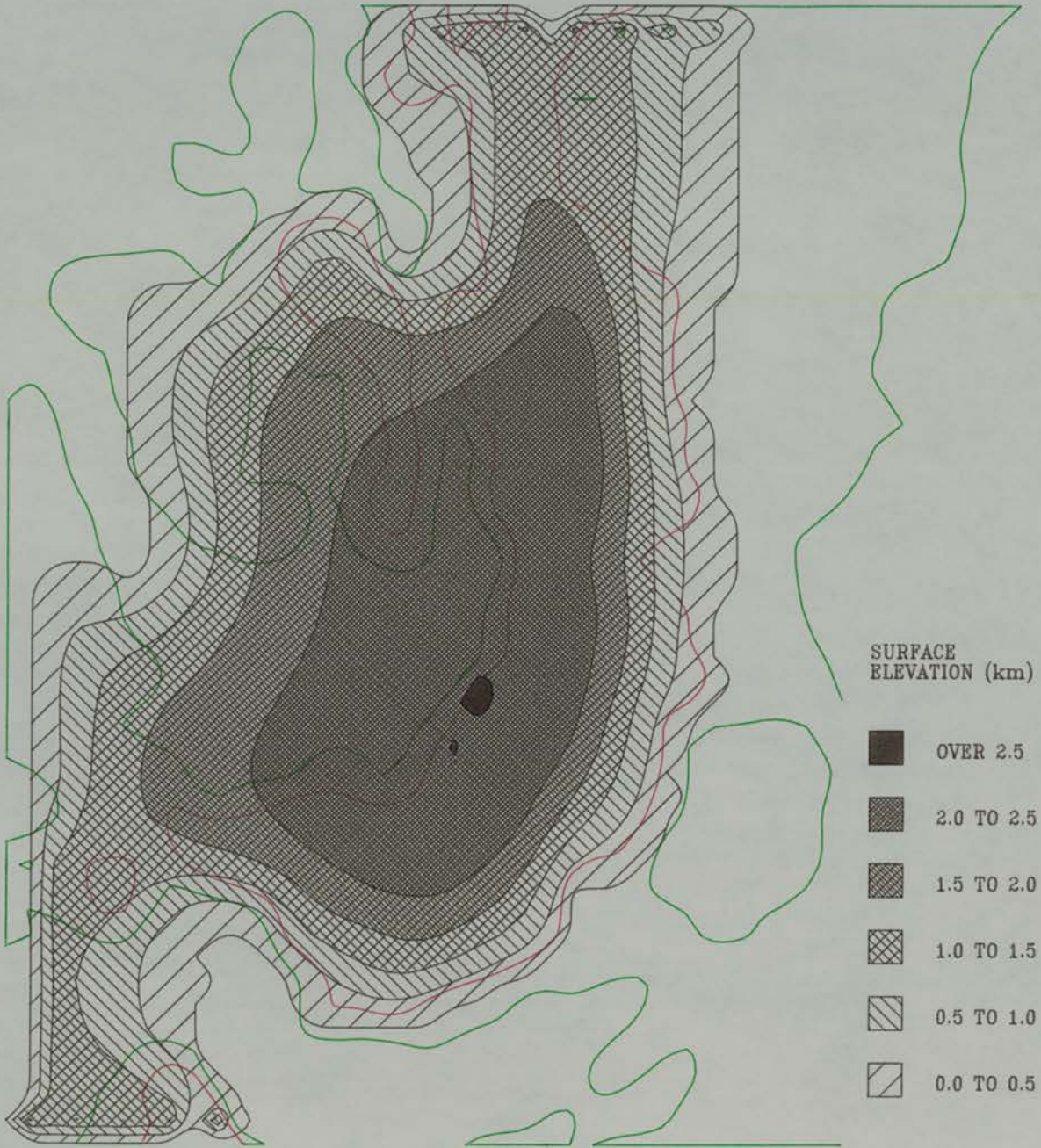
FIGURE 3.14 THE PREDICTION OF THE STANDARD RUN FOR ICE SHEET VELOCITIES AT 30.0 KA (10.0 KA BP). THE RED LINE REPRESENTS SEA LEVEL AND THE GREEN LINE REPRESENTS A WATER DEPTH OF 0.5 KM.

VELOCITY
(km/a)

OVER 0.5

0.4 TO 0.5

0.3 TO 0.4

0.2 TO 0.4

0.1 TO 0.2

0.0 TO 0.1

FIGURE 3.15 THE PREDICTION OF THE STANDARD RUN FOR ICE SHEET MORPHOLOGY AT 33.0 KA (7.0 KA BP). THE RED LINE REPRESENTS SEA LEVEL AND THE GREEN LINE REPRESENTS A WATER DEPTH OF 0.5 KM.

SURFACE
ELEVATION (km)

OVER 2.5

2.0 TO 2.5

1.5 TO 2.0

1.0 TO 1.5

0.5 TO 1.0

0.0 TO 0.5
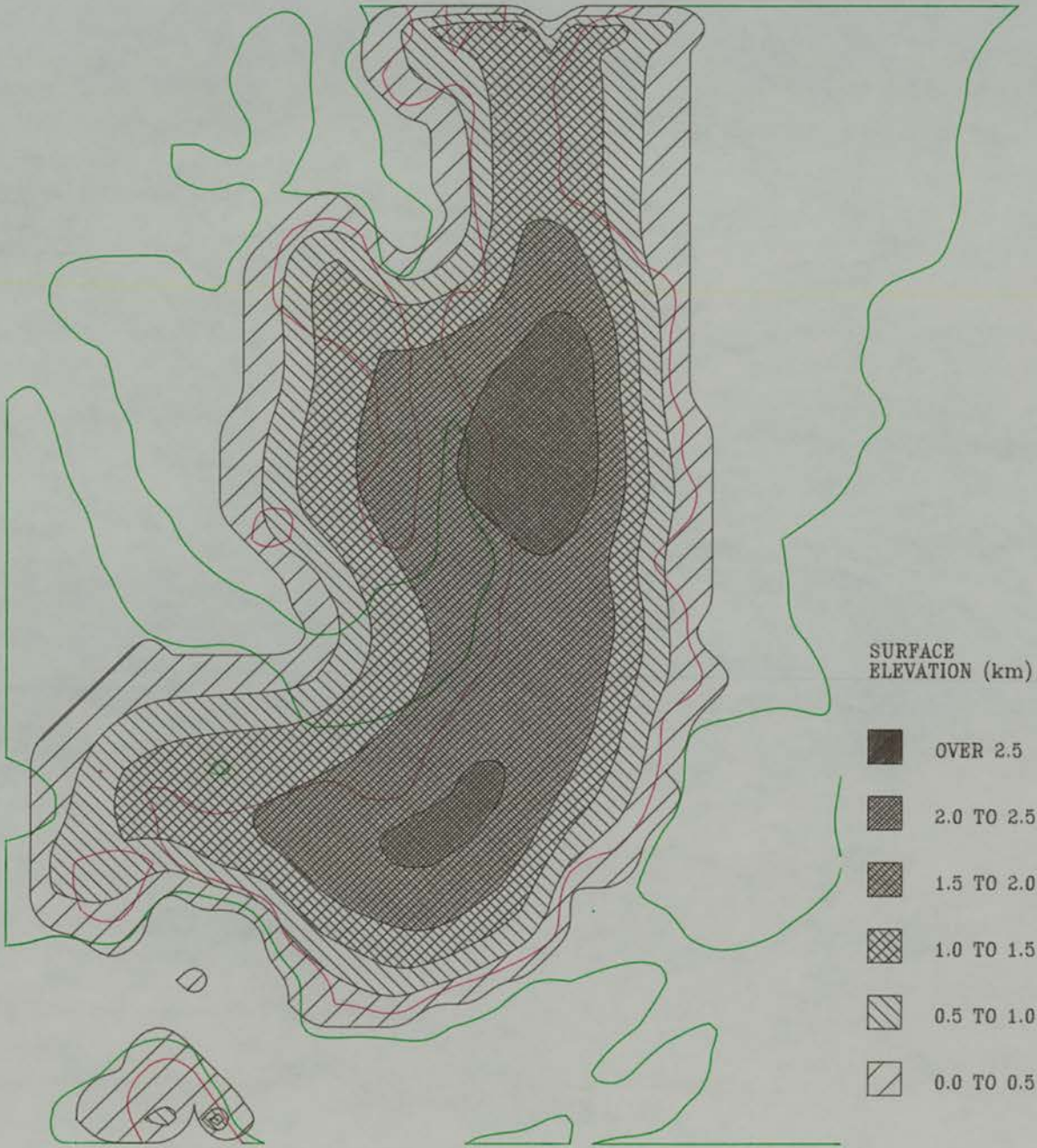
FIGURE 3.16 THE PREDICTION OF THE STANDARD RUN FOR ICE SHEET VELOCITIES AT 33.0 KA (7.0 KA BP). THE RED LINE REPRESENTS SEA LEVEL AND THE GREEN LINE REPRESENTS A WATER DEPTH OF 0.5 KM.

VELOCITY
(km/a)

OVER 0.5

0.4 TO 0.5

0.3 TO 0.4

0.2 TO 0.4

0.1 TO 0.2

0.0 TO 0.1

FIGURE 3.17 THE PREDICTION OF THE STANDARD RUN FOR ICE SHEET MORPHOLOGY
AT 36.0 KA (4.0 KA BP). THE RED LINE REPRESENTS SEA LEVEL AND
THE GREEN LINE REPRESENTS A WATER DEPTH OF 0.5 KM.

SURFACE
ELEVATION (km)

OVER 2.5

2.0 TO 2.5

1.5 TO 2.0

1.0 TO 1.5

0.5 TO 1.0

0.0 TO 0.5
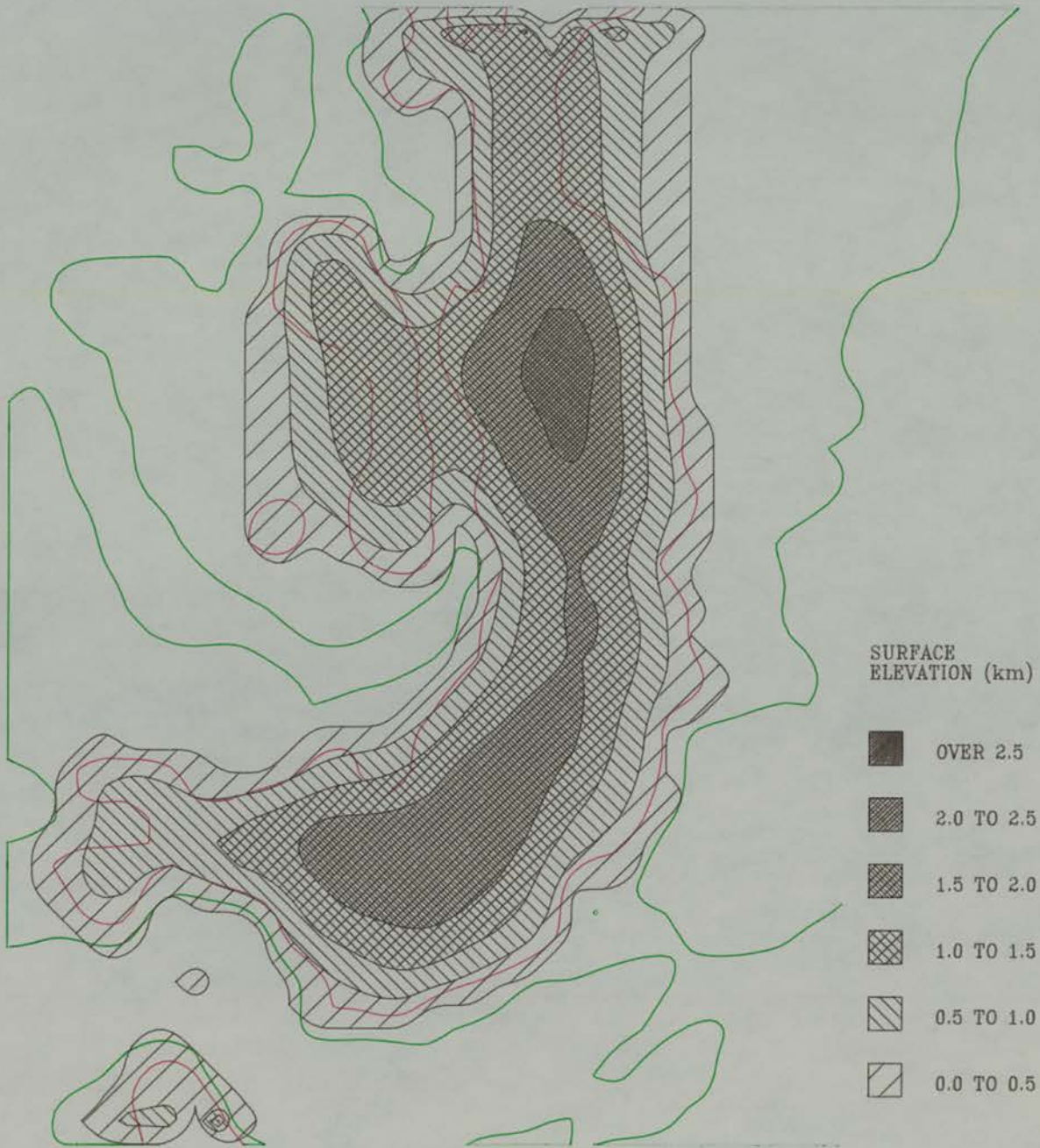
FIGURE 3.18 THE PREDICTION OF THE STANDARD RUN FOR ICE SHEET VELOCITIES AT 36.0 KA (4.0 KA BP). THE RED LINE REPRESENTS SEA LEVEL AND THE GREEN LINE REPRESENTS A WATER DEPTH OF 0.5 KM.

VELOCITY
(km/a)

OVER 0.5

0.4 TO 0.5

0.3 TO 0.4

0.2 TO 0.4

0.1 TO 0.2

0.0 TO 0.1

3.19 Reconstruction of the ice sheet flow lines for George VI Sound during the last glacial maximum. A. Ablation Point, F. Fossil Bluff, T. Two Step Cliffs, B. Batterbeee Mountains. After Clapperton and Sugden (1982).
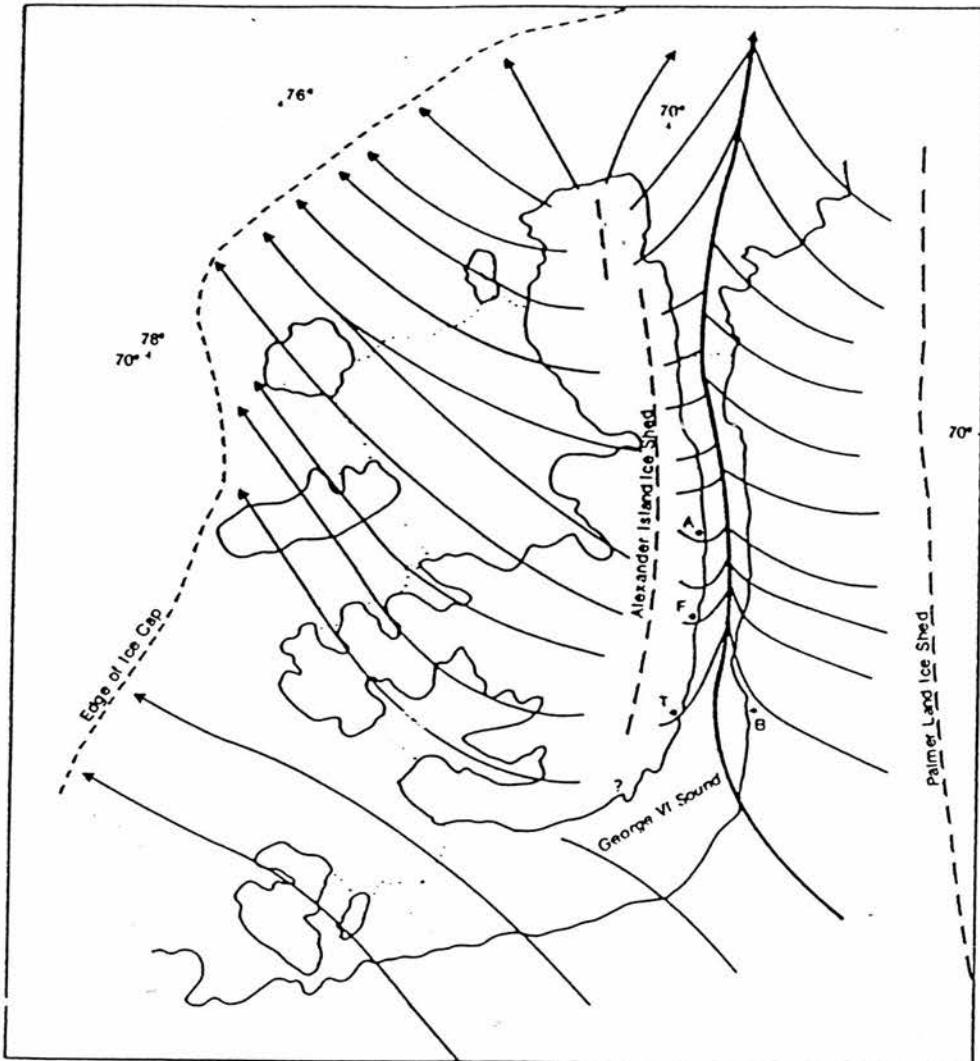
FIGURE 3.20 THE PREDICTION OF THE STANDARD RUN FOR ICE SHEET THICKNESS
AT 25.0 KA (15.0 KA BP). THE RED LINE REPRESENTS SEA LEVEL
AND THE GREEN LINE REPRESENTS A WATER DEPTH OF 0.5 KM.

ICE
THICKNESS (km)

OVER 3.5

3.0 TO 3.5

2.5 TO 3.0

2.0 TO 2.5

1.5 TO 2.0

1.0 TO 1.5

0.5 TO 1.0

0.0 TO 0.5
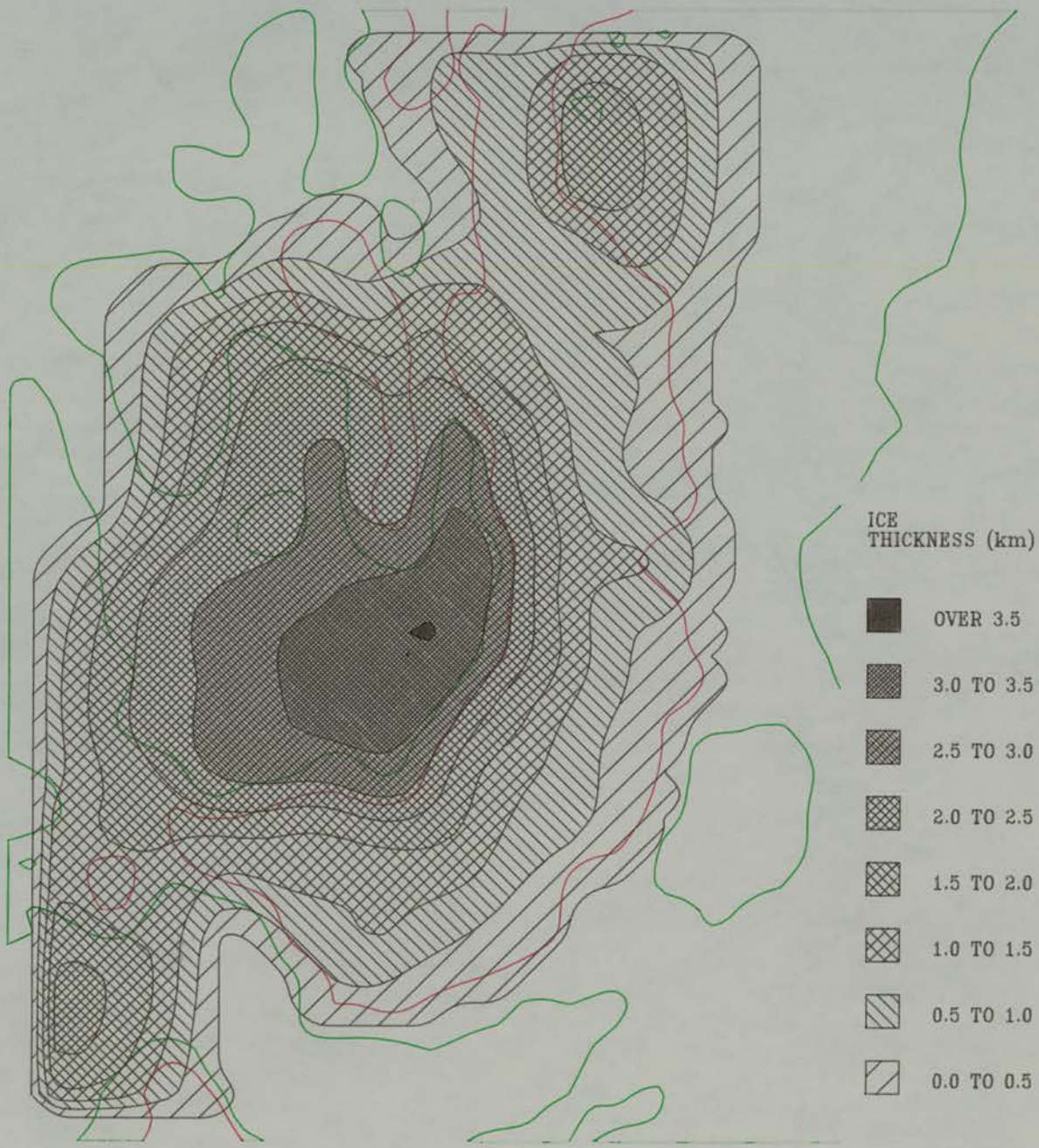
FIGURE 3.21 THE PREDICTION OF THE STANDARD RUN FOR UPLIFT PATTERN
BETWEEN 25.0 AND 40.0 (THE LAST 15.0 KA), CALCULATED BY
SUBTRACTING THE BEDROCK TOPOGRAPHY AT 25.0 KA FROM THE
BEDROCK TOPOGRAPHY AT 40.0 KA. THE RED LINE REPRESENTS
SEA LEVEL AND THE GREEN LINE REPRESENTS A WATER DEPTH OF
0.5 KM.

PREDICTED
UPLIFT (km)

BELOW 0.00

0.15 TO 0.00

0.30 TO 0.15

0.45 TO 0.30

0.60 TO 0.45

ABOVE 0.60
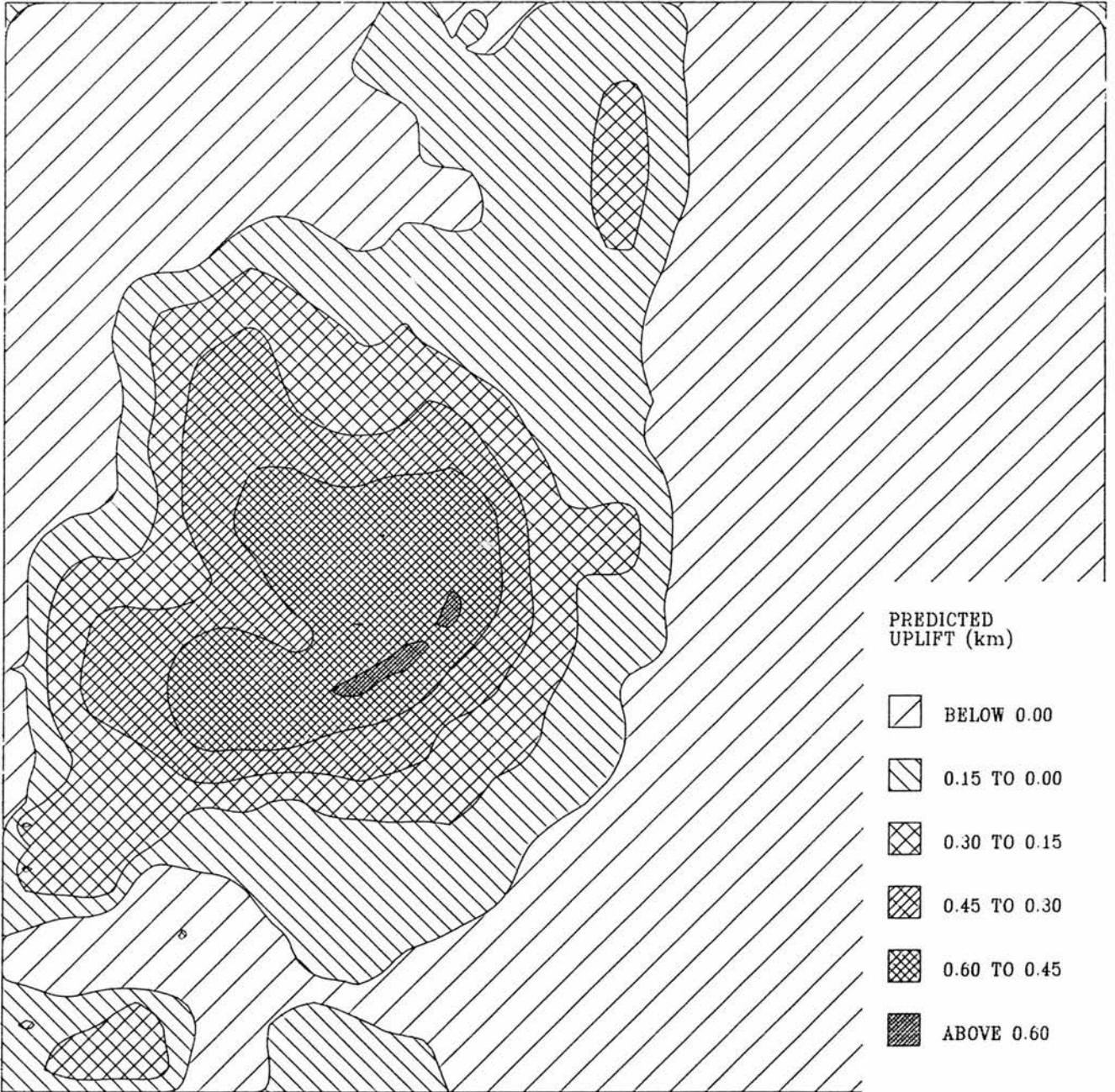
3.22   The   distribution   of   nuntaks   across   the   Antarctic
Peninsula. The nunataks are divided into six groups according to
the type of geomorphological evidence they offer.
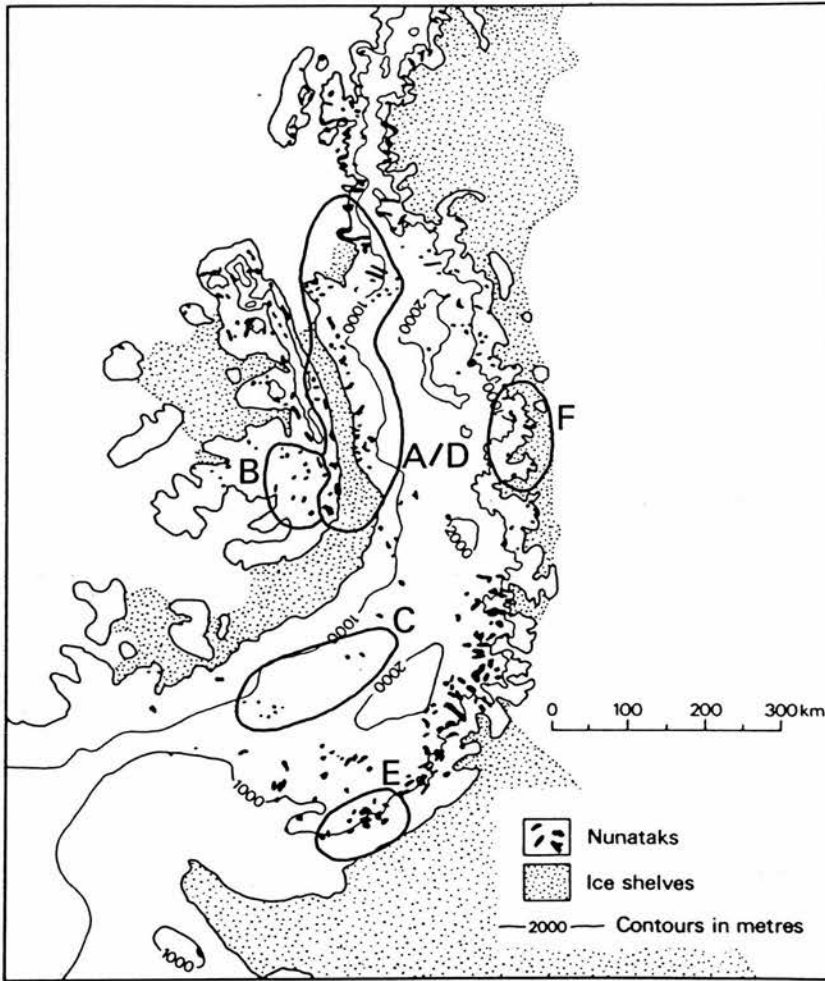
FIGURE 3.23 SENSITIVITY ANALYSIS OF THE ICE SHEET VOLUMES PRODUCED BY
BY THE MODEL WHEN IT IS FORCED BY EITHER USING SEA LEVEL
OR BASAL MELT RATE ALONE.

1000 x CUBIC KM

ICE SHEET VOLUME

LINE TYPES:
STANDARD
BASAL MELT ONLY
SEA LEVEL ONLY

TIME A
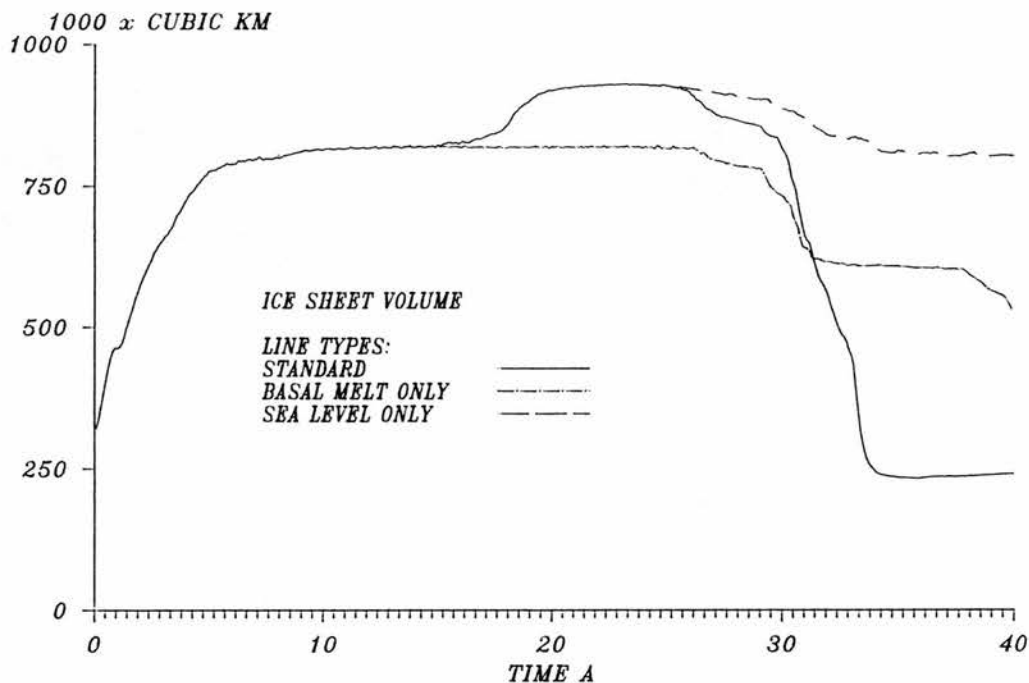
FIGURE 3.24 SENSITIVITY ANALYSIS OF THE EFFECT OF ISOSTASY ON THE ICE
SHEET VOLUMES PRODUCED BY THE MODEL. THE RUNS SHOWN ARE
THE STANDARD, A RUN INCORPORATING SLOW ISOSTATIC RESPONSE,
A RUN INCORPORATING FAST ISOSTATIC RESPONSE AND A RUN
INCORPORATING NO ISOSTATIC RESPONSE.

1000 x CUBIC KM

ICE SHEET VOLUME

LINE TYPES:
STANDARD (Da = 35)
Da = 20 RUN
Da = 50 RUN
NO ISOSTASY RUN

TIME A
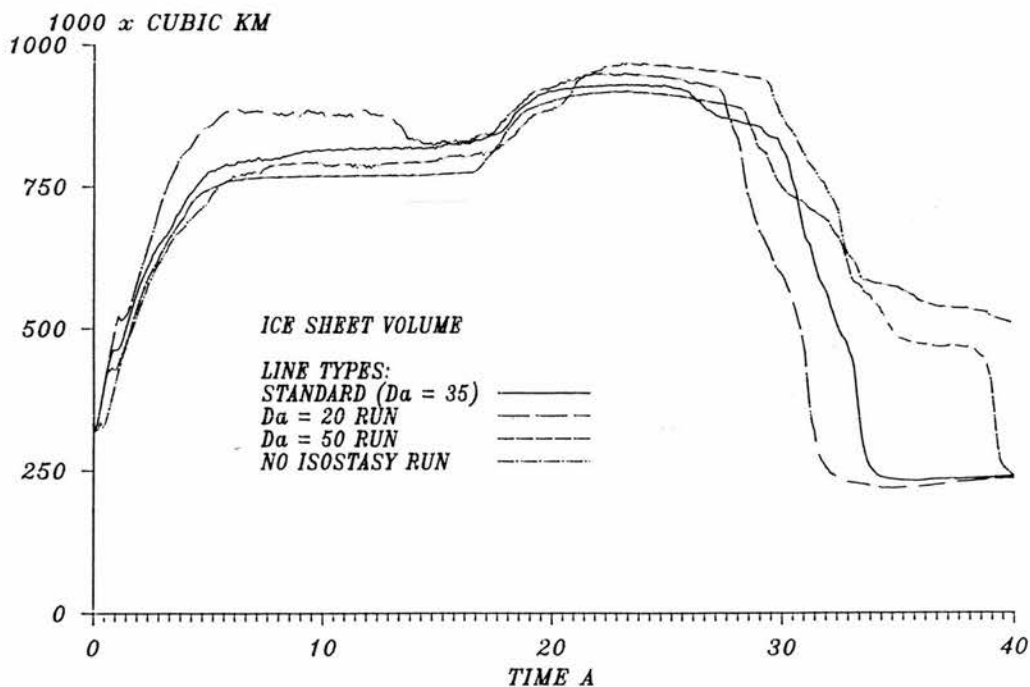
FIGURE 3.25 THE MINIMUM ICE COVER PREDICTED AT 32.0 KA (8.0 KA BP) BY A
MODEL INCORPORATING SLOW ISOSTATIC RESPONSE. THE RED LINE
REPRESENTS SEA LEVEL AND THE GREEN LINE REPRESENTS A WATER
DEPTH OF 0.5 KM.

SURFACE
ELEVATION (km)

OVER 2.5

2.0 TO 2.5

1.5 TO 2.0

1.0 TO 1.5

0.5 TO 1.0

0.0 TO 0.5
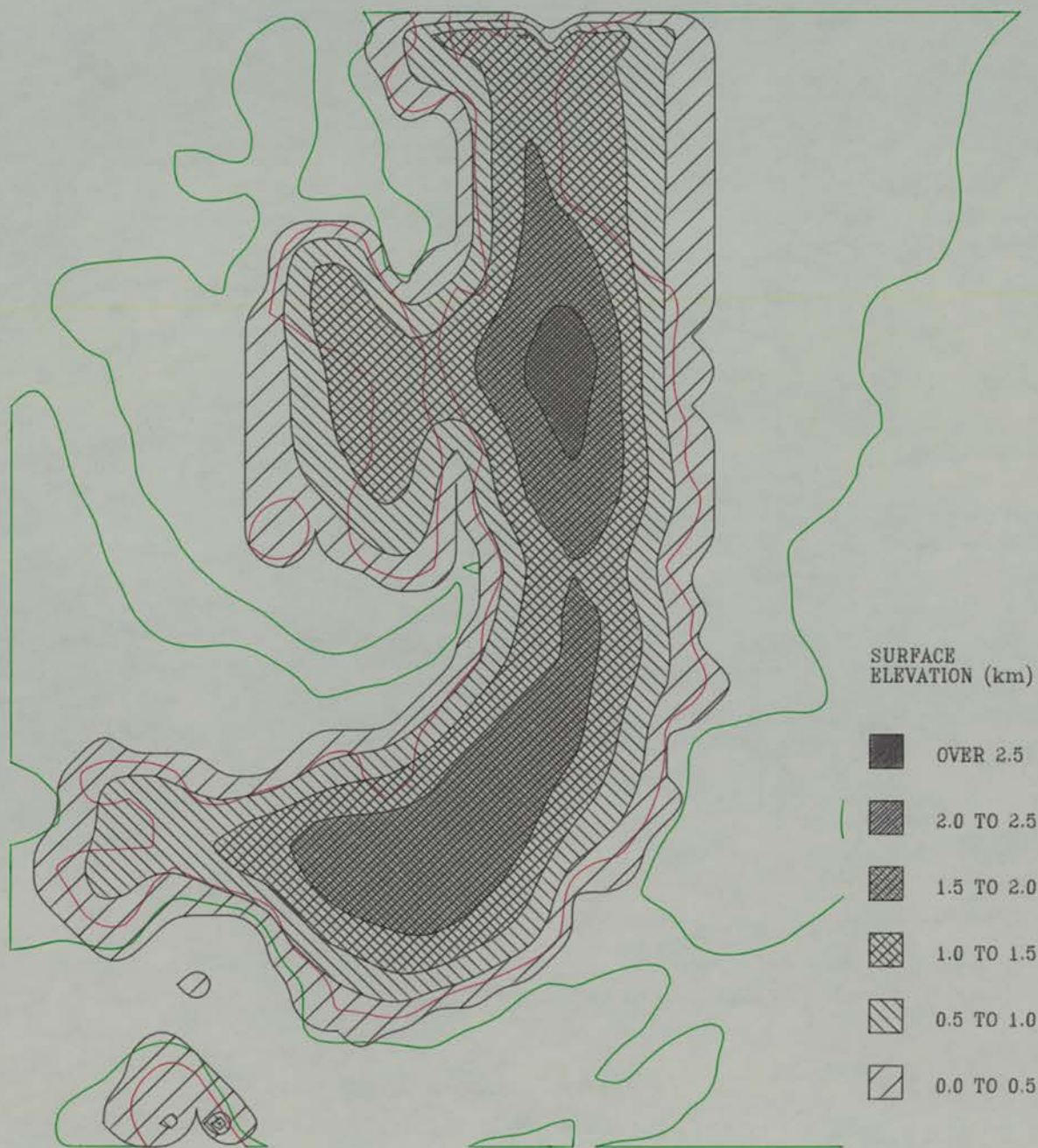
FIGURE 3.26 THE MAXIMUM ICE COVER PREDICTED AT 25.0 KA (15.0 KA BP) BY A MODEL INCORPORATING NO MERIDONAL SURFACE ACCUMULATION GRADIENT. THE RED LINE REPRESENTS SEA LEVEL AND THE GREEN LINE REPRESENTS A WATER DEPTH OF 0.5 KM.

SURFACE ELEVATION (km)

OVER 2.5

2.0 TO 2.5

1.5 TO 2.0

1.0 TO 1.5

0.5 TO 1.0

0.0 TO 0.5
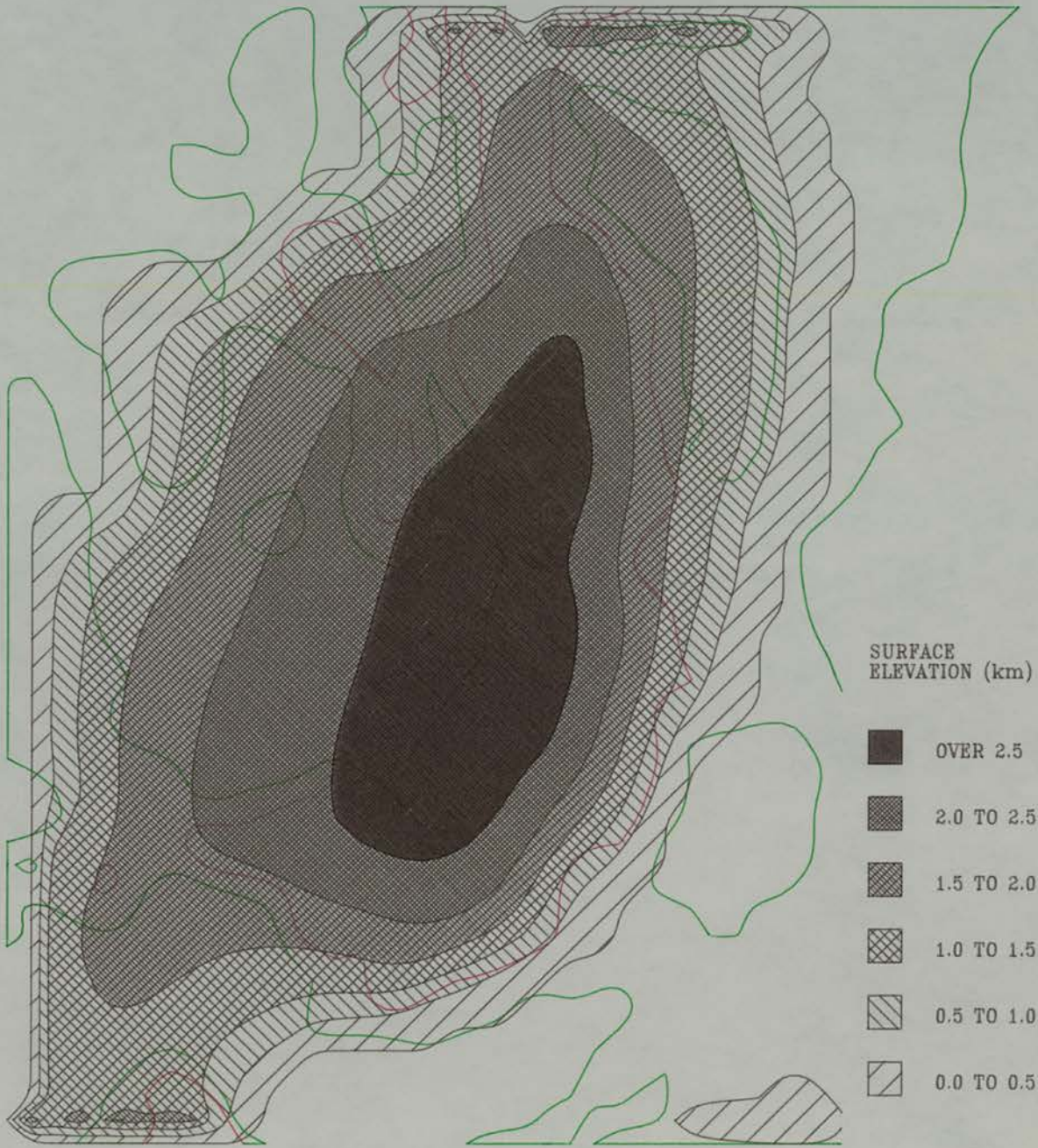
FIGURE 3.27 SENSITIVITY ANALYSIS OF THE EFFECT OF MEAN SURFACE ACCUMULATION ON ICE SHEET GROWTH. THE ICE VOLUME CURVES ARE FOR THE FIRST 10.0 KA OF THE MODEL RUN (40.0 TO 30.0 KA BP).
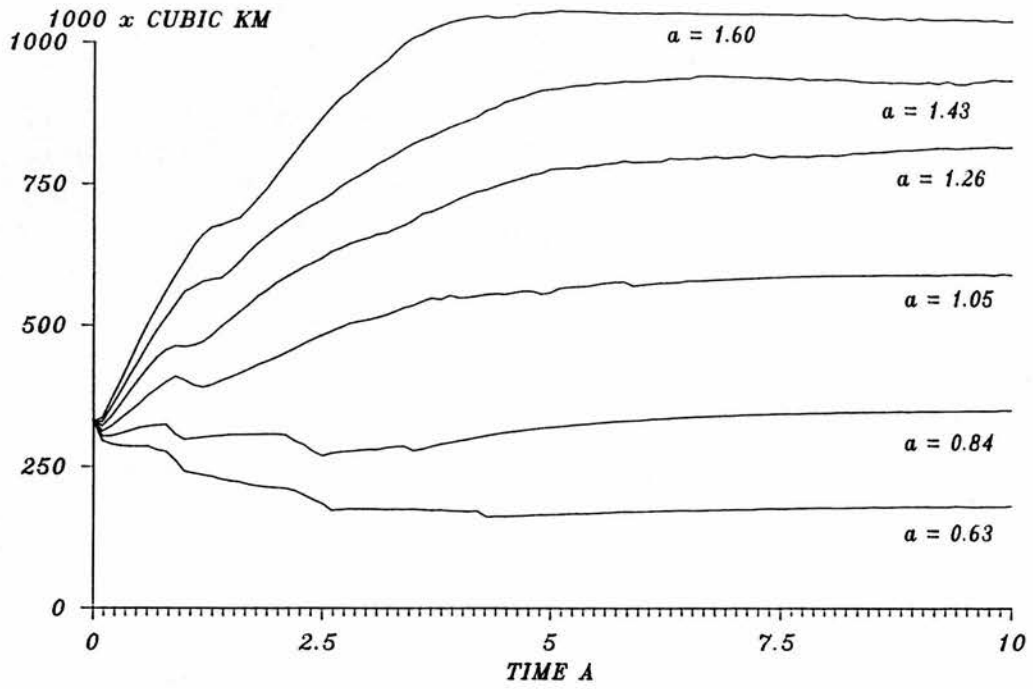
FIGURE 3.28 SENSITIVITY ANALYSIS OF THE EFFECT OF CALVING ON ICE
SHEET GROWTH. THE ICE VOLUME CURVES ARE FOR THE
FIRST 10.0 KA OF THE MODEL RUN (40.0 TO 30.0 KA BP).
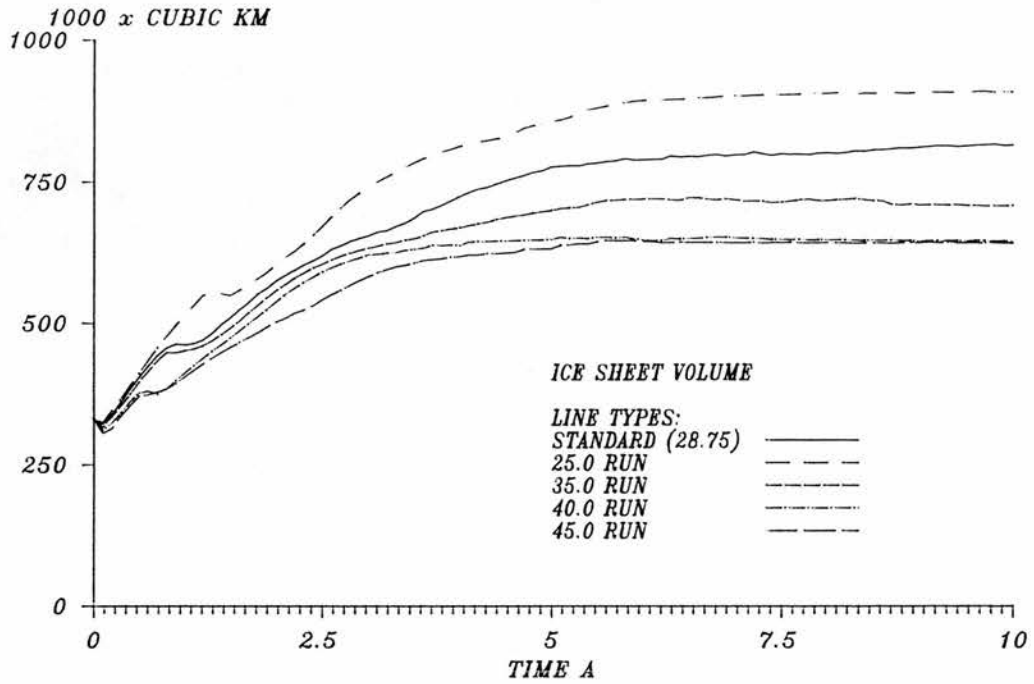
FIGURE 3.29 COMPARISON OF THE ICE VOLUMES PRODUCED BY THE STANDARD
RUN, AND BY A RUN THAT EMPLOYED ONLY SEA LEVEL FORCING
BUT INCORPORATED INCREASED CALVING.

188
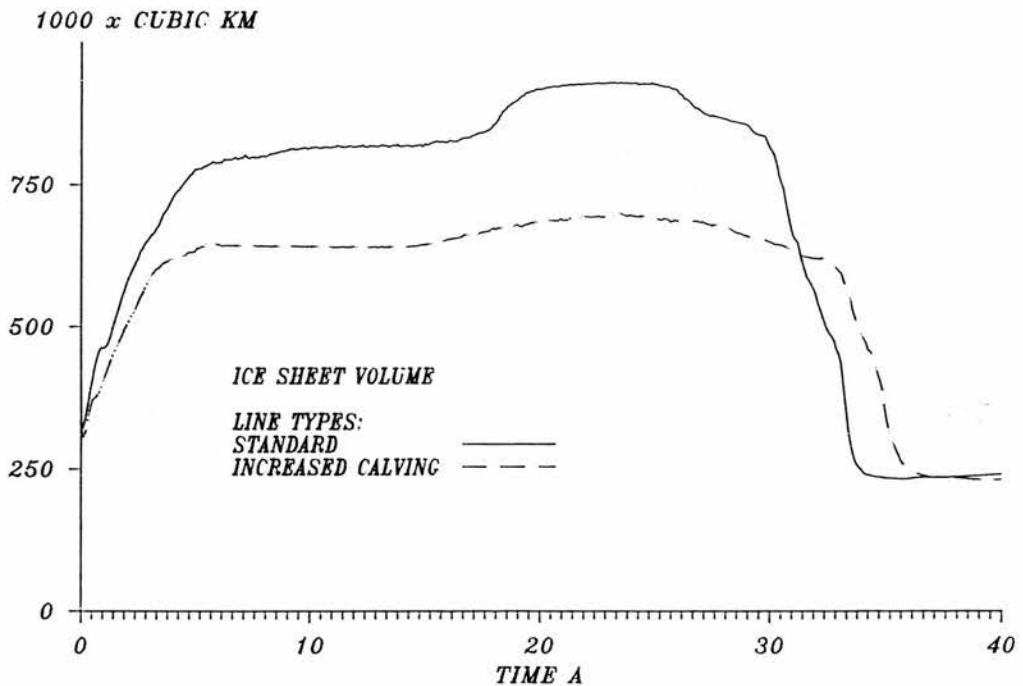
FIGURE 3.30 SENSITIVITY ANALYSIS OF THE EFFECT OF MARINE BASAL MELT ON ICE SHEET GROWTH. THE ICE VOLUME CURVES ARE FOR THE FIRST 10.0 KA OF THE STANDARD RUN (40.0 TO 30.0 KA BP).
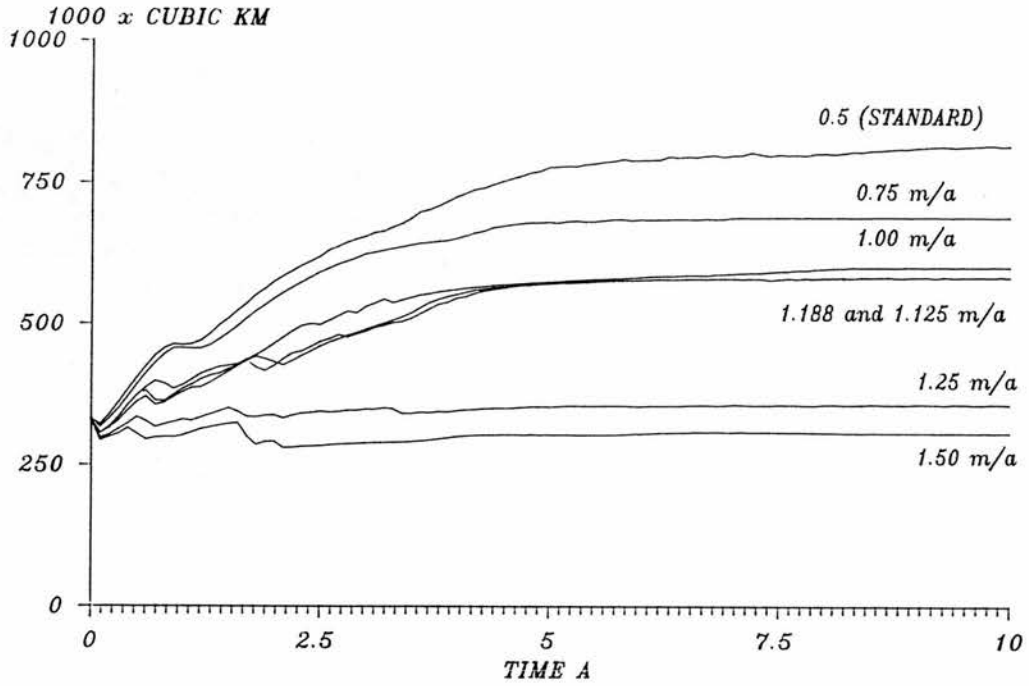
FIGURE 3.31 SENSITIVITY ANALYSIS OF THE EFFECT OF MARINE BASAL MELT ON ICE SHEET DECAY. THE ICE VOLUME CURVES ARE FOR THE LAST 15.0 KA OF THE MODEL RUN (25.0 KA BP TO THE PRESENT).

189
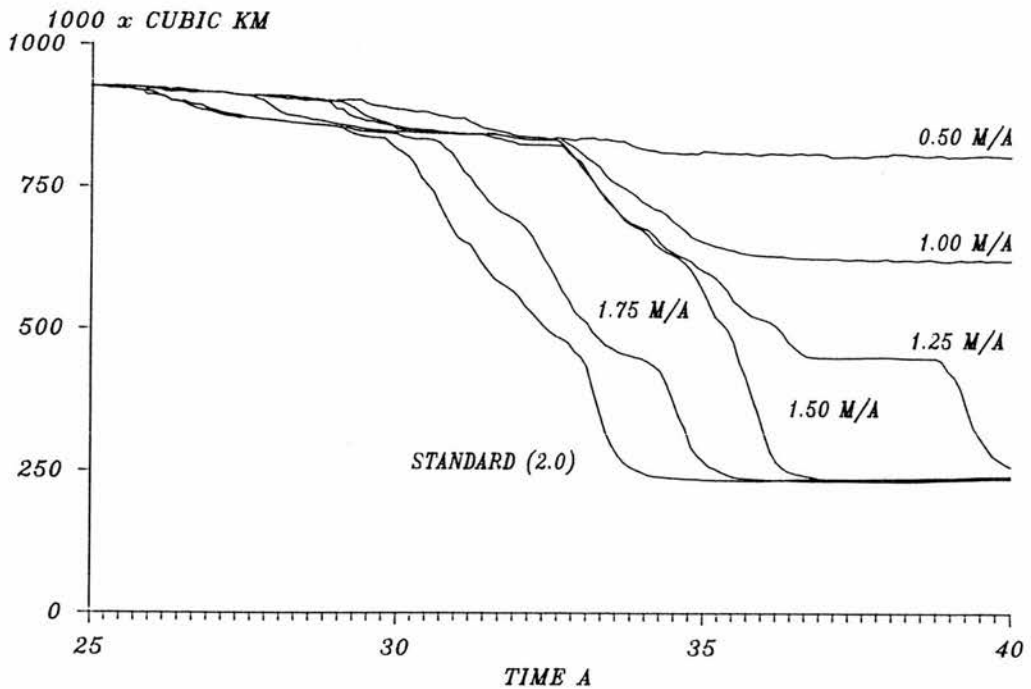
FIGURE 3.32 SENSITIVITY ANALYSIS OF THE EFFECT OF VELOCITY VARIATION
ON ICE SHEET GROWTH. THE ICE VOLUME CURVES ARE FOR THE
FIRST 10.0 KA OF THE MODEL RUN (40.0 TO 30.0 KA BP).
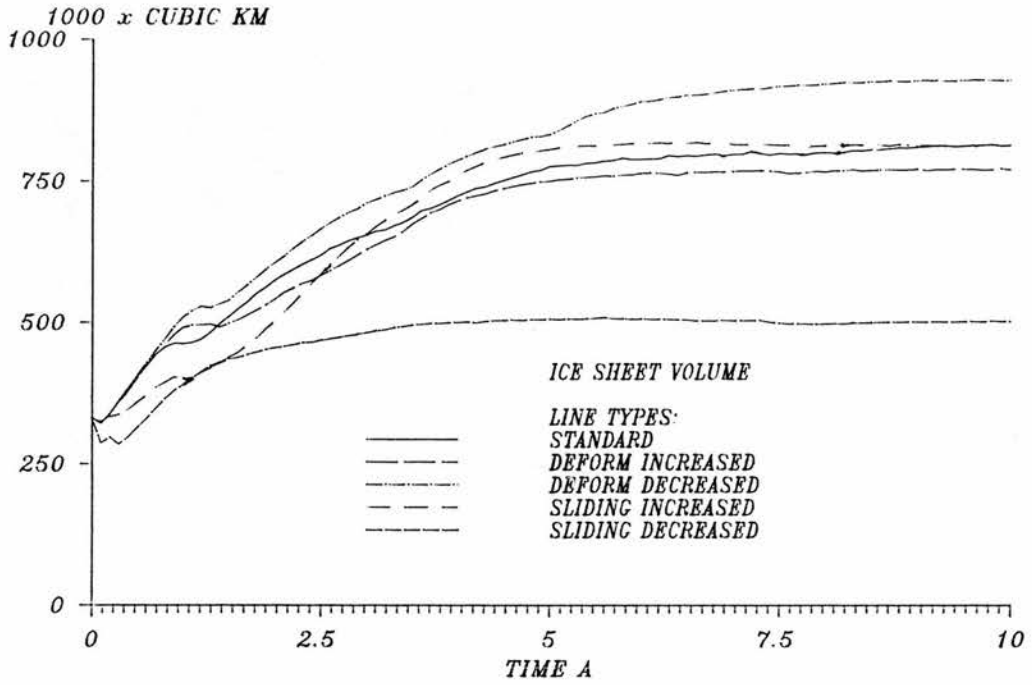
FIGURE 3.33 SENSITIVITY ANALYSIS OF THE EFFECT OF VELOCITY VARIATION
ON ICE SHEET DECAY. THE ICE VOLUME CURVES ARE FOR THE
LAST 15.0 KA OF THE MODEL RUN (25.0 KA BP TO THE PRESENT).
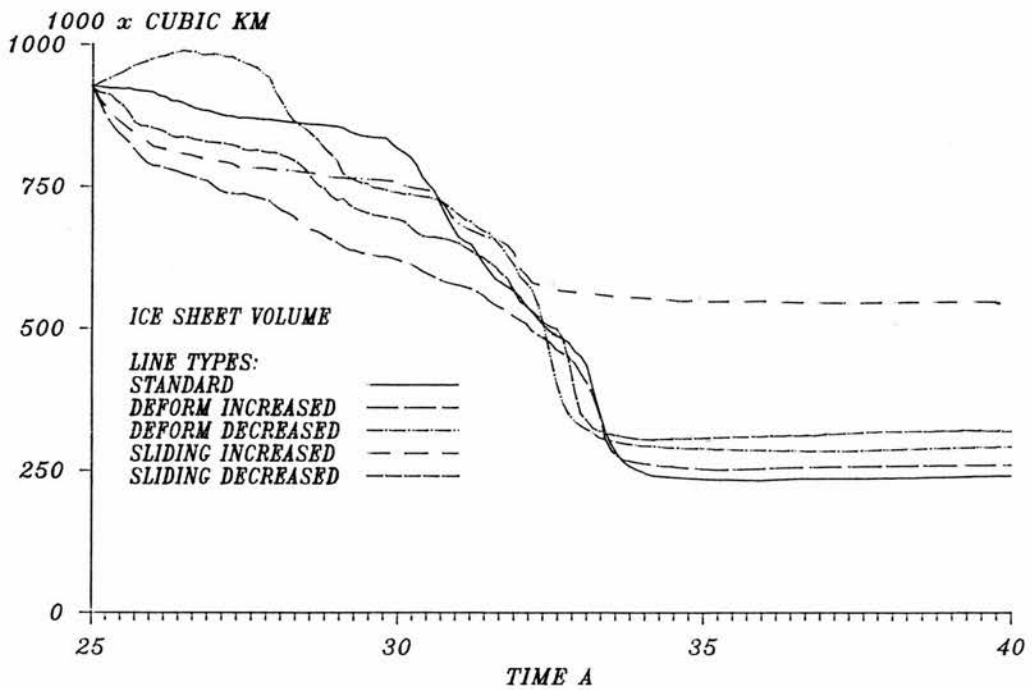
CHAPTER FOUR : THE LOCH LOMOND STADIAL ICE SHEET IN SCOTLAND.

(4.1) THE AIMS OF THE CASE STUDY.

The Loch Lomond stadial in Scotland spanned the period 12.5 to 9.5 ka BP. It saw dramatic changes in regional air temperatures, which initiated the development of a large ice mass in western Scotland. The modelling of this ice mass is a useful case study because a large body of information exists on its form, which can be used as an effective source of test data.

The aims of this case study are:

(i) to use the model to derive estimates of former ice sheet form from a palaeoclimatic input;

(ii) to use these estimates to test the model against field evidence from the area; and, if the model is found to be adequate,

(iii) to use the model to investigate the dynamics of the Loch Lomond ice sheet.

Three particular aspects of ice sheet dynamics are investigated. First, the likelihood of the ice sheet developing an equilibrium form is assessed. The question of whether the ice sheet maximum represented a phase of long term steady state or a fleeting turn-around between phases of growth and decay is also addressed. Second, the model is used to investigate the likely growth and decay rates of the Loch Lomond ice sheet. And third, the model is used to identify the dominant climatic and ice flow factors affecting the ice sheet's behaviour.

(4.2) MODEL MODIFICATIONS AND INPUT DATA.

The model described in Chapter 2 was used with the following three amendments. First, eustatic sea level change was not used as a driving variable. The Loch Lomond ice sheet was almost entirely land-based, thus oceanic changes would have had little influence on the behaviour of the ice sheet. Second, the marine loss terms of calving and basal melt are not applied. Third, isostasy is not incorporated. Sutherland (1981) estimates a relative sea level depression of 4 m at 10.0 ka BP in the Loch Fyne/Loch Long area, which he attributes to isostasy produced by the adjacent Loch Lomond ice mass. This minor effect is well within the limits of the model's accuracy.

The model requires three sets of input data that are specific to the case study. The first set of input data is initial bedrock topography. It is assumed that bedrock topography during the Loch Lomond stadial was similar to the present day Scottish topography. This implies that isostatic recovery from the Devensian maximum ice sheet was at a similar stage to present. This assumption is supported by Sissons (1983), who indicates that relative sea level during the Loch Lomond was within 6 m of the present day level.

192

The envelope topography scheme is employed and the envelope constant ('a' in equation 2.8) is given the value 1.0. This means that the envelope representation of topography is equivalent to the maximum distribution of bedrock altitude (sub-section 2.3.2).

Present day surface elevation contours were digitised from the Ordnance Survey Physical Map of Great Britain (Sheet 2) and from Admiralty Chart Number INT160. The resultant irregularly spaced data was then interpolated onto a rectangular grid of 81 (North-South) by 91 (East-West) 5x5 km elements. Two topographic grids were produced. One grid represents the mean surface altitude within each grid element and the other represents the maximum surface altitude. A contoured representation of the maximum topography is shown in Figure 4.1. The main upland features of the Cairngorms, Lochnagar, Breadalbane, Badenoch, Ben Nevis and the Carn Eige area are all easily recognised, as are the main basins and valleys of Rannoch Moor/Strath Tay, Glen Mor, Braemar, Strath Spey and Strath Conon.

The second model input is precipitation. Again the assumption of a present day distribution is made. The implications of this assumption are discussed later. The distribution of mean annual precipitation rate is based on the same grid as topography and is shown in Figure

4.2. The original data was obtained from Reed and Elliot (1979) and the Meteorological Office (1968). The main features of importance are the orographic enhancement on the West coast and the deep precipitation shadow to the East. The third model input is latitudinal range. This is required in the net mass balance section of the model. The bottom of the grid used in the model lies at 55.7^O North and the top lies at 59.3^O North.

The Scottish place names used in Chapter 4 are shown in Figure 4.3. The three model inputs of topography, precipitation and latitude represent boundary conditions that govern model behaviour but do not change during the course of a simulation. The model is driven by changes in regional air temperature. The derivation of an air temperature record for this area and its integration into the model are discussed in sub-section (2.2.1). Air temperature drives the model via regional changes in both ablation rate and precipitation effectiveness. The model's response to this forcing is via the twin feedback loops of net mass balance/ice thickness/surface elevation and ice thickness/ ice flow.

(4.3) RESULTS : THE STANDARD MODEL AND ITS TESTING.

The results discussed in this section were obtained using the parameter values given in Table 4.1 unless otherwise stated. The model produced output at a

specified time interval, which included total ice volume
and distributions of ice thickness, surface elevation,
velocity and net mass balance. All of the model runs were
for the period 12.5 to 7.5 ka BP. In the following
discussion time is given relative to the model's starting
time of 12.5 ka BP, thus a time of 3.0 ka is equivalent
to 9.5 ka BP.

(4.3.1) The net mass balance model.

Figures 4.4 and 4.5 relate net mass balance to its
four determinants (surface elevation, precipitation,
latitude and imposed temperature depression). The values
used to obtain these graphs are typical of the Loch
Lomond stadial. In each graph net mass balance is the
dependent variable and altitude the independent variable.
The trends for temperature depressions of zero ^{o}C
(present day conditions), -4.0 and -8.0 ^{o}C are shown by
different line types. For each temperature depression
three sets of results are given. Figure 4.4 shows results
for varying latitudes and Figure 4.5 shows results for
varying precipitation rates.

The Equilibrium Line Altitude (ELA) is indicated in
both graphs and is a useful aid to their interpretation.
The model predicts a fall in the ELA of 260 m between the
southern and northern boundaries of the model grid. This
difference is the same for all temperature depressions.

Variation in precipitation also produces shifts in the ELA. For a latitude of 57 ^{O}N an increase in precipitation from 0.8 to 2.4 m a^{-1} leads to an ELA depression of 497 m. This range of precipitation values is typical of the East-West contrast over Scotland, and implies a considerable meridional ELA gradient over the area. This East-West gradient (248 m ^{O}E^{-1}) remains the same for varying air temperature depressions and dominates the spatial distribution of ELA predicted by the model. The latitudinal gradient is minor in comparison to this meridional gradient and amounts to 72 m ^{O}N^{-1}. The spatial distribution of the ELA predicted by the model forms a complex surface, whose altitude varies in response to imposed air temperature depression. The exact rate of ELA change with respect to temperature varies around 180 m ^{O}C^{-1}.

Several calculations were performed to investigate the size of temperature depression required to initiate areas of positive net mass balance and ice accumulation in Scotland. The results are given in Table 4.2, for both mean and envelope (maximum) topographic representations (see sub-section 2.3.2). The envelope representation requires a depression of -3.0 ^{O}C to initiate positive net mass balances, whereas a depression of -6.0 ^{O}C is required by the mean topographic representation. Larger temperature depressions produce a great increase in the

196

area of positive net mass balance. The geographical extent of these areas (Figure 4.6) shows three interesting features. First, the area of positive net mass balance in the Cairngorms is always fairly restricted. Second, the crescent of mountains around Rannoch Moor and the area around Carn Eige are the most likely sites for ice sheet initiation because they have both large precipitation rates and high surface altitudes. Third, outlying areas of net accumulation exist in the North around Ben More Assynt and on the islands of Mull, Skye and Lewis.

(4.3.2) The standard model.

The variation of net mass balance described above is now linked to the rest of the ice sheet model and driven by the use of the air temperature depressions described in sub-section (2.2.1). Predicted ice volume for this standard run is shown in Figure 4.7, as are the temperature changes used to force the model. Ice sheet volume increases exponentially until slightly after the maximum temperature depression. The volume then starts to decrease rapidly and the ice sheet disappears 200 a later.

The exponential nature of ice sheet growth is a consequence of both the increasingly severe temperature depression and the positive feedback between ice

thickness, surface elevation and net mass balance. The former is to be expected from the above discussion on net mass balance trends, while the latter arises because ice accumulation raises surface elevations to higher, cooler altitudes where ablation decreases and precipitation effectiveness increases. The growth and decay of the ice sheet is asymmetrical because the abrupt rise of the ELA at 2.6 ka exposes a large ice sheet surface area to ablation. Ice volume changes during decay are therefore greater than ice volume changes during growth, when smaller ice sheet areas are involved.

Unfortunately the volume output of the model has no equivalent geological record which could be used as a means of testing. The volume estimates obtained from deep sea core oxygen isotope records are correlated to global ice volume and are not applicable to testing at the regional scale of this study. Testing is restricted to model predictions of ice sheet extent and thickness. In common with most former ice sheets, the majority of the available geological evidence concerns the maximum Loch Lomond ice sheet. Evidence of maximum spatial extent can be obtained from geomorphological features such as terminal moraines and drift borders (Lowe and Walker 1984). In addition estimates of ice thickness may be obtained from the mapping of trim-lines, which mark the altitudinal boundary between zones of glacial and

periglacial material (Thorp 1981).

The model predicts that maximum volume is reached at 2.6 ka and ice sheet thickness at this time is shown in Figure 4.8. This prediction can be compared with the geomorphological estimate of Sissons (1979b) shown in Figure 4.9. There is reasonable agreement between the two. The prediction of ice extent over the South-West Grampians and the southern North-West Highlands is good. Local ice is predicted in Lewis, Skye and Mull, which again agrees with field interpretations (Sissons 1974). The quite extensive, though thin, ice cover centred around Ben More Assynt represents an over-prediction in comparison with field evidence, as does the northerly extension of the main ice mass into the An Teallach/Beinn Dearg area. These mismatches probably reflect inaccuracies in the model rather than poor field interpretation because well defined terminal moraines form the main elements of the field evidence in these areas (Sissons 1977).

A likely explanation for this mismatch between field evidence and model prediction is the topographic representation used in the model. The highland areas of the Grampians, Cairngorms and southern North-West Highlands are dominated by plateau-type topography, whereas isolated peaks are more typical of the northerly

199

areas. *The envelope scheme used in the model over-estimates the general altitude of areas with distinct mountain peaks and may be over-predicting in these areas while coping well with the plateau topography of other areas. This error leads to a net mass balance over-prediction in northerly areas but leaves southerly areas unaffected.*

A less dramatic mismatch between model prediction and field evidence lies within the Cairngorm area. The extent of ice here is again over-predicted, although the model does identify the Gaick and Lochnagar ice caps. A potential explanation for this over-prediction is in the assumption of a constant precipitation pattern. If airflow during the Loch Lomond was predominantly westerly then the present precipitation shadow in the East of Scotland is likely to have been deepened by the topographic barrier of the West Grampian ice mass. Precipitation values over the East would therefore have been smaller than those used in the model. Thus the model is probably over-predicting the build up of ice in the Cairngorms.

Predicted ice thickness can also be tested against field evidence. Sissons (1974) estimates ice thicknesses over Rannoch Moor as 400 m, over the head of Loch Lomond as 600 m and over the Gaick plateau as 110 m. These

values are less than the predictions of maximum ice thickness made by the model and possible reasons for this discrepancy are discussed shortly.

There is little field evidence against which ice velocity predictions can be tested, it is therefore sufficient to say that the predicted ice velocity has a fairly uniform distribution and a typical range of 0.01 to 0.15 km a^{-1}.

Where?

(4.3.3) The dynamics of the standard model.

Figures 4.10 and 4.11 show the predicted stages of ice sheet growth and decay. At 1.5 ka air temperatures are sufficiently low for extensive areas of positive net mass balance to develop in the vicinity of Carn Eige and Ben Nevis. After a further 500 a ice covers the majority of uplands above 600 m, with the exception of the easterly mountain plateaux. Comparison with the areas of positive net mass balance shown in Figure 4.6 indicates that the majority of this expansion is caused by the ELA reduction consequent on cooling from -5.6 to -7.2 ^{O}C.

The next 500 a of the run sees volume trebled and extent expanded to cover areas down to 400 m in the West and down to 600/700 m in the East. This expansion is not simply a consequence of the further temperature reduction because ice extends into areas where the topography is

*lower than the predicted ELA. In particular Strath Conon,
Glen Mor and Rannoch Moor are occupied by thick ice but
have bedrock elevations that are too low to allow local
ice accumulation. Ice accumulation in these areas is
caused by ice flow from the adjacent highlands; the ice
thicknesses arising from this flow result in increased
local surface elevations, which exceed the local ELA and
allow snow to accumulate. A strong feedback can then
develop between net mass balance and ice thickness. This
is particularly true of Rannoch Moor, where ice flow
within the basin is constrained on three sides by the
surrounding highlands. The increased outflow that would
normally be associated with increased ice thickness
cannot develop and ice thickening therefore accelerates.*

*In other areas, such as the southern margin of the ice
sheet, the positive feedback between net mass balance and
ice thickness is countered by increased ice outflow. Ice
volumes increase less in these areas because ice can flow
freely to regions of lower surface elevation where
ablation prevails. The accelerated infilling of Rannoch
Moor (and the other topographic basins)   therefore
appears to be a major factor in the exponential increase
of the ice sheet's volume.*

*At 2.5 ka air temperature depression is at a maximum.
However it is not until 100 a later that ice volume*

reaches a maximum. At this time the temperature depression has fallen from -8.0 ^{O}C to -7.6 ^{O}C. In this 100 a period a further 1000 km^3 is added to the ice sheet's volume; however the ice sheet's margins remain almost stationary. The location of these margins is therefore partially divorced from interior volume increases. During this period the altitude at which ablation predominates is fairly constant because air temperature varies only slightly. However increasing interior ice thicknesses appear incapable of increasing ice outflow and extending the margin to lower altitudes. This lack of coupling between interior and margin is a consequence of the restricted ice flow over the mountainous rim of Rannoch Moor.

When air temperatures start their steep rise between 2.6 and 2.8 ka, ice volumes fall dramatically. Figure 4.11 shows the retreat of the ice sheet. Rates of retreat are tied to ice thickness; the areas of greatest thickness (Rannoch Moor and Glen Mor) survive the longest. This scenario is consistent with the stagnation and down-wasting of an ice sheet rather than with active retreat.

The predicted behaviour of the ice sheet over time is difficult to test because it requires evidence from periods other than the maximum. However two specific

field estimates can be used to test the above scenario.
First, the glaciation is constrained by field radiocarbon
dates to have started between 11.8 and 11.3 ka BP
(Sissons 1967, Peacock 1971, and Gray and Brooks 1972)
and to have ended around 10.8 ka BP (Lowe and Walker
1976, and Walker and Lowe 1979). These dates for ice
sheet initiation and termination differ from those of the
model, which predicts extensive glaciation between 2.0
and 2.6 ka (10.5 and 9.9 ka BP). However, these
predictions are sensitive to the dating of the
palaeoecological estimates used to drive the model and
may therefore be inaccurate. The field and model
estimates of the time span of extensive glaciation do
agree and both lie between 0.5 and 1.0 ka.

A second confirmatory set of field evidence is
suggested by Sissons (1974 and 1977). The terminal
moraines of Loch Lomond glaciers are often well formed,
particularly those in the West, but series of concentric
moraines are seldom present. This implies a stable ice
sheet maximum followed by a continuous, rapid retreat.
The stability of the margins at the maximum allows time
for large terminal moraines to form, while their rapid
retreat leaves little time for additional moraines to
develop. The rapidity of the Loch Lomond ice sheet's
retreat is also indicated by the presence of hummocky
moraine. One interpretation of this controversial feature

is that it represents the random dumping of debris from stagnant, down-wasting ice (Sissons 1977). This interpretation agrees with the rapid decay predicted by the model.

The dynamic behaviour of the ice sheet model agrees fairly well with field interpretations and the model has survived testing; thus its dynamics probably reflect the dynamics of the real Loch Lomond ice sheet. The experiments discussed in the next section are therefore used to investigate the dynamics of the model itself and attempt to reveal the underlying mechanics of the response to climatic change.

(4.4) RESULTS : EXPERIMENTS WITH THE MODEL.

The experiments performed on the tested model are summarized in Table 4.3. They fall into two sections. The first section uses a time series of air temperature as its forcing function, and aims to ascertain which areas of the model are critical in determining the model's overall behaviour. This first section is further subdivided into the analysis of net mass balance and the analysis of ice flow. The experiments of the second section employ a constant air temperature input. The discussion concerning the exponential growth of the Loch Lomond ice sheet identified two important factors. They were the progressive increase in imposed temperature

depression and the positive feedback between ice thickness, surface elevation and net mass balance. The aim of the second set of experiments is to isolate the effects of the latter feedback factor.

(4.4.1) Time Dependent Forcing.

Net mass balance sensitivity.

Net mass balance is determined principally by surface altitude; a useful first step in assessing the net mass balance sensitivity of the model is therefore to alter the model's topographic representation. The model was run without the envelope topography, which was used in the standard run. Ice was therefore grown solely on a mean bedrock topography. The ice volume history of this second run is shown in Figure 4.7 and the maximum ice thickness distribution is shown in Figure 4.12. Ice volumes, thicknesses and extent are smaller than those predicted in the standard envelope topography run (maximum volume is only 30 % of the standard run's maximum). This is because overall bedrock elevation is reduced and net mass balances are therefore smaller (Table 4.2). This indicates that the quantities of ice involved in growth and decay are sensitive to the representation of topography. The dynamic behaviour of the mean topography run is, however, similar to the behaviour of the envelope topography run.

206

Net mass balance sensitivity can also be assessed by
repeating the standard, maximum topography run using air
temperature forcing functions that are uniformly 1 ^{O}C
cooler and 1 ^{O}C warmer. This range is similar to the
± 2 ^{O}C error estimated by Atkinson et al (1987) for
Coleoptera reconstructions of air temperature. The
results of this pair of experiments are shown for volume
(Figure 4.13) and for ice sheet extent (Figure 4.14). The
ice sheet in the 1 ^{O}C warmer run reaches a maximum volume
that is only 24 % of the maximum volume achieved in the
original standard run. In contrast the ice sheet in the
1 ^{O}C cooler run reaches a maximum volume that is 251 %
of the original maximum.

The ice sheet produced by the 1 ^{O}C warmer run has a
maximum thickness of 450 m and occupies only the western
highland areas above 600 m. Comparison with the areas of
positive net mass balance shown in Figure 4.6 indicates
that some flow has occurred, but that this is restricted
to highland areas and the infilling of topographic
hollows has not occurred. In contrast the 1^O C cooler run
has a maximum thickness of 1300 m and occupies most of
Western Scotland down to sea level. These results
emphasize the importance of climate as an input to the
model.

An additional experiment was performed to assess whether the model showed a similar sensitivity to precipitation. Rind et al (1986) indicate that Scottish precipitation rates during the stadial were half of their present day values. A run using a precipitation decrease of 50 % and the standard air temperature curve produced both reduced volume (Figure 4.13) and reduced extent (Figure 4.15). In this run ice is restricted to areas above 800 m, and the run achieves a maximum volume that is only 7 % of the standard run's maximum volume. This result implies that the parameterization of climate in the present model is inconsistent with the use of a precipitation rate that is much lower than the present day value. This theme will be discussed further in Chapter 5. However the model does appear to be very sensitive to the variation of both precipitation and imposed air temperature.

Ice flow sensitivity.

It has been established that the model is sensitive to the net mass balance parameters. The following section describes experiments with the flow section of the model and investigates whether a similar sensitivity exists in this section of the model. There are two important velocity parameters, the first is associated with deformation (A) and the second is associated with sliding (K_2). Four model runs were completed using the standard

model and the standard input data. In each run one of the two parameters' value was either increased or decreased by 50 %.

The ice volumes attained in these four runs are shown in Figure 4.16 and their maximum ice thickness distributions are shown in Figures 4.17 to 4.20. The model is less sensitive to these velocity parameters than to the net mass balance parameters. For example, a 50 % decrease in K_2 produces only a 17 % increase in maximum volume, and a 50 % increase in K_2 reduces maximum volume by only 11 %.

These velocity experiments also indicate that varying the sliding parameter by a fixed fraction of its value has a greater effect than varying the deformation parameter by the same fraction. Thus a 50 % change in the value of the sliding parameter has a greater effect on ice sheet volume than a 50 % change in the deformation parameter's value. This is somewhat surprising because the sliding law was originally derived from marine ice streams. The Loch Lomond ice sheet was almost entirely land-based, so deformation is likely to have been the dominant velocity component.

The model may be more sensitive to sliding because a 50 % change of value represents a greater proportion of

the natural variation of the sliding parameter than of the deformation parameter. The deformation parameter can vary by an order of magnitude (Paterson 1981), a change of ± 50 % change is thus comparatively minor. The papers in which the sliding law was derived (Budd et al 1984, 1985) quote no range for the parameter, however it is unlikely to vary by an order of magnitude. Variation by a fixed fraction may therefore perturb the sliding parameter more that the deformation parameter.

The maximum thickness distributions for runs in which the deformation parameter was varied (Figures 4.19 and 4.20) show few differences compared to the standard run (Figure 4.8). However the runs in which the sliding parameter was varied have slight differences (Figures 4.17 and 4.18). In general both of the latter have similar extents to the standard, while thicknesses are greater when sliding is reduced and are decreased when sliding is increased. These differences arise through the feedback mechanism of net mass balance, ice thickness and surface elevation. In a run where ice velocity is reduced the surface elevation of the accumulation area is higher than in the standard run. Surface elevation/net mass balance feedback is therefore stronger and ice accumulates more rapidly. This results in a generally thicker ice sheet with a larger volume. The reverse argument applies in a run with reduced velocity. Despite

the above mechanism the sensitivity of the ice flow parameters is minor in comparison to that of the net mass balance parameters.

(4.4.2) Constant forcing.

The above discussion concerned the model dynamics associated with a time dependent air temperature history. The following section investigates the dynamics associated with constant forcing. The principal interest in studying model response to constant forcing is to isolate the contribution of internal feedback to ice sheet growth.

The likelihood of steady state.

As a first step it is useful to ascertain whether an ice sheet that is the size of the Loch Lomond maximum can be maintained in steady state by a constant air temperature. Figure 4.21 presents the results of a series of experiments which attempted to maintain such an ice sheet in steady state. The first 2.6 ka of these runs is identical to the standard run, but the rate of warming after 2.6 ka is progressively reduced. Warming rates of 0.011 and 0.006 ^oC a^{-1} (in comparison to the standard rate of 0.025 ^oC a^{-1}) are both sufficient to induce rapid decay. However, the latter rate allows a slight volume increase to occur before this decay. It appears that slow growth is possible when the temperature depression is in

excess of -6.25 ^{O}C. To test this idea a further experiment was performed in which the temperature depression subsequent to 2.8 ka was limited to -6.25 ^{O}C and held at this level for 500 a. A constant volume ice sheet is maintained, the thickness distribution of which is in steady state. It therefore appears that, given an ice sheet similar to that in Figure 4.8:

(i) a temperature depression in excess of -6.25 ^{O}C leads to continued growth;

(ii) a temperature depression smaller than -6.25 ^{O}C leads to decay; and

(iii) a temperature depression of -6.25 ^{O}C leads to a steady state.

The importance of net mass balance/ice thickness/surface elevation feedback.

The above conclusions apply only to an existing Loch Lomond ice sheet. It is now interesting to investigate the consequences of a constant temperature depression without a pre-existing ice mass. This allows an assessment to be made of the roles of topography and ice sheet internal feedback in determining rates and patterns of ice sheet growth.

The volume response of the standard model (Table 4.1) to various constant air temperature depressions is shown in Figure 4.22, which should be compared to a typical Loch Lomond maximum ice volume of 6000 to 7000 km^3. Two modes of behaviour are apparent. First, small temperature

212

depressions produce small, steady state ice sheets. Second, more severe temperature depressions initiate ice sheets that continually expand.

This abrupt jump between modes of behaviour, known as bifurcation, arises because of the topographic variation in the model. Once a highland ice sheet has developed the present model provides two ways in which it can expand to a steady state; by altitudinal flow or by latitudinal flow. In the former, flow is over fairly short distances and transfers ice accumulated at higher altitudes to lower altitudes where it can be lost via ablation. In the second mode of behaviour flow within an ice sheet carries ice over far wider distances from accumulation areas in high latitudes to ablation areas in lower latitudes. This second case is associated with far larger ice sheets.

The $-6.5\ ^{O}C$ and $-6.625\ ^{O}C$ model runs (Figure 4.22) provide contrasting examples of steady state and continually expanding ice sheets; they also illustrate the key role of temperature depression in switching between these modes of behaviour. The $-6.5\ ^{O}C$ run is an example of a small ice sheet reaching dynamic equilibrium by altitudinal flow alone. This situation is illustrated in Figure 4.23 and is only possible if there is sufficient altitudinal variation for a large contrast to

exist between rates of accumulation and ablation.

More severe temperature depressions compress the altitudinal width of the ablation zone and therefore make the potential ablation sink less effective. The -6.625 ^{o}C run is an example of this. Ice sheet extent during this run is shown at successive 1.0 ka intervals in Figures 4.24 to 4.27. After 1.0 ka the ice sheet in this run (Figure 4.24) is very similar to the steady state ice sheet of the -6.5 ^{o}C run (Figure 4.23). However the additional temperature depression of the -6.625 ^{o}C run allows accumulation to overcome ablation and the next 1.0 ka sees continued ice sheet expansion (Figure 4.25), in particular ice is present at 500 m above sea level in Rannoch Moor. After 3.0 ka this Rannoch Moor ice is thick enough to become part of the ice sheet's accumulation area (Figure 4.26). At this stage the ice sheet's volume is growing rapidly and by 4.0 ka a large ice sheet of 4972 km^{3} has developed (Figure 4.27). The ice sheet continues to grow until the end of the model run. The only way that such an ice sheet can reach steady state is by latitudinal flow, which balances ice accumulation in northerly areas by ice ablation in more southerly areas. In the present model ice sheets that have outgrown local topographic variation must therefore expand until they reach latitudinal constraints.

The above discussion illustrates the role of temperature depression in determining ice sheet volume bifurcation. The actual mechanism that leads to bifurcation is now investigated. This mechanism is intimately linked to topography. The ice sheet extents shown in Figures 4.23 to 4.27 indicate that volume growth is largely a consequence of ice sheet dynamics in the Rannoch Moor area, because the major difference between the $-6.5\ ^{o}C$ run and the $-6.625\ ^{o}C$ run is the infilling of Rannoch Moor. The North-West Highlands ice sheet has a more passive role. Ice sheet expansion in this area is minimal during the first 4.0 ka of the $-6.625\ ^{o}C$ model run. In addition the extent of the North-West Highland ice sheet in the $-6.625\ ^{o}C$ is similar to that in the $-6.5\ ^{o}C$ run.

The topography of the North-West Highlands forms a relatively simple North-South ridge (Figure 4.1). Ice sheet growth away from this ridge's accumulation area is constrained by ablation at lower altitudes. This ridge-type topography means that the size of the area above the ELA is not particularly sensitive to temperature variation and ice sheet extent varies consistently with different temperature depressions. There is also little opportunity for volume expansion via net mass balance/ice thickness/surface elevation positive feedback, because increased ice thicknesses are associated with greater

outflow and increased ice wastage in the ablation zone.

In contrast the Rannoch Moor area is associated both with a pronounced sensitivity to imposed temperature depression and with volume expansion via the net mass balance/ice thickness/surface elevation loop. As discussed above, Rannoch Moor is susceptible to accelerated infilling because of its basin shape. This mechanism implies a sensitivity to imposed temperature depression because there is a limit to the capacity of the Moor to ablate incoming ice flow. Once this limit is exceeded, local ice accumulation can occur and the ice sheet's overall accumulation area becomes vastly increased.

In summary, the model shows three modes of behaviour when it is run without a pre-existing ice sheet:

(i) if the temperature depression is less than -3.0 ^{o}C, no ice accumulates;

(ii) if the temperature depression is between -3.0 and -6.5 ^{o}C, small steady state ice masses develop; and

(iii) if the temperature depression is in excess of -6.5 ^{o}C, large ice sheets develop.

The ice sheet volumes produced by the second, steady state mode of behaviour are considerably less than the size of the maximum ice sheet predicted by the standard model. Imposed temperature determines the model's mode of behaviour. However the transition between control by

altitudinal flow (producing small, steady state ice sheets) and control by latitudinal flow (producing large, expanding ice sheets) is determined by topography. In particular the Rannoch Moor basin is crucial in determining the nature of this transition.

The influence of the topographic representation on net mass balance/ice thickness/surface elevation feedback.

The above discussion places much emphasis on the role of topography in determining ice sheet response to climatic change. A reasonable next stage is to explore whether such a response is sensitive to the topographic representation used in the model. A series of constant temperature depression runs were completed in which the standard model's envelope scheme and was replaced by a mean topographic representation. The resultant volume curves are shown in Figure 4.28.

Ice volumes still bifurcate with imposed temperature depression, but this bifurcation occurs at more severe temperature depressions than in the standard run. A volume of around 2000 km^3 again appears critical, because a temperature depression of -7.0 ^{o}C leads to continuous growth, while a depression of -6.85 ^{o}C produces a near steady state ice sheet of 1474 km^3.

The curves in Figure 4.28 have two crossing points which are related to topography. These are at 2.0 ka between the -6.5 and -6.75 ^{O}C runs, and at 2.6 ka between the -6.85 and -6.9 ^{O}C runs. Figures 4.29 and 4.30 display ice sheet extent at 5.0 ka for the -6.85 and -6.9 ^{O}C runs. In the -6.85 ^{O}C run ice is limited to the North-West Highlands above 500 m. However, in the -6.9 ^{O}C run ice covers both the North-West Highlands and the Rannoch Moor area. The additional 0.05 ^{O}C temperature depression must therefore initiate sufficient extra accumulation around Rannoch Moor for ice to flow into and fill the Moor. The ice sheet in the -6.85 ^{O}C run reaches steady state after 2.1 ka because it is limited to the North-West Highland 'ridge', while the ice sheet in the -6.9 ^{O}C run continues to grow because of the infilling of Rannoch Moor. This illustrates the different ice sheet dynamics associated with 'ridge' and 'basin' topographies, and leads to the crossing of the two volume curves.

The volume curves in Figures 4.22 and 4.28 have contrasting types and degrees of inflection. Here inflection is defined as the transition from a decelerating rate of volume increase to an accelerating rate of volume increase, or vice versa. The former case is termed upward inflection, while the latter is termed downward inflection. The standard envelope topography runs show significant upward inflection, this is

particularly true of the -6.625^O C run. However the mean topography runs have either no inflection or slight downward inflection. This contrast arises from the use of an envelope topography and from the link between a point's surface elevation and its net mass balance.

In the envelope topography runs the net mass balance of a point is determined using either the point's maximum bedrock altitude or the sum of its mean bedrock altitude and its ice thickness, depending on which is the greater. Initially, ice thicknesses in the accumulation area of an ice sheet are shallow and the maximum bedrock elevation is used to determine net mass balance. At this stage overall accumulation input to the ice sheet remains constant because net mass balance values are determined by the constant altitude of hill tops. However lateral ice flow to lower altitudes increases both ablation and overall ice loss from the ice sheet. The constant rate of input and the increasing rate of output lead to a decelerating rate of ice sheet volume growth.

Eventually ice in the accumulation area of the ice sheet becomes thick enough to inundate the maximum bedrock topography (ice thickness is greater than the difference between maximum and mean bedrock altitude). As this happens accumulation ceases to be constant and begins to increase as surface elevations rise. The

overall input to the ice sheet begins to increase because progressively more nunataks become engulfed by ice. The rate of volume growth therefore starts to accelerate and a point of upward inflection is created.

The mean topography runs do not have upward inflection. This is because there is no phase of constant ice input and increasing ice output. Net mass balance in the ice sheet accumulation area is always determined by mean bedrock altitude plus ice thickness. Net mass balance must therefore increase as soon as ice forms and continues to increase as surface elevations rise. The overall growth rate of the ice sheet accelerates until ice flows to lower altitudes and suffers ablation, at which point the input rate is countered by a rapidly increasing ablation output rate. Volume growth thus switches from an accelerating rate of increase to a decelerating rate of increase, and a point of downward inflection is created.

Despite this contrast in the rate of ice sheet volume growth, the topographic representation used in the model has little effect on the basic bifurcation of ice volume with imposed temperature depression.

The influence of ice flow on net mass balance/ice thickness/surface elevation feedback.

Changing ice sheet velocity has also been found to

have an effect on net mass balance, because of its association with ice thickness. A further constant temperature experiment was therefore performed to assess this mechanism's influence on bifurcation. The standard envelope model was employed with a sliding constant (K_2) 1.5 times the original. Comparison of this run (Figure 4.31) with the standard (Figure 4.22) shows that increasing the sliding constant has little effect on the model's bifurcation but increases the degree of inflection in individual volume curves. This is particularly true of the -6.75 ^{O}C run, which closely approaches steady state, whereas previously it showed only slight inflection.

This behaviour can be explained by the fact that outflow from the accumulation area is greater than in the standard run. Ice thicknesses in the accumulation area are therefore less than in the standard run. This leads to an increase in the time required for ice thickness to overcome the envelope topography, which results in a greater degree of volume inflection because net mass balance calculations rely on the constant maximum topography for a longer period of time.

These three experiments reveal that the bifurcation of ice volume with temperature depression is a stable feature of the system. This behaviour can now be related

221

to larger, Loch Lomond sized ice sheets. A temperature depression of -6.25 ^{O}C allows a pre-existing Loch Lomond sized ice sheet to reach steady state. But the same depression is not sufficient to allow the growth of an ice sheet of similar size from an initially ice-free state. The difference between the temperatures needed to initiate an ice sheet and to maintain an ice sheet in a steady state arises from the need to counter the ice sheet's inherent positive net mass balance/ice thickness/surface elevation feedback. This feedback loop is a source of hysteresis within the ice sheet system because the effect of a specific temperature input differs according to the ice distribution already present. The current model implies that a steady state ice sheet of the Loch Lomond's size could not develop as the result of a constant temperature depression.

(4.5) CONCLUSIONS.

This case study uses a general ice sheet model to study the Loch Lomond stadial in Scotland. The model links many separately derived components in order to simulate the growth and decay of an ice sheet. The main model inputs are the distributions of precipitation and bedrock elevation, both of which remain constant throughout a model run. The model is driven using an estimated July air temperature time series and produces predictions of ice sheet extent, thickness and net mass

balance. The model forms a link between independent palaeo-climatic and glacial geomorphological reconstructions. The former drive the model, while the latter are used to test it.

Output from the model indicates that the Loch Lomond ice sheet was highly dynamic. Once air temperatures fall sufficiently to allow local ice accumulation, ice volumes rise exponentially. This exponential rise is a consequence of both the progressive nature of the air temperature decline and the positive feedback within the ice sheet system. The latter arises when ice accumulation raises the ice surface elevation. This leads to a further increase in ice accumulation because ice surface temperatures are cooler, ablation is reduced and precipitation effectiveness is increased. However, this feedback loop is not strong enough to allow significant ice volume growth after temperatures begin to rise. Ice sheet retreat is extremely rapid and is dominated by ablation over virtually the whole ice surface.

Field evidence allows the model to be tested. Tests are made in relation to ice sheet maximum extent and thickness, and in relation to the ice sheet's residence time and the nature of its decay. This field evidence and the model's predictions agree tolerably well.

The model's behaviour has several interesting features that concern the dynamics of ice sheet growth and decay. In the model maximum ice sheet volume is a fleeting turn-around between phases of rapid growth and decay, while ice sheet maximum extent is a fairly long lived feature. Temperature is relatively constant for 200 a around the maximum depression. During this period ice volumes vary dramatically. This volume change can be attributed to internal net mass balance feedback. However it is not associated with similar changes in ice sheet extent. It appears that the relatively constant temperature during this period can stop the margins of the ice sheet advancing but cannot control the thickening of the ice sheet's interior. During this period the ice sheet's interior and its margins appear to exhibit partially independent behaviour. This type of model prediction implies that a high resolution topographic representation is important in the modelling of small ice masses and that the use of either steady state or flowline modelling techniques may not capture the essential features of the system.

The nature of the ice sheet's response to climatic change is more easily studied if model behaviour is simplified. To this end a number of experiments were performed using a constant temperature depression. The above description of ice sheet behaviour indicates that

strong feedback within the ice sheet system can lead to rapid variations in ice volume. Despite this a Loch Lomond maximum ice sheet can be maintained in steady state with a constant temperature depression of -6.25 ^{O}C. In this case ice accumulation, ablation and flow balance each other so that ice thicknesses remain constant through time. This demonstrates that it is possible to constrain the ice sheet's positive net mass balance feedback loop.

The effects of this net mass balance loop were investigated with several model runs using constant imposed temperature and an initially ice-free topography. Three types of behaviour occur. First, for temperature depressions smaller than -3.0 ^{O}C no ice develops. Second, for temperature depressions between -3.0 and -6.5 ^{O}C, small steady state ice sheets develop. Third, for temperature depressions in excess of -6.5 ^{O}C ice sheets expand continuously. The second and third cases differ in the degree to which the positive net mass balance feedback loop is constrained. In the second case (as in the steady state maximum ice sheet above) the loop is constrained by ice flow within the ice sheet, while in the third case this flow is insufficient to stop ice sheet growth.

Two implications arise from these experiments. The first concerns the conditions necessary to develop a Loch Lomond maximum sized ice sheet of between 6000 and 7000 km³. The temperature depression required to develop a 6000 km³ ice sheet (greater than -6.5 °C) is in excess of the temperature depression needed to maintain steady state once this size has been reached (-6.25 °C). This illustrates the non-linearity of the ice sheet system, which stems principally from the net mass balance feedback described above.

A second feature is the contrast between small steady state and continuously expanding ice sheets. Detailed analysis of the output from individual runs reveals that this bifurcation is caused by the topographic representation used in the model. Varying bedrock elevations allow a spectrum of net mass balance conditions to exist within the model because net mass balance is strongly dependent on altitude. Small steady state ice sheets can exist because there is sufficient contrast between highland positive net mass balances and adjacent lowland negative net mass balances. Further temperature depression reduces ablation, allowing larger ice sheets to develop and expand continuously. The amplitude of relief is therefore important in determining ice sheet response to climatic change.

The spatial distribution of topography also influences this response. Two particular cases have been discussed; those of basin and ridge type topographies. An ice sheet developed on ridge topography responds to climatic change more uniformly than an ice sheet developed on basin topography. In the former case the effect of variation in net mass balance on ice thickness is buffered by changes in ice flow. For instance a temperature drop increases net mass balance, and leads to larger ice thicknesses and greater ice flow downhill to areas where ablation predominates. This produces an increase in overall ablation which counters the initial increase in ice accumulation. The behaviour of ice sheets developed on basin topography is not buffered to the same extent. This is because ice flow within the hollow of the basin is restricted by the surrounding bedrock walls. This produces a threshold in ice sheet response to climatic change. Up to a certain point local ablation within the bedrock hollow can cope with ice inflow from the adjacent highland areas and a steady state can exist. Beyond this point ice flow from the highlands overcomes local ablation and accelerated infilling of the hollow is initiated.

The effect of topography on ice sheet behaviour persists through several different versions of the model and is a stable feature of the model. It may therefore be

important in the behaviour of real world ice sheets, particularly where the ice sheet is small and occupies an area of varied topography. This case study predicts that ice sheet behaviour in the North-West Highlands of Scotland is determined by ridge topography. While ice sheet behaviour in the South-West Grampians is determined by basin topography. Ice sheet response to climatic change is therefore more abrupt in the South-West Grampians. Bifurcation of the Loch Lomond ice sheet's overall volume with temperature depression is caused by the behaviour of the western Grampian ice sheet, while the North-West Highlands ice sheet has a more passive role in determining overall dynamics. These predictions need to be tested against field evidence, however the appropriate evidence is not yet available.

It is clear from these constant temperature experiments that the way in which the model responds to climatic change is both complex and strongly determined by topography. Both the topography's amplitude and its geographical distribution are important in determining this response. Further experiments indicate that behaviour of the ice sheet model is far more sensitive to the representation of climate than to the parameterization of ice flow.

The model determines deformational and sliding velocities from ice thickness and surface slope. Variation in the exact form of these relationships does not affect model ice sheet behaviour significantly. In contrast the variation of either the imposed air temperature time series or the precipitation input leads to dramatic changes in model behaviour. It therefore appears that more importance should be attached to the modelling of the interaction between ice sheet and climate than to the nature of the flow within the ice sheet.

<u>Table 4.1</u> <u>Summary of the parameter values used in the standard</u>
<u>run of the model.</u>

Parameter	Standard value	Units
<u>Net mass balance</u>		
lapse rate	6.5	$^{o}C\ km^{-1}$
July to annual temperature correction	2.571	--
effectiveness		
-linear function		
-intercept	-0.698	--
-latitude multiplier	0.014	$^{o}N^{-1}$
-elevation multiplier	0.224	km^{-1}
ablation		
-exponential function base 10		
-intercept	5.708	$m\ a^{-1}$
-latitude multiplier	-0.071	$m\ a^{-1}\ ^{o}N^{-1}$
-elevation multiplier	$0.833\ x\ 10^{-3}$	a^{-1}
precipitation		
-elevation multiplier	$0.5\ x\ 10^{-3}$	a^{-1}
<u>Ice flow</u>		
deformation		
-flow law multiplier	$5.3\ x\ 10^{-33}$	$m^3 s^5 kg^{-3}$
-flow law power	3.0	--
sliding		
-sliding law multiplier	$5.0\ x\ 10^6$	$m^3 (bar\ a)^{-1}$
-minimum ice thickness at which sliding occurs	0.1	km
maximum velocity constraint	2.0	$km\ a^{-1}$
gravitational acceleration	9.81	$m\ s^{-2}$
density of ice	870.0	$kg\ m^{-3}$
<u>General</u>		
grid unit	5.0	km
time step	1.0	a
topographic representation	maximum	

<u>Table 4.2</u> <u>The predictions of the model for areas of positive</u>
<u>net mass balance over Scotland. Given as a function of</u>
<u>temperature depression, for both the envelope and the</u>
<u>mean topographic representations.</u>

Imposed temperature depression $^{\circ}C$	Area with positive net mass balance (km^2)	
	Envelope representation	Mean representation
3.0	25	--
4.0	225	--
5.0	1425	--
6.0	3750	90
7.0	7950	1450
8.0	14925	6725

<u>Table 4.3 Summary of the experiments carried out using the model, showing relevant figures and, for the runs in sub-section (4.4.1), the maximumvolume achieved as a percentage ofthe standard run's maximum volume.</u>

Description	Relevant Figures			Effect on volume (%)
	Volume	Thickness	Extent	
Standard	4.7	4.8	4.10 4.11	100
<u>Sub-section (4.4.1)</u>				
mean topography	4.7	4.12	--	30
1 °C warmer	4.13	--	4.14	24
1 °C cooler	4.13	--	4.14	251
precipitation halved	4.13	4.15	--	7
sliding constant x 0.5	4.16	4.17	--	117
sliding constant x 1.5	4.16	4.18	--	89
deformation constant x 0.5	4.16	4.19	--	102
deformation constant x 1.5	4.16	4.20	--	98
<u>Sub-section (4.4.2)</u>				
reduced rates of warming	4.21	--	--	--
constant temperature: standard	4.22	--	4.23 4.24 4.25 4.26 4.27	--
mean topography	4.28	--	4.29 4.30	--
sliding constant x 1.5	4.31	--	--	--

FIGURE 4.1 A CONTOURED REPRESENTATION OF THE PRESENT DAY BEDROCK TOPOGRAPHY, WHICH IS USED AS THE TOPOGRAPHIC INPUT IN THE MODEL.

BEDROCK
ELEVATION (km)

OVER 1.0

0.8 TO 1.0

0.6 TO 0.8

0.4 TO 0.6

0.2 TO 0.4

0.0 TO 0.2
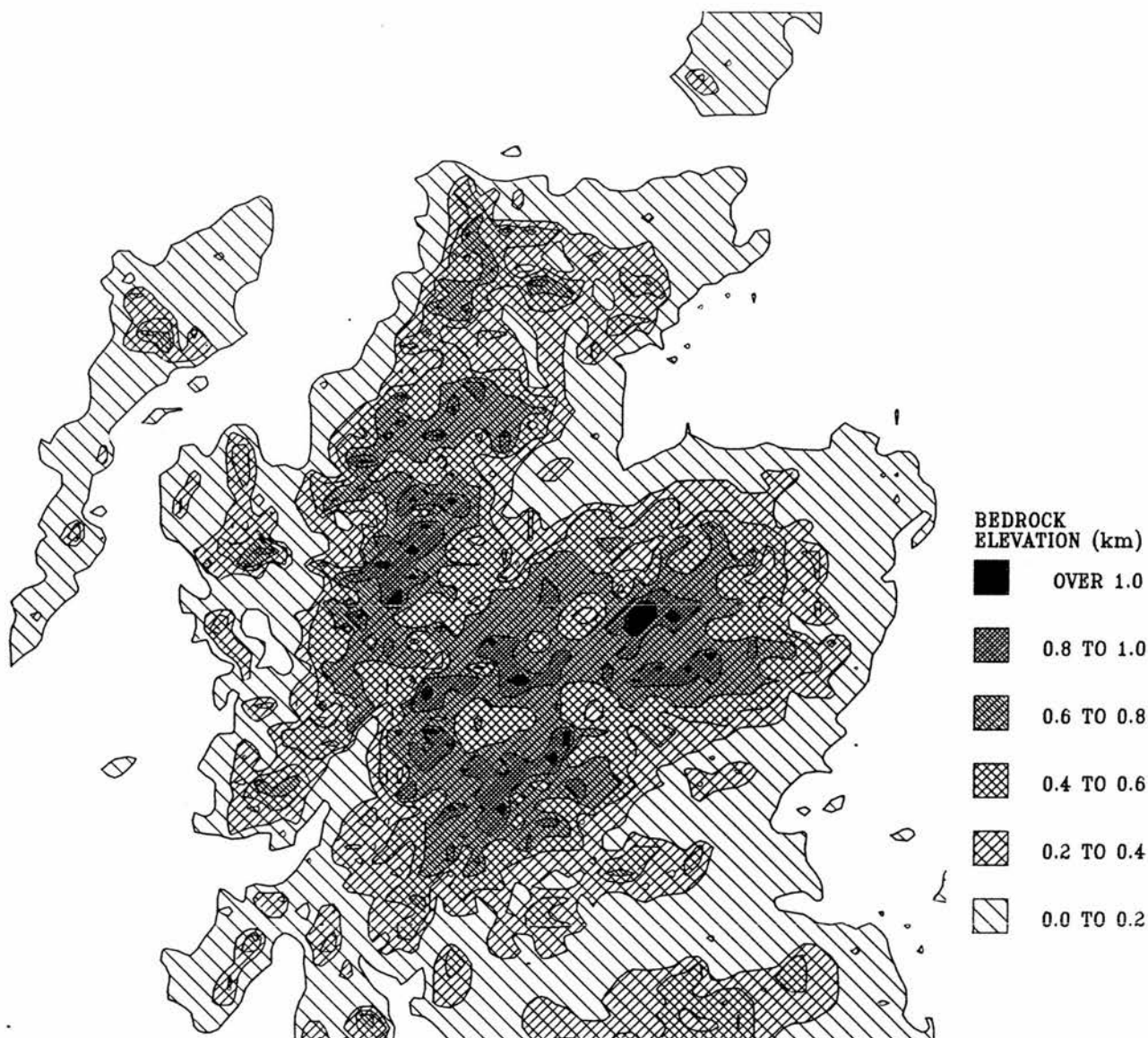
FIGURE 4.2 A CONTOURED REPRESENTATION OF THE PRESENT DAY PRECIPITATION DISTRIBUTION, WHICH IS USED AS A NET MASS BALANCE INPUT IN THE MODEL. THE SCOTTISH COASTLINE IS ALSO SHOWN.

PRECIPITATION
(m/a)

OVER 2.25

2.00 TO 2.25

1.75 TO 2.00

1.50 TO 1.75

1.25 TO 1.50

1.00 TO 1.25

0.75 TO 1.00

UNDER 0.75
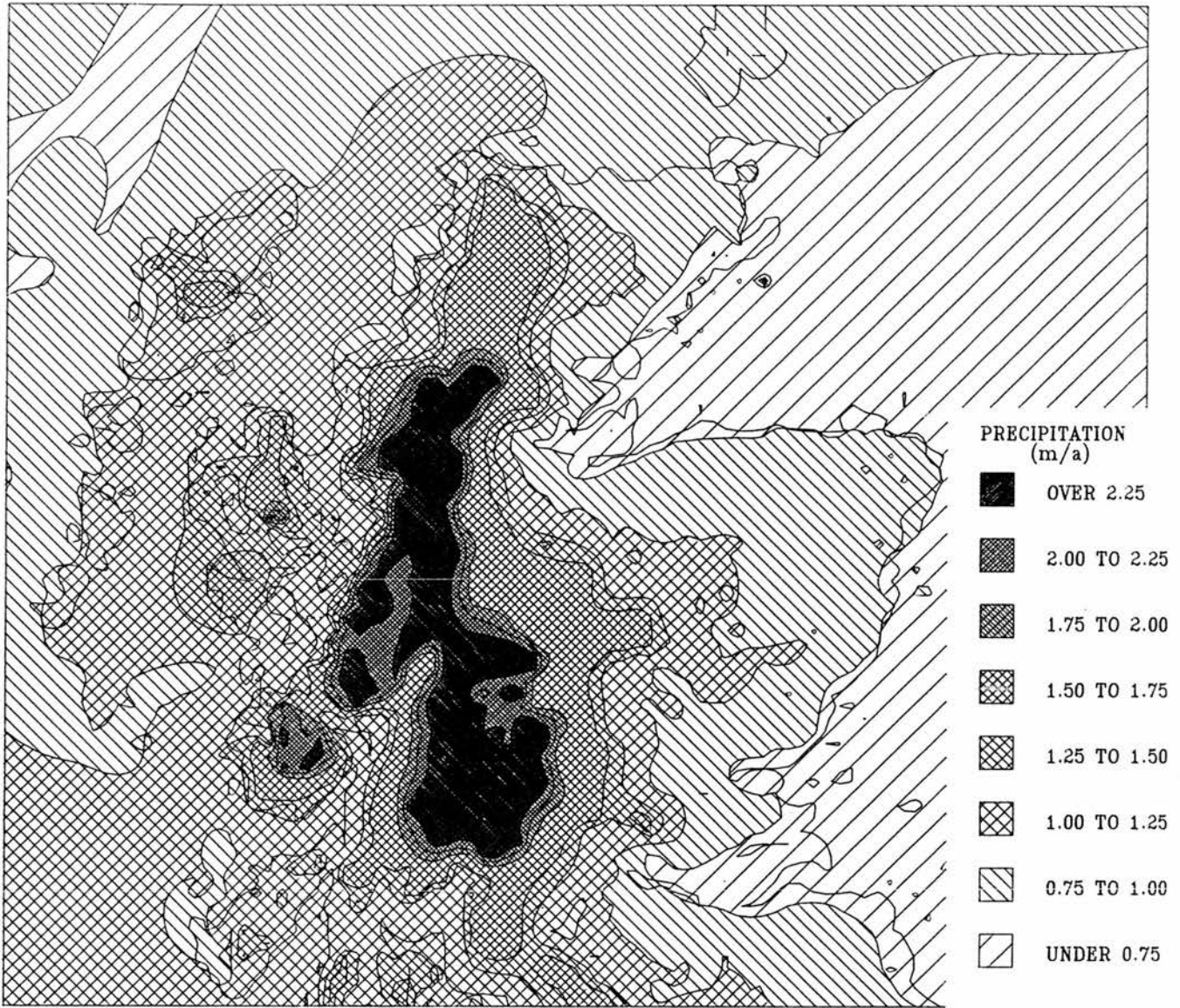
FIGURE 4.3 PLACE NAMES USED IN CHAPTER 4, WITH THE PRESENT DAY
BEDROCK TOPOGRAPHY.

BEDROCK
ELEVATION (km)

OVER 0.6

0.0 TO 0.6

KEY:

(1) AN TEALLACH
(2) BADENOCH
(3) BEINN DEARG
(4) BEN MORE ASSYNT
(5) BEN NEVIS
(6) BRAEMAR
(7) BREADALBANE
(8) CAIRN EIGE
(9) CAIRNGORMS
(10) GAICK

(11) GLEN MORE
(12) LEWIS
(13) MULL
(14) LOCH LOMOND
(15) LOCH LONG/LOCH FYNE
(16) LOCHNAGAR
(17) RANNOCH MOOR/
        STRATH TAY
(18) STRATH CONON
(19) STRATH SPEY
(20) SKYE

FIGURE 4.4 NET MASS BALANCE SHOWN AS A FUNCTION OF SURFACE ELEVATION, TEMPERATURE DEPRESSION AND LATITUDE.
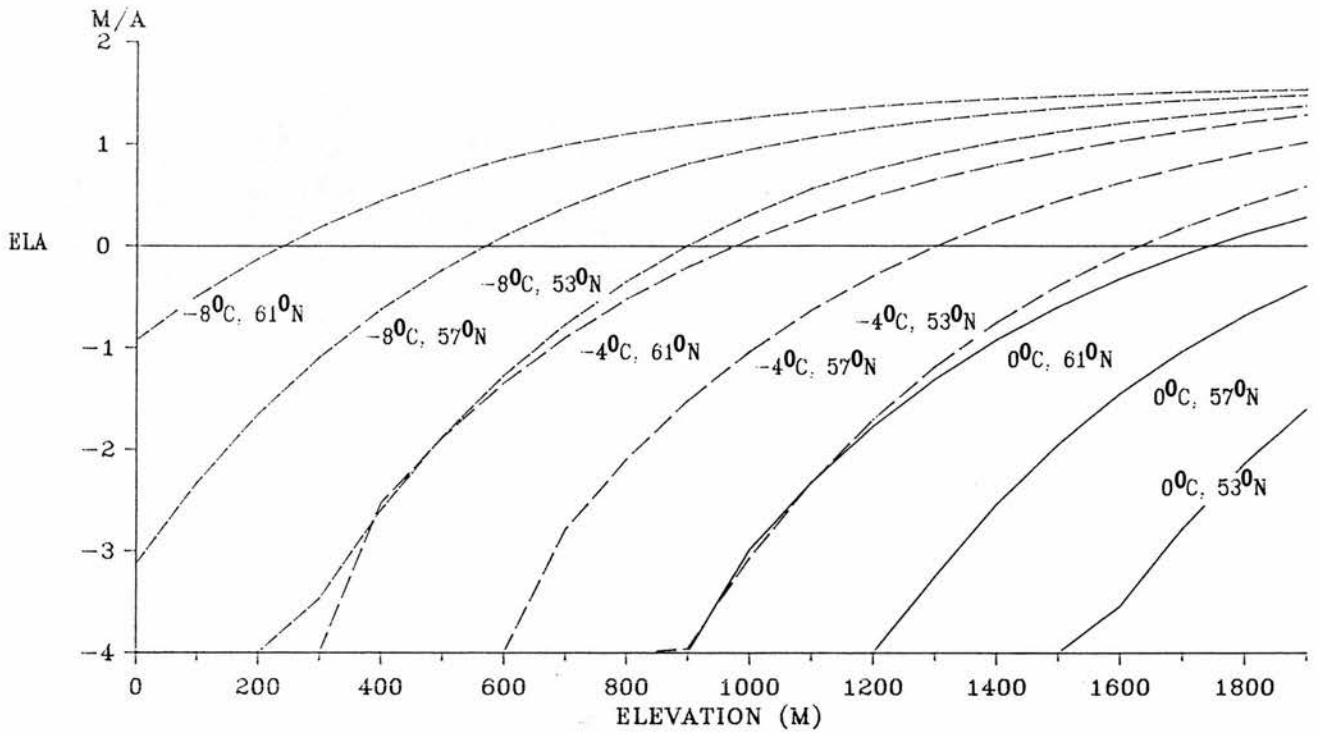
FIGURE 4.5 NET MASS BALANCE SHOWN AS A FUNCTION OF SURFACE ELEVATION, TEMPERATURE DEPRESSION AND PRECIPITATION RATE.

236
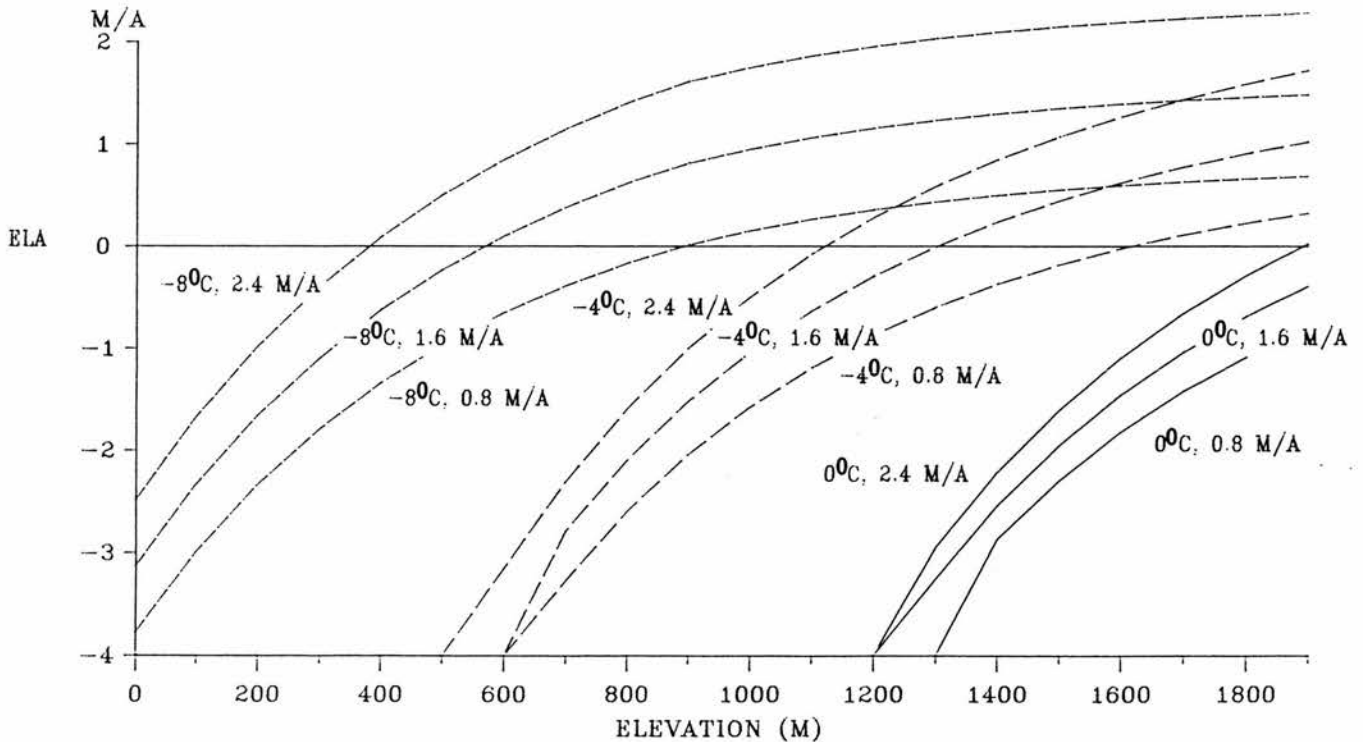
FIGURE 4.6 THE EXTENT OF AREAS WITH POSITIVE A NET MASS BALANCE FOR
VARYING TEMPERATURE DEPRESSIONS. RESULTS ARE SHOWN
TEMPERATURE DEPRESSIONS OF −6.0, −7.0 AND −8.0 ^{0}C. IN
ALL CASES THE MAXIMUM BEDROCK TOPOGRAPHY WAS USED.
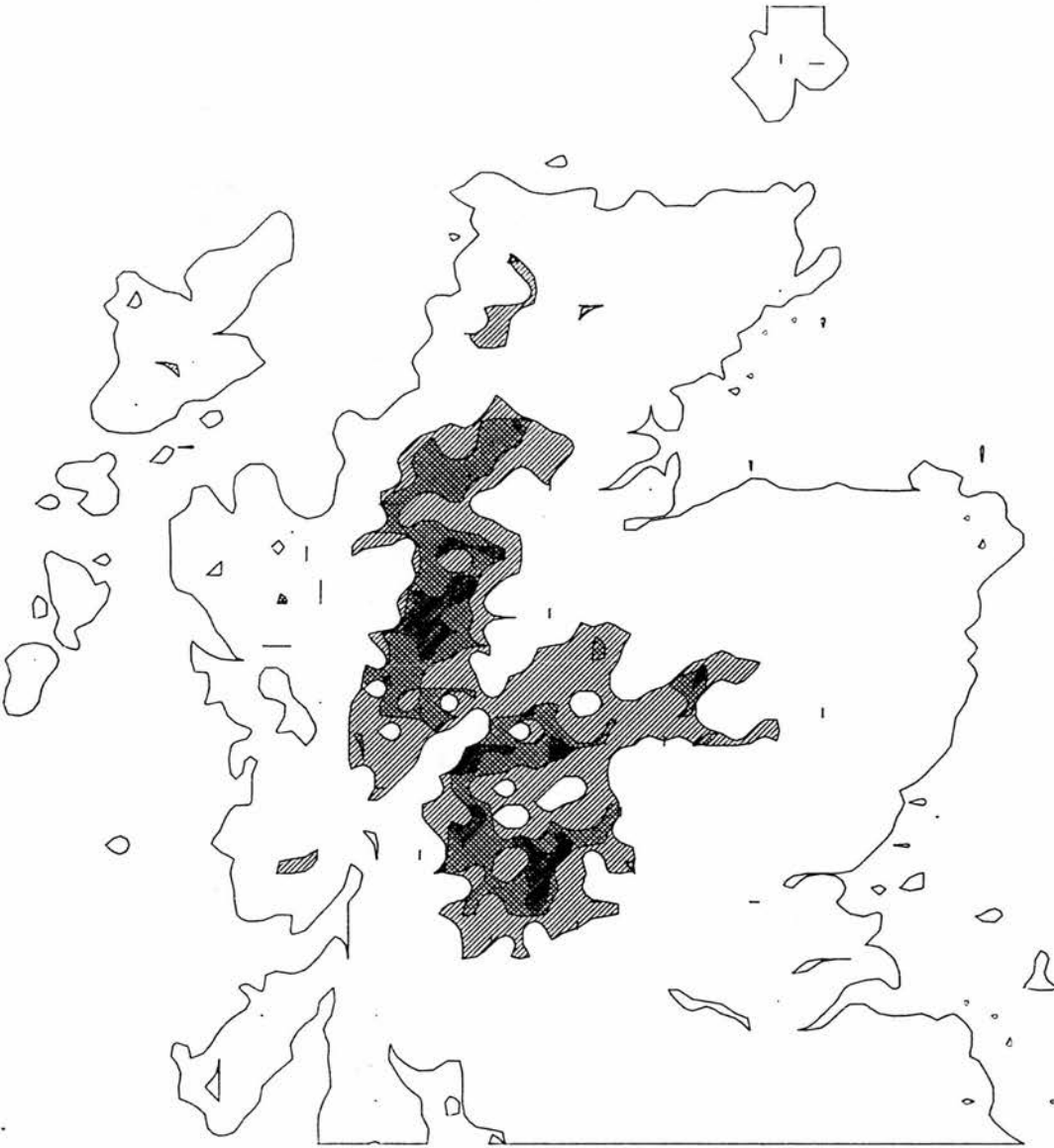
AREA HAS A POSITIVE NET MASS BALANCE
WHEN TEMPERATURE DEPRESSION IS:

IN EXCESS OF 6.0 DEGREES C

IN EXCESS OF 7.0 DEGREES C

IN EXCESS OF 8.0 DEGREES C

FIGURE 4.7 THE ICE SHEET VOLUME OUTPUT PRODUCED BY THE STANDARD RUN, WHICH USED AN ENVELOPE TOPOGRAPHY, AND BY A RUN THAT USED ONLY A MEAN TOPOGRAPHY.
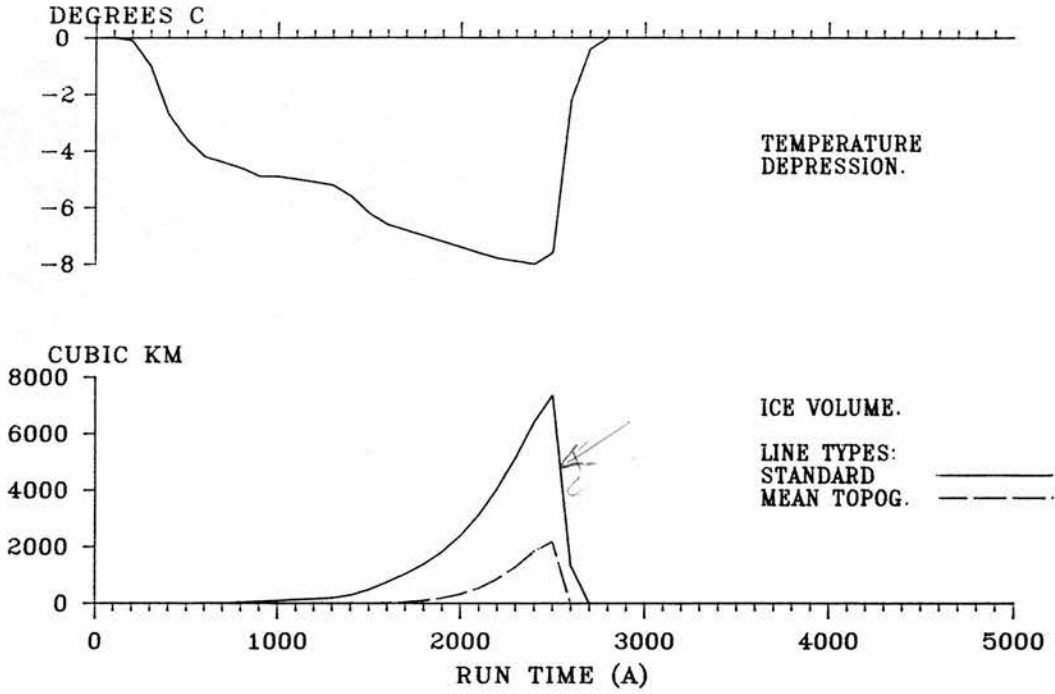
FIGURE 4.8 THE PREDICTION OF THE STANDARD RUN FOR ICE SHEET THICKNESS
AT 2.6 KA. THIS REPRESENTS THE MAXIMUM ICE SHEET ATTAINED
IN THE STANDARD RUN.

ICE
THICKNESS (m)

OVER 700

600 TO 700

500 TO 600

400 TO 500

300 TO 400

200 TO 300

100 TO 200

0 TO 100
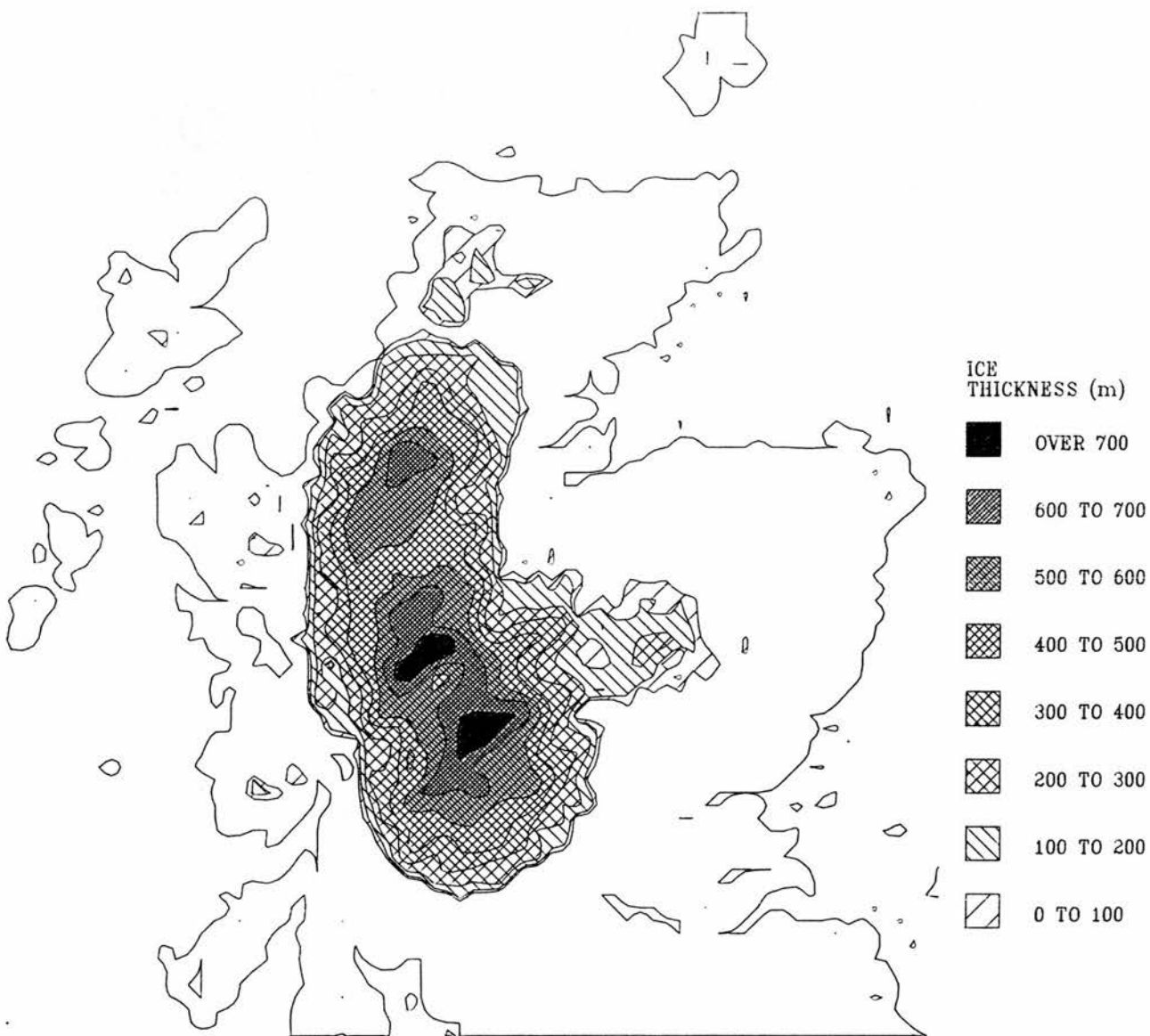
Figure 4.9 An estimate of the extent of the maximum Loch Lomond ice sheet based on geomorphological evidence, after Sissons (1979b).
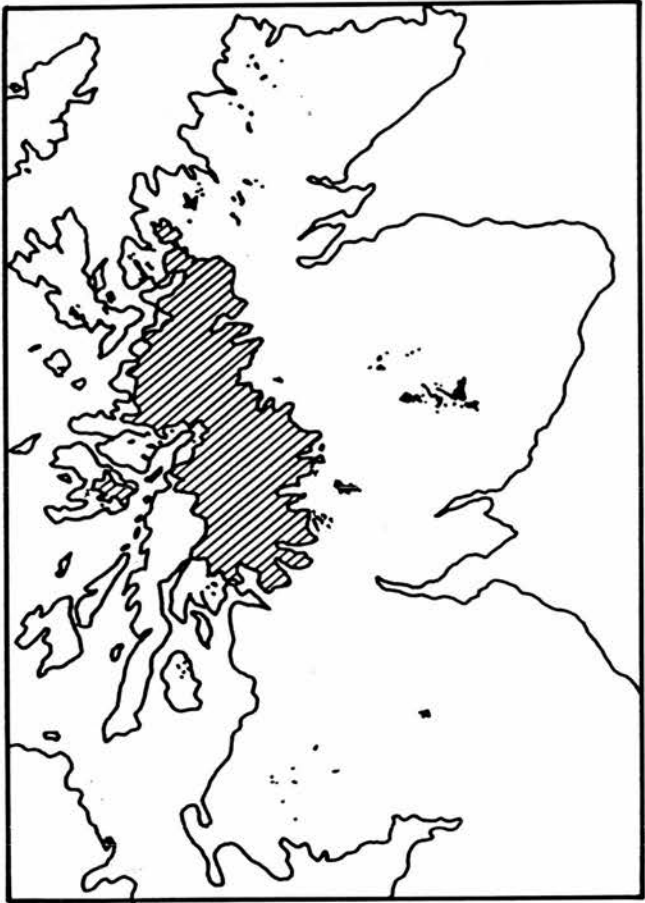
FIGURE 4.10 THE PREDICTION OF THE STANDARD RUN FOR ICE EXTENT
DURING ICE SHEET GROWTH. THE AREA OF THE ICE SHEET
IS SHOWN AT 1.5, 2.0, 2.5 AND 2.6 KA.
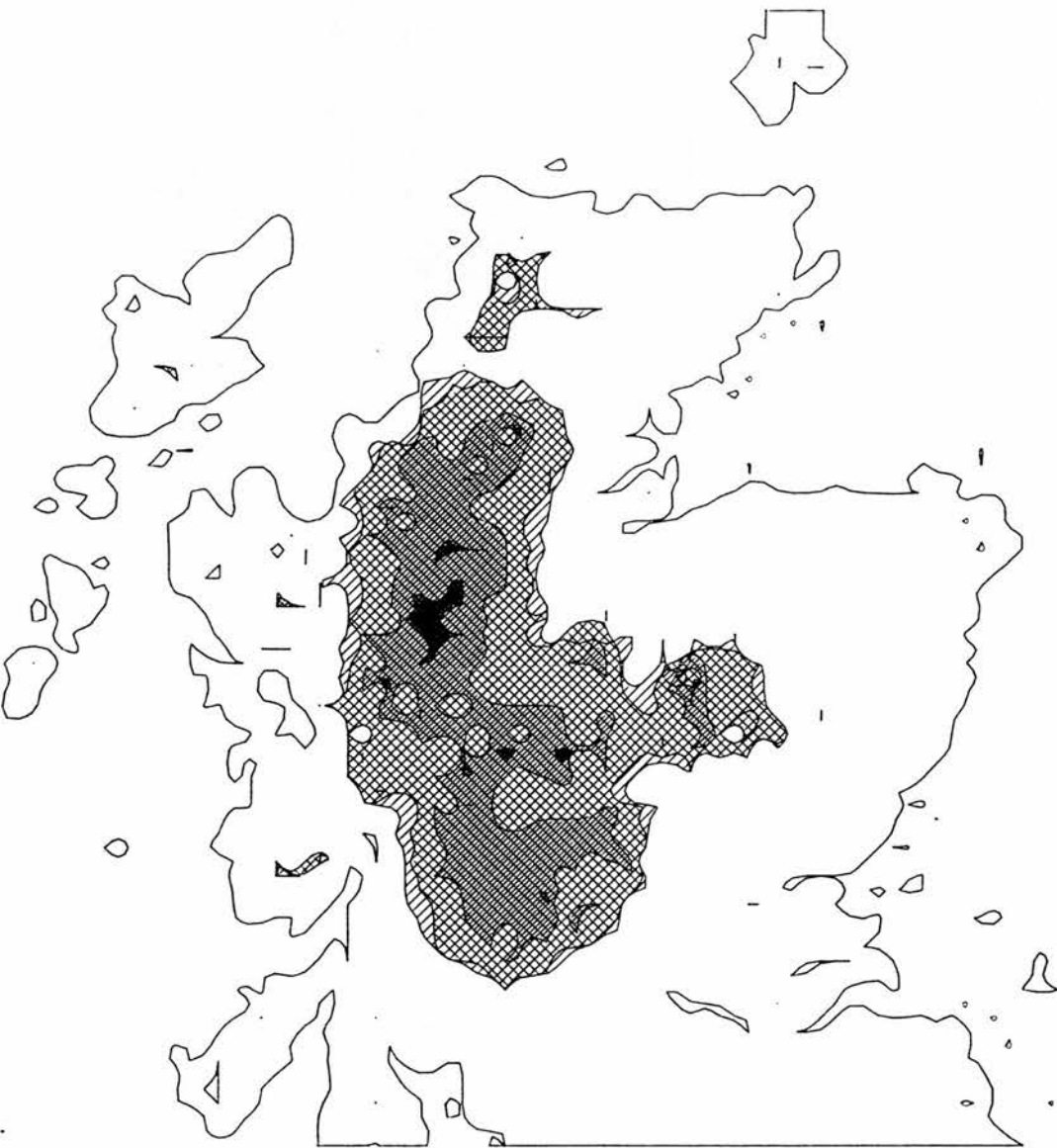
TIMES AT WHICH THE AREA IS COVERED BY ICE:

ICE COVERED AT 2.6 KA

ICE COVERED AT 2.5 KA

ICE COVERED AT 2.0 KA

ICE COVERED AT 1.5 KA

FIGURE 4.11 THE PREDICTION OF THE STANDARD RUN FOR ICE EXTENT
DURING ICE SHEET DECAY. THE AREA OF THE ICE SHEET
IS SHOWN AT 2.6, 2.7 AND 2.75 KA.
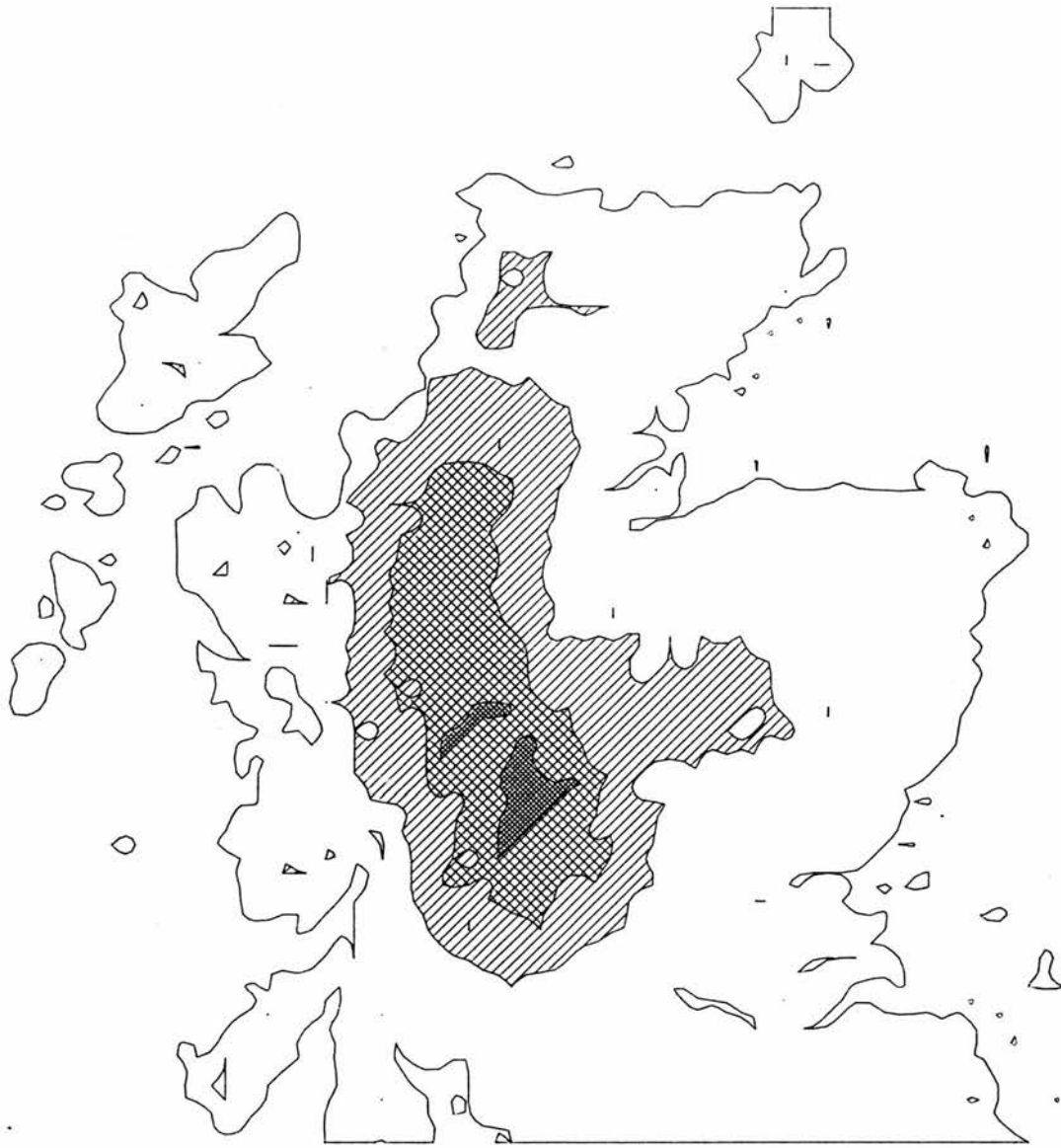
TIMES AT WHICH THE AREA IS COVERED BY ICE:

ICE COVERED AT 2.6 KA

ICE COVERED AT 2.7 KA

ICE COVERED AT 2.75 KA

FIGURE 4.12 THE PREDICTION OF A RUN USING ONLY THE MEAN TOPOGRAPHY
FOR ICE SHEET THICKNESS AT 2.6 KA. THIS REPRESENTS THE
MAXIMUM ICE SHEET ATTAINED IN THE RUN.
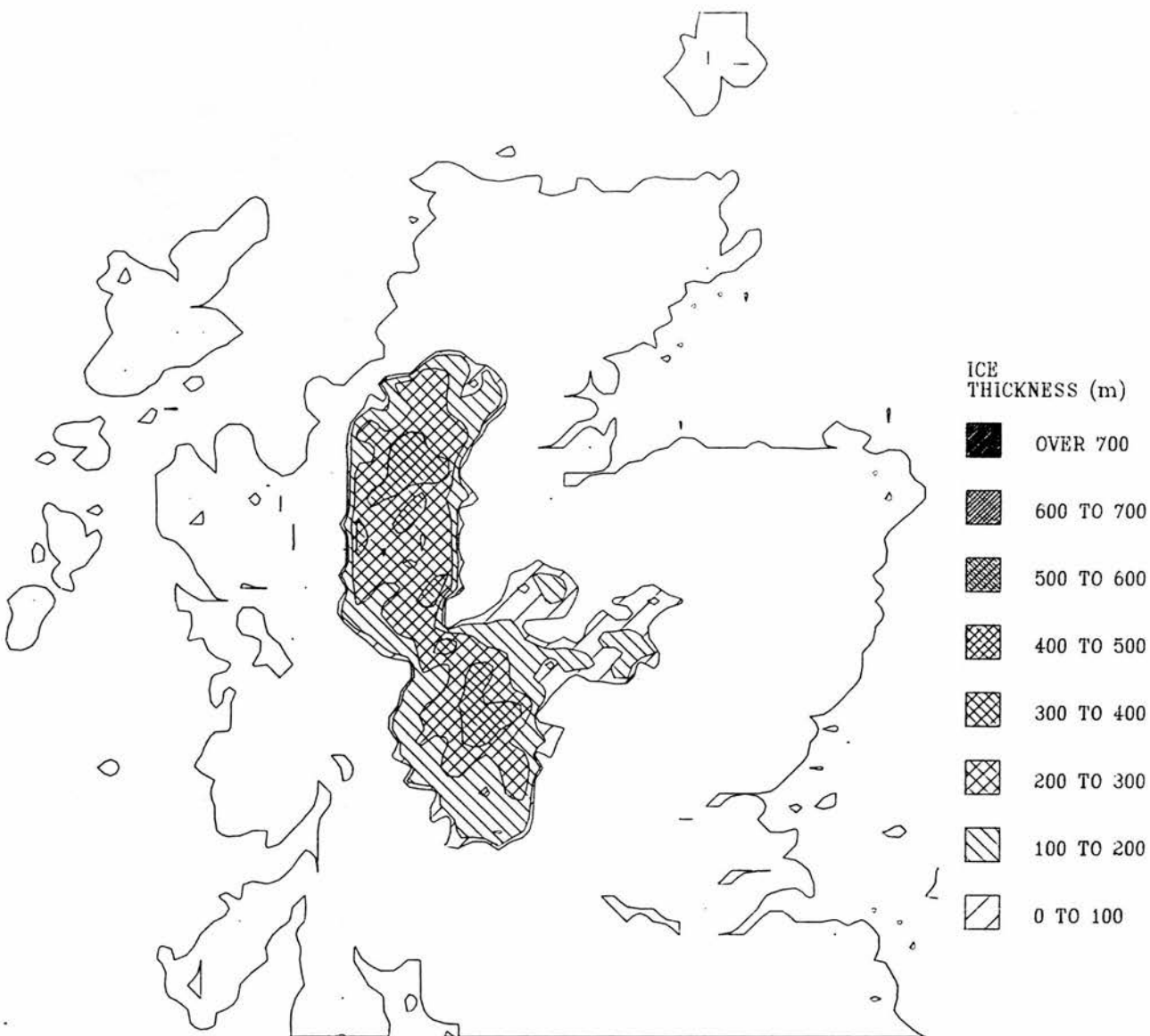
FIGURE 4.13 SENSITIVITY ANALYSIS OF THE EFFECT OF CLIMATE ON THE ICE SHEET VOLUMES PRODUCED BY THE MODEL. ONE OF THE RUNS SHOWN USED A TEMPERATURE TIME SERIES THAT WAS ONE DEGREE WARMER THAN THE STANDARD, WHILE THE OTHER USED A TEMPERATURE TIME SERIES THAT WAS ONE DEGREE COOLER. A RUN WHICH USED HALF OF THE STANDARD PRECIPITATION RATE IS ALSO SHOWN.
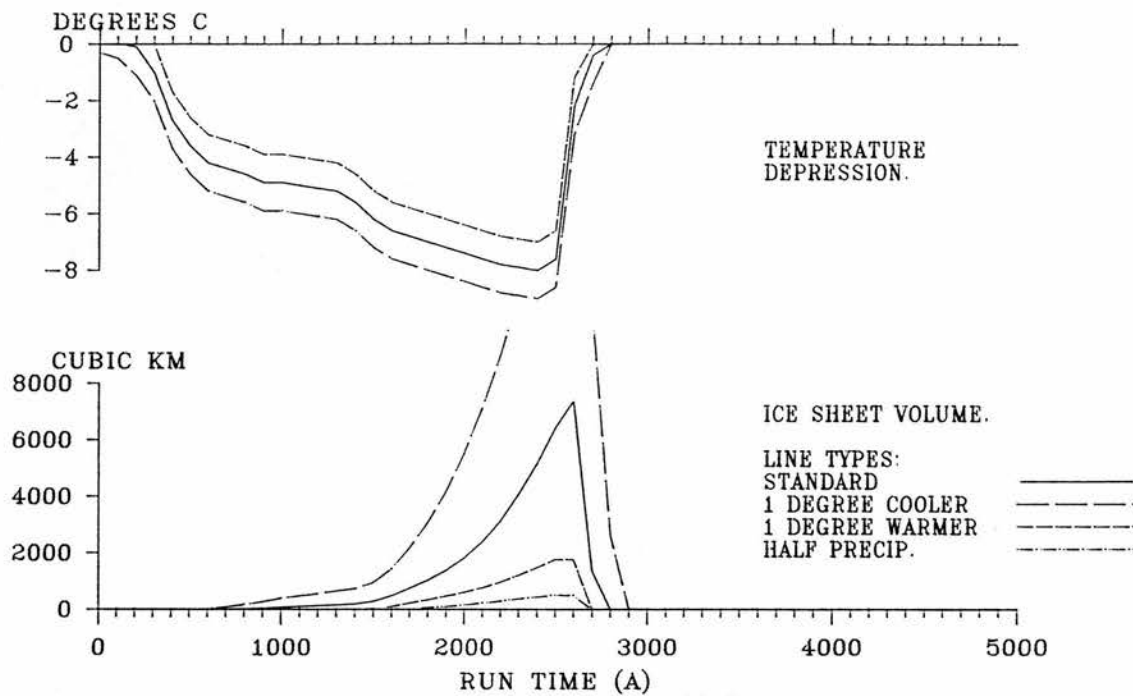
FIGURE 4.14 THE PREDICTED MAXIMUM ICE SHEET EXTENT FOR THE STANDARD RUN AND FOR A PAIR OF RUNS WHICH USED TEMPERATURE TIME SERIES THAT WERE ONE DEGREE WARMER AND ONE DEGREE COOLER THAN THE STANDARD TIME SERIES.
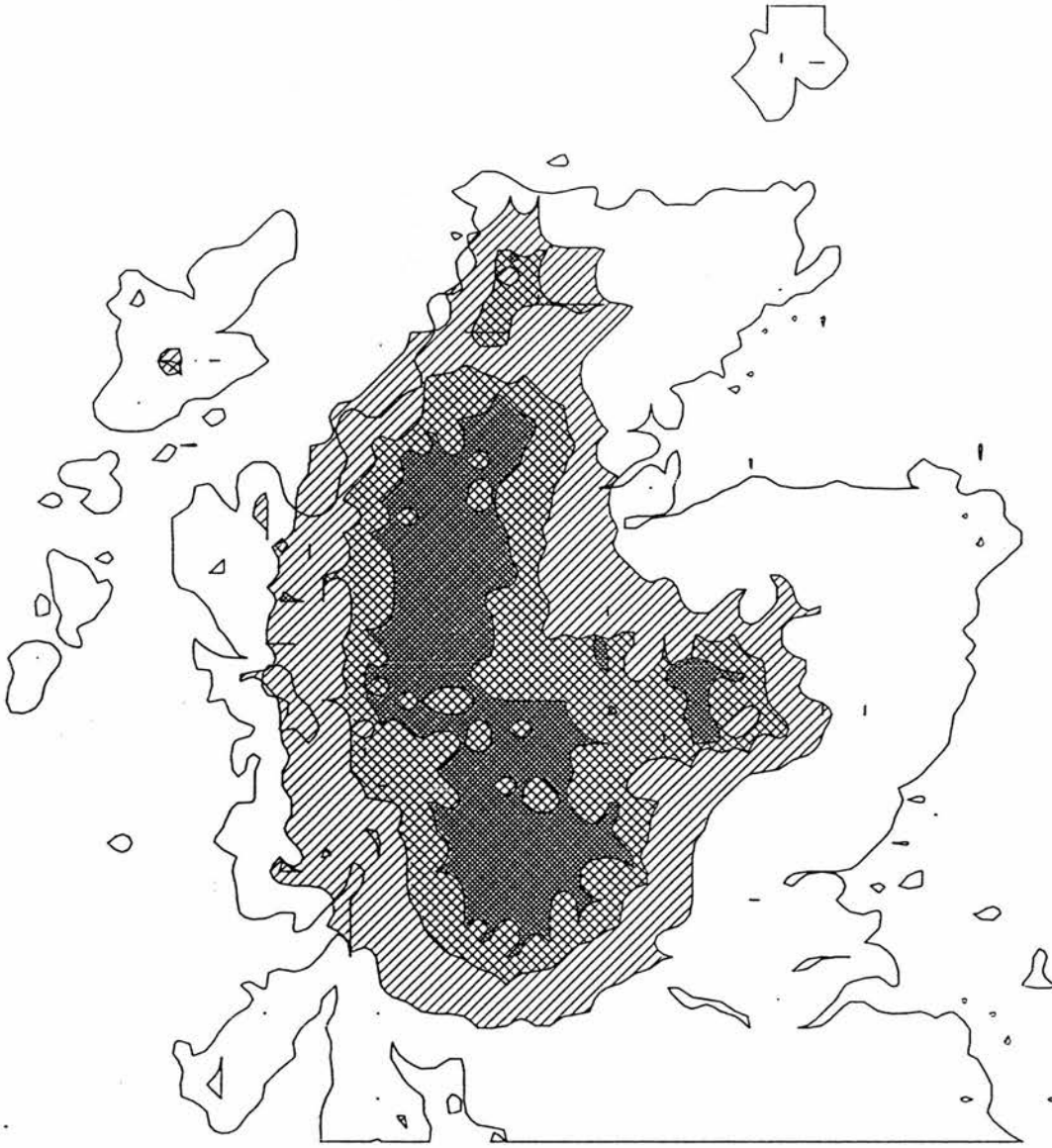
ICE SHEET EXTENT FOR:

1 DEGREE C COOLER RUN

STANDARD RUN

1 DEGREE C WARMER RUN

FIGURE 4.15 THE PREDICTION OF A RUN USING HALF OF THE STANDARD
PRECIPITATION RATE FOR ICE SHEET THICKNESS AT 2.6 KA.
THIS REPRESENTS THE MAXIMUM ICE SHEET ATTAINED IN THE
RUN.

ICE
THICKNESS (m)

OVER 700

600 TO 700

500 TO 600

400 TO 500

300 TO 400

200 TO 300

100 TO 200

0 TO 100
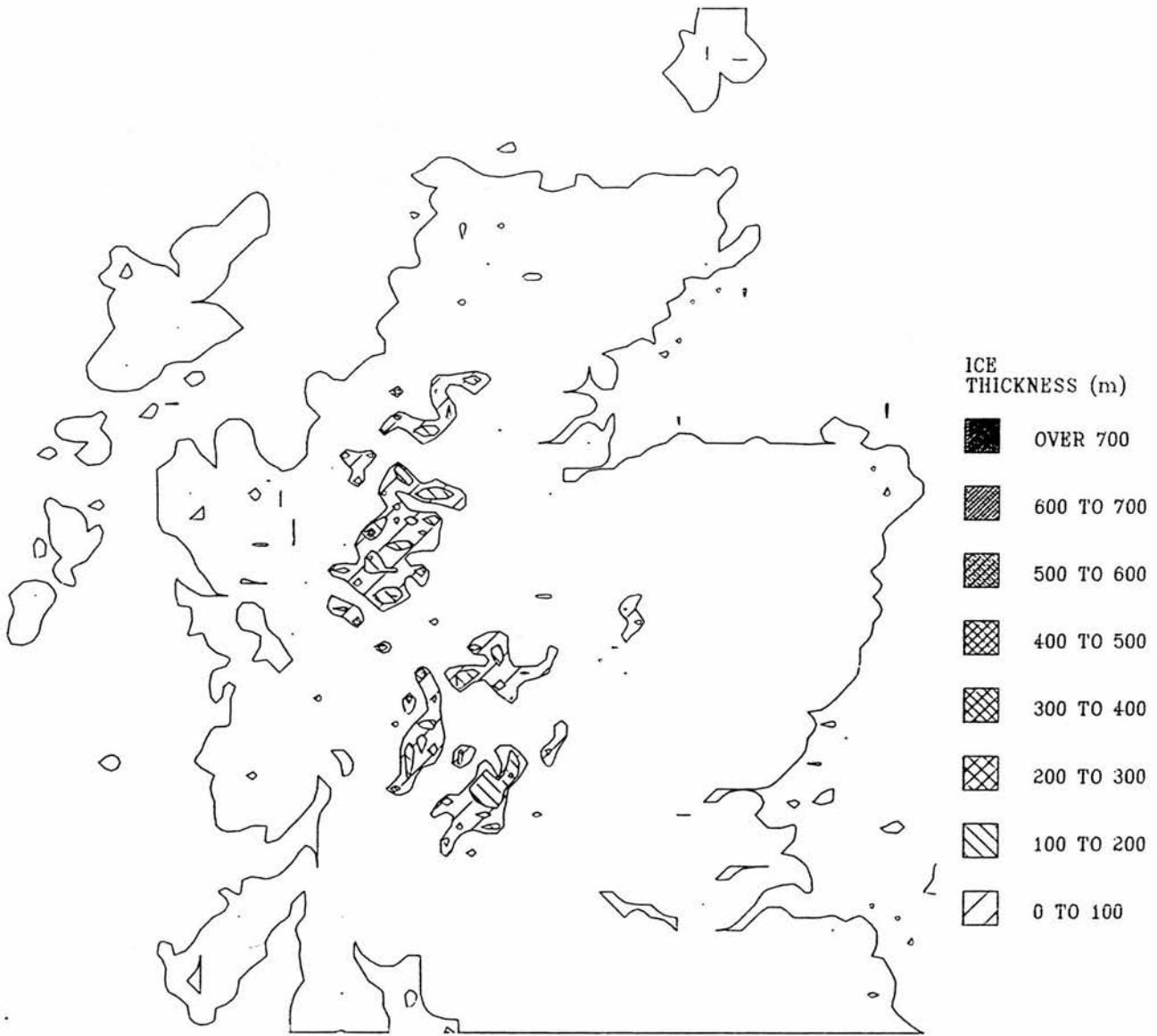
FIGURE 4.16 SENSITIVITY ANALYSIS OF THE EFFECT OF VELOCITY VARIATION ON THE ICE SHEET VOLUMES PRODUCED BY THE MODEL. THE RUNS SHOWN USED 50 % INCREASES AND 50 % DECREASES ON THE STANDARD DEFORMATION AND SLIDING PARAMETER VALUES.
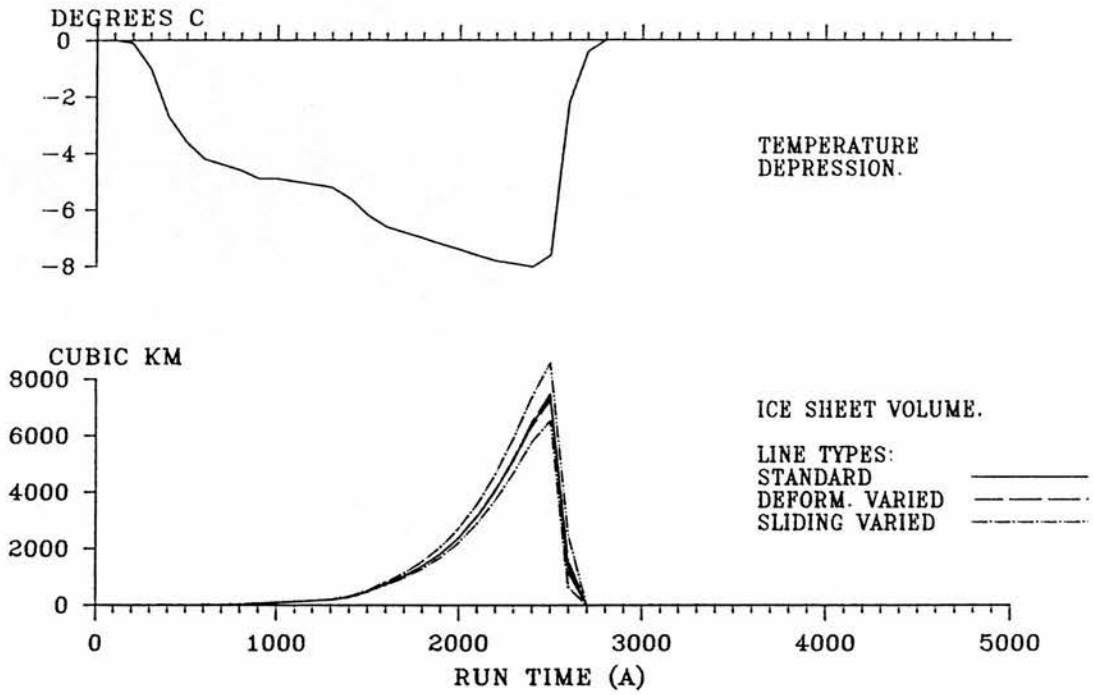
FIGURE 4.17 THE PREDICTION OF A RUN WITH DECREASED SLIDING
          VELOCITY FOR ICE SHEET THICKNESS AT 2.6 KA. THIS
          REPRESENTS THE MAXIMUM ICE SHEET ATTAINED IN THE
          RUN.

ICE
THICKNESS (m)

OVER 700

600 TO 700

500 TO 600

400 TO 500

300 TO 400

200 TO 300

100 TO 200

0 TO 100
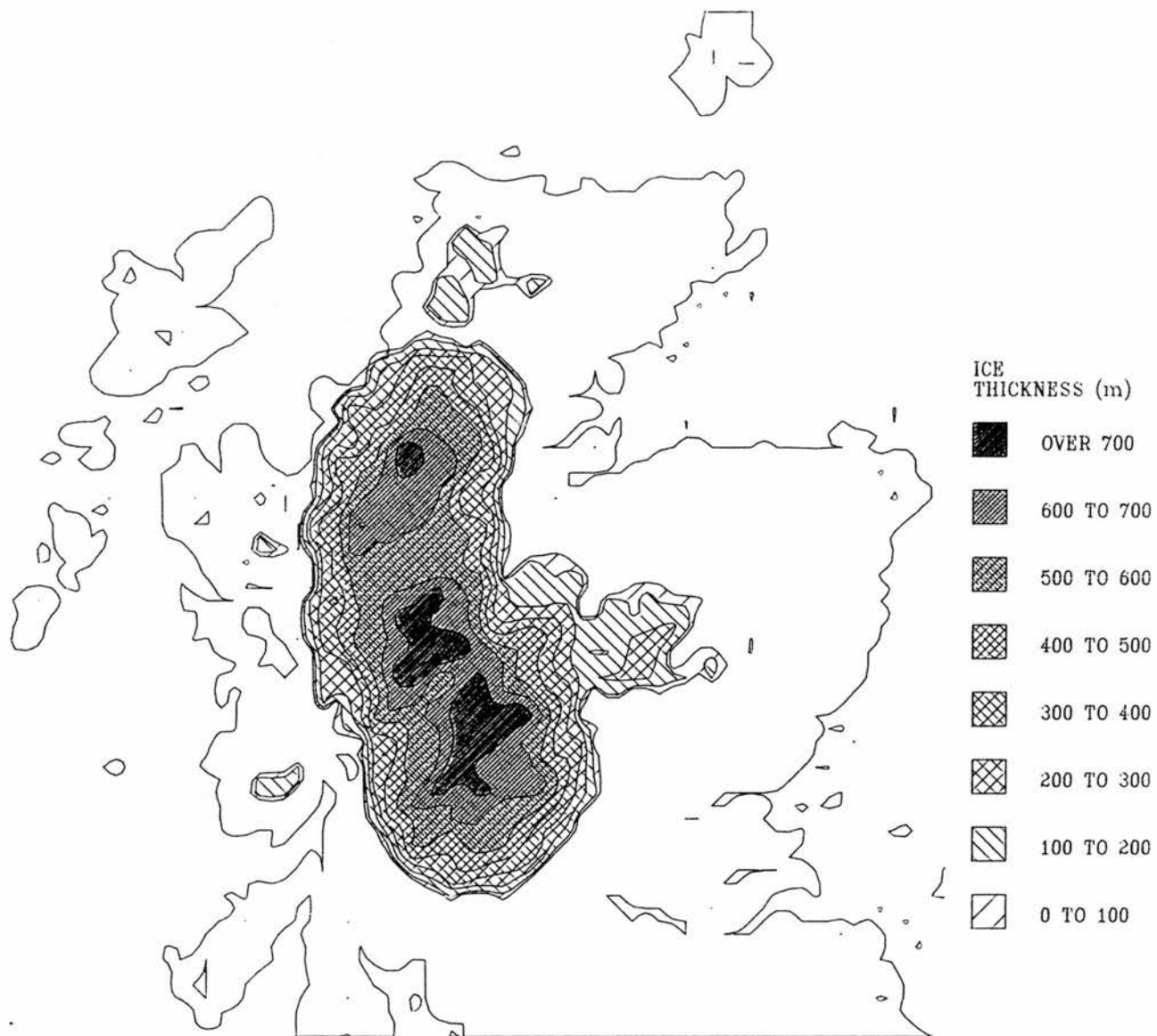
FIGURE 4.18 THE PREDICTION OF A RUN WITH INCREASED SLIDING
          VELOCITY FOR ICE SHEET THICKNESS AT 2.6 KA. THIS
          REPRESENTS THE MAXIMUM ICE SHEET ATTAINED IN THE
          RUN.

ICE
THICKNESS (m)

OVER 700

600 TO 700

500 TO 600

400 TO 500

300 TO 400

200 TO 300

100 TO 200

0 TO 100
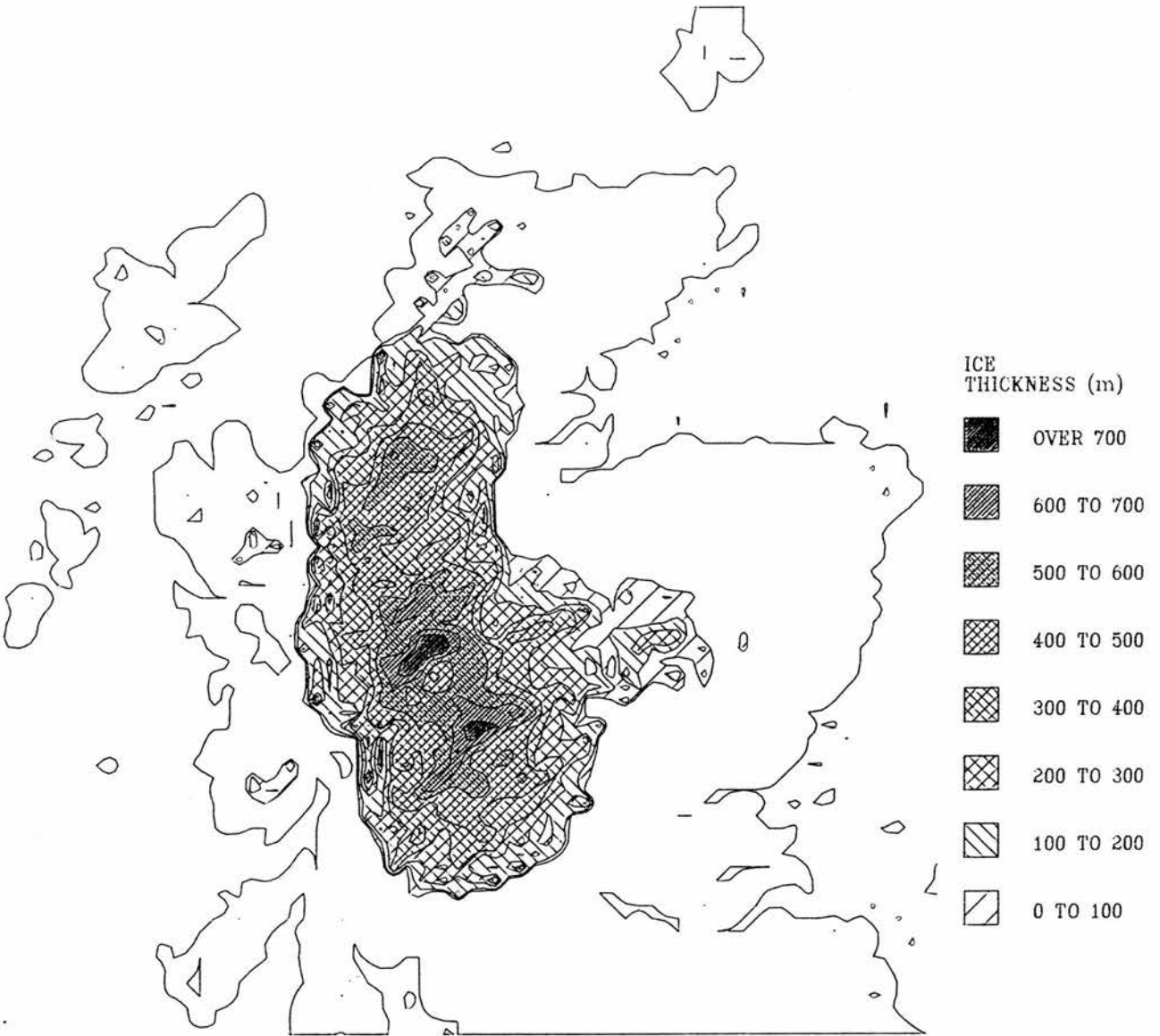
FIGURE 4.19 THE PREDICTION OF A RUN WITH DECREASED DEFORMATION
         VELOCITY FOR ICE SHEET THICKNESS AT 2.6 KA. THIS
         REPRESENTS THE MAXIMUM ICE SHEET ATTAINED IN THE
         THE RUN.

ICE
THICKNESS (m)

OVER 700

600 TO 700

500 TO 600

400 TO 500

300 TO 400

200 TO 300

100 TO 200

0 TO 100
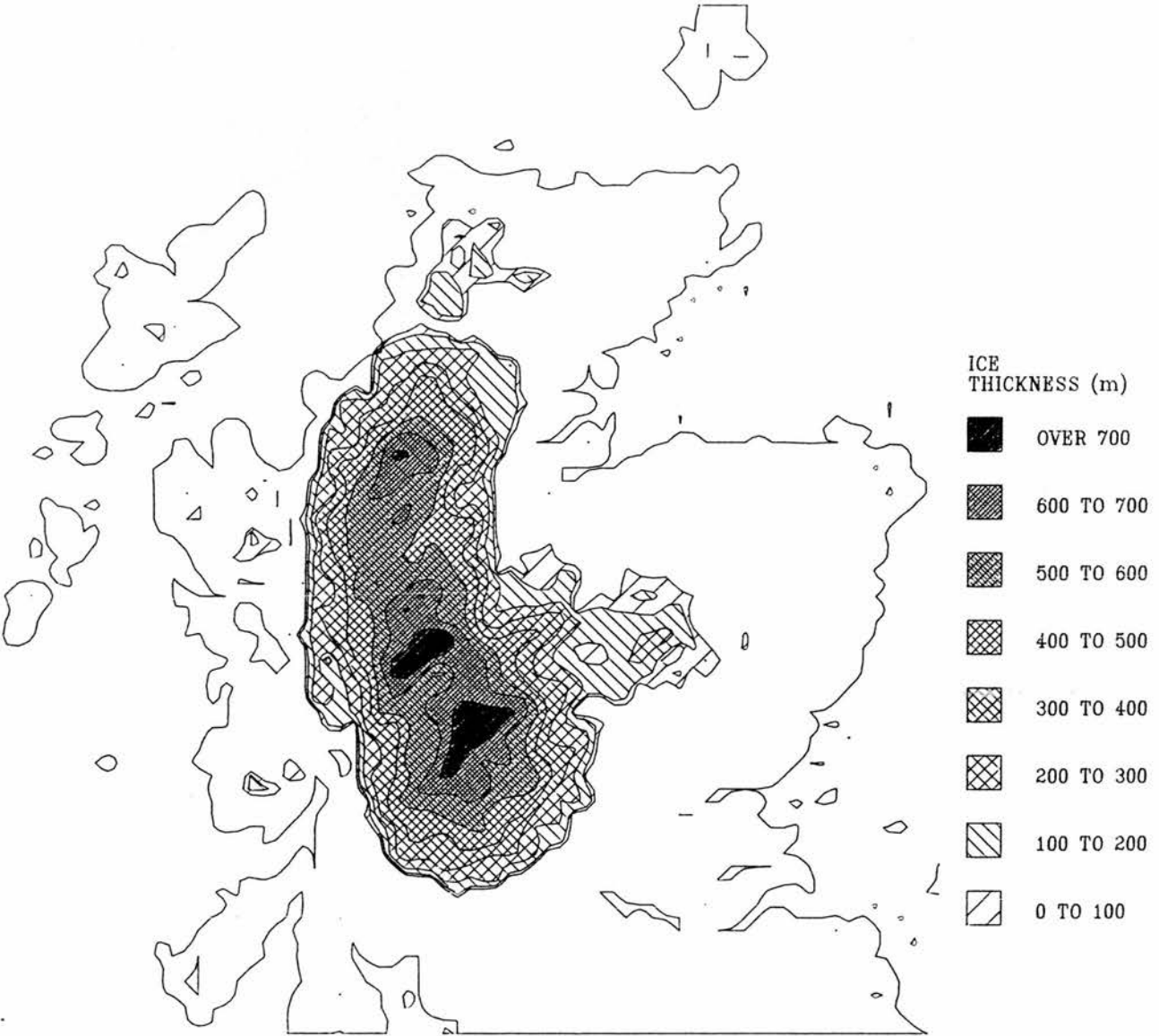
FIGURE 4.20 THE PREDICTION OF A RUN WITH INCREASED DEFORMATION
VELOCITY FOR ICE SHEET THICKNESS AT 2.6 KA. THIS
REPRESENTS THE MAXIMUM ICE SHEET ATTAINED IN THE
THE RUN.

ICE
THICKNESS (m)

OVER 700

600 TO 700

500 TO 600

400 TO 500

300 TO 400

200 TO 300

100 TO 200

0 TO 100
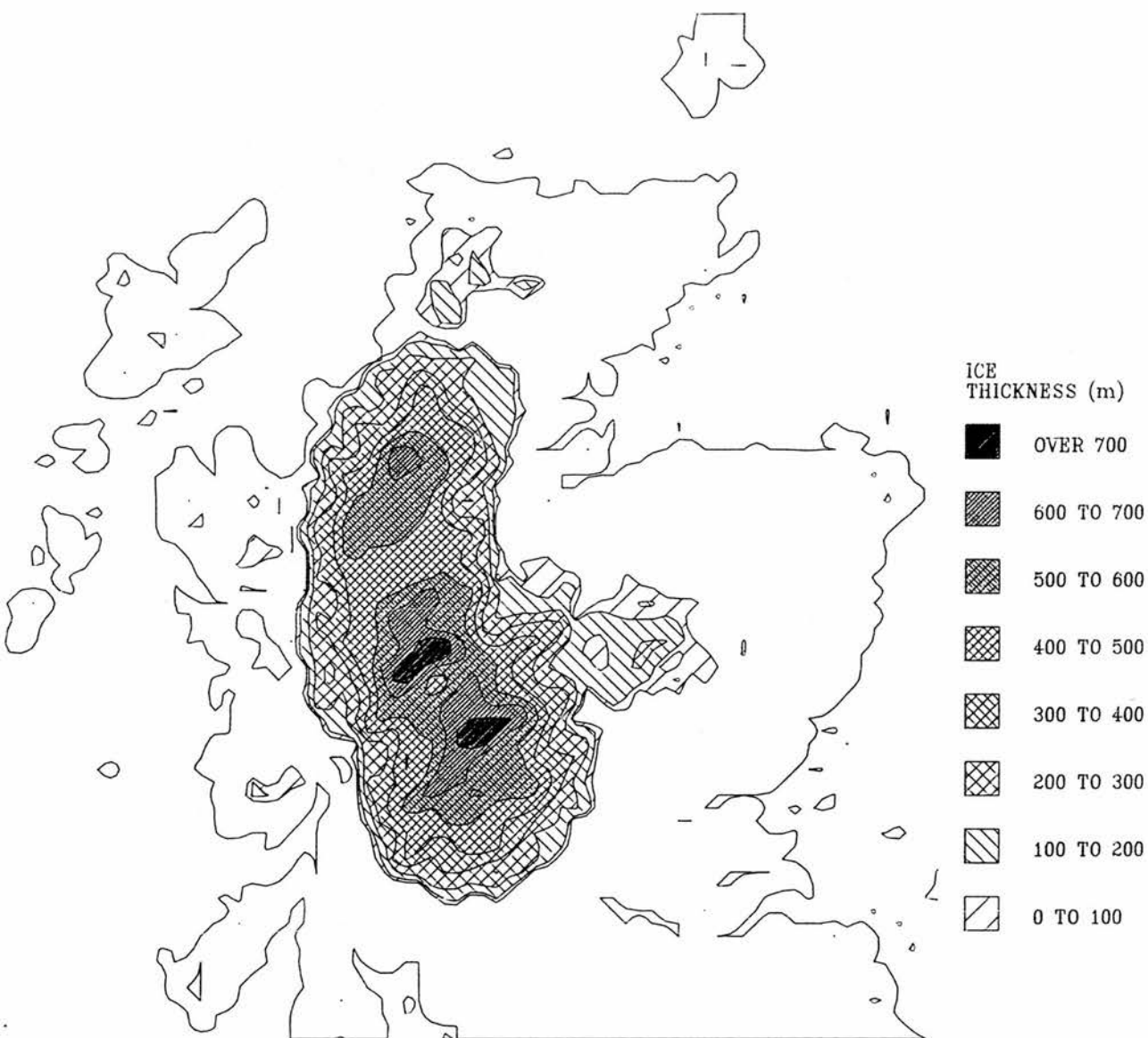
FIGURE 4.21 COMPARISON OF THE ICE VOLUMES PRODUCED BY THE STANDARD RUN,
AND BY RUNS EMPLOYING SLOWER RATES OF WARMING AFTER 2.6 KA.
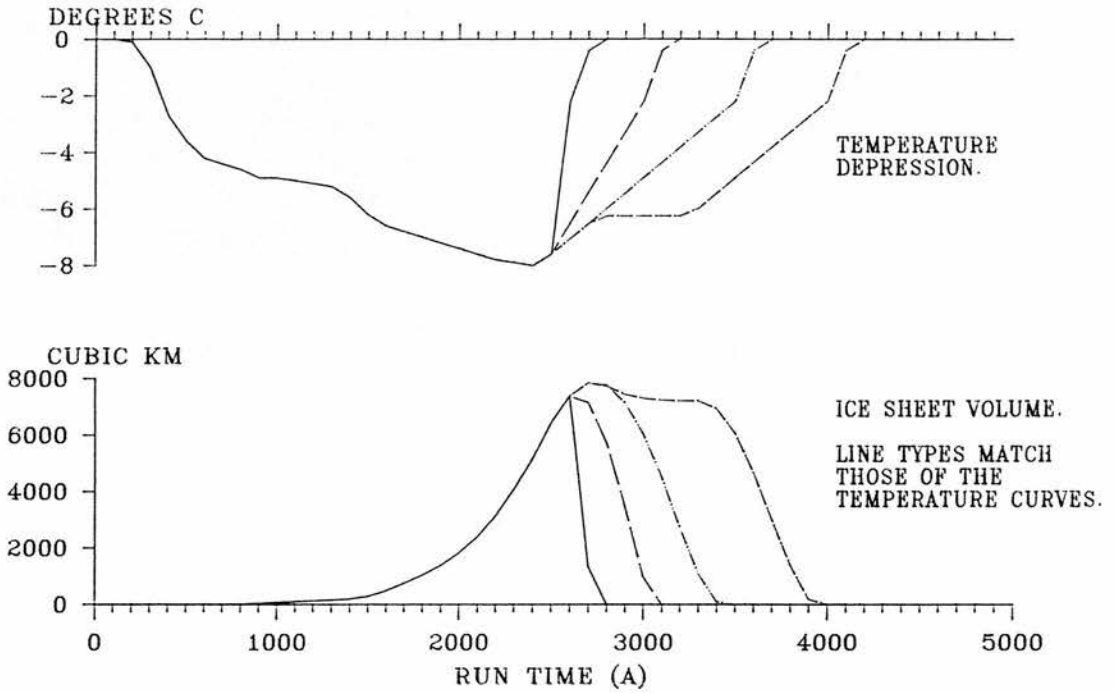
FIGURE 4.22 THE ICE SHEET VOLUME OUTPUT PRODUCED BY THE STANDARD MODEL
WHEN IT IS FORCED USING CONSTANT IMPOSED TEMPERATURE
DEPRESSIONS.

252
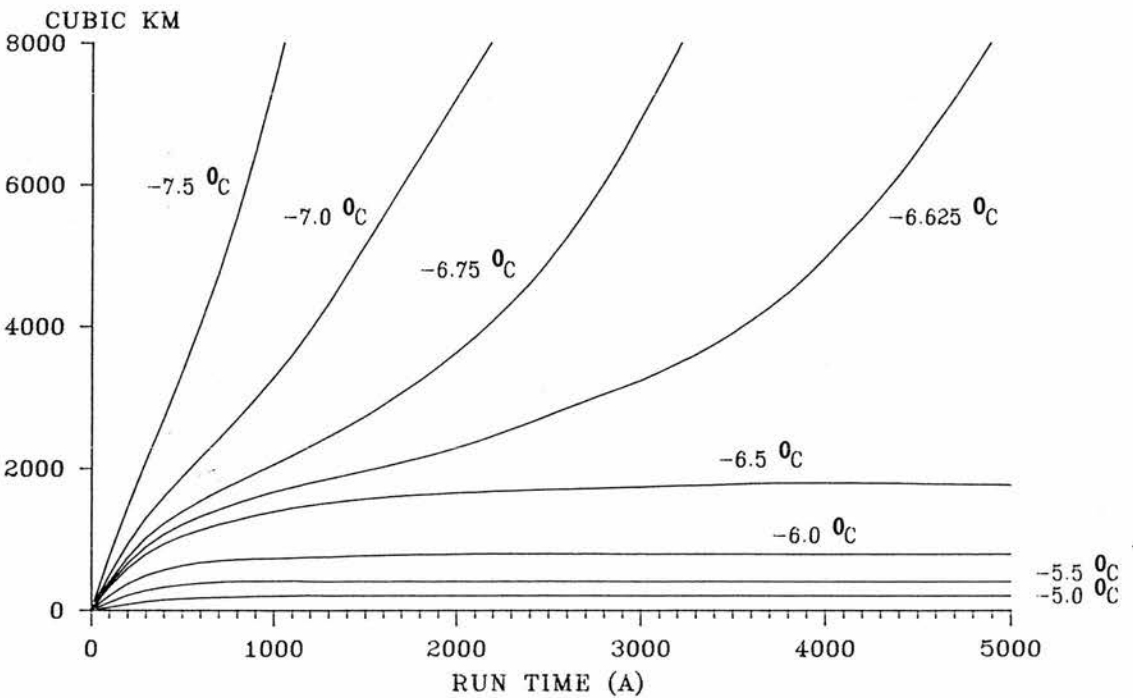
FIGURE 4.23 THE PREDICTION OF THE STANDARD MODEL FOR ICE SHEET EXTENT
AT 5.0 KA IN A RUN USING A CONSTANT TEMPERATURE DEPRESSION
OF −6.5 °C. THE ABLATION AND ACCUMULATION AREAS OF THE ICE
SHEET ARE INDICATED.

NET MASS
BALANCE

ACCUMULATION
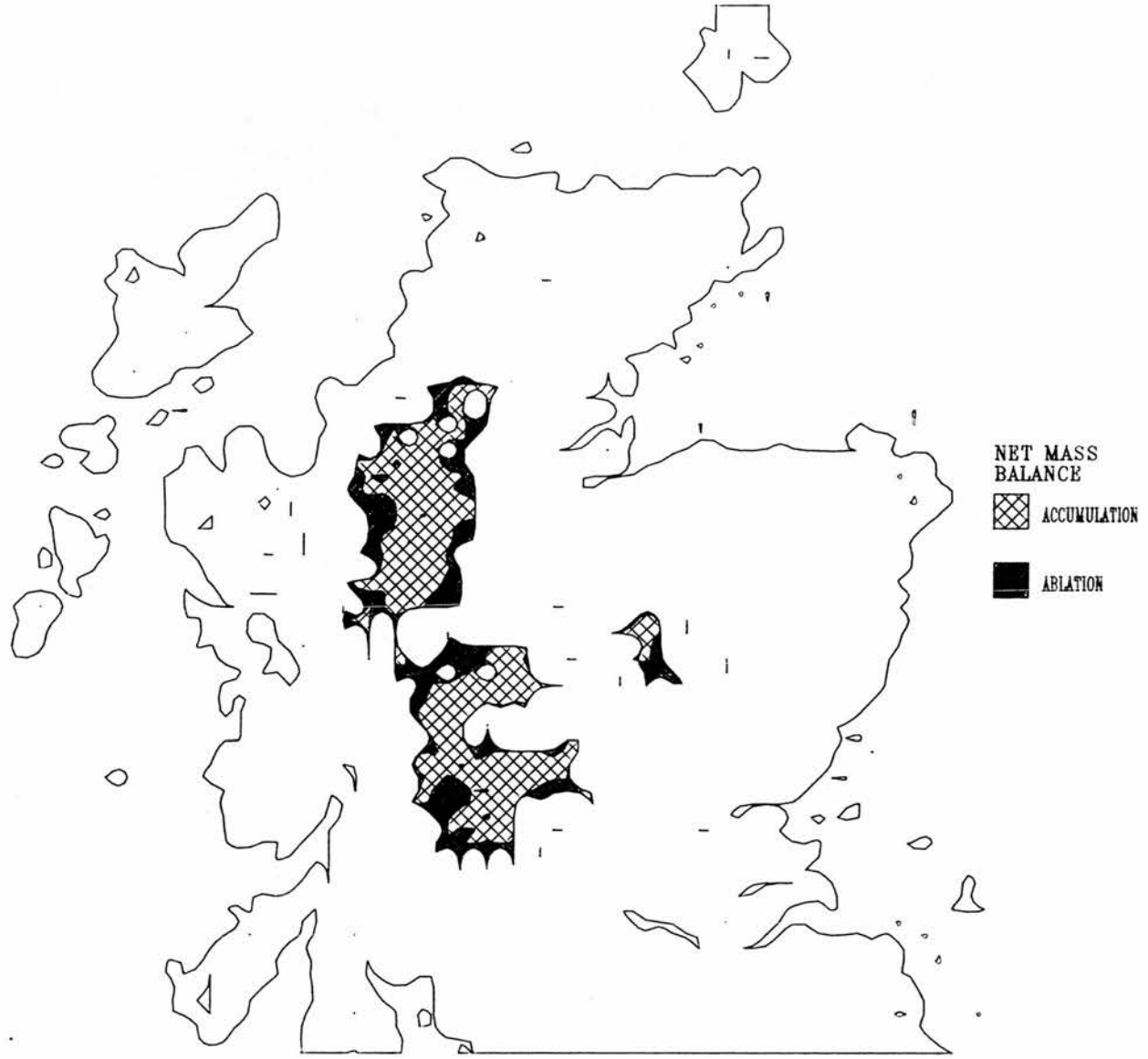
ABLATION

FIGURE 4.24 THE PREDICTION OF THE STANDARD MODEL FOR ICE SHEET EXTENT
AT 1.0 KA IN A RUN USING A CONSTANT TEMPERATURE DEPRESSION
OF -6.625 ^{0}C. THE ABLATION AND ACCUMULATION AREAS OF THE ICE
SHEET ARE INDICATED.

NET MASS
BALANCE

ACCUMULATION
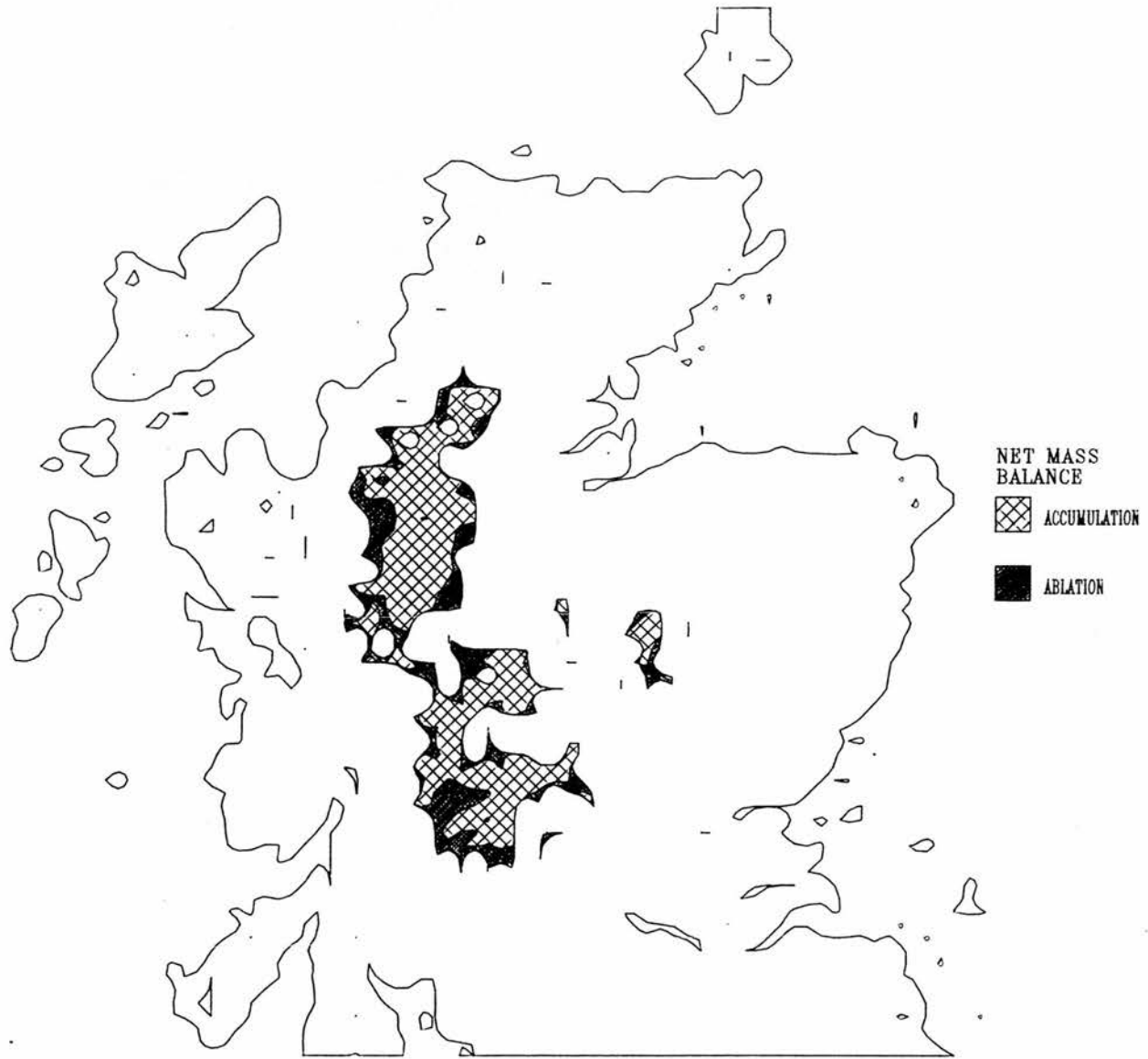
ABLATION

FIGURE 4.25 THE PREDICTION OF THE STANDARD MODEL FOR ICE SHEET EXTENT AT 2.0 KA IN A RUN USING A CONSTANT TEMPERATURE DEPRESSION OF -6.625 ^{0}C. THE ABLATION AND ACCUMULATION AREAS OF THE ICE SHEET ARE INDICATED.

NET MASS BALANCE

ACCUMULATION
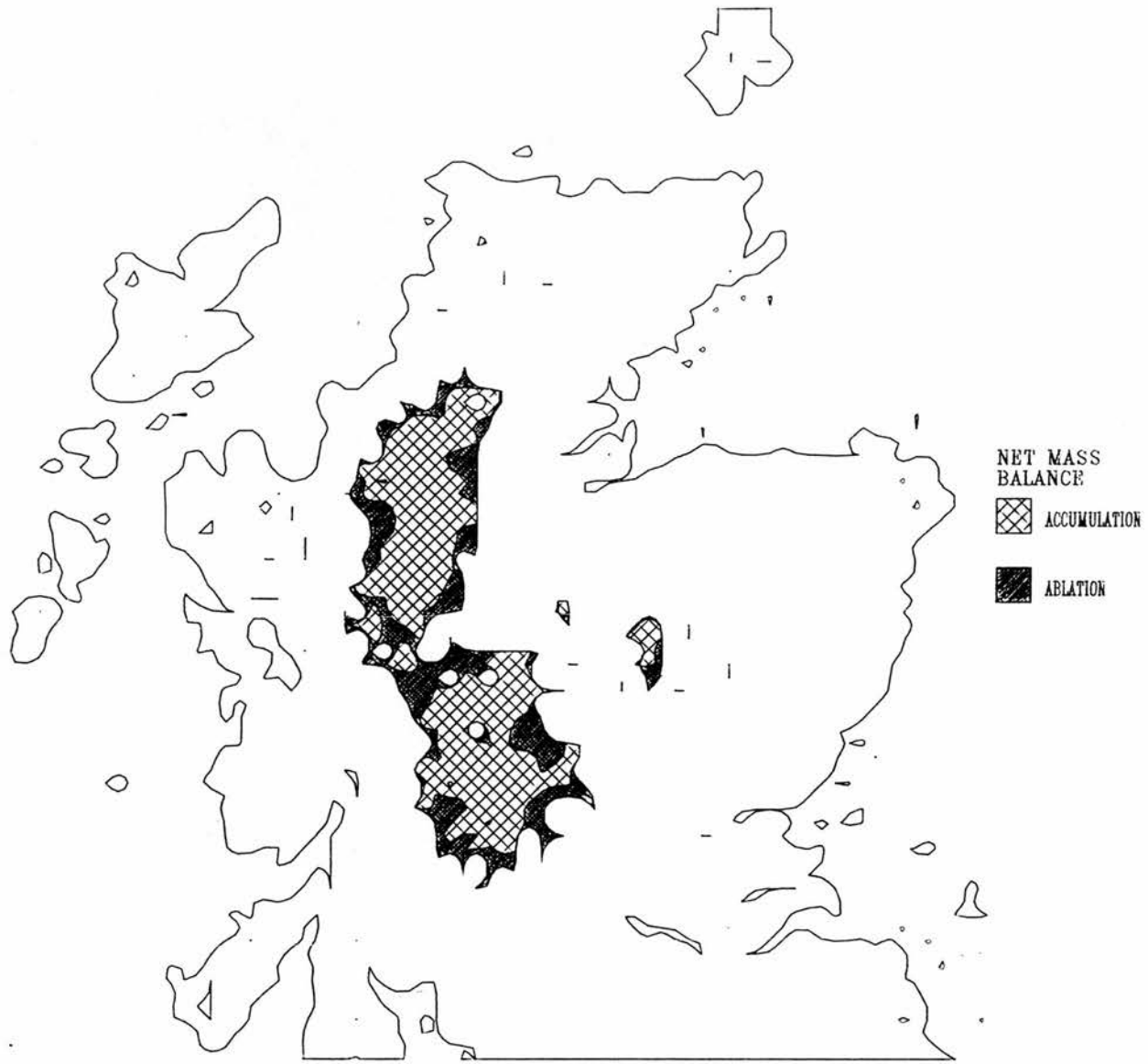
ABLATION

FIGURE 4.26 THE PREDICTION OF THE STANDARD MODEL FOR ICE SHEET EXTENT
AT 3.0 KA IN A RUN USING A CONSTANT TEMPERATURE DEPRESSION
OF −6.625 °C. THE ABLATION AND ACCUMULATION AREAS OF THE ICE
SHEET ARE INDICATED.

NET MASS
BALANCE

ACCUMULATION
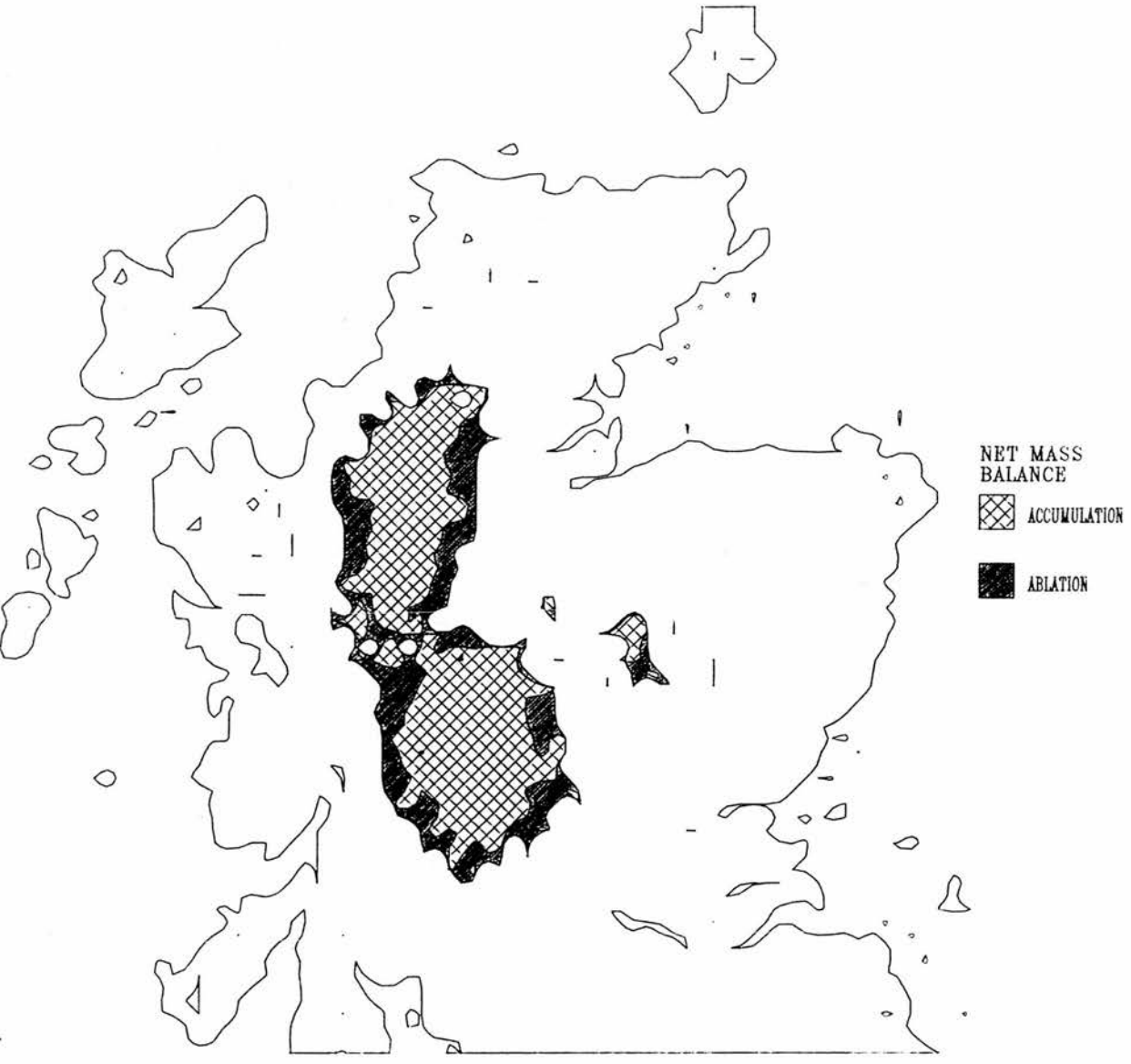
ABLATION

FIGURE 4.27 THE PREDICTION OF THE STANDARD MODEL FOR ICE SHEET EXTENT
AT 4.0 KA IN A RUN USING A CONSTANT TEMPERATURE DEPRESSION
OF −6.625 °C. THE ABLATION AND ACCUMULATION AREAS OF THE ICE
SHEET ARE INDICATED.

NET MASS
BALANCE

ACCUMULATION

ABLATION
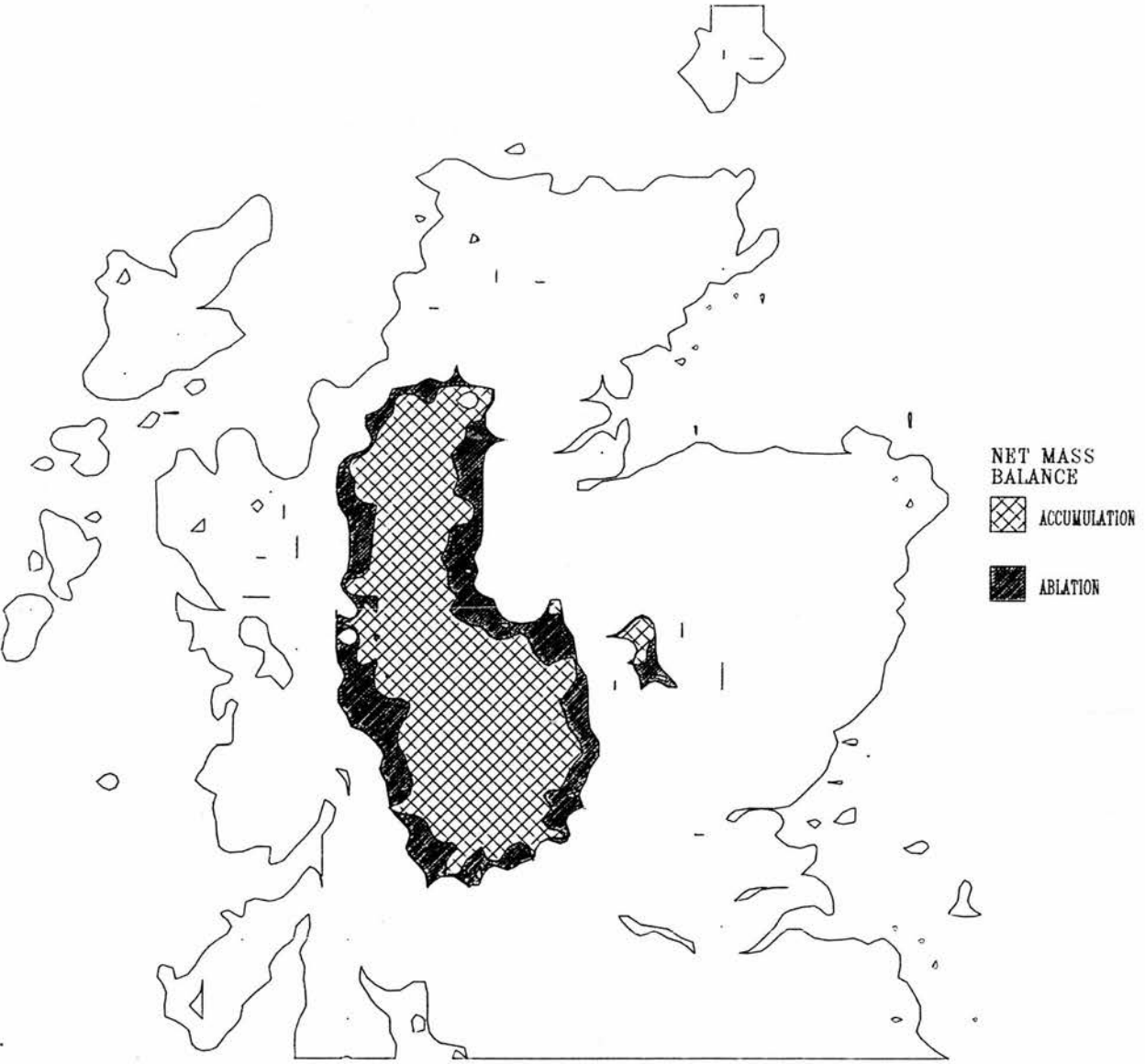
FIGURE 4.28 THE ICE SHEET VOLUME OUTPUT PRODUCED BY A MODEL THAT EMPLOYS ONLY THE MEAN TOPOGRAPHY, WHEN IT IS FORCED USING CONSTANT IMPOSED TEMPERATURE DEPRESSIONS.
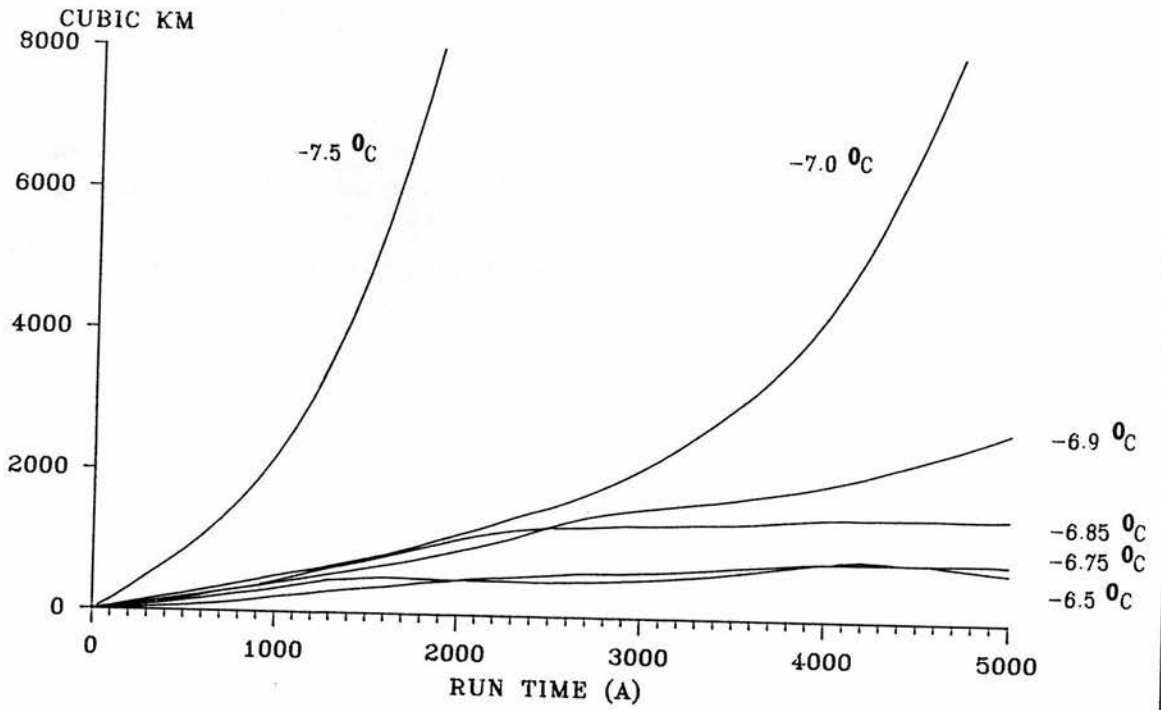
FIGURE 4.29 THE PREDICTED ICE SHEET EXTENT AT 5.0 KA IN A RUN USING ONLY THE MEAN TOPOGRAPHY AND A CONSTANT TEMPERATURE DEPRESSION OF -6.85 ^{0}C. THE ABLATION AND ACCUMULATION AREAS OF THE ICE SHEET ARE INDICATED.

NET MASS BALANCE

ACCUMULATION
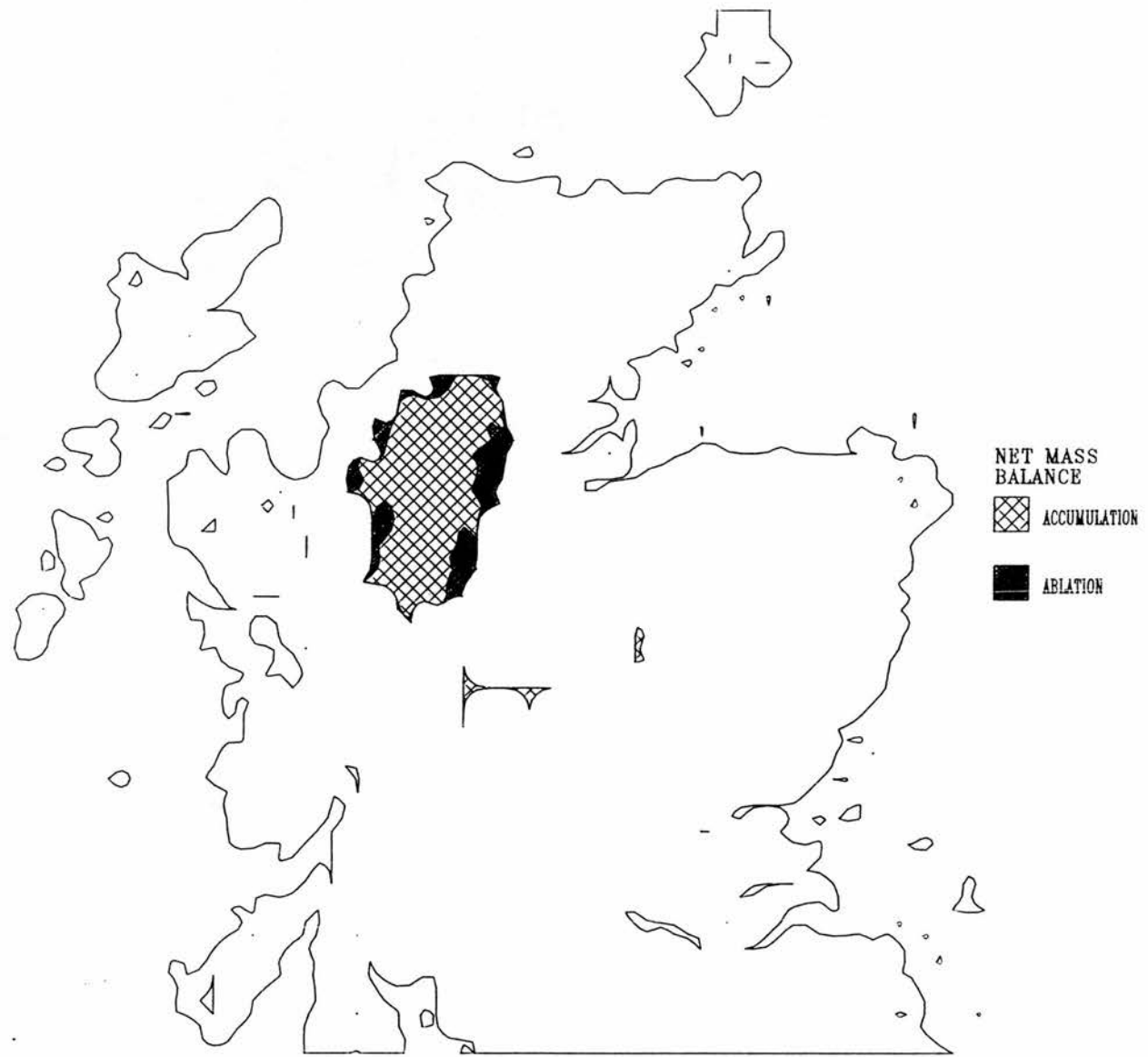
ABLATION

FIGURE 4.30 THE PREDICTED ICE SHEET EXTENT AT 5.0 KA IN A RUN USING ONLY THE MEAN TOPOGRAPHY AND A CONSTANT TEMPERATURE DEPRESSION OF −6.9 ^{0}C. THE ABLATION AND ACCUMULATION AREAS OF THE ICE SHEET ARE INDICATED.

NET MASS BALANCE

ACCUMULATION

ABLATION
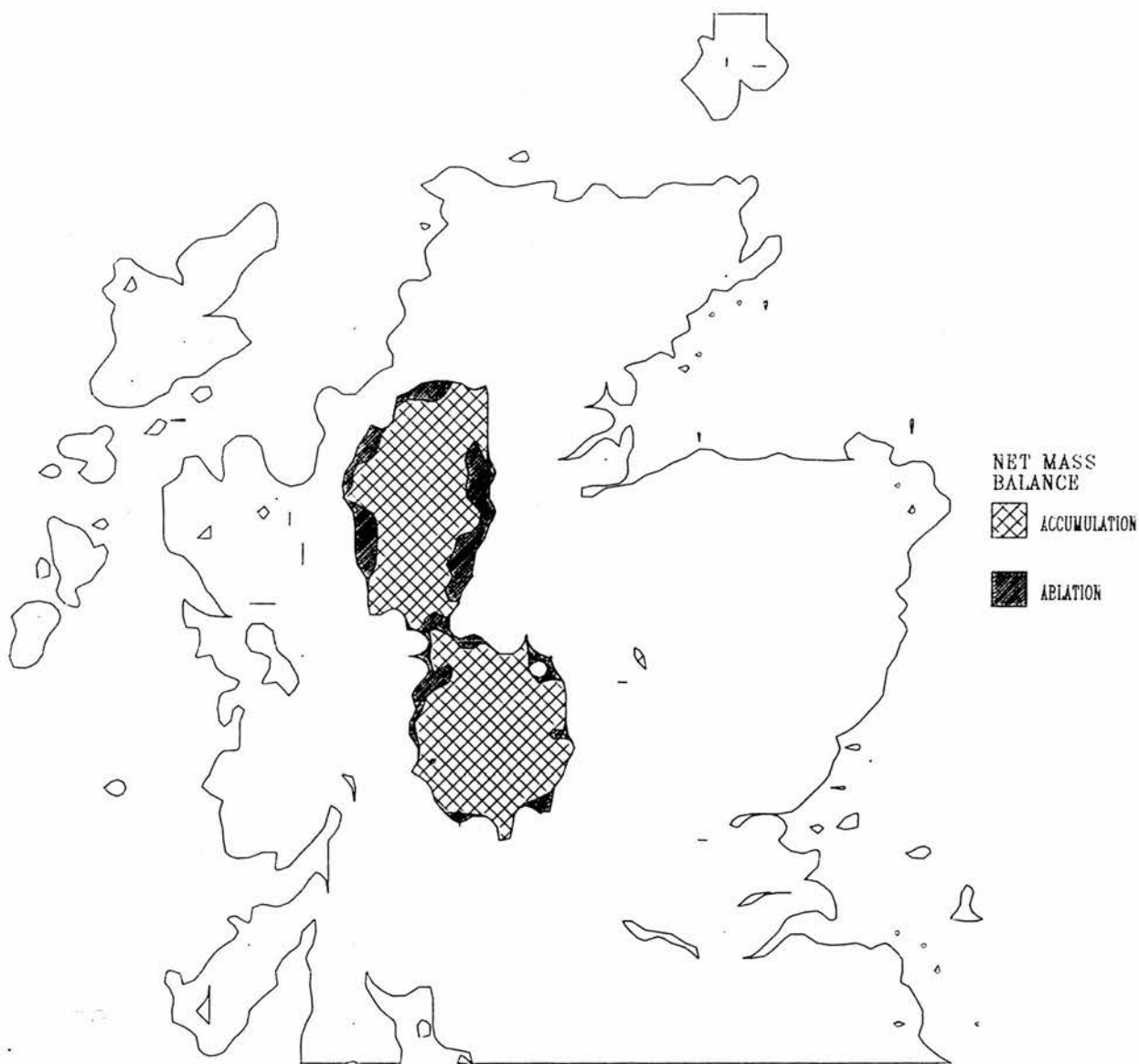
FIGURE 4.31 THE ICE SHEET VOLUME OUTPUT PRODUCED BY A MODEL WITH INCREASED SLIDING VELOCITY, WHEN IT IS FORCED USING CONSTANT IMPOSED TEMPERATURE DEPRESSIONS.
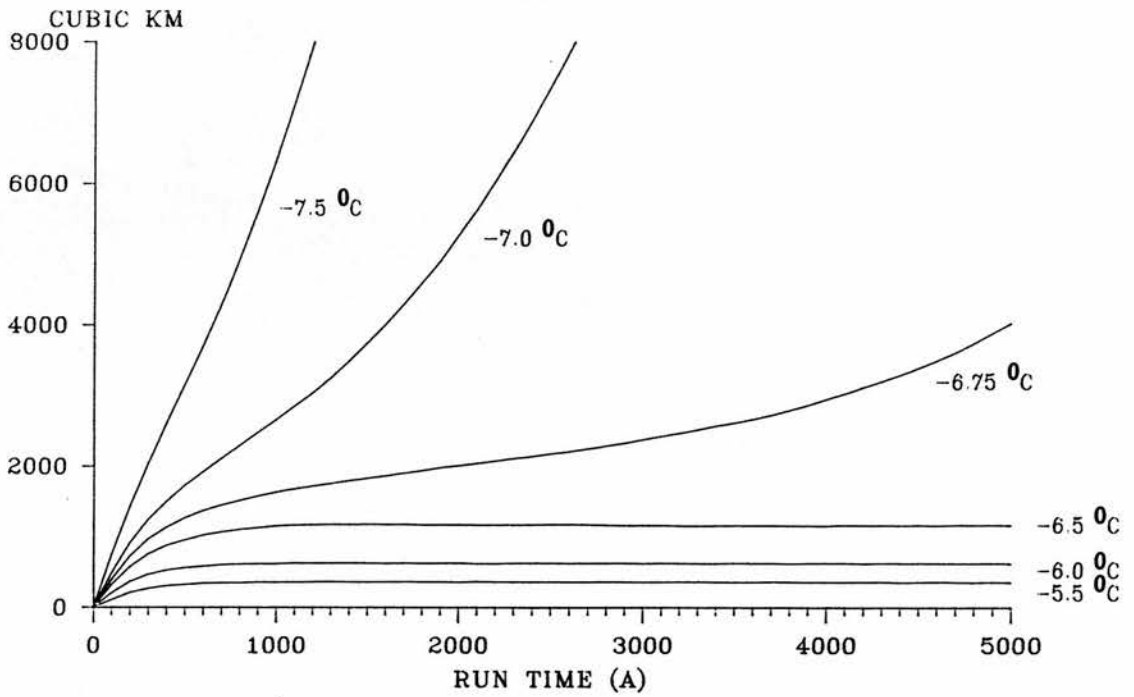
CHAPTER FIVE : THE CLIMATE OF THE LOCH LOMOND STADIAL IN SCOTLAND.

(5.1) THE AIMS OF THE CASE STUDY.

One of the main conclusions of the previous chapter was that the Loch Lomond ice sheet in Scotland was particularly sensitive to changes in climate; experiments which used varying air temperature and precipitation inputs had greatly differing outcomes. In contrast ice flow dynamics were found to have a relatively unimportant role in determining the behaviour of the ice sheet. The purpose of this case study is to assess the validity of the climate assumptions used in the initial Loch Lomond ice sheet model.

There were two sets of climate assumptions. First, precipitation distribution during the stadial was assumed to be both constant and similar to the present day distribution. This further implies that falling air temperatures had no effect on atmospheric moisture contents and precipitation rates, and that the southerly migration of the oceanic North Atlantic polar front had no effect on Scotland's precipitation. This case study attempts to test the validity of these assumptions by explicitly modelling atmospheric moisture and precipitation over Scotland during the stadial.

A second set of climatic assumptions in the initial Loch Lomond ice sheet model are those associated with ablation and the fraction of precipitation falling as snow (effectiveness). In both cases crude relationships to altitude, latitude and imposed temperature change were used. The validity of these relationships is impossible to test independently because there is no evidence relating to the actual values of ablation and effectiveness during the stadial. As an alternative, more sophisticated methods of determining ablation and effectiveness are used in this case study. The aim is to assess the difference in model behaviour produced by employing these more sophisticated methods. The aims of the case study are therefore:

(i) to develop an atmospheric moisture model that is capable of predicting the precipitation rates over Scotland during the Loch Lomond stadial;

(ii) to couple this model to the Loch Lomond ice sheet model and to assess the effect of changing precipitation distributions on the dynamics of the Loch Lomond ice sheet;

(iii) to develop an alternative method of modelling ablation and effectiveness variations during the Loch Lomond stadial; and

(iv) to substitute this latter alternative into the coupled ice sheet model and to assess its effects on overall model behaviour.

The structure of this case study reflects these aims, and consists of four sections that discuss the models and their results. The first section (Section 5.2) discusses the precipitation model and is divided into three sub-

sections:- a general atmospheric moisture model; its application to the problem of determining atmospheric moisture fluxes over the Atlantic Ocean; and a higher resolution model that couples Atlantic atmospheric moisture fluxes to a detailed Scottish model. The second section (Section 5.3) describes the results obtained when the above precipitation model is coupled to the Loch Lomond ice sheet model. A sensitivity analysis of these results is also presented.

An important element of the first two sections is the treatment of contrasting wind direction. Thus results are replicated for one model in which the predominant wind direction is from the West and for another using a predominantly south-westerly wind direction. The importance of these contrasting experiments is to test the contention of Sissons (1979b) that wind directions during the Loch Lomond stadial where not westerly, as they are at present, but were south-westerly. The section concludes with an analysis of the model output and addresses questions such as the likelihood of the inheritance of pre-Loch Lomond ice and the effect of North Atlantic polar front migration on frontogenesis in the Scottish area.

The third section (5.4) deals with the development of alternative ablation and effectiveness models. These

models, in contrast to the ones initially used, explicitly include an estimate of surface air temperature. There are three sub-sections:- development of a simple surface air temperature model; development of alternative ablation and effectiveness models using surface air temperature input; and comparison with the initial ablation and effectiveness models. The fourth and final section of this case study links these alternative models of ablation and effectiveness with those of precipitation and ice sheet flow, and assesses the implications of the model's output for the behaviour of the Loch Lomond ice sheet.

(5.2) THE ATMOSPHERIC MOISTURE - PRECIPITATION MODEL.
(5.2.1) GENERAL DESCRIPTION OF THE MODEL.

The model is derived from the work of Sanberg and Oerlemans (1983), who modelled the effects of orographically enhanced precipitation and atmospheric moisture depletion on ice sheet evolution. The model is useful to the present study because it allows the effects of atmospheric and oceanic temperature changes on precipitation to be assessed in a relatively simple manner. The sophistication of the model is intermediate between a purely empirical model and a full global circulation model. It is based around the continuity equation for vertically integrated atmospheric moisture and contains terms dealing with evaporation,

precipitation, advection and diffusion. Changes in
atmospheric moisture content through time (t, in s) are
determined using the equation:

$$\frac{\partial W}{\partial t} = \frac{W_{sat} - W}{T_*} - W(f_0 + f_1 S) - U.\nabla W + D_W.\nabla^2 W \quad (5.1)$$

where W is the amount of water vapour in a vertical
column extending from the ground surface to the 'top' of
the atmosphere, and has units of kg m^{-2}; W_{sat} is the
amount of moisture held in this column when the air is
saturated, and has units of kg m^{-2}; T_* is the time scale
over which evaporation occurs from a surface, in s; S is
upwind ground surface slope, and is dimensionless; f_0 and
f_1 are parameters that determine the exact relationship
between surface slope, atmospheric moisture and
precipitation (units s^{-1}); U is a specified wind velocity
field (ms^{-1}) and D_W is the diffusivity of atmospheric
moisture (m^{2}s^{-1}).

Evaporation in the model.

The first term in equation (5.1) represents the
moisture flux entering the atmospheric store via
evaporation. The magnitude of this flux depends on the
difference between the current moisture content and the
saturated moisture content and on the time scale over
which evaporation occurs. In the model this latter is
dependent solely on the ground surface type and
different time scales are used for water, land and ice

surfaces.

The saturated water content of the atmosphere depends on two factors, surface temperature and elevation. The derivation of a series of curves relating saturation moisture content to temperature and altitude is now discussed. The saturation vapour pressure (e, mbar) above a fresh water surface is a function of air temperature (T, ^{o}C):

$$e = 6.1 \times 10^{(aT/T+b)}$$

(5.2)

where a and b are parameters with values of 7.5 and 237.3 respectively (Haurwitz 1941). The exact form of this relationship varies with water salinity and the presence of ice, but numerical experiments reveal that this variation is extremely minor. For a given air temperature, saturation vapour pressure can be found and converted to an equivalent moisture density (χ , $kg\ m^{-3}$) using:

$$\chi = \frac{217\,e}{273+T}$$

(5.3)

The next stage in determining the saturation moisture content of the atmospheric column is to obtain both a relationship between altitude and air temperature and boundary values for the problem. The variation of temperature with altitude is modelled as a linear decrease from a specified surface temperature at a lapse

267

rate of 6.5 ^{O}C km^{-1} (Barry 1981). This relationship is used for the lowest 5.5 km of the atmosphere, which holds the bulk of the atmosphere's moisture content (Barry and Chorley 1982). This relationship and that of equation (5.3) are substituted into equation (5.2), which is then integrated with respect to altitude producing a relationship that estimates vertically integrated saturation moisture content (W_{sat}, kg m^{-2}) for a column running between the ground surface and 5.5 km. This equation requires surface air temperature and surface elevation to be specified. The former is required as a boundary from which to start the integration, while the latter affects saturation moisture content because the depth of moisture-bearing atmosphere above the ground surface is altered by surface altitude.

Several curves of saturation moisture content as a function of sea level air temperature and altitude are shown in Figure 5.1. The relationship between saturation moisture content and surface elevation is particularly strong for warmer sea level air temperatures and is partially the cause of the 'elevation desert effect' of Budd and Smith (1981) and Sugden (1977). In addition, the saturation moisture content above the oceans, where surface elevation is equal to zero, is very sensitive to air temperature. The information shown in Figure 5.1 is fed into the the model as a 'look up' table. Exact values

*are determined using an interpolation routine. Despite
having been determined independently, the values
presented in Figure 5.1 agree closely with those of
Sanberg and Oerlemans (1983).*

Precipitation in the model

*The second term in the continuity equation (5.1)
represents the moisture flux lost from the atmospheric
store via precipitation. This term is particularly
important because it represents the link between the
atmospheric moisture model and the Loch Lomond ice sheet
model. Precipitation responds to variations in both
atmospheric moisture content and upwind ground surface
slope. The orographic enhancement of precipitation is
caused by increased surface slopes, and the
'precipitation shadow' effect is the result of reduced
moisture contents. Upwind surface slope is specified and
is crucial to the model's prediction of spatial
precipitation pattern. The model does not simulate
precipitation changes that arise from varying circulation
patterns. Thus the variation of precipitation rates
produced by shifting cyclone tracks (Keen 1984) is not
incorporated in the model.*

Advection and diffusion in the model.

*The third and fourth terms in equation (5.1) represent
advection and diffusion respectively and are concerned*

269

with the movement of moisture horizontally through the atmosphere. Both involve the 'grad' operator which represents the derivatives of W in both horizontal dimensions (x and y). The 'grad squared' operator of the diffusion term involves the second derivatives of W. The diffusion term also involves a diffusivity constant for atmospheric moisture (D_W). The advection term is the product of 'grad W' and a specified vertical-mean wind velocity.

Numerical considerations.

The response time of the atmospheric moisture system is shorter than those of ice sheet and ocean systems. It is therefore assumed that the distribution of atmospheric moisture comes into equilibrium with a given set of temperature, ice sheet and topographic conditions. Equation (5.1) is integrated forward through time until a steady state moisture distribution is achieved. A straight-forward finite difference scheme is used, where the 'grad' terms are approximated using centred differences in space and the derivative of moisture content (W) with time (t) is integrated using a forward scheme (see Section 2.5). The end condition used in the model assumes that a steady state is achieved if the change in total atmospheric moisture content produced by a single iteration falls below a certain level. Several model experiments indicate that the moisture and

precipitation distributions do indeed reach a steady state at this stage. The exact levels used as end conditions are specified in the relevant Atlantic Ocean and Scottish sub-sections.

(5.2.2) ATMOSPHERIC MOISTURE FLUXES OVER THE ATLANTIC OCEAN DURING THE LOCH LOMOND STADIAL.

The model is now applied to the problem of determining atmospheric moisture fluxes across the Atlantic Ocean during the Loch Lomond stadial. This sub-section details the various inputs to the model; indicates the parameter values, end conditions and boundary values used; and presents model output for atmospheric moisture contents and precipitation rates.

The simulation of Scottish precipitation during the Loch Lomond stadial must begin with a consideration of Atlantic atmospheric moisture fluxes because the climate of Scotland is dominated by the westerly advection of moisture from the Atlantic. A one-dimensional flowline form of the atmospheric moisture model is used. This is computationally more efficient than the full two-dimensional model because the 'grad' terms only consider derivatives along the direction of air flow. This simplification is justifiable because advection dominates diffusion as the main form of horizontal moisture transport at the large spatial scales of the

Atlantic Ocean.

Atlantic model input data.

As mentioned above, two models are developed, one using westerly airflow and the other south-westerly airflow. These contrasting wind directions have three consequences. Two are concerned with the finer resolution Scottish model and relate to the aspect of the upwind ground surface slope and the direction of advection over the area. The third concerns the direction from which Atlantic moisture is advected into the Scottish area; thus one flowline model is concerned with a wind fetch to the West of Scotland and the other to the South-West.

The two model flowlines are shown in Figure 5.2, each follows a linear course and contains 20 elements each of 220 km length. The curl shown in the trajectory of the South-West transect in Figure 5.2 is produced by the geometric distortion of the projection used. For the model to be used the following input data are required at each of the 220 km elements:

(i)   topography (mean surface altitudes), used in the determination of upwind surface slope (S), the determination of saturation atmospheric moisture content (W_{sat}) and the allocation of evaporation time scale constants (T_*);

(ii) vertical-mean wind velocity (U), used in the advection term; and

(iii) sea level air temperatures, used in the determination of saturated atmospheric moisture contents.

The dry land topography of the area (the first set of input data) is used to calculate upwind surface slopes using:

$$S = \max\left(0.0, (B_i - B_{i-1})/\triangle X\right) \qquad (5.4)$$

where B_i and B_{i-1} are mean bedrock elevations in km at the current element (i) and the adjacent upwind (i-1) element, and $\triangle x$ is the element size (in this case 220 km). The zero constraint is used to ensure that negative precipitation values do not occur on the lee side of mountain ranges!

The use of a horizontal element size of 220 km is prompted by considerations of the origins of orographic precipitation in Scotland. The work of Sawyer (1956) and of Atkinson and Smithson (1972 and 1974) indicates that upland areas in Britain are associated with high precipitation rates because of the increased cyclogenesis of frontal depressions passing over orographic barriers. The slope of a typical front lies between 0.01 (for a warm front) and 0.02 (for a cold front, Barry and Chorley 1982). The effect of the Scottish highland massif is therefore likely to manifest itself over distances of between 100 and 200 km, assuming a general upland altitude of 1 km and a frontal slope of 0.01 to 0.02. Thus an element size of 220 km gives sufficient horizontal resolution.

273

The second set of model input data relate to the specified wind field, which can be represented as series of magnitudes rather than as a series of vectors. A constant value of 4.0 m s^{-1} is used in the model for both transect directions, principally for the sake of convenience. Experiments with a more realistic set of wind magnitudes indicated that model behaviour was not sensitive to the exact wind magnitudes used.

The third set of input data relates to surface air temperatures. Variation in sea level air temperatures are used to drive the model and are affected by the migrations of the North Atlantic polar front. This oceanic front separates polar water to the North from sub-polar water to the South. Its migrations have been accurately tracked by the analysis of deep sea core sediments (as discussed in Section 2.2.1). During the Loch Lomond stadial the front migrated from a position between Newfoundland and Iceland to its maximum southerly extent at 45 ^{O}N and then retreated rapidly to its present day position around Greenland. The model used in this section is applied at eleven specific times, starting at 12.5 ka BP and then at every 500 a to 7.5 ka BP. The positions of the front at these times, shown in Figures 5.3 and 5.4, are derived from the data of the Ruddiman and McIntyre (1981 a and b), McIntyre et al (1976) and Kellogg T. B. (1977).

The following steps are used to determine the required

sea level air temperatures:

*(i)   present   day   summer   and   winter   sea   level   air
        temperatures   and   sea surface   temperatures   are
        obtained from Tucker and Barry (1984);*

*(ii)   an idealized sea surface temperature   cross-section
        is estimated from the data of Ruddiman et al (1977)
        and CLIMAP (1981);*

*(iii) a series of sea surface temperature profiles along
        the two model   transects are constructed using the
        present day sea surface temperature data   of (i),
        the   idealized   cross-section   of   (ii)   and   the
        estimates of North Atlantic polar front position in
        Figures 5.3 and 5.4; and*

*(iv)   these   sea   surface temperature profiles are
        converted to sea   level air temperatures using a
        regression equation based on the present day data
        of (i).*

The present summer and winter data is first averaged

to produce annual estimates of sea surface temperature

and sea level air temperature. The former refers to the

water temperature at the ocean/air boundary, while the

latter refers to the air temperature at this surface. The

40 annual estimates   are regressed to give the following

relationship between sea surface temperature (T_w, ^oC) and

sea level air temperature (T_a, ^oC):

$$T_a = -4.19 + 1.26 T_w$$
(5.5)

This regression equation explains   99.3 % of the

variation within the data sets. It is used later to

convert the final sea surface temperature profiles into

the sea level air temperatures used in the model.

275

The second stage is the derivation of an idealized sea surface temperature cross-section of the North Atlantic polar front. The available data (Ruddiman et al 1977 and CLIMAP 1981) were used to obtain the cross-section in Figure 5.5, which shows the temperatures on a transect running perpendicular to the front and intersecting the front at the fourth unit of the transect. This profile captures the basic structure of the front, namely a dramatic fall in sea surface temperatures preceding the front (12.7×10^{-3} ^{o}C km^{-1}) and a gentler decrease behind the front (1.5×10^{-3} ^{o}C km^{-1}). The effect of North Atlantic polar front migration on sea surface temperatures is modelled in this way because actual time dependent estimates of sea surface temperatures during the Loch Lomond are limited to a few geographical locations and do not provide a complete spatial distribution.

Sea surface temperature distributions can now be estimated. Ruddiman et al (1977) indicate that Atlantic sea surface temperatures at 7.5 ka BP were similar to their present day values, with the North Atlantic polar front located close to its present day position around Greenland. The present day distribution of temperatures is therefore used as the 7.5 ka BP model input data set. For the earlier times of interest a sea surface temperature distribution is synthesised by overlaying the

276

idealized profile on this present day distribution. Sea

surface temperatures at the nodes of the model transects

(see Figure 5.2) are obtained from this overlay using the

following rules:

*(i)   the   position of the North Atlantic polar front is
        identified, this   point is   given the temperature
        4.5 ^{o}C (Figure 5.5);*

*(ii)   data   points falling inside the front are assigned
        temperatures according to the idealized profile;*

*(iii)   data points falling outside the front are given a
        temperature based on the idealized profile if they
        are less than three transect units from the front
        and the idealized profile temperature is less than
         the node's present day   temperature; otherwise
        the node's present day temperature is used; and*

*(iv)   an allowance is made for the angle of intersection
        between the transect and the North Atlantic polar
        front; the decline in temperature used behind the
         front is less when the transect crosses the front
        at an acute angle.*

The sea surface temperatures derived using the above

rules were then converted to sea level air temperatures

using equation (5.5). The results are shown in Figures

5.6 and 5.7 for the West and South-West transects

respectively and at 7.5 ka BP (present day data), 8.0,

8.5, 9.0, 9.5, 10.0, 10.5, 11.0, 11.5, 12.0, and 12.5 ka

BP. Also shown in the figures are the topographic input

data used for the transects.

Parameter values and numerical considerations.

The complete set of parameter values used in the model

are shown in Table 5.1. Initially atmospheric moisture

content at each node was set to a value of 5.0 kg m^{-2}. Equation (5.1) was then iterated forward through time until the change in total atmospheric moisture content produced by a single iteration was less than 0.0001 kg m^{-2} (7×10^{-5} % of its final value), this condition was generally met after 1500 to 2100 iterations. The boundary conditions employed set advection and diffusion equal to zero at the first and final nodes of the model transect.

Atlantic model output.

This sub-section has three aims. First, the output of the Atlantic model is compared to estimates of actual precipitation and evaporation over the present day Atlantic Ocean. Second, the effect of North Atlantic polar front migration on the distribution of moisture over the Atlantic is ascertained. Third, boundary condition data are selected for the finer resolution Scottish study .

The predicted patterns of precipitation along the two model transects are shown in Figures 5.8 and 5.9, for the West and South-West runs respectively. The present day, West transect run was used to tune the model. Precipitation rates vary between 600 and 800 mm a^{-1} in the oceanic sector of the transect and reach a peak value of 2400 mm a^{-1} over Scotland, which is in accord with the

estimates of Tucker (1961) Reed and Elliot (1979) for the Atlantic, and of the Meteorological Office (1968) for Scotland. The model predicts evaporation rates of 800 to 1200 mm a^{-1} over the ocean, which is in agreement with the estimates of Zubenok and Strokina (1963). Precipitation in the cooler than present West transect runs has a generally similar pattern to that of the present day run, but oceanic precipitation rates fall to a minimum of 500 mm a^{-1} and Scottish precipitation rates reach a minimum of 1300 mm a^{-1}. The South-West transect runs have generally higher precipitation rates with oceanic values typically in excess of 1800 mm a^{-1}.

The equivalent atmospheric moisture patterns are shown in Figures 5.10 and 5.11. They reflect the distribution of sea level air temperature (Figures 5.6 and 5.7). The West transect runs show a progressive reduction in atmospheric moisture content as a result of the southerly migration of the North Atlantic polar front. The main implication of these runs for the Scottish model is the reduction in the amount of advected atmospheric moisture over the area during the Loch Lomond stadial. In contrast the South-West transect runs are relatively unaffected by North Atlantic polar front migration and moisture advection over Scotland remains considerable in all runs.

No sensitivity analysis is presented for the flowline model of Atlantic atmospheric moisture because it represents just one of several inputs to the more important Scottish atmospheric moisture model. The role of the Atlantic model is to provide boundary conditions for the Scottish model, in particular moisture advection. The sensitivity of these boundary conditions in the Scottish model is analysed later. The important information to be carried forward as boundary conditions for the Scottish model is shown in Table 5.2. This information consists of the steady state atmospheric moisture content over Scotland (transect nodes 17 and 18) and over the two transect nodes adjacent to Scotland (16 and 19).

(5.2.3) ATMOSPHERIC MOISTURE FLUXES OVER SCOTLAND DURING THE LOCH LOMOND STADIAL.

In the application of the atmospheric moisture model to the Scottish climate during the Loch Lomond stadial the model reverts to a two dimensional form. The grid is the same as that used in the Loch Lomond ice sheet model and consists of 91 (East - West) by 81 (North - South) cells of 5 x 5 km size.

This sub-section is divided into three parts. First, there is a discussion of the data input required by the model. Second, the parameterizations, the initial conditions, the boundary conditions and the end points

used to run the model are discussed. Third, there is a discussion of model output and a sensitivity analysis of the model.

Scottish model input data.

The Scottish model requires surface air temperature, vertical mean wind velocity and topography to be specified. The surface air temperatures used are derived from the air temperature difference time series (Section 2.2.1) at the eleven specific times of interest. Surface air temperatures are derived from these differences using a present day sea level air temperature of 8.5 ^{o}C and a lapse rate 6.5 ^{o}C km^{-1}. Apart from the changes caused by varying surface elevations, Scottish surface air temperatures are assumed constant at a particular time for the whole area. The second model input is vertical mean wind speed, for which a constant value of 4.0 m s^{-1} is assumed for the whole area and for both wind directions.

The final model input of surface topography uses the gridded representation of mean bedrock topography introduced in Chapter 4. Saturation moisture content (W_{sat}) is derived using this topographic data (in addition to the surface air temperatures discussed above), as are the evaporation time scales (T_{*}). However the principal use of topography is in determining upwind

surface slope distribution. This is found using:

$$S_i = \max\left(0.0, \left(B_i - \left(\sum_{k=i}^{i-n} B_k\right)/n\right)/\triangle x_n\right) \qquad (5.6)$$

where B_i is mean elevation at the current grid cell, which incorporates any ice thicknesses present. The summation term finds the mean elevation of the n upwind grid cells, and $\triangle x_n$ refers to the horizontal distance separating the current grid cell from the middle grid cell of the summation set. Since orographic enhancement occurs at horizontal distances of 100 to 200 km, the number of 5 km grid cells over which topographic averaging is appropriate amount to 20 ($n=20$).

Equation (5.6) refers to the case of westerly airflow, and i refers to grid points along a West - East row (x dimension). The second wind direction to be modelled is south-westerly. The upwind slopes in this case are found by using:

$$S_{i,j} = \max\left(0.0, \left(B_{i,j} - \left(\sum_{k=i,m=j}^{i-n,j-n} B_{k,m}\right)/n\right)/\triangle x_n\right) \qquad (5.7)$$

where the summation subscripts refer to changing x and y positions within the grid, and $\triangle x_n$ is corrected to give a diagonal South-West distance rather than a westerly distance. The distributions of upwind slope produced by equations (5.6) and (5.7) are shown in Figure 5.12 and 5.13 respectively.

Parameter values and numerical considerations.

The parameter values used in the model are shown in Table 5.3. The slight differences between these parameter values and those used in the Atlantic model arise because of the different scales of the two models. Three specific numerical considerations need further consideration, they are initial values, boundary conditions and end point.

Initial atmospheric moisture values are set equal to those predicted by the Atlantic model over Scotland (Table 5.2). The Scottish model's domain is divided into two halves, each of which takes its initial atmospheric moisture content from the Atlantic transect nodes 17 and 18 (for both West and South-West wind directions). In this way iterations of the Scottish model alter the distribution of moisture within the model domain but do not significantly alter the total moisture held within the model. This reduces the number of iterations that the model requires to reach steady state and saves on the computation time needed to run the model.

The boundary conditions allow Atlantic moisture to advect into the Scottish model. In the case of the westerly airflow net import and export of moisture to and from the model occurs solely along the flowline of the Atlantic model (West to East). Thus both advection and diffusion are set equal to zero at the northern and

southern boundaries of the model. At the eastern and western boundaries diffusion is also set equal to zero. This is done principally for the sake of convenience, because diffusion only accounts for a small amount of atmospheric moisture movement within the model. The following three step scheme is used to estimate advection at the western and eastern boundaries of the model.

First, mean atmospheric moisture contents are found for the westerly and easterly halves of the model domain. Second, the derivative of atmospheric moisture content is found using this varying mean value and the fixed value at the adjacent Atlantic transect node. The equation used is:

$$\frac{\partial W}{\partial x} \approx \frac{W_w - W_{i-1}}{\triangle X_a} \, , \, \frac{\partial W}{\partial x} \approx \frac{W_{i+1} - W_e}{\triangle X_a} \qquad (5.8)$$

where $\triangle x_a$ refers to the distance between Atlantic transect nodes (220 km); W_w and W_e are the calculated means of atmospheric moisture in the two halves of the model domain (West and East respectively); and W_{i-1} and W_{i+1} are, respectively, the fixed atmospheric moisture values at the adjacent upwind and downwind Atlantic transect nodes (16 and 19). The third step is to find advection over the boundary as the product of the above derivative and the specified wind velocity (U). This estimate is then used in the next iteration of the continuity equation (5.1) and a new atmospheric moisture

284

distribution is determined, from which the half-domain means are calculated.

This scheme is used principally because it allows the Scottish atmospheric moisture distribution to develop an equilibrium with the adjacent Atlantic moisture values and thus with the whole Atlantic moisture transect. This is more realistic than a scheme which specifies constant derivatives at the model boundaries.

The above boundary scheme is used in the south-westerly wind direction model with the following amendments. The Scottish model domain is divided into South-West and North-East halves rather than East and West halves. The advection derivatives are then found using these values and those at the two adjacent South-West transect nodes. Derivatives at the southern and western boundaries use the South-West mean and moisture at Atlantic node 15, while derivatives at the northern and eastern boundaries use the North-East mean and moisture at Atlantic node 19.

The final numerical consideration is that of the end condition used to estimate when the modelled atmospheric moisture distribution has reached steady state. As with the Atlantic atmospheric moisture model a check is kept on total atmospheric moisture content. The model is

assumed to have reached a steady state when the change in mean moisture content produced by a single iteration of the model is less than 0.0001 kg m^{-2} (0.002 % of the final value). In general 1400 iterations are required for this condition to be met.

Scottish model output.

This section is concerned with three aspects of Scottish model output. First, a detailed description is given of a model run using present day conditions. Second, a sensitivity analysis of the model is presented using perturbations around this present day model run. And third, example runs are presented for different times during the Loch Lomond stadial and for the two contrasting wind directions. The model was initially run using present day air temperatures and boundary conditions, and with a westerly wind direction. Figures 5.14, 5.15 and 5.16 show the distributions of saturated moisture content, steady state moisture content and precipitation, respectively. Comparison of the saturated and steady state moisture contents indicates that the saturation of the atmosphere varies between 20 and 35 %. The expected atmospheric moisture depletion to the East is present and moisture contents in the East are 50 % of the values in the West. This pattern of atmospheric moisture and the distribution of upwind surface slopes (Figure 5.12) determine the modelled precipitation

pattern. There is a close agreement between this distribution and the actual distribution (Figure 4.2). The crucial high precipitation rates over the South-East Grampians and the North-West Highlands are accurately modelled, as are the moderate rates over the Cairngorms in the East.

The results of the sensitivity analysis performed on the model are shown in Figures 5.17 and 5.18 and in Table 5.4. In each model run the present day model inputs are held constant while the value of one parameter is either increased or decreased by 50 %. Histograms of the precipitation distributions produced in these sensitivity runs are shown in Figures 5.17 and 5.18, along with the histogram of the present day modelled precipitation distribution. The goodness of fit index values shown in Table 5.4 are calculated using (Kirkby et al 1987):

$$\text{G.F.I.} = \sum_{i=1,j=1}^{n,m} \left(P_{i,j}^{stan} - P_{i,j}^{sens} \right) \qquad (5.9)$$

where n and m refer to the overall model domain (91 by 81); and $P^{sens}_{i,j}$ and $P^{stand}_{i,j}$ are the precipitation rates at point i,j in the particular sensitivity run and in the standard present day modelled run.

The indices calculated from equation (5.9) use the overall precipitation distribution and do not highlight

areas of high precipitation. The arguments of Chapter 4 imply that areas of high precipitation are very important in the initiation of the Loch Lomond ice sheet. Thus a second goodness of fit index is included in Table 5.4 that uses only areas with a modelled present day precipitation rate in excess of 1800 mm.

The modelled precipitation distribution is particularly sensitive to a decrease in saturation moisture content (W_{sat}), decreased boundary conditions (the amount of atmospheric moisture advected into the area from the Atlantic Ocean) and a decrease in precipitation parameters f_0 and f_1. The latter sensitivity is to be expected because of the effect of surface slope on precipitation. The former two sensitivities indicate the importance of moisture input into the atmosphere via evaporation and advection.

Precipitation during the Loch Lomond stadial can now be simulated using the atmospheric moisture model. Two model runs were performed to assess the effect of falling air temperatures on precipitation during the stadial. The model used Loch Lomond stadial input data and boundary conditions. The input data are shown in Table 5.5. The estimated Atlantic moisture fluxes come from the Atlantic modelling work of sub-section (5.2.2) and the air temperatures come from the forcing function used in the

Loch Lomond ice sheet model (sub-section 2.2.1). Topographic and wind velocity input data are the same as in the present day run. The topographic data does not incorporate elevation changes caused by the growth of the Loch Lomond ice sheet, and thus the simulated precipitation patterns reflect changes in air temperature alone.

Histograms of the predicted precipitation patterns for 12.0 and 10.0 ka BP and for the present day are shown in Figure 5.19. These times are chosen to investigate the effects of a range of air temperatures in the model. The 12.0 ka BP run has an air temperature roughly 4 ^{o}C cooler than the present day air temperature and the 10.0 ka BP run has an air temperature that is roughly 8 ^{o}C cooler. There is a progressive decrease of the mean precipitation rate with these falling air temperatures, such that the mean precipitation rate is 1083 mm a^{-1} at the present day, 852 mm a^{-1} at 12.0 ka BP, and 597 mm a^{-1} at 10.0 ka BP. This decrease reflects both a general reduction of non-orographic precipitation and a dramatic fall in orographic precipitation. This latter feature has important implications for the Loch Lomond ice sheet model, because ice sheet growth is related to the presence of high precipitation areas over the West coast of Scotland. The decline is such that the area with a precipitation rate in excess of 1800 mm a^{-1} falls from

9.4 % of the overall model domain at the present day, to 4.2 % at 10.0 ka BP and 0.05 % at 12.0 ka BP. The precipitation pattern produced in these two Loch Lomond stadial runs is similar to that of the present day, with a distinct East-West gradient.

Figures 5.20 and 5.21 show, respectively, the modelled distributions of steady state atmospheric moisture and precipitation obtained using the south-westerly wind direction. This output was obtained using the same present day air temperature and topographic data as the westerly airflow run. The distribution of saturated moisture content is therefore the same in both run runs (Figure 5.14). The boundary conditions did, however, differ from those of the westerly airflow run (see Table 5.5).

The steady state atmospheric moisture distribution (Figure 5.20) reflects the south-westerly airflow in that moisture depletion increases progressively from the South-West to the North-East. The precipitation distribution (Figure 5.21) is determined by this pattern and by that of the south-westerly upwind surface slopes (Figure 5.13). This precipitation distribution is similar to that produced by the present day westerly airflow run. However overall precipitation is higher because of the increased atmospheric moisture advection. In addition,

precipitation over the South-West Grampians becomes proportionally more important than that over the North-West Highlands. The high precipitation rates over the Southern Uplands arise because of inaccuracies at the boundary of the model.

The two experiments (Figure 5.19) investigating the effects of atmospheric cooling on precipitation at 10.0 and 12.0 ka BP are repeated using the south-westerly airflow model. Equivalent air temperature and topography inputs are used in both sets of runs, but the differing boundary conditions lead to greater atmospheric moisture advection in the south-westerly run. Mean precipitation rates fall from 1146 mm a^{-1} (present day) to 1088 mm a^{-1} (12 ka BP) and 745 mm a^{-1} (10 ka BP). The fraction of the model domain which has a precipitation rate in excess of 1800 mm a^{-1} falls from 13.9 % (present day) to 8.7 % (12 ka BP) and 0.2 % (10 ka BP). Both of these features indicate that precipitation rates are generally higher than those of the equivalent westerly airflow run.

The atmospheric moisture model discussed in this section contains a large number of assumption and uses a variety of input data sets. However, the predictions of the model remain relatively stable when the parameters and inputs of the model are altered. The model provides a useful method of predicting the accumulation input to

the Loch Lomond ice sheet. A sensitivity analysis of the coupled ice sheet - atmospheric moisture model can be used to assess the sensitivity of the the atmospheric moisture assumptions in the overall coupled model. This procedure will allow the effects of inaccuracies in the atmospheric moisture model on the behaviour of the overall coupled model to be assessed.

(5.3) A COUPLED ATMOSPHERIC MOISTURE - ICE SHEET MODEL.
(5.3.1) INTRODUCTION.

The aim of this section is to build on this previous work and to assess the effect of varying precipitation on the growth and decay of the Loch Lomond ice sheet. The previous section indicates that significant changes in the distribution of precipitation could have arisen during the Loch Lomond stadial. For instance, the maximum temperature depression of 8.0 ^{o}C at 10.0 ka BP led to a 45 % reduction in mean precipitation rate and a 99.5 % reduction in the size of the area over which precipitation exceeded 1800 mm a^{-1}. The consequences of this variation for ice sheet behaviour are now investigated by coupling the new atmospheric moisture model of Section (5.2) with the ice sheet model of Chapter 4. The following sub-sections discuss the coupled model's output for both westerly and south-westerly airflow; a sensitivity analysis of the key controlling variables and parameters; and the wider implications.

(5.3.2) OUTPUT FROM THE COUPLED MODEL FOR WESTERLY AND SOUTH-WESTERLY AIRFLOWS.

The ice sheet model used in this section is identical to the one used in Chapter 4 and, as before, the model is run for the 5.0 ka period between 12.5 and 7.5 ka BP. The chronological conventions of Chapter 4 are used, and time is given relative to the model start time of 12.5 ka BP. A time of 2.6 ka should therefore be taken as 9.9 ka BP.

The coupled model is partially driven by the atmospheric moisture model which calculates precipitation every 500 a. At these times the atmospheric moisture model is run to steady state as described in Section (5.2). The final distributions of atmospheric moisture and precipitation produced at these times depend on the model inputs and boundary conditions. Three of these inputs and boundary conditions are specified and are not affected by the behaviour of the ice sheet model. They are wind speed/direction, air temperature and boundary moisture advection. The boundary moisture conditions in each of the eleven atmospheric moisture model runs (one every 500 a) and for both airflow directions are shown in Table 5.5. Wind speed is held at 4.0 m s^{-1}, while air temperatures are derived from the forcing function of sub-section (2.2.1). The values of the model parameters are the same as those shown in Table 5.3.

Topography varies in accord with the growth and decay of the ice sheet, which affects the distributions of both upwind surface slope and orographic precipitation. In addition, the steady state atmospheric moisture distribution is altered because the saturated atmospheric moisture content is affected by surface elevation and enhanced orographic precipitation produces downwind moisture deficits.

Ice volume and mean precipitation rate from the coupled model using westerly airflow are shown in Figure 5.22. Ice thickness and precipitation distributions at 2.6 ka into the model run are shown in Figures 5.23 and 5.24 respectively. A maximum ice sheet volume is achieved at 2.6 ka and is only 13 % of the maximum volume achieved in the constant precipitation run of Chapter 4 (Figure 5.22, the standard volume curve). The phase of exponential ice sheet growth found in this latter, constant precipitation run does not occur when precipitation is allowed to vary in response to climatic change. The high precipitation rates (above 1800 mm a^{-1}, shown in Figure 4.2) that are associated with ice sheet growth in the constant precipitation run are replaced by values that are typically below 1200 mm a^{-1} (Figure 5.24). The exponential growth typical of the constant precipitation run depends on high precipitation rates. When these high rates are absent, ice volumes increase

linearly and the combined effect of falling air temperature and positive net mass balance / ice thickness / surface elevation feedback is insufficient to induce accelerated ice sheet growth.

Comparison of Figure 4.8, which shows ice thickness distribution at 2.6 ka in the constant precipitation run of Chapter 4, and Figure 5.23, which shows ice thickness in the run employing varying precipitation, indicates that, when precipitation is allowed to change, ice growth is restricted to the highland areas around Rannoch Moor and to the North-West Highlands. Ice thicknesses are typically below 300 m. In addition the infilling of topographic basins that typified the constant precipitation run does not occur.

Comparison of Figures 5.16 and 5.24 (modelled precipitation distributions for the present and at 2.6 ka) indicates that the modelled precipitation rates at 2.6 ka are uniformly 500 mm a^{-1} lower than those predicted for the present day. Orographic enhancement occurs in the West, in particular over the North-West Highlands. Here the two factors of reduced precipitation through atmospheric cooling and enhanced orographic precipitation through ice sheet growth counteract each other.

Ice volumes and mean precipitation using the south-westerly airflow model is shown in Figure 5.25. Ice thickness and precipitation distributions at 2.6 ka are shown in Figure 5.26 and 5.27 respectively. South-westerly airflow brings more Atlantic moisture into the Scottish area than westerly airflow. Precipitation is therefore higher and larger ice sheet volumes are achieved. The ice sheet volume at 2.6 ka in the south westerly airflow run is 171 % of that in the westerly airflow run. The ice sheet at 2.6 ka in this run is more extensive than that of the westerly airflow run (Figures 5.23 and 5.26) and some infilling of topographic hollows has occurred, in particular the Rannoch Moor basin. This infilling is possible because the south-westerly airflow maintains areas of high precipitation in excess of 2000 mm a^{-1} over the South-West Grampians (Figure 5.27).

(5.3.3) SENSITIVITY ANALYSIS OF THE COUPLED MODEL.

The sensitivity analysis of the atmospheric moisture model (Section 5.2.3) indicated that the model's behaviour was particularly sensitive to variation in the following parameters and variables:

(i)   the precipitation parameters f_0 and f_1;

(ii) the saturated atmospheric moisture content; and

(iii) the imposed boundary conditions (atmospheric moisture advection from the Atlantic Ocean).

The precipitation parameters are not included in the present sensitivity analysis because changes in their values are extremely hard to quantify. For instance, the changing circulation regimes postulated by Sissons (1976 and 1980) could lead to the time dependent variation of these parameters during the Loch Lomond stadial. The implications of such changes are explored later.

Variation in the saturated moisture content and the imposed boundary conditions affect the moisture content of the modelled atmosphere. In the former case the effect occurs via evaporation while, in the latter case, it occurs via moisture advection. The analysis of these effects can be used to investigate the sensitivity of the model to air temperature variation. Air temperature is the main driving variable in the model and affects moisture contents and precipitation rates via its association with evaporation rate and saturated moisture content (Figure 5.1). If the model over-predicts the effect of air cooling on saturated moisture content then Loch Lomond stadial precipitation rates will be under-estimated.

The coupled model was run for the whole Loch Lomond stadial using, alternatively, 50 % and 150 % of the standard values for saturated moisture content and for the Atlantic Ocean boundary conditions. This set of

four runs was repeated for both the westerly and the south-westerly airflow models. Model output for the runs is shown in Figures 5.28, 5.29 (both westerly), 5.30 and 5.31 (both south-westerly). In these diagrams the predicted time series are shown for ice volume and for mean precipitation rate.

In all cases maximum ice volume is restricted to below 50 % of the maximum achieved in the constant precipitation run of Chapter 4. The rate of ice volume growth is related to the precipitation distribution at the time of maximum air temperature depression (between 2.0 and 3.0 ka). Table 5.6 shows the maximum ice volume and the areas of the model domain with precipitation rates in excess of 1800, 2000 and 2200 mm a^{-1}, for each of the above runs and for the constant precipitation run. These indices show that the crucial precipitation rate for ice sheet growth is 2200 mm a^{-1}; large ice volumes develop when an area in excess of 40×10^{-3} has precipitation rates greater than 2200 mm a^{-1}, while far smaller ice volumes are produced when this area is reduced to below 20×10^{-3}. The 1800 and 2000 mm a^{-1} indices show a similar, but not so abrupt, pattern of change.

This sensitivity analysis indicates that a fall in predicted precipitation during the Loch Lomond stadial is

a stable feature of the model's behaviour. The ice sheet section of the model is very sensitive to these falling precipitation rates and, in particular, precipitation rates greater than 2200 mm a^{-1} appear crucial in promoting ice sheet growth.

(5.3.4) CONCLUSIONS AND IMPLICATIONS ARISING FROM THE COUPLED MODEL.

The experiments described in this section use a coupled atmospheric moisture and ice sheet model. Output from this coupled model indicates that varying precipitation rates during the Loch Lomond stadial had a profound effect on the dynamics of the Loch Lomond ice sheet in Scotland. If, as in Chapter 4, a constant precipitation distribution is used throughout the stadial, then ice sheet volumes rise exponentially to a maximum of 7370 km^3. This exponential growth is a product of progressive air temperature cooling (affecting ablation rates) and net mass balance / ice thickness / surface elevation feedback. If precipitation is allowed to vary in response to both air temperature change and North Atlantic polar front migration then ice sheet volumes rise linearly to a maximum of 950 km^3 for a westerly wind direction. This indicates that the combined effects of air cooling and North Atlantic polar front migration on atmospheric moisture content, precipitation and ice sheet growth rate counteract the growth rate increases caused by air cooling and ice sheet net mass

balance feedback.

The scenario of ice sheet growth, maximum and decay inferred in Chapter 4 from a model using constant precipitation was found to agree with field interpretations. The scenarios of ice sheet behaviour produced by the coupled models of this chapter do not agree with field interpretations; the predicted maximum ice sheet is thinner and far less extensive than that which would be expected from field evidence. Thus the initial simple model produces predictions of ice sheet behaviour that are in accord with field evidence, while a more realistic coupled model does not. Three hypotheses can be advanced to account for this apparent anomaly. They concern the atmospheric moisture model itself, the possibility of ice inheritance from earlier times and the parameterization of ablation.

The atmospheric moisture model.

The first hypothesis is that the atmospheric moisture model over-estimates the effect of falling air temperature on atmospheric moisture content and precipitation. One reason for this over-estimation has already been explored, namely an alternative airflow direction. A south-westerly airflow allows more Atlantic moisture advection into the Scottish area because moisture is drawn from areas to the South of the North

Atlantic polar front.

This contrast between present day westerly and former south-westerly airflow directions was postulated by Sissons (1979b and 1980) on the basis of reconstructed Loch Lomond stadial glacier equilibrium line altitudes, and has received support from the work of Larsen et al (1984) on Norwegian cirques. The modelling work reported here supports the idea of an alternative wind direction for two reasons.

First, ice sheet growth in the south-westerly airflow model is centred around Rannoch Moor and very little ice is present in the northern North-West Highlands (Figure 5.26). This is not merely a consequence of the small ice sheet volumes produced in this run because many other south-westerly airflow runs produce larger ice volumes but make the same predictions about the geographical distribution of ice sheet growth. One of the main mismatches between field evidence and the predictions of the constant precipitation ice sheet model of Chapter 4 (Section 4.3.1) was the over-prediction of ice in the North-West Highlands. The predictions of the south-westerly airflow model imply that this mismatch may have arisen because of the westerly airflow assumption implicit in the use of a present day precipitation distribution. These arguments lend support to the idea of

a south-westerly wind direction during the Loch Lomond stadial.

Another aspect of the modelling work adds support to the hypothesis of south-westerly airflow: a model using a south-westerly airflow predicts a larger maximum ice sheet than a model using a westerly wind direction. The predictions are closer to the extent and thickness expected from field estimates than those of the westerly airflow model. This support is obviously not a conclusive test of the hypothesis of a south-westerly wind direction, but does add weight to the argument. However the use of a south-westerly airflow direction in the model still leaves a disparity between model predictions and field interpretations. Further explanations must therefore be sought.

The model may also over-estimate the effect of falling air temperatures on atmospheric moisture content and precipitation rates because it overlooks an important atmospheric process. For instance Sissons and Sutherland (1976) and Sissons (1979b) postulate a band of enhanced frontogenesis and increased precipitation sweeping over Scotland with the passage of the North Atlantic polar front. This zone of high precipitation may have led to an extremely rapid phase of ice sheet growth, which was followed by a general stagnation as precipitation rates

fell immediately behind the North Atlantic polar front.

This hypothesis was tested by uniformly doubling the precipitation rate during the 500 a period between 1.0 and 1.5 ka (11.5 to 11.0 ka BP). This represents the period during which the North Atlantic polar front was adjacent to the U.K. (Figure 5.3). The results for ice sheet volume are shown in Figures 5.32 and 5.33 for both westerly and south-westerly wind directions. The increased precipitation rates from 1.0 to 1.5 ka produce early accelerated ice sheet growth in both runs. However, the maximum ice sheets produced in these runs still are considerably smaller and thinner than those expected from field evidence.

The above increased precipitation experiments exaggerate the effect of enhanced frontogenesis for two reasons. First, Sissons and Sutherland (1976) indicate that precipitation rates at this time were similar to those of the present day. The uniform doubling is therefore likely to over-predict any precipitation effect. Second, the duration of the precipitation increase (a period of 500 a) is likely to be an over-estimate because of the North Atlantic polar front's migration speed. If the North Atlantic polar front travelled from its position at 11.0 ka BP (66 ^{O}N) to its position at 10.0 ka BP (44 ^{O}N) at a uniform rate

(2.5 km a^{-1}) then it would have occupied a position adjacent to the Scottish highlands for only 120 a. The exact length of time for which the North Atlantic polar front increased Scottish precipitation rates would have depended on the width of the zone of enhanced frontogenesis. However, such an effect would have lasted for less than 500 a. Increased initial ice sheet growth triggered by enhanced frontogenesis can, therefore, be rejected as an explanation for the mismatch between model prediction and field interpretation because numerical experiments which deliberately exaggerate this effect under-predict the extent and thickness of the maximum ice sheet.

Literature on the climate of the Loch Lomond stadial in Scotland indicates that precipitation rates were lower than those of the present day. The global circulation modelling of Rind et al (1986) predicts an overall lowering of 400 mm a^{-1} over Western Europe. While various field estimates from Scotland indicate: a rate of 200 to 300 mm a^{-1} for the lowland Spey Valley (Birks and Mathewes 1978 and Sissons 1979a); a rate of 500 to 600 mm a^{-1} for the North-West Cairngorms (Sissons 1980); a rate of 2700 to 4000 mm a^{-1} for the western Grampians (Sissons 1980); and a rate of 1650 mm a^{-1} for the South-East Grampians (Sissons and Sutherland 1976). The latter two values are higher than those predicted by the

westerly airflow model (Figure 5.24) but agree with the predictions of the south-westerly airflow model (Figure 5.27). It therefore appears that the reduced precipitation rates predicted by the atmospheric moisture model agree with other estimates of climate during the Loch Lomond. However the degree of the precipitation reduction may be over-predicted by the models, especially by the westerly airflow model.

A sensitivity analysis of the coupled model indicates that even minor reductions in precipitation rate can have a marked effect on ice sheet growth. Once the precipitation rates in the highlands fall below 2200 mm a^{-1} then Loch Lomond ice sheet growth is suppressed. Given the sensitivity of ice sheet growth to precipitation and the likelihood of reduced precipitation rates during the Loch Lomond stadial then some slowing of Loch Lomond ice sheet growth is inevitable.

The above discussion attempts to test the hypothesis that the failure of the coupled model to produce realistic ice volumes is wholly attributable to inaccurate precipitation modelling. Two mechanisms are used to explain this inaccuracy. They are south-westerly airflow and enhanced frontogenesis. Neither is wholly satisfactory. In addition, a sensitivity analysis of the

coupled model and literature on the Loch Lomond stadial climate both support the predictions of the atmospheric moisture model. The initial hypothesis that the atmospheric moisture model is inadequate can therefore be rejected, and an alternative explanation for the disparity between model predictions and field interpretations must be sought.

The inheritance of pre-Loch Lomond ice.

A second hypothesis that can be used to explain the mismatch between the predictions of the coupled model and field interpretations is that of ice inheritance from pre-Loch Lomond glaciations. This hypothesis questions the initial ice-free conditions used in the model so far.

The late Devensian glaciation reached a maximum at 18.0 ka BP, and at this time covered the majority of mainland Britain. It is possible that the warm Late Glacial interstadial which preceded the Loch Lomond stadial saw only incomplete decay of the late Devensian ice sheet, leaving isolated pockets of ice in some Scottish glens. This ice would then raise the surface elevation of the initial Loch Lomond topography and make ice sheet growth more likely because of the strong positive relationship between net mass balance and surface elevation.

Field evidence relating to the ice cover immediately prior to the Loch Lomond stadial is conflicting; some authors suggest a complete deglaciation (Sissons 1972, Sissons and Grant 1972), while others favour the existence of ice masses (Sugden 1970, Peacock 1970). A series of model experiments were performed to assess the likelihood of pre-existing ice affecting the behaviour of the Loch Lomond ice sheet. In these experiments a variety of initial ice coverages were used. These coverages were drawn from the Loch Lomond ice sheet decay sequence of Chapter 4 (Figure 4.10) on the assumption that the last decay stages of the late Devensian ice sheet occupied the same areas. None of these initial ice coverages survived in the model run long enough to influence the behaviour of the Loch Lomond ice sheet itself. This was the case for all initial ice volumes (including a Loch Lomond maximum sized ice sheet of 7370 km^3) and for a variety of precipitation distributions (including the present day distribution used in Chapter 4).

These experiments indicate that the Loch Lomond ice sheet could only have been affected by the inheritance of ice if the pre-existing ice mass was larger than the Loch Lomond ice sheet maximum. In this case the growth of the Loch Lomond ice sheet represents a phase of minor re-growth rather than a distinct phase of glaciation. Field evidence suggests that the growth of the Loch Lomond ice

sheet was distinct and was not a stand-still in the decay of a larger ice sheet (Sissons 1967, Peacock 1971, and Gray and Brooks 1972). The hypothesis of ice inheritance affecting the dynamics of the Loch Lomond ice sheet can therefore be rejected.

The parameterization of ablation and effectiveness in the coupled model.

The third and final hypothesis that can be used to explain the disparity between the predictions of the coupled model and field interpretations is that the ablation and/or effectiveness parameterizations used in the model are inaccurate. The actual rates of ablation and effectiveness during the Loch Lomond stadial are unknown and it is unlikely that an appropriate set of field data will become available to test the model's ablation and effectiveness predictions. These predictions are therefore untestable. However an alternative method of assessing the validity of the predictions is to compare them with the predictions of other, more sophisticated ablation/effectiveness models. To this end alternative ablation and effectiveness parameterizations need to be incorporated into the model. The aim is to compare their predictions with those of the initial ablation and effectiveness parameterizations and, if the predictions differ, to investigate the behaviour of a model coupling ice sheet flow, atmospheric moisture and these new ablation/effectiveness parameterizations.

(5.4) AN ALTERNATIVE ABLATION/EFFECTIVENESS MODEL.

The ablation/effectiveness model used so far is based upon the three equations (2.3), (2.4) and (2.5):

$$Ab = 10^{(E_o - E)/1\cdot2} \qquad (2.3)$$

$$E_0 = 6\cdot85 - 0\cdot085\phi + \Delta E_J \qquad (2.4)$$

$$Eff = -0\cdot698 + 0\cdot014\phi + 0\cdot224(E - \triangle E_A) \qquad (2.5)$$

Both ablation (Ab) and effectiveness (Eff) are predicted from the three independent variables of surface altitude (E), latitude (ϕ) and imposed afr temperature change (expressed as an imposed isotherm shift, see Figure 2.7; ΔE_J, July and ΔE_A, annual). An alternative ablation/effectiveness model is developed in this section. Although this model is still empirical in nature, its derivation is distinctly different from that of the model outlined by the above equation set. The aim of this work is to test the validity of the original ablation/effectiveness model using the predictions of the alternative model. The comparison of the two models cannot offer a critical test; however, it does allow the behaviour of the coupled model discussed in Section (5.3) to be put in perspective.

The alternative ablation/effectiveness model has four main components:

(i) the derivation of a seasonal air temperature curve from surface altitude, latitude and imposed air temperature change inputs;

(ii) the use of this curve to obtain mean monthly temperatures;

(iii) the calculation of monthly effectiveness values from the mean monthly temperatures; and

(iv) the calculation of monthly ablation rates from the mean monthly temperatures using the sum of monthly degree days.

The first two components are treated in sub-section (5.4.1), while the latter two are discussed in sub-section (5.4.2). Finally sub-section (5.4.3) compares the original and the alternative ablation/effectiveness models.

(5.4.2) SURFACE AIR TEMPERATURE ESTIMATION.

A monthly air temperature curve (such as that shown in Figure 2.6) can be approximated using a cosine function:

$$T_m = Off - Amp.\cos\left(\frac{\pi n}{6}\right) \qquad (5.10)$$

where T_m is mean monthly air temperature ($^{\circ}C$) and n is a 'month number' running from 6.5 (for July) to 11.5 (for December). The symmetry of the cosine curve means that only the latter half of the year needs to be considered. The parameter 'Off' refers to the offset of the mean annual temperature (around which the cosine curve varies) from 0.0 $^{\circ}C$, and the parameter 'Amp' refers to the amplitude of the annual temperature wave (peak to mean

difference). The monthly air temperature curve for the present day (Figure 2.5, curve A) has an offset of 10.0 ^{o}C and an amplitude of 7.0 ^{o}C.

The offset and amplitude of the mean air temperature curve vary geographically and through time. In the model this variation is empirically related to altitude, latitude and imposed air temperature change. Two equations are derived which have either the offset or the amplitude as their dependent variable and altitude, latitude and temperature change as independent variables. The values of the parameters involved in these equations are derived from the literature relating to the present day and former climate of the British Isles.

The first two relationships are between imposed air temperature change and offset, and between imposed air temperature change and amplitude. Two of the few papers investigating the changes in monthly air temperature curves during the Loch Lomond stadial are those of Williams (1975) and Coope et al (1971), which use data derived from periglacial and Coleoptera sources. The authors predict similar changes in the amplitude and offset of the monthly temperature curve. These changes can be related to the air temperature difference time series that is used as a forcing function in the ice sheet model (Figure 2.4). The time series represents the

difference between former July air temperatures and those of the present day. It varies between 0.0 ^{o}C for the present day and -8.0 ^{o}C for the Loch Lomond stadial. A linear relationship is used to link the air temperature differences to the amplitude and offset of the monthly air temperature curve.

The second set of relationships are those between surface altitude and offset, and between altitude and amplitude. A standard lapse rate of 6.5 ^{o}C km^{-1} is used to approximate the variation of offset with altitude and is the Meteorological Office standard value for mean annual temperature. The amplitude of the monthly temperature curve also varies with altitude. The lapse rates of maximum and minimum annual temperatures differ by 2.0 ^{o}C km^{-1} (Green and Harding 1980), so that the annual temperature range becomes progressively compressed as altitude increases. The amplitude of the monthly temperature curve therefore decreases at the rate of 2.0 ^{o}C km^{-1}.

The third and final set of relationships are those between latitude and offset, and between latitude and amplitude. The present day January and July air temperatures over the British Isles are used to estimate these effects (Chandler and Gregory 1976, and Manley 1970). The influences of latitude and altitude on the

monthly air temperature curve are assumed to remain constant and independent of changes in imposed air temperature difference.

The final equations used to approximate changing monthly air temperature curves are:

$$\text{Amp} = 7.0 - 1.57\triangle T_J - 0.25(\phi - 50.5) - 2.0E \qquad (5.11)$$

$$\text{Off} = 10.0 + 2.57\triangle T_J - 0.38(\phi - 53.17) - 6.5E \qquad (5.12)$$

These equations and equation (5.10) allow monthly air temperatures to be estimated throughout the whole of the Loch Lomond stadial model run and over the whole of the Scotland.

The varying influences of latitude, altitude and imposed temperature change on monthly air temperatures are analysed in Table 5.7. This table presents for each of the three independent variables: the multipliers used in equations (5.11) and (5.12); the expected range of the variable's value; and the influence of the variable on offset and amplitude (the product of the range and the multiplier value, expressed in ^{o}C and as a percentage of the total possible variation). Offset and amplitude are both dominated by imposed air temperature change, but variation in altitude can also have a significant effect on the offset.

313

Monthly air temperature curves may also be influenced by the surface conditions of ice and ice-free ground. The partitioning of energy at the ground surface changes dramatically when ice is present. This variation stems principally from: the high albedo of snow and ice surfaces (Lian and Cess 1977, and Manabe and Broccoli 1985); the strength of the inversion layer above an ice surface (Schwerdtfeger 1970); and the reduced atmospheric moisture content above ice surfaces (Oerlemans and van der Veen 1984). These processes may alter the heat budget of the overlying atmospheric boundary layer and produce a layer of 'chilled' air above the ice sheet. The transition from an ice-free surface to an ice sheet surface may therefore be mirrored by a change in regional climate. It is possible that this layer of chilled air could insulate the ice sheet from the effects of global temperature changes and alter the overall ice sheet response to imposed air temperature changes.

The variation of mean annual temperature over large ice sheets typically reflects a lapse rate of 10.0 ^{o}C km^{-1} (Greenland: Mock and Weeks 1966 and Putnins 1970, Antarctica: Schwerdtfeger 1968). This lapse rate consists of two separate components, one vertical and the other horizontal. The former reflects the air temperature variation produced by altitudinal changes alone and should therefore equal the environmental lapse rate

(6.5 ^{o}C km^{-1}). The latter reflects the horizontal changes in regional climate caused by the presence of an ice surface. These horizontal changes have an altitudinal effect because horizontal and vertical distances are linked via ice sheet surface slope. The overall lapse rate (dT/dE) is related to these vertical ($\partial T/\partial E$) and horizontal ($\partial T/\partial x$) components:

$$\frac{dT}{dE} = \frac{\partial T}{\partial E} + \frac{\partial T}{\partial x} \cdot \frac{\partial x}{\partial E} \qquad (5.13)$$

where $\partial x/\delta E$ is the reciprocal of ice sheet surface slope. Typical values of ice sheet surface slope are 1.0 x 10^{-2} to 1.0 x 10^{-3}. If these value are substituted into equation (5.13) along with the values of overall lapse rate (10.0 ^{o}C km^{-1}) and environmental lapse rate (6.5 ^{o}C km^{-1}), then an estimate can be made of the horizontal variation of mean annual temperature over an ice sheet ($\delta T/\delta x$). An estimate of 0.02 ^{o}C km^{-1} is obtained from the above values of overall and environmental lapse rates.

This calculation suggests that, direct altitudinal effects aside, mean annual air temperatures over an ice sheet decrease at the rate of 0.02 ^{o}C per km from the ice sheet perimeter. This is only a gross estimate of the effect of varying regional climate on air temperatures, but it can be used to obtain an order of magnitude

315

estimate of the effect over the Loch Lomond ice sheet. If the ice sheet had a maximum width of 100 km then horizontal effects could have produced an interior air temperature fall of 1.0 ^{o}C. Although this represents a maximum estimate, it is far smaller than the effects of altitude, latitude and imposed temperature change on air temperatures. Table 5.7 shows that it represents only 3.3 % of the total possible variation of the offset. This implies that the Loch Lomond ice sheet was too small to have developed its own regional climate and that the effects of differing surface types can be omitted in further modelling work.

(5.4.2) THE PREDICTION OF ABLATION AND EFFECTIVENESS USING SURFACE AIR TEMPERATURES.

The mean monthly air temperatures obtained from equations (5.10) to (5.12) can now be used to estimate monthly values of effectiveness and ablation. This is done by using empirical relationships derived from the present distribution of these variables.

The effectiveness model uses the work of Lauscher (1976), who studied the changing fraction of precipitation falling as snow (the effectiveness) for varying altitudes throughout Western Europe. He obtained the following relationship for monthly periods:

$$Eff_m = 0.50 - 0.05T_m \qquad (5.14)$$

where Eff_m is monthly effectiveness. This relationship operates between mean monthly temperatures of -10.0 and 10.0 $^{\circ}$C, outside of this range effectiveness is either 0.0 or 1.0.

The ablation model is based upon the work of Braithwaite and Thomsen (1984), who derived a series of relationships between mean monthly temperature, the sum of monthly degree days and monthly ablation rate. Mean monthly temperature is related to the sum of all temperatures above melting point (0.0 $^{\circ}$C) during a month (S_m, the positive degree day sum expressed per day):

$$S_m = 1.74 + 0.50 T_m + 0.03 T_m^2 \qquad (5.15)$$

This regression equation ($R^2 = 99.9$ %) is based on the tabulated data presented in Braithwaite (1984). The original relationship was developed from statistical considerations and was successfully tested in the Swiss Alps and in West Greenland.

The second stage is to estimate monthly ablation rate (Ab_m, expressed per day) from the sum of positive degree days (Braithwaite and Olesen 1984):

$$Ab_m = \max(0.0, -0.36 + 0.54 S_m) \qquad (5.16)$$

This regression equation ($R^2 = 82.0$ %) is based on 29 samples from two glacier sites in West Greenland

317

(Nordbogletscher and Qamanarssup sermia). A correction factor of 0.068 has been applied to the original equation to convert the original units of kg m^{-2} d^{-1} to units of m a^{-1}. The equations (5.15) and (5.16) are used when mean monthly air temperature is between -8.0 ^{o}C and 10.0 ^{o}C. Outside this range ablation is set to either 0.0 or a monthly maximum rate of 5.12 m a^{-1}.

This completes the description of the ablation/effectiveness model. For a particular location and time, the monthly mean air temperatures are found using equations (5.10), (5.11) and (5.12). Monthly values for effectiveness (equation 5.14) and ablation (equations 5.15 and 5.16) are then found and summed to obtain annual estimates which are related to the rest of the ice sheet model, using:

$$b = P \cdot Eff - Ab \qquad (5.17)$$

(5.4.3) COMPARISON OF THE ORIGINAL AND THE ALTERNATIVE ABLATION/EFFECTIVENESS MODELS.

The old model is defined by equations (2.3), (2.4) and (2.5), while the new model defined is by equations (5.10), (5.11), (5.12), (5.14), (5.15) and (5.16). This section compares, firstly, separate ablation and effectiveness predictions; secondly, the combined predictions (using equation 5.17); and, thirdly, the spatial distribution of the accumulation areas predicted

by the two models using Scottish Loch Lomond input data.

The effect of changing imposed temperature and surface altitude on ablation and effectiveness is shown in Figures 5.34 and 5.35 for the new model. Equivalent graphs for the old model are shown in Figures 2.9 and 2.10. All four graphs show predictions at latitude 57.0 ^{O}N. The new effectiveness model predicts lower values than the old model, especially for large air temperature depressions. In addition the rate of effectiveness change produced by varying temperature depression and surface altitude is slower in the new model. A final contrast between the two graphs of effectiveness is their degree of linearity. Effectiveness changes at a constant rate in the old model, whereas it varies non-linearly in the new model. This contrast is produced by the use of the cosine curve to predict mean monthly temperatures in the new model. The predictions of ablation contrast in the same ways. Thus, the new ablation model predicts generally lower ablation rates which vary more rapidly than those of the old model. There is also evidence of greater non-linearity in the predictions of the new model.

The use of the new combined effectiveness/ablation model decreases both predicted ablation rates and effectiveness values. These changes have contrasting

effects on the overall net mass balance. The former tends to increase the net mass balance while the latter tends to decrease it. The effect of temperature, surface altitude and latitude on predicted net mass balance is shown in Figure 5.36, and the effect of temperature, surface altitude and precipitation rate on predicted net mass balance is shown in Figure 5.37. Equivalent graphs for the old model are shown in Figures 4.4 and 4.5.

Predicted equilibrium line altitudes are lower in the new model, although the difference between the two models is reduced at lower surface altitudes, lower precipitation rates and lower latitudes. The rates of mass loss below the equilibrium line are lower in the new model and the rates of mass gain above the equilibrium line are slightly higher.

The spatial distribution of the accumulation areas predicted for Scotland by the new model are shown in Table 5.8. The specific input data are the Scottish maximum topography (Figure 4.1), the present day Scottish precipitation distribution (Figure 4.2) and the Scottish precipitation distribution predicted for 10.0 ka BP by the westerly airflow model (Figure 5.24).

When the present day precipitation distribution is used, the old and new models predict the initiation of

accumulation areas at similar temperature depressions. However, the size of predicted accumulation areas is always far greater in the case of the new model. When the 10.0 ka BP precipitation distribution is used the contrast between the models is increased.

The geographical extent of the accumulation areas predicted by the new model are shown in Figure 5.38 for the present day precipitation distribution and imposed temperature depressions of -4.0, -6.0 and -8.0 ^{O}C. The predictions of the old model for imposed temperature depressions of -6.0, -7.0 and -8.0 ^{O}C are shown in Figure 4.6. The extent of the accumulation area predicted by the old model for a -8.0 ^{O}C temperature depression is similar to that predicted by the new model for a -6.0 ^{O}C temperature depression. The old model's prediction for a -7.0 ^{O}C depression and the new model's prediction for a -6.0 ^{O}C depression are also similar. These features indicate that accumulation area size is far more sensitive to imposed temperature depression in the new model. The new model's prediction of accumulation area extent for depression of -8.0 ^{O}C is far in excess of any other prediction and covers virtually all upland areas above 300 m altitude.

The new model predicts net mass balances which are always more positive than the predictions of the old

model. This leads to lower equilibrium line altitudes and larger accumulation areas than predicted by the old model. This contrast is mainly a function of reduced ablation rates in the new model, which more than compensate the reduced effectiveness values.

(5.5) INCORPORATING THE NEW ABLATION/EFFECTIVENESS MODEL INTO THE COUPLED ATMOSPHERIC MOISTURE – ICE SHEET MODEL.

The new ablation/effectiveness model described in Section (5.4) is now incorporate into the coupled atmospheric moisture - ice sheet model described in Section (5.3). The old coupled model used in Section (5.3) dramatically under-predicted the extent and the thickness of the maximum Loch Lomond ice sheet. The new ablation/effectiveness model was developed in order to investigate the possibility that the under-predictions of the old coupled model could be attributed to poor ablation/effectiveness parameterization.

Two complete runs of the new coupled model are now described, with the aim of assessing the effects of altering ablation-effectiveness model. One run used the westerly airflow model, while the other used the south-westerly airflow model. The input data and the parameter values used in the atmospheric model are shown in Tables 5.3 and 5.5, respectively. The output of both model runs for ice volume and for mean precipitation rate is shown

322

in Figures 5.39 and 5.40. Also shown in these graphs are model outputs from both the constant precipitation run of Chapter 4 and the coupled models of Section (5.3) which used the old ablation/effectiveness model.

Both of the new coupled model runs produce ice volumes in excess of those produced in the constant precipitation run. Maximum ice volume is 128 % of the constant precipitation maximum volume for the westerly airflow run, and 225 % for the south-westerly airflow run. Ice volumes show an exponential rise and a dramatic fall similar to those of the constant precipitation run of Chapter 4. The maximum ice sheet extent and thickness is similar to that achieved by the constant precipitation run, although both are slightly greater.

There are two differences between the maximum ice sheets produced by the new model when westerly airflow is used and when south-westerly airflow is used. First, the south-westerly maximum is larger because of the larger precipitation rates in the run (sub-section 5.3.2). Second, the geographical distribution of the maximum ice sheet of the south-westerly airflow model has a better fit with field evidence because maximum ice thicknesses are centred over Rannoch Moor and not over the Glen Mor and An Teallach/Beinn Dearg areas. In addition, outlying ice masses in the North-West Highlands are reduced in the

south-westerly airflow model.

The dynamics of ice sheet growth and decay exhibited in both of these runs are similar to those described in Chapter 4 for the old constant precipitation model. A sensitivity analysis of the new coupled model was performed and revealed similar results. For this reason the results are not discussed further.

The results produced by the new coupled model indicate that the parameterization of net mass balance is crucial in determining the behaviour of the ice sheet. Although precipitation rates are likely to have been considerably reduced during the Loch Lomond stadial, this does not affect the dynamics of ice sheet growth and decay when the new ablation-effectiveness scheme is incorporated into the model.

There are two ways of interpreting the Loch Lomond modelling experiments. One hypothesis is represented by the old model using a constant precipitation rate. In Chapter 4 modelled precipitation rates are the same as those of the present day and ablation rates are relatively high. The second hypothesis is represented by the new ablation/effectiveness modelling of this chapter. In this second hypothesis precipitation rates are reduced during the Loch Lomond stadial, however this

324

reduction is compensated by decreased ablation rates. Uncertainty remains as to which of these hypotheses is correct, or whether an intermediate situation existed. Both scenarios lead to similar maximum ice sheet extent and similar ice sheet growth and decay dynamics, it is therefore unlikely that field data based relating to the glacial geology of the area could be used to test the two scenarios. Indirect evidence relating to precipitation rates may, however, offer a means of testing the two rival scenarios of constant and varying precipitation rate.

The relative validity of the two scenarios is indicated by two points relating to the assumptions used in the two contrasting ablation/effectiveness models. First, the old ablation relationship was originally derived in Budd and Smith (1981). The net mass balance model used in Budd and Smith's work did not incorporate varying effectiveness, but assumed that all precipitation fell as snow. The ablation relationship is likely to have been tuned to exaggerate ablation because accumulation was being over-estimated by the assumption of 100 % effectiveness. The old Loch Lomond ice sheet model (using constant precipitation) uses the same ablation relationship in conjunction with varied effectiveness. This model may, therefore, over-estimate ablation and compensate this over-estimation by the use of an over-

estimated precipitation distribution. This argument favours the use of the new ablation relationship which predicts lower ablation rates.

A second point relating to the modelling assumptions is the use of a maximum envelope topography in the old Loch Lomond ice sheet model of Chapter 4. The fact that a maximum topography was needed in order to produce sufficient ice accumulation implies that net mass balances were being under-estimated and that ablation was being over-estimated. Although the exact topographic representation required in the net mass balance section of the model is uncertain and should be greater than the mean representation (Section 2.3.2), the use of the maximum seems unrealistic.

It is suggested that the results of the old ablation/effectiveness model using constant precipitation, the old ablation/effectiveness using varied precipitation and the new ablation/effectiveness model using varied precipitation are related in the following way. First, the old ablation/effectiveness model using constant precipitation predicts ice sheet size correctly because it balances an over-estimate of ablation with an over-estimate of accumulation. Second, when the old ablation/effectiveness model is used in conjunction with the atmospheric moisture - precipitation

model, precipitation rates are reduced and the over-estimated ablation rate leads to an under-estimate of ice sheet size. Finally, when the new ablation/effectiveness model is used in conjunction with the atmospheric moisture - precipitation model, the over-estimation of accumulation and the over-estimation of ablation are both removed and ice sheet size is correctly predicted.

In one respect it is not particularly important which of the scenarios is correct. In both cases ice sheet growth is exponential, ice sheet retreat extremely rapid and the ice sheet survives for approximately 1.0 ka.

Table 5.1 Parameter values in the atmospheric moisture model when it is used to predict moisture fluxes over the Atlantic Ocean during the Loch Lomond stadial.

Parameter	Symbol	Value	Units
evaporation time constant	T_*	3.0 (ocean) 30.0 (land)	days
precipitation parameters	f_0 f_1	4.0×10^{-3} 3.5×10^{-6}	s^{-1} s^{-1}
diffusion constant	D_w	5.8×10^6	$m^2 \, s^{-1}$
grid spacing	Δx	220.0	km
time interval	Δt	500.0	s

Table 5.2 The steady state atmospheric moisture values predicted over the Scottish area by the Atlantic Ocean atmospheric moisture model. These values are used as boundary conditions to the Scottish precipitation model.

Wind dir.	Time (ka BP)	Atmospheric moisture (kg m^{-2}) at node:			
		Left adjacent (16)	Left Scottish (17)	Right Scottish (18)	Right adjacent (19)
West	12.5	6.7	6.4	6.6	7.3
West	12.0	5.2	5.2	5.7	6.7
West	11.5	4.5	4.5	5.2	6.3
West	11.0	3.7	3.5	3.5	3.8
West	10.5	3.5	3.3	3.2	3.3
West	10.0	3.5	3.3	3.2	3.3
West	9.5	5.2	5.2	5.7	6.7
West	9.0	6.6	6.3	6.5	7.2
West	8.5	6.7	6.4	6.6	7.3
West	8.0	6.7	6.4	6.6	7.3
West	7.5	6.7	6.4	6.6	7.3
South-West	12.5	9.5	8.8	8.4	8.1
South-West	12.0	9.1	8.1	7.2	6.1
South-West	11.5	9.0	7.9	7.0	5.9
South-West	11.0	7.0	6.2	5.6	4.8
South-West	10.5	6.0	5.3	4.9	4.3
South-West	10.0	6.0	5.3	4.9	4.3
South-West	9.5	9.1	8.1	7.2	6.1
South-West	9.0	9.5	8.8	8.4	8.1
South-West	8.5	9.5	8.8	8.4	8.1
South-West	8.0	9.5	8.8	8.4	8.1
South-West	7.5	9.5	8.8	8.4	8.1

Table 5.3 The parameter values used in the atmospheric moisture model when the model is used to predict precipitation rates over Scotland during the Loch Lomond stadial.

Parameter	Symbol	Value	Units
evaporation time constant	T_*	3.0 (ocean) 30.0 (land) 60.0 (ice)	days
precipitation parameters	f_0 f_1	2.8×10^{-3} 5.5×10^{-6}	s^{-1} s^{-1}
diffusion constant	D_w	6.0×10^4	$m^2 \, s^{-1}$
grid spacing	Δx	5.0	km
time interval	Δt	100.0	s

Table 5.4 *Goodness of fit indices applied to the sensitivity analysis of the atmospheric model, present day precipitation distribution.*

Parameter	Perturbation	Goodness of fit [*]	
		Whole model domain.	Areas with actual precipitation in excess of 1800 mm.
f_0	x 50 %	103700	22000
	x 150 %	29240	4970
f_1	x 50 %	31070	250500
	x 150 %	9600	57320
T_*	x 50 %	40920	42850
	x 150 %	14240	26020
U	x 50 %	41220	130280
	x 150 %	32690	67250
W_{sat}	x 50 %	70205	159815
	x 150 %	30610	35260
Boundary values.	x 50 %	83280	229460
	x 150 %	15870	16760
	none	27830	67914

[*] *relevant sensitivity run in comparison to standard run.*

Table 5.5 The boundary moisture values and the air temperature input data fed into the atmospheric moisture model when it is used to predict precipitation rates over Scotland during the Loch Lomond stadial.

Time of run and wind direction	Boundary conditions (in kg m^{-2}) at node				July air temperature (°C)
	16	17	18	19	
west present day	6.7	6.4	6.6	7.3	8.5
west 12.0 ka BP	5.2	5.2	5.7	6.7	4.9
west 10.0 ka BP	3.5	3.3	3.2	3.3	0.9
south-west present day	9.5	8.8	8.4	8.1	8.5
south-west 12.0 ka BP	9.1	8.1	7.2	6.1	4.9
south-west 10.0 ka BP	6.0	5.3	4.9	4.3	0.9

Table 5.6 Sensitivity analysis of the coupled model: the effect of changing precipitation rates on the maximum ice sheet volume. The indices presented here are for both of the modelled wind directions and for the constant precipitation model of Chapter 4.

Model Run	Fraction of model domain with precipitation rate in excess of (mm a^{-1})			Maximum ice volume (km^3)
	2200	2000	1800	
		x 0.001		
Constant precipitation (from Chapter 4)	40.8	49.8	55.8	7370.0
Westerly air-flow: standard	0.0	0.5	2.3	950.0
Westerly air-flow: 150 % Saturated moisture content	1.1	4.3	13.0	1470.0
Westerly air-flow: 50 % Saturated moisture content	0.0	0.0	0.0	380.0
Westerly air-flow: 150 % Boundary condition	0.4	2.0	7.7	1200.0
Westerly air-flow: 50 % Boundary condition	0.0	0.0	0.0	340.0
South-westerly air-flow: standard	1.1	6.4	14.5	1620.0
South-westerly air-flow: 150 % Saturated moisture content	19.8	31.5	45.6	3600.0
South-westerly air-flow: 50 % Saturated moisture content	0.0	0.7	0.1	630.0
South-westerly air-flow: 150 % Boundary condition	21.4	36.1	49.9	3700.0
South-westerly air-flow: 50 % Boundary condition	0.0	0.0	0.0	200.0

Table 5.7 The effect of variation in imposed temperature change, latitude and altitude on the predicted amplitude and offset of the mean monthly air temperature curve (based on equations 5.11 and 5.12).

	Mean monthly temperature curve dependent variable	Independent Variables		
		Imposed temperature difference (^{o}C)	Altitude (km)	Latitude (^{o}N)
Multiplier in equation (5.14) and (5.15).	Amplitude	x 1.57	x -2.00	x -0.25
	Offset	x -2.57	x -6.50	x -0.38
Range of variable in the Loch Lomond model.		0.0 to -8.0	0.0 to 1.3	55.7 to 59.3
Influence on the parameter value:				
- in ^{o}C*	Amplitude	12.6	0.9	2.6
	Offset	20.6	1.4	8.5
- as a percentage of the total** possible effect	Amplitude	78.2	5.6	16.2
	Offset	67.5	4.6	27.9

* found as the product of the range and the multiplier for each parameter (offset and amplitude) and variable (imposed temperature change, latitude and altitude) combination.

** found as the percentage of the total amplitude or offset variation (ie the sum of the variations produced by imposed temperature change, latitude and altitude).

Table 5.8 The accumulation area sizes predicted by the original and alternative net mass balance models, for varying air temperature depressions and for different precipitation distributions.

Predicted accumulation area size in km^2 for specific model and precipitation distribution used.

Imposed temperature difference (^{o}C)	Alternative (new) model		Original (old) model	
	Present day precip.	Predicted 10.0 ka BP precip.	Present day precip.	Predicted 10.0 ka BP precip.
0.0	--	--	--	--
-1.0	--	--	--	--
-2.0	50	--	25	--
-3.0	775	25	225	--
-4.0	3175	225	1125	--
-5.0	5200	1425	2975	150
-6.0	10525	3750	5600	1200
-7.0	16550	7950	10000	2900
-8.0	24725	14925	14675	6150

FIGURE 5.1 SATURATED ATMOSPHERIC MOISTURE CONTENT AS A FUNCTION OF
SEA LEVEL AIR TEMPERATURE AND SURFACE ELEVATION.
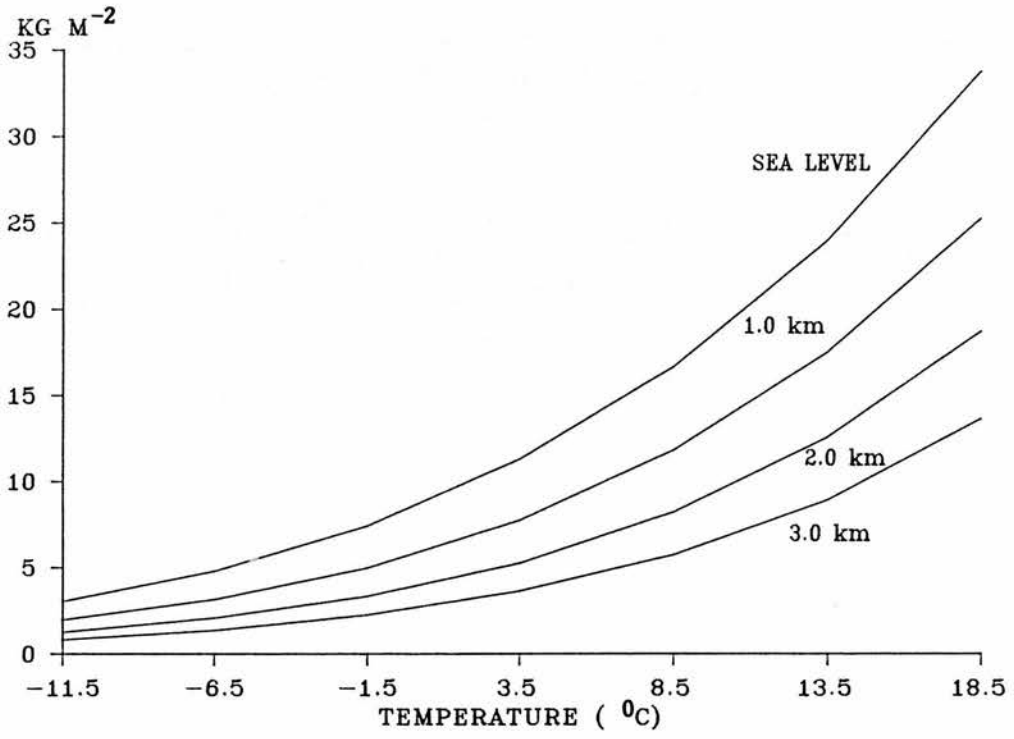
Figure 5.2 The westerly and south-westerly transects used in the modelling of atmospheric moisture fluxes over the Atlantic Ocean during the Loch Lomond stadial.
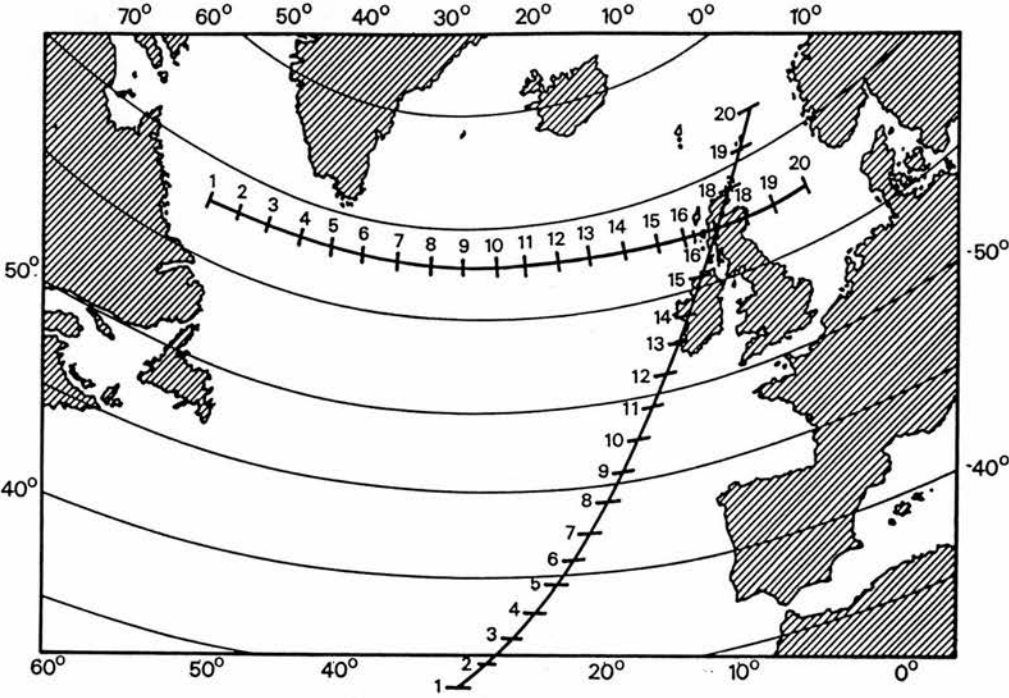
Figure 5.3 The positions of the North Atlantic polar front between 10.0 and 8.0 ka BP, shown at successive 0.5 ka intervals. This data is used to estimate sea surface temperatures at these times. After Ruddiman and McIntyre 1981a.
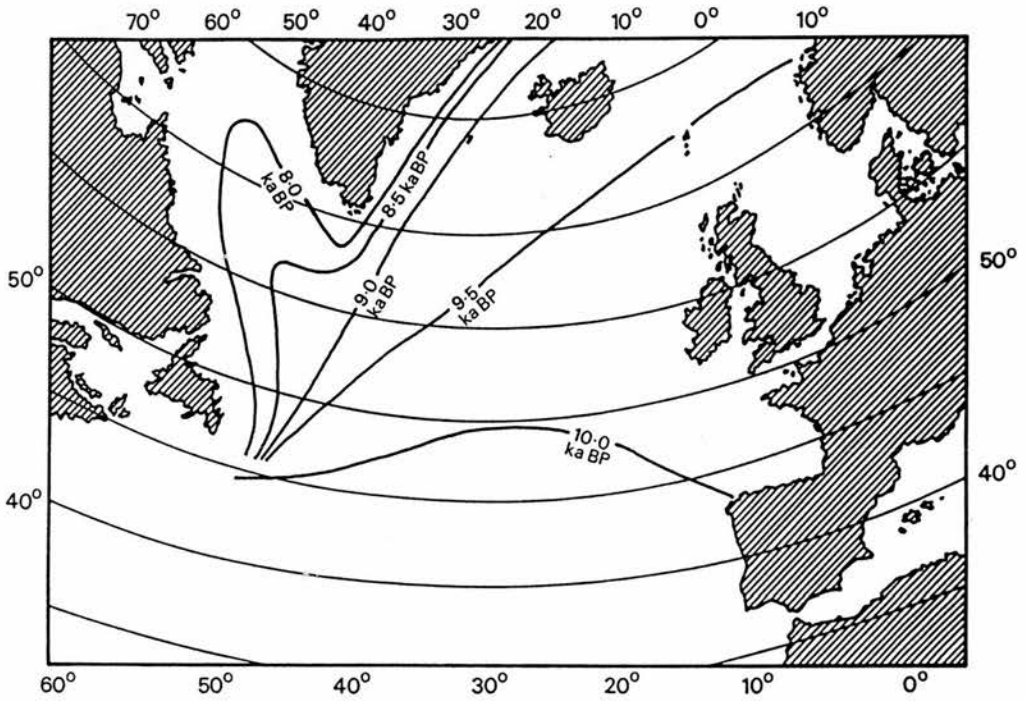
Figure 5.4 The positions of the North Atlantic polar front
between 12.5 and 10.5 ka BP, shown at successive 0.5 ka
intervals. This data is used to estimate sea surface temperatures
at these times. After Ruddiman and McIntyre 1981a.
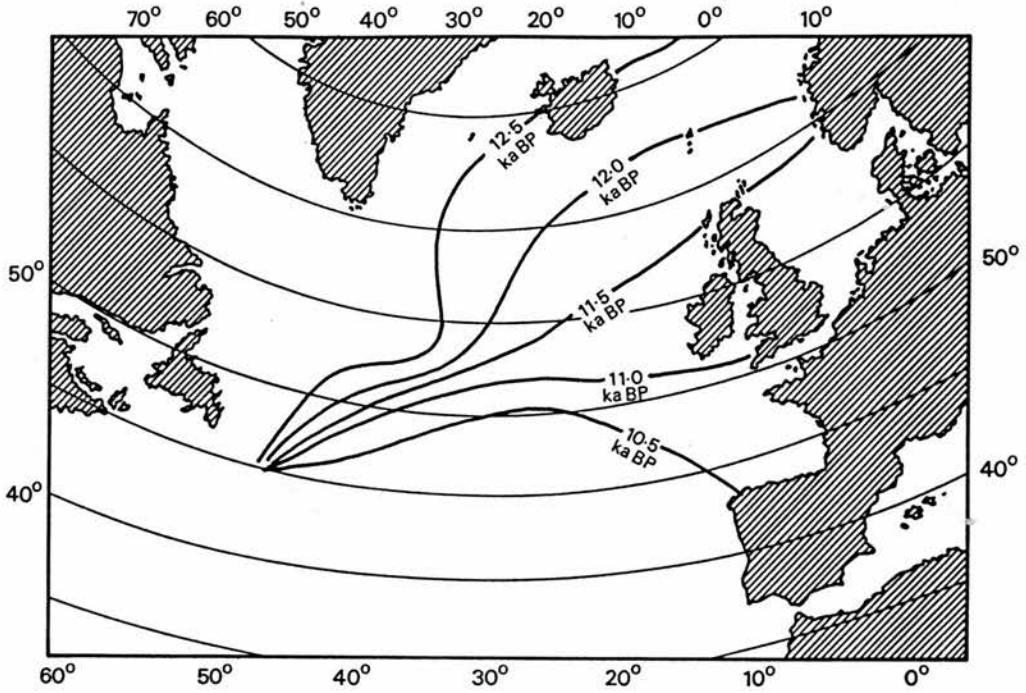
FIGURE 5.5 AN IDEALIZED CROSS-SECTION OF THE SEA SURFACE TEMPERATURE STRUCTURE OF THE NORTH ATLANTIC POLAR FRONT. THIS DATA IS USED TO ESTIMATE NORTH ATLANTIC SEA SURFACE TEMPERATURES DURING THE LOCH LOMOND STADIAL.
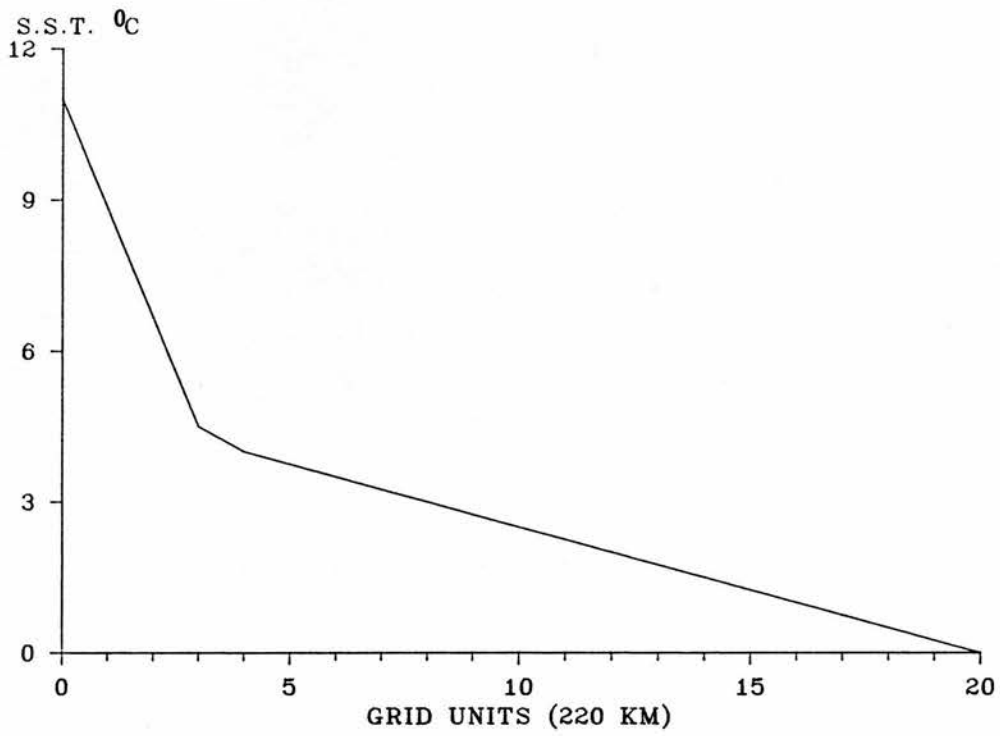
FIGURE 5.6 THE ATLANTIC OCEAN MODEL INPUT DATA FOR THE WESTERLY TRANSECT.
THE TRANSECTS SHOWN ARE FOR TOPOGRAPHY (IN KM), AND FOR SEA
LEVEL TEMPERATURE (IN ^{0}C) AT 0.5 KA INTERVALS BETWEEN 12.5 AND
7.5 KA BP.
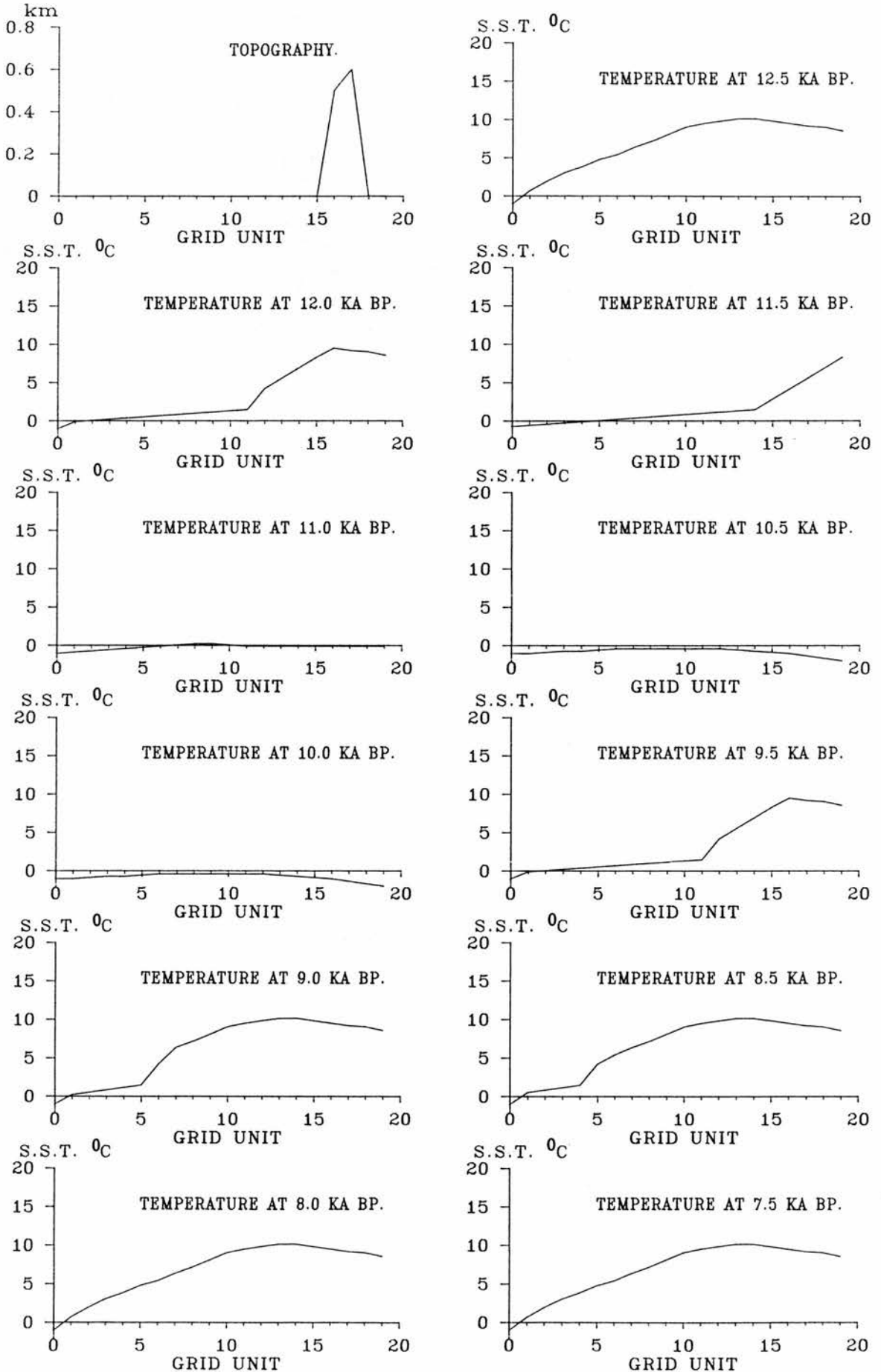
FIGURE 5.7 THE ATLANTIC OCEAN MODEL INPUT DATA FOR THE SOUTH—WESTERLY
TRANSECT. THE TRANSECTS SHOWN ARE FOR TOPOGRAPHY (IN KM),
AND FOR SEA LEVEL AIR TEMPERATURE (IN ^{0}C) AT 0.5 KA INTERVALS
BETWEEN 12.5 AND 7.5 KA BP.
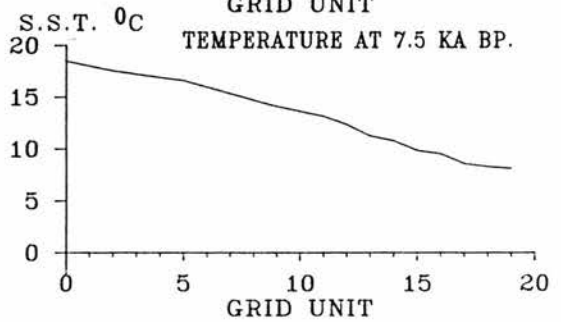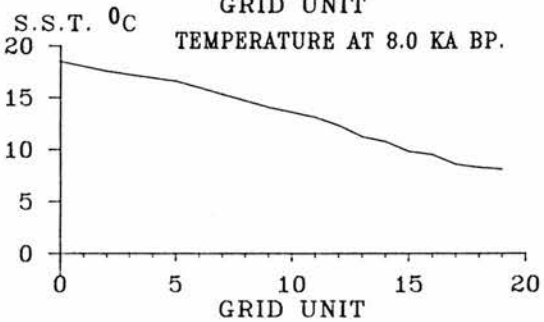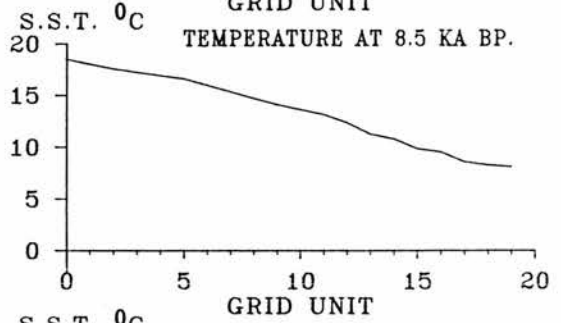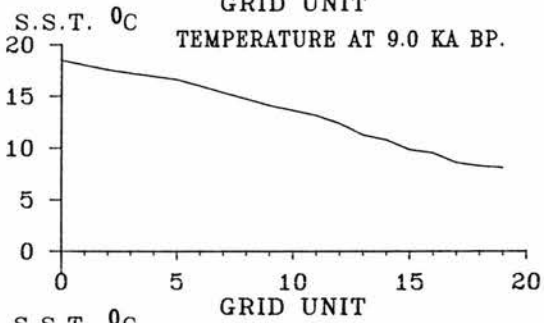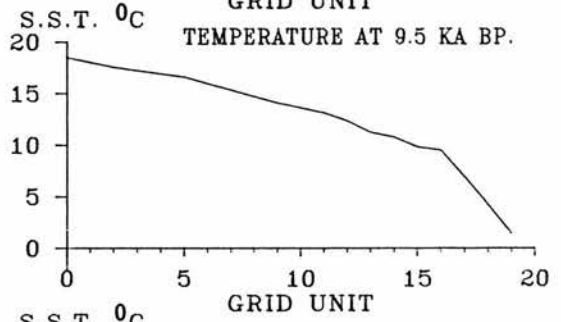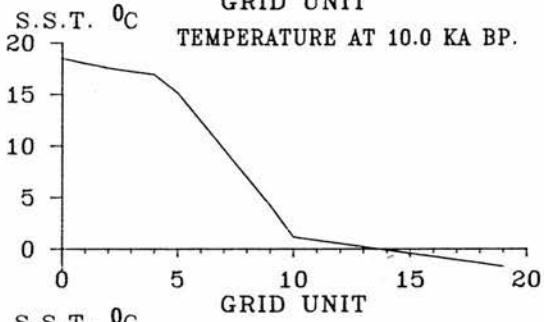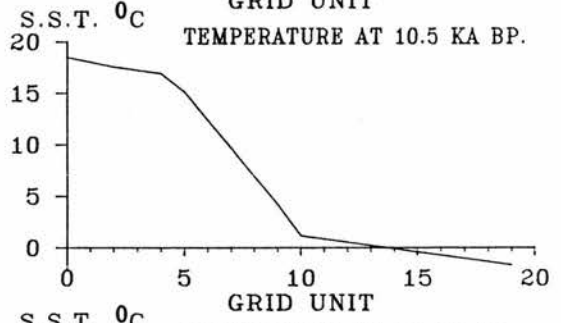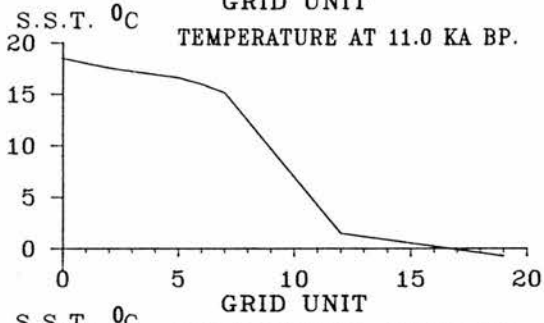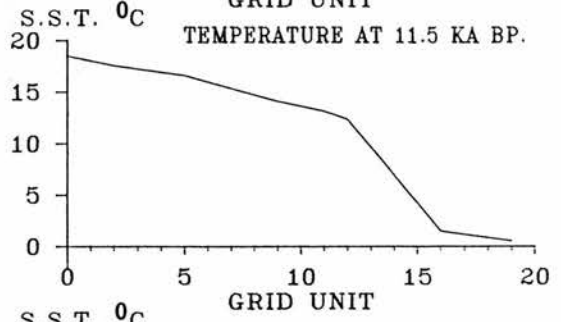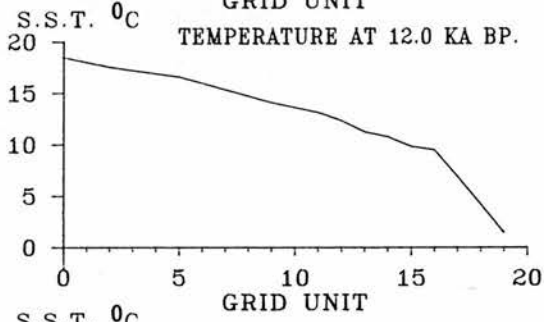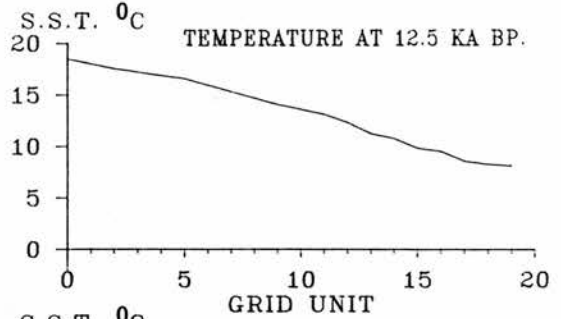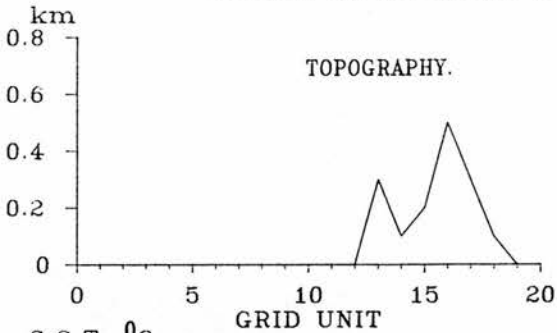
FIGURE 5.8 THE ATLANTIC OCEAN MODEL OUTPUT FOR THE WESTERLY TRANSECT. THE TRANSECTS SHOWN ARE FOR ANNUAL PRECIPITATION RATE (IN MM A^{-1}) AT 0.5 KA INTERVALS BETWEEN 12.5 AND 7.5 KA BP.
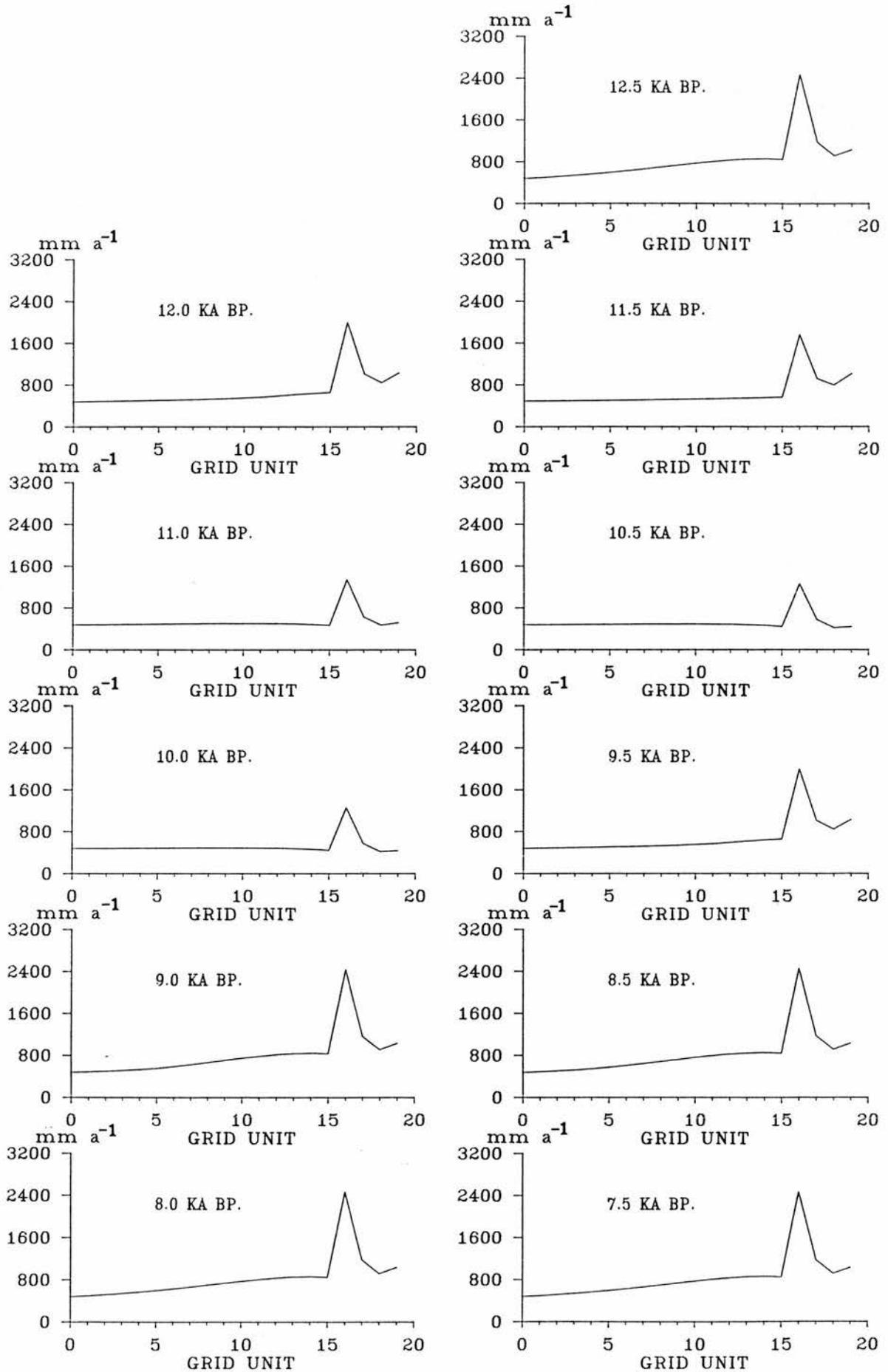
FIGURE 5.9 THE ATLANTIC OCEAN MODEL OUTPUT FOR THE SOUTH—WESTERLY TRANSECT. THE TRANSECTS SHOWN ARE FOR ANNUAL PRECIPITATION RATE (IN MM A^{-1}) AT 0.5 KA INTERVALS BETWEEN 12.5 AND 7.5 KA BP.
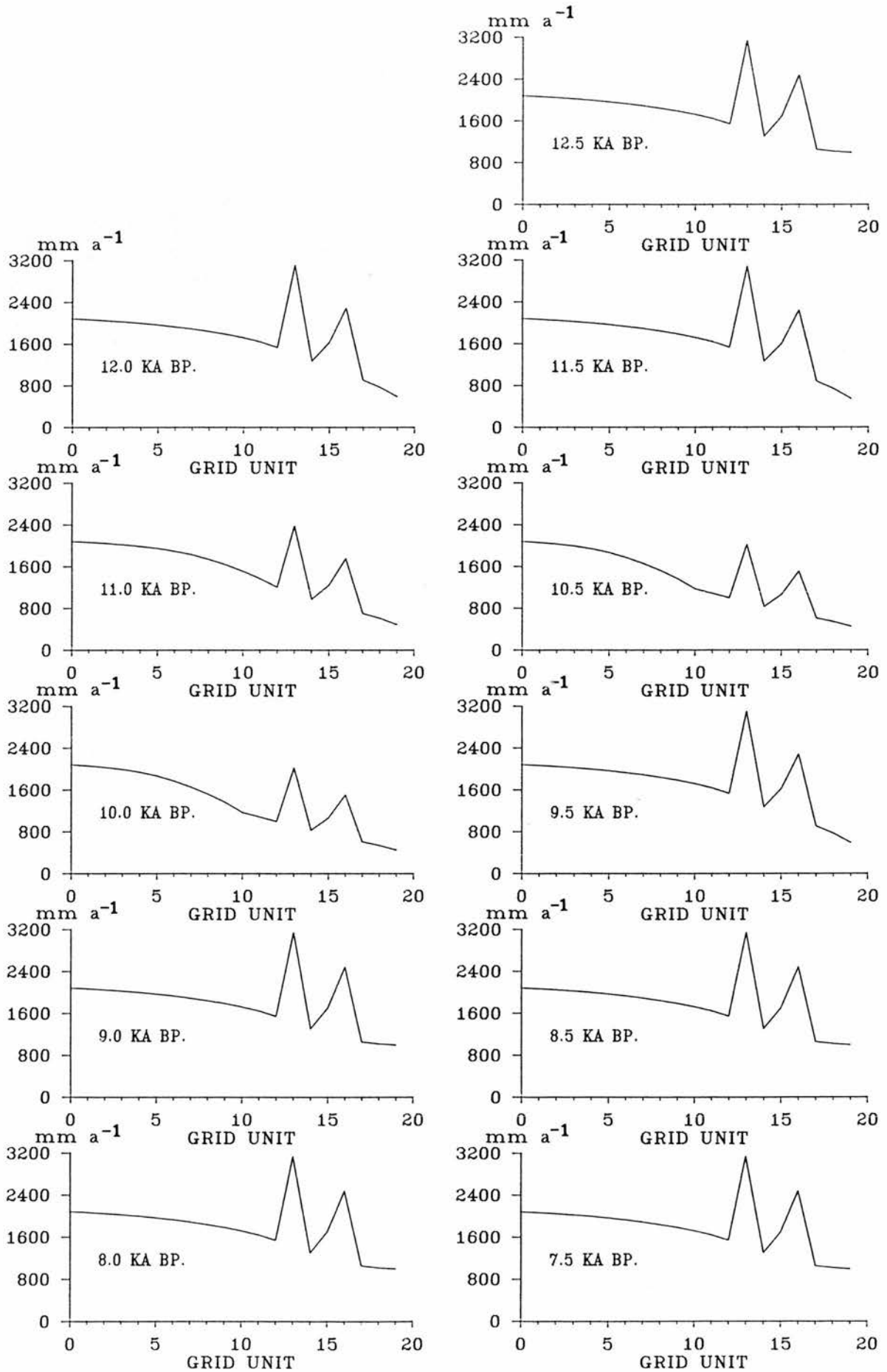
344

FIGURE 5.10 THE ATLANTIC OCEAN MODEL OUTPUT FOR THE WESTERLY TRANSECT. THE TRANSECTS SHOWN ARE FOR ATMOSPHERIC MOISTURE CONTENT (IN KG M⁻²) AT 0.5 KA INTERVALS BETWEEN 12.5 AND 7.5 KA BP.
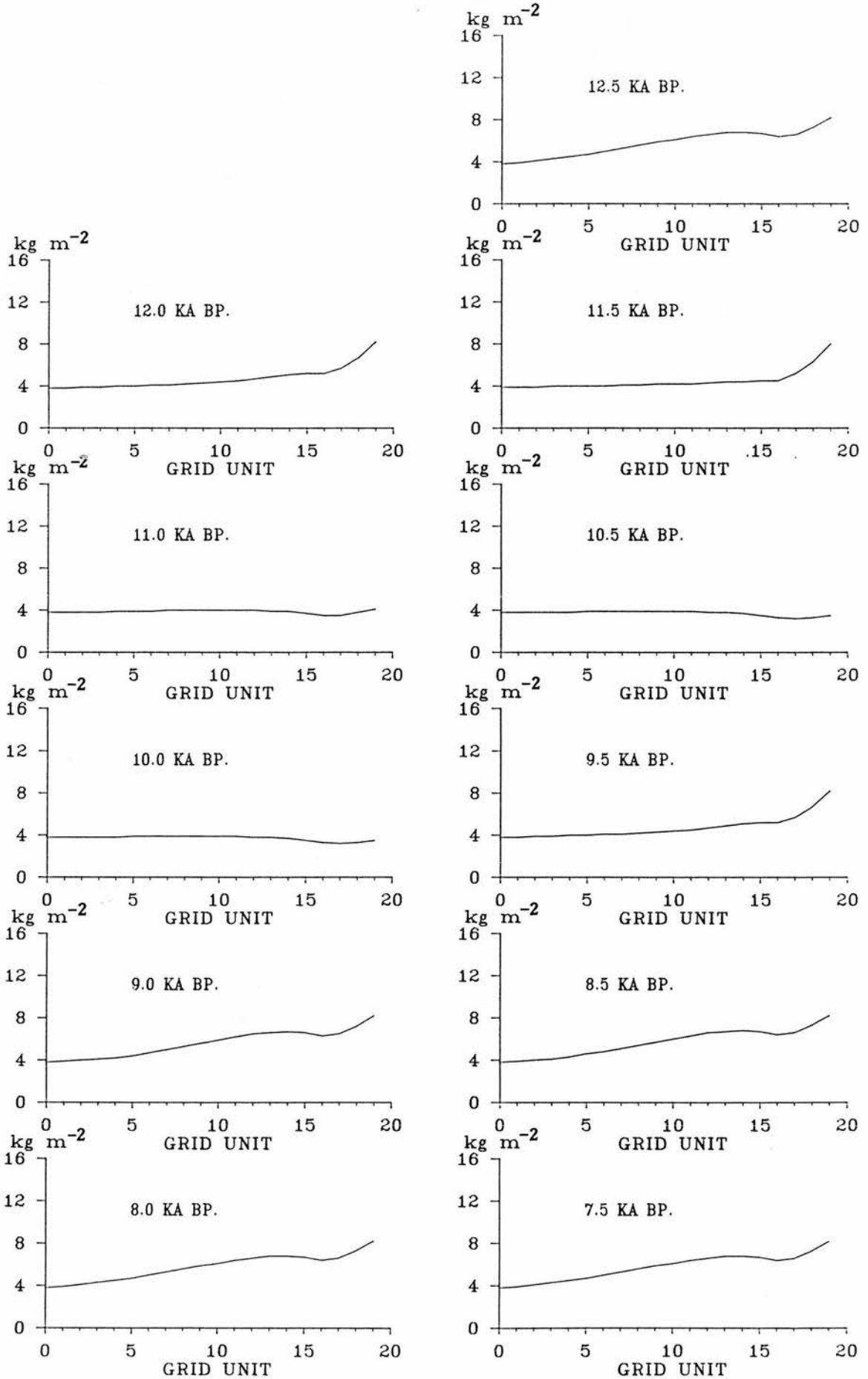
FIGURE 5.11 THE ATLANTIC OCEAN MODEL OUTPUT FOR THE SOUTH-WESTERLY TRANSECT. THE TRANSECTS SHOWN ARE FOR ATMOSPHERIC MOISTURE CONTENT (IN KG M^{-2}) AT 0.5 KA INTERVALS BETWEEN 12.5 AND 7.5 KA BP.
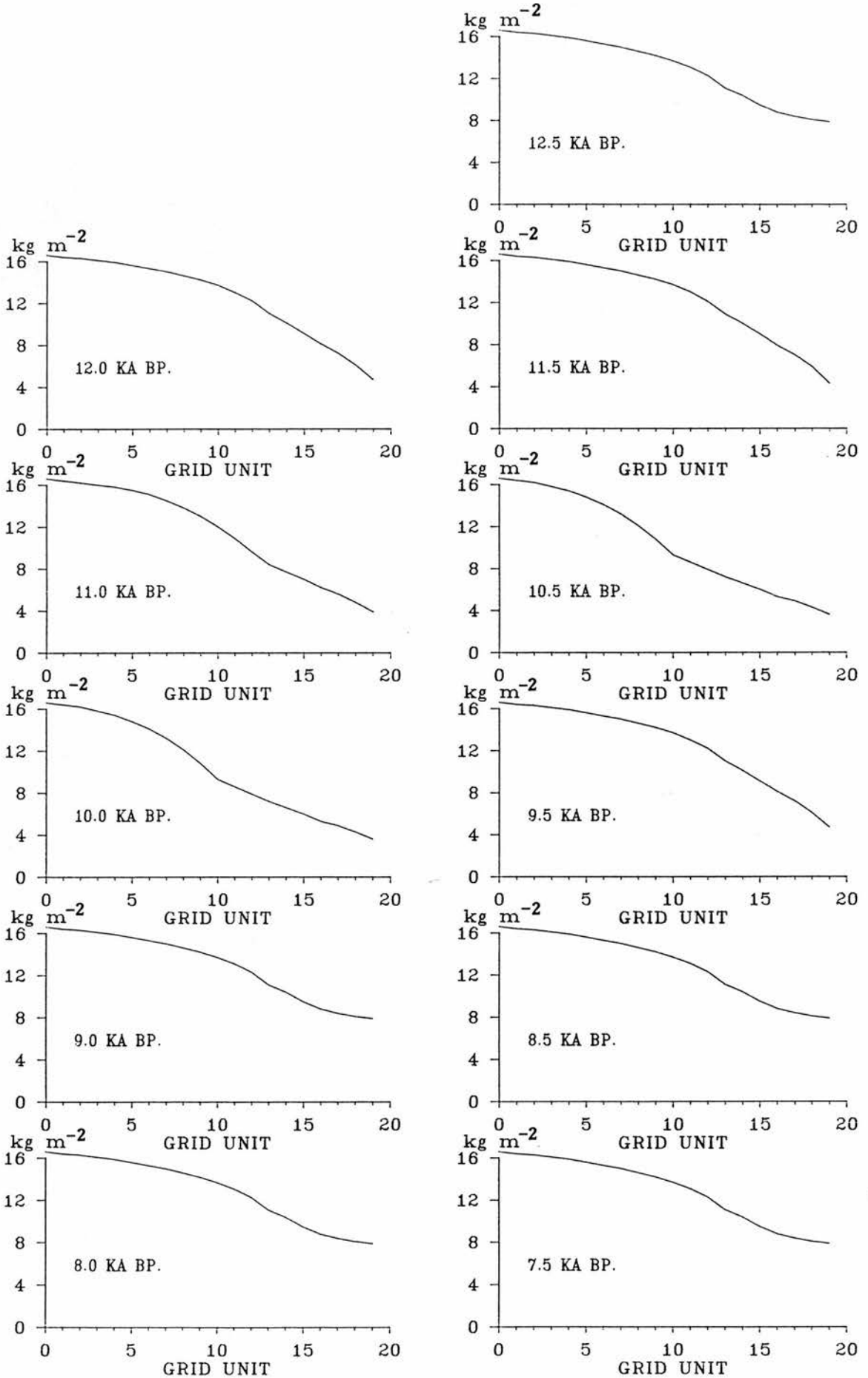
FIGURE 5.12 THE DISTRIBUTION OF UPWIND SURFACE SLOPES CALCULATED
IN THE SCOTTISH MODEL FOR A WESTERLY WIND DIRECTION.

FIGURE 5.13 THE DISTRIBUTION OF UPWIND SURFACE SLOPES CALCULATED IN THE SCOTTISH MODEL FOR A SOUTH-WESTERLY WIND DIRECTION.

FIGURE 5.14 THE DISTRIBUTION OF SATURATED ATMOSPHERIC MOISTURE CONTENT CALCULATED IN THE SCOTTISH MODEL FOR THE PRESENT DAY.
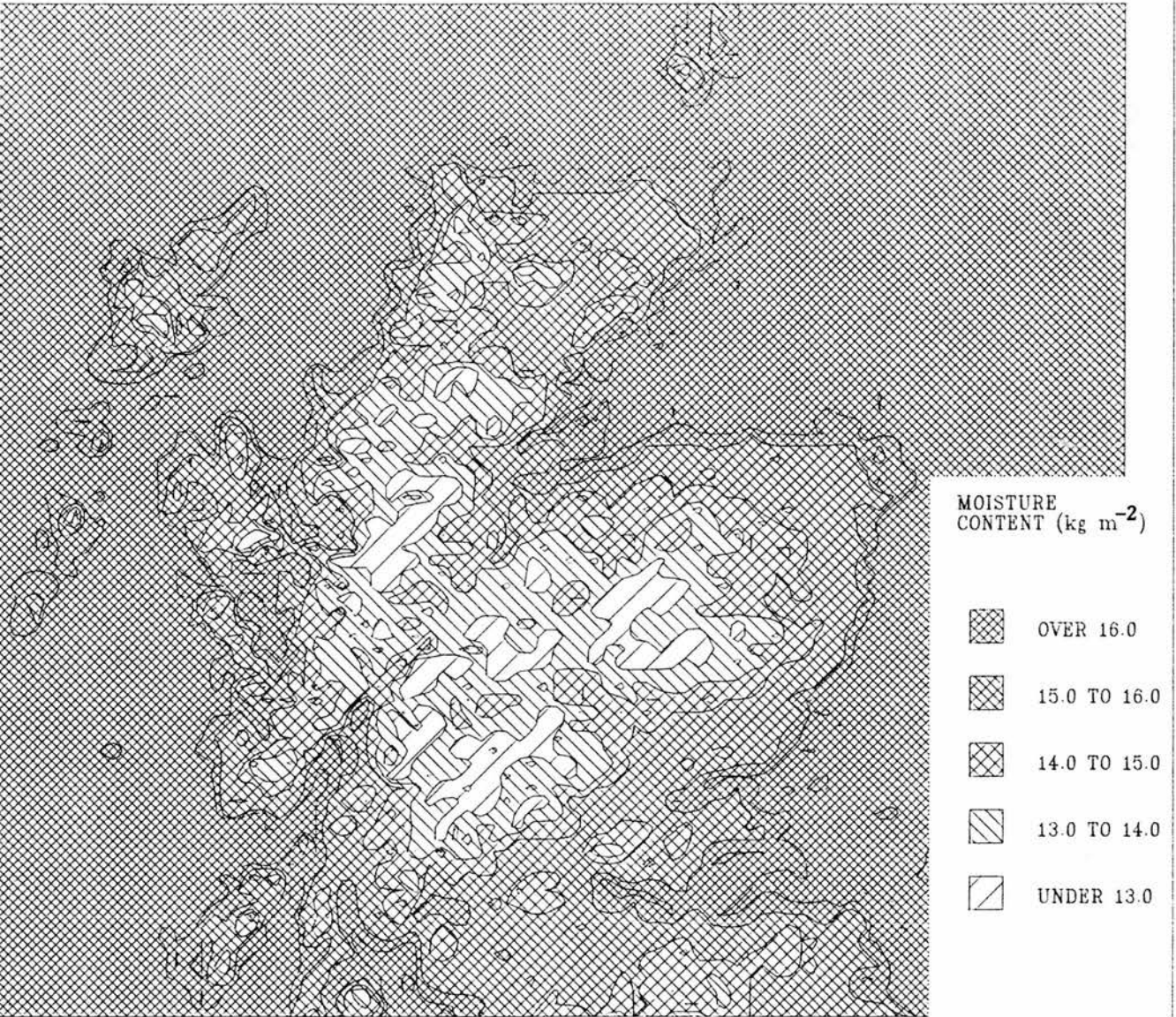
MOISTURE CONTENT (kg m^{-2})

OVER 16.0

15.0 TO 16.0

14.0 TO 15.0

13.0 TO 14.0

UNDER 13.0

FIGURE 5.15 THE DISTRIBUTION OF ATMOSPHERIC MOISTURE CONTENT
CALCULATED IN THE SCOTTISH MODEL FOR THE PRESENT
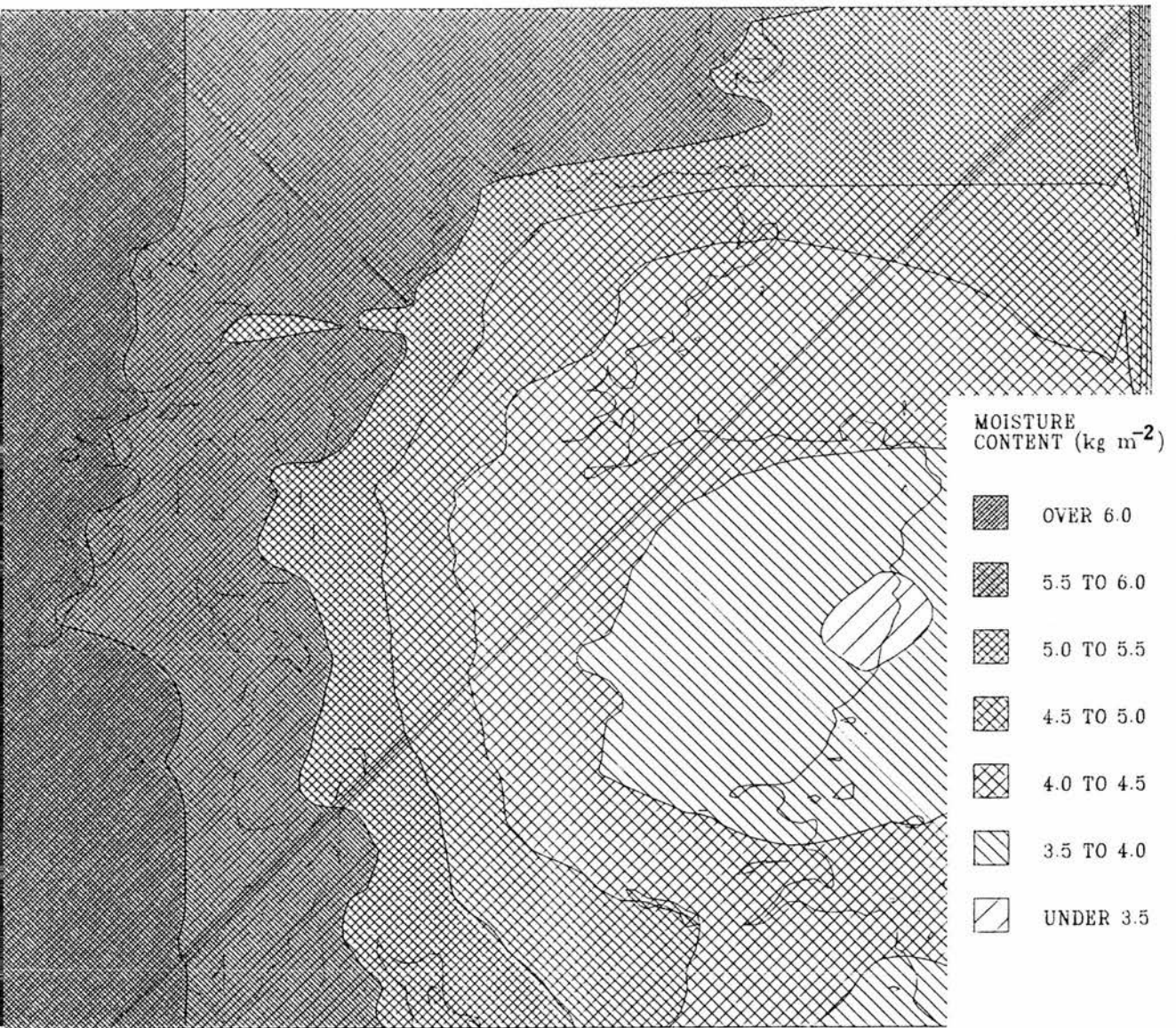DAY WITH A WESTERLY WIND DIRECTION.

MOISTURE
CONTENT (kg m^{-2})

OVER 6.0

5.5 TO 6.0

5.0 TO 5.5

4.5 TO 5.0

4.0 TO 4.5

3.5 TO 4.0

UNDER 3.5

FIGURE 5.16 THE DISTRIBUTION OF ANNUAL PRECIPITATION RATE CALCULATED IN THE SCOTTISH MODEL FOR THE PRESENT DAY WITH A WESTERLY WIND DIRECTION.

PRECIPITATION (m/a)

OVER 2.25

2.00 TO 2.25

1.75 TO 2.00

1.50 TO 1.75

1.25 TO 1.50

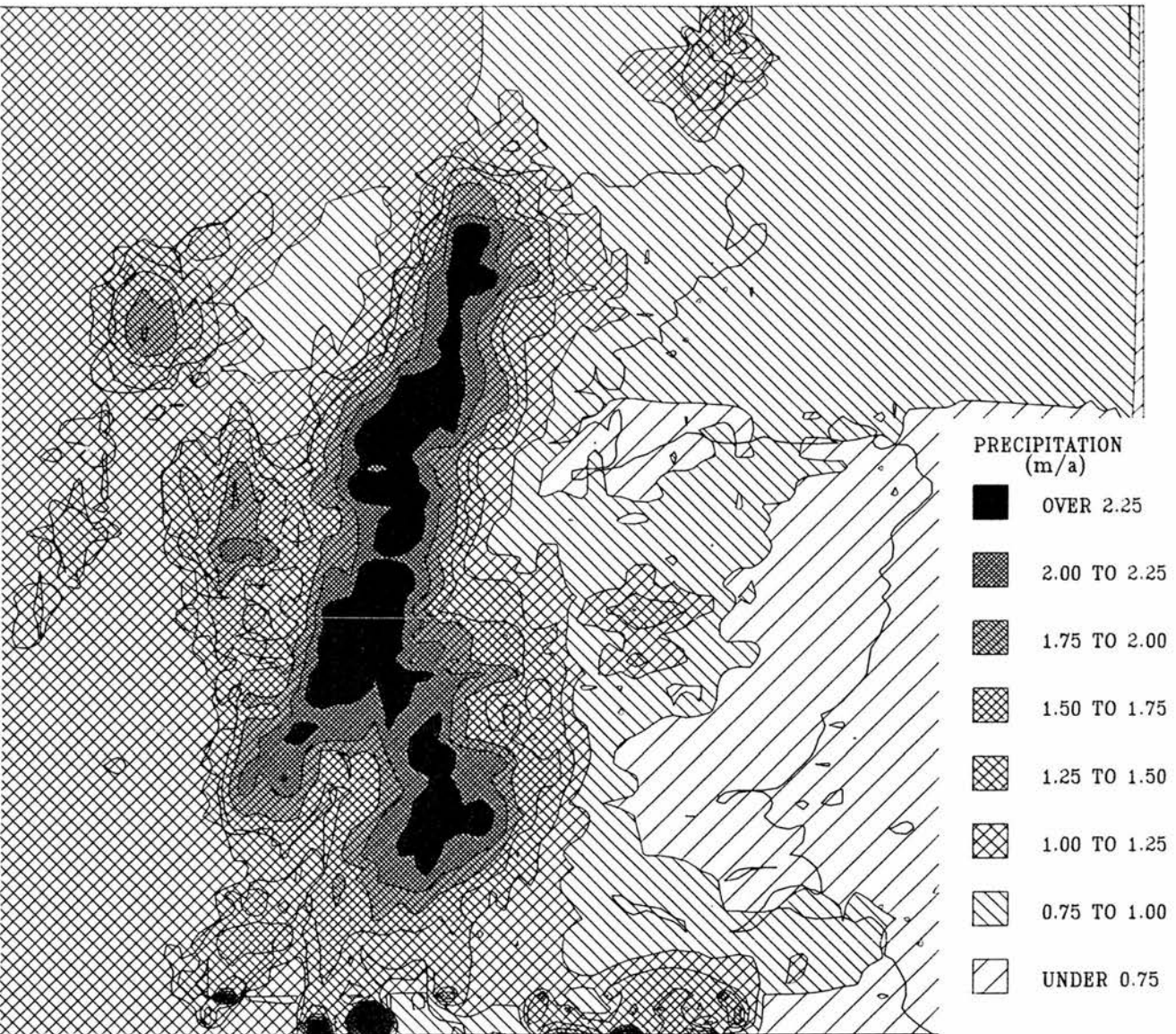1.00 TO 1.25

0.75 TO 1.00

UNDER 0.75

FIGURE 5.17 HISTOGRAMS OF THE ANNUAL PRECIPITATION RATES PREDICTED BY THE SCOTTISH MODEL DURING THE SENSITIVITY ANALYSIS. RESULTS ARE SHOWN FOR THE STANDARD WESTERLY RUN, AND FOR WESTERLY RUNS IN WHICH THE PRECIPITATION PARAMETERS (f_0 AND f_1) AND THE EVAPORATION TIME SCALE (T_*) WERE EITHER INCREASED OR DECREASED BY 50 %.
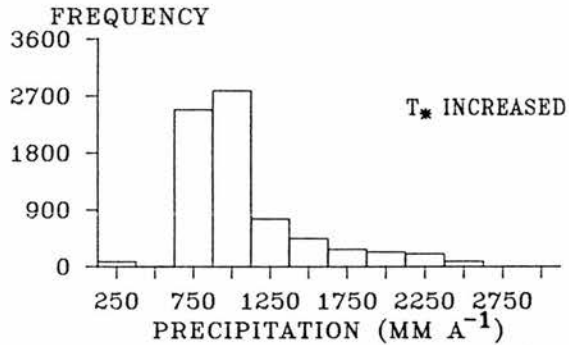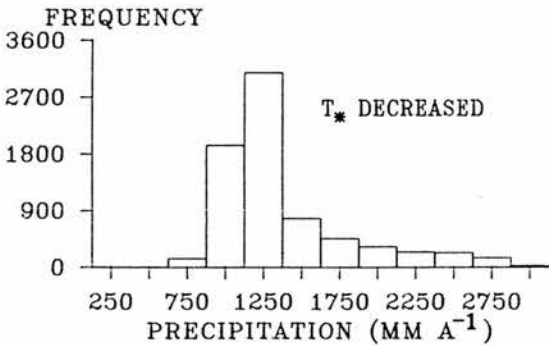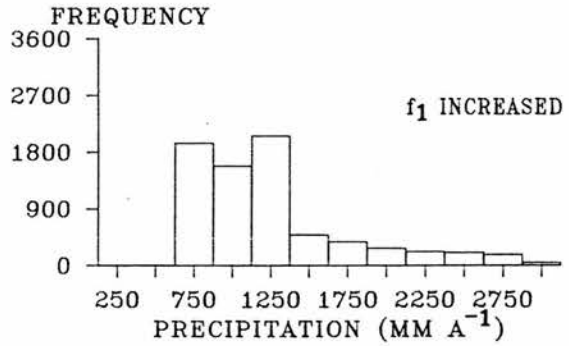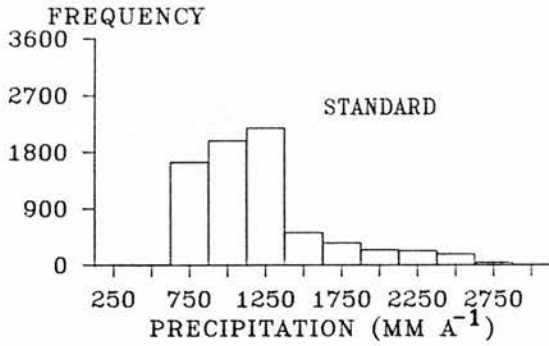
FIGURE 5.18 HISTOGRAMS OF THE ANNUAL PRECIPITATION RATES PREDICTED BY THE SCOTTISH MODEL DURING THE SENSITIVITY ANALYSIS. RESULTS ARE SHOWN FOR WESTERLY RUNS IN WHICH THE SPECIFIED WIND VELOCITY (U) AND THE SATURATED MOISTURE CONTENT DISTRIBUTION (Wsat) WERE EITHER INCREASED OR DECREASED BY 50 %. RESULTS ARE ALSO SHOWN FOR WESTERLY RUNS IN WHICH THE VALUE OF THE BOUNDARY MOISTURE CONTENT WAS EITHER INCREASED OR DECREASED BY 50 %, OR REMOVED ENTIRELY.
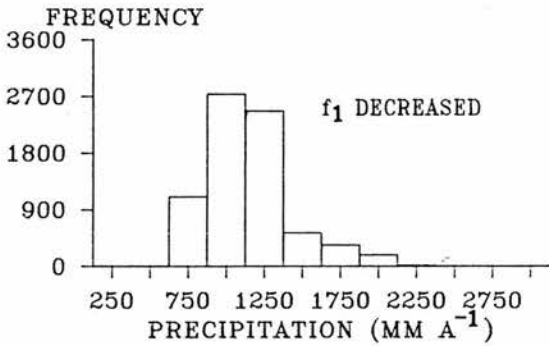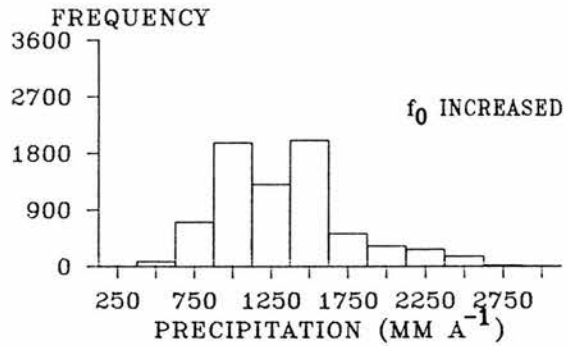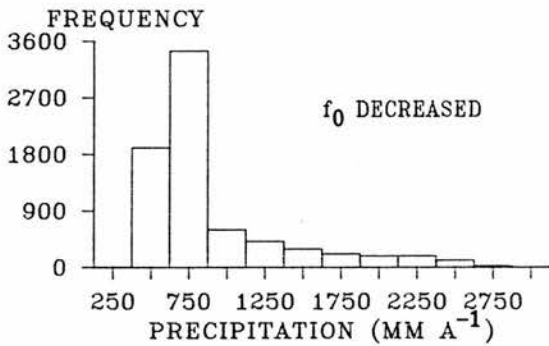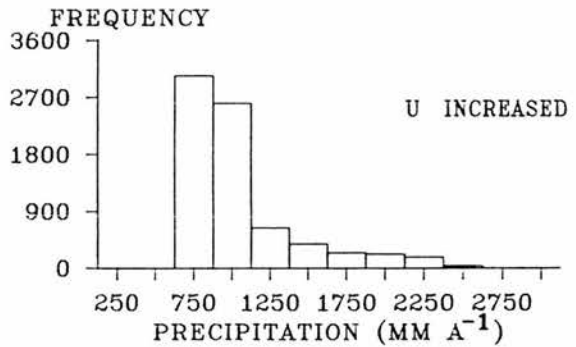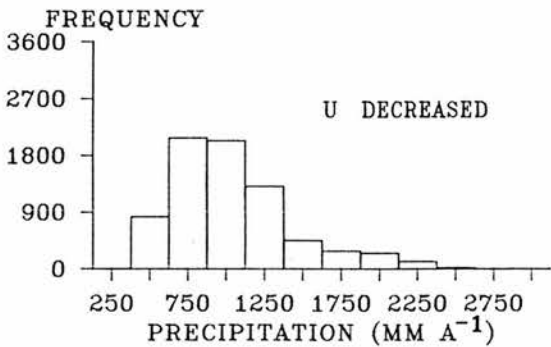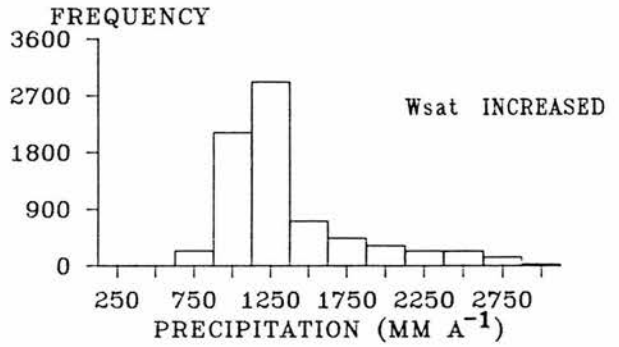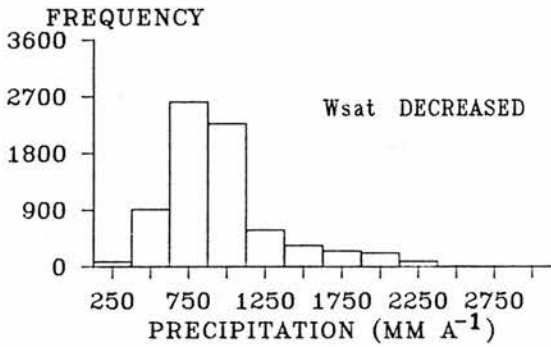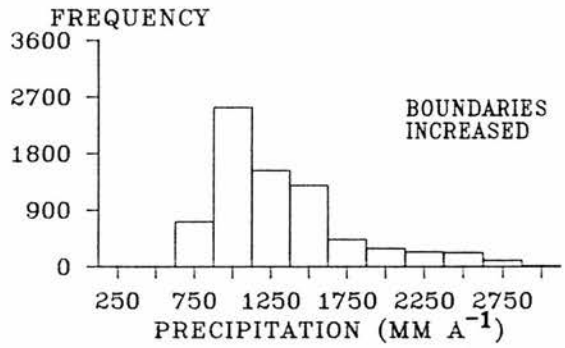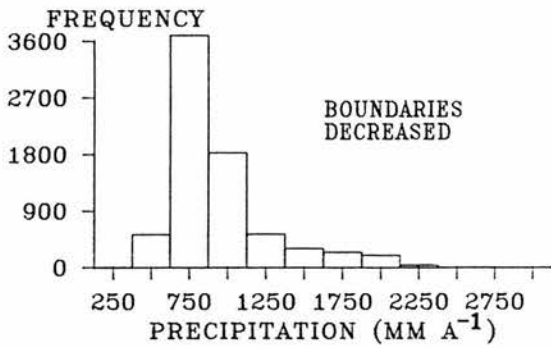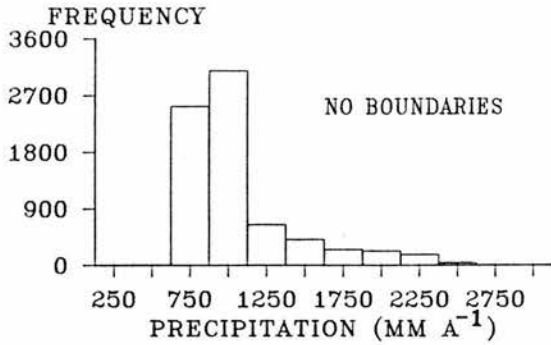
FIGURE 5.19 HISTOGRAMS OF THE ANNUAL PRECIPITATION RATES PREDICTED BY
THE SCOTTISH MODEL DURING THE SENSITIVITY ANALYSIS. RESULTS
ARE SHOWN FOR WESTERLY AND SOUTH—WESTERLY RUNS IS WHICH
IMPOSED SURFACE AIR TEMPERATURES HAD THEIR PRESENT DAY VALUES,
THEIR VALUES AT 12.0 KA BP AND THEIR VALUES AT 10.0 KA BP.
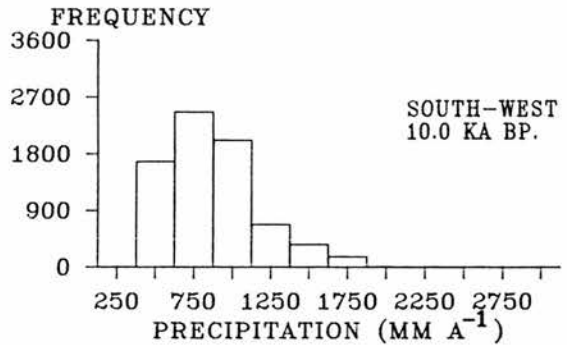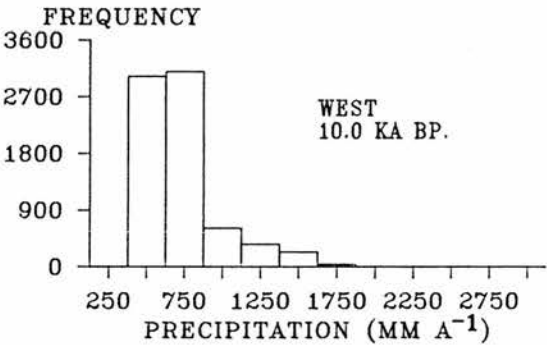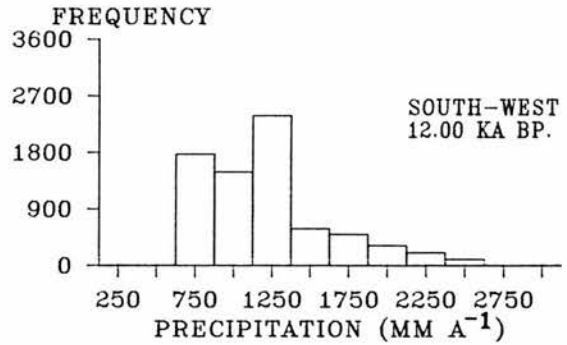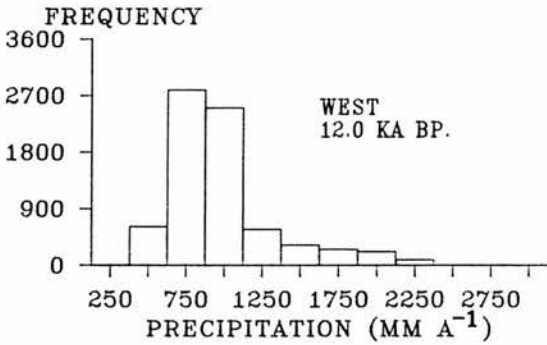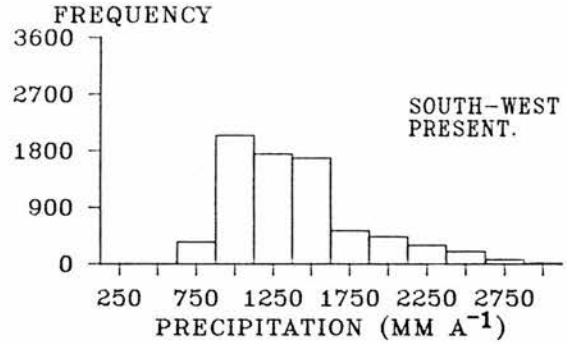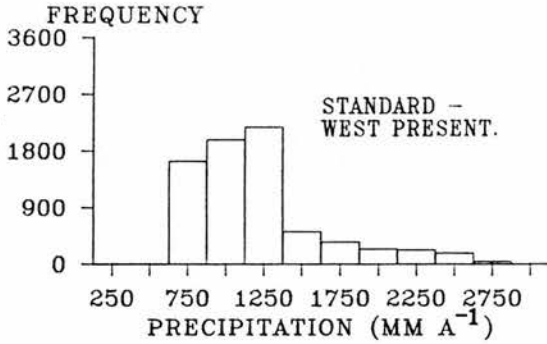
FIGURE 5.20 THE DISTRIBUTION OF ATMOSPHERIC MOISTURE CONTENT
CALCULATED IN THE SCOTTISH MODEL FOR THE PRESENT
DAY WITH A SOUTH–WESTERLY WIND DIRECTION.

MOISTURE
CONTENT (kg m^{-2})

OVER 6.0

5.5 TO 6.0

5.0 TO 5.5

4.5 TO 5.0

4.0 TO 4.5

3.5 TO 4.0

UNDER 3.5
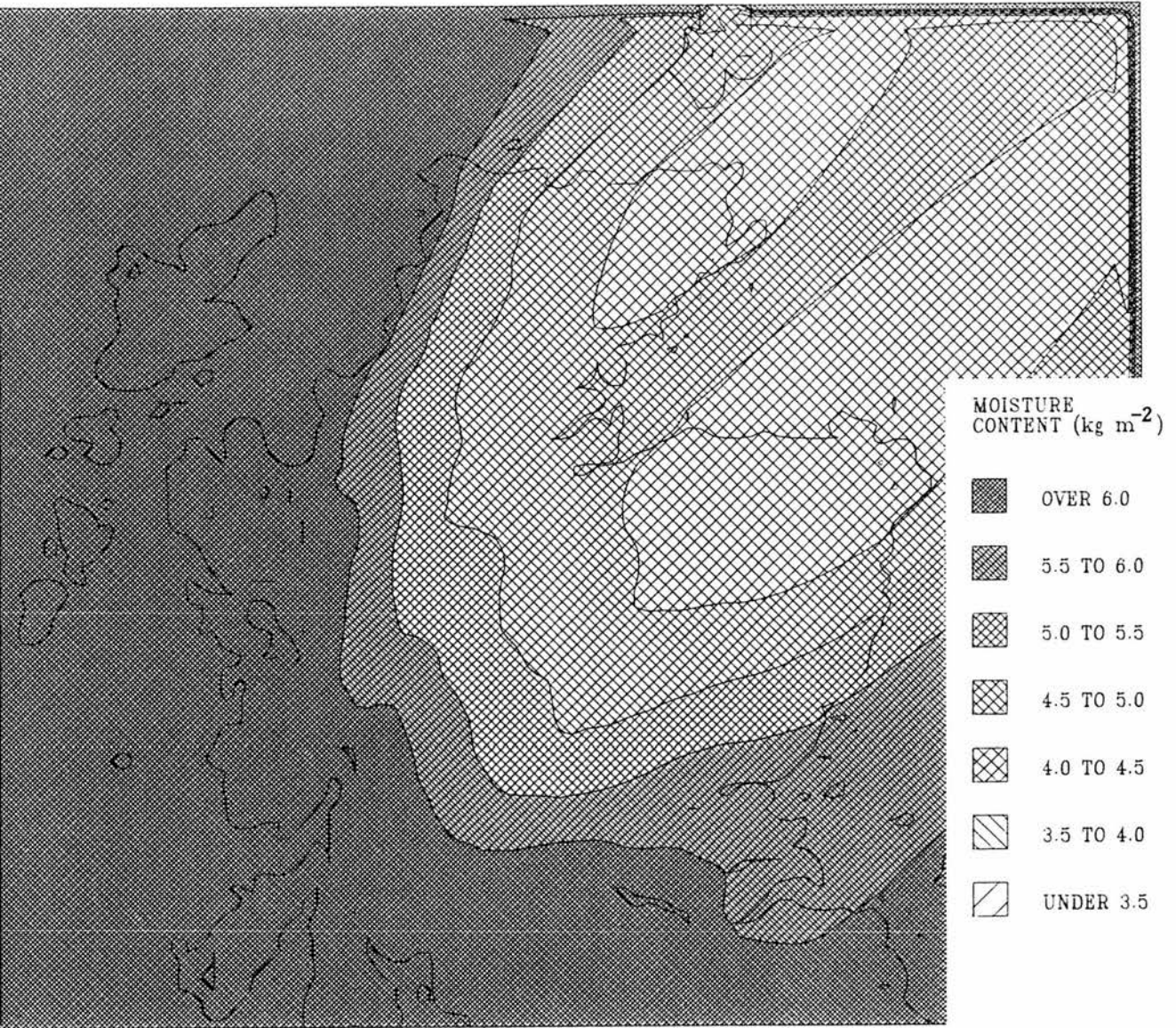
FIGURE 5.21 THE DISTRIBUTION OF ANNUAL PRECIPITATION RATE
CALCULATED IN THE SCOTTISH MODEL FOR THE PRESENT
DAY WITH A SOUTH-WESTERLY WIND DIRECTION.

PRECIPITATION
(m/a)

OVER 2.25

2.00 TO 2.25

1.75 TO 2.00

1.50 TO 1.75

1.25 TO 1.50

1.00 TO 1.25

0.75 TO 1.00

UNDER 0.75
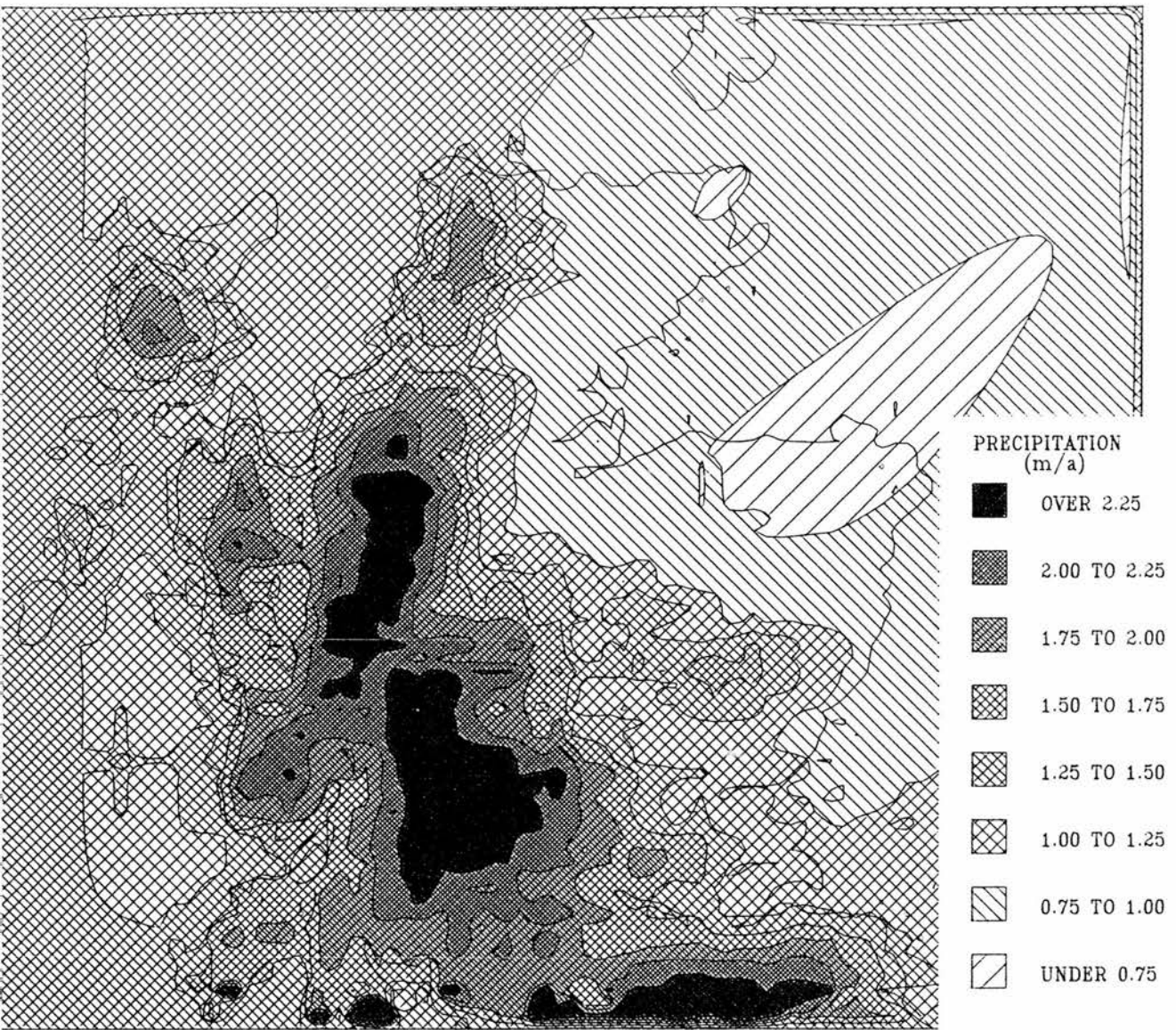
FIGURE 5.22 THE ICE SHEET VOLUME OUTPUT PRODUCED BY THE COUPLED MODEL
WHEN A WESTERLY WIND DIRECTION IS EMPLOYED. THE ICE SHEET
VOLUME OUTPUT FROM THE STANDARD RUN OF CHAPTER 4 IS ALSO
SHOWN. THE TOP GRAPH SHOWS THE AIR TEMPERATURE DEPRESSION
INPUT AND THE MEAN PRECIPITATION RATE OUTPUT.
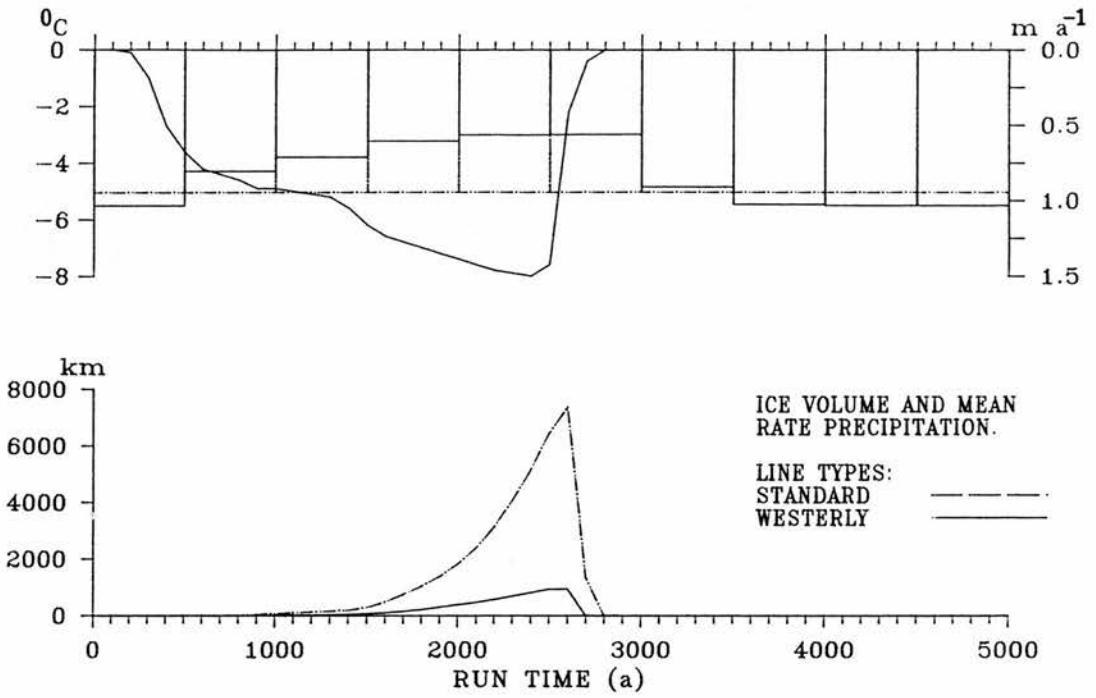
FIGURE 5.23 THE PREDICTION OF THE COUPLED MODEL FOR ICE SHEET THICKNESS AT 2.6 KA. WHEN A WESTERLY WIND DIRECTION IS EMPLOYED. THIS REPRESENTS THE MAXIMUM ICE SHEET ATTAINED IN THE THE RUN.

FIGURE 5.24 THE PREDICTION OF THE COUPLED MODEL FOR ANNUAL PRECIPITATION
RATE AT 2.6 KA WHEN A WESTERLY WIND DIRECTION IS EMPLOYED.
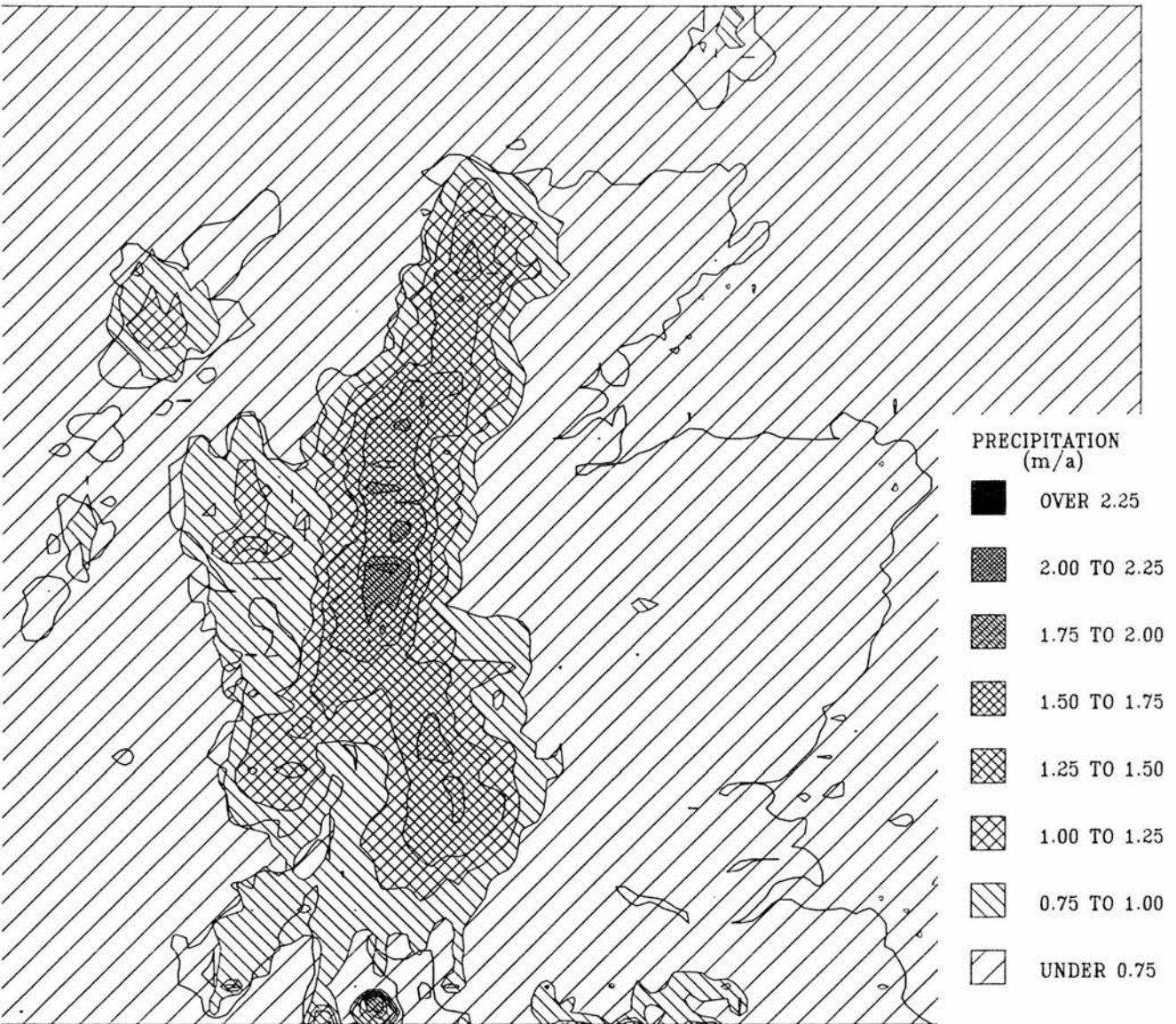
FIGURE 5.25 THE ICE SHEET VOLUME OUTPUT PRODUCED BY THE COUPLED MODEL WHEN A SOUTH-WESTERLY WIND DIRECTION IS EMPLOYED. THE ICE SHEET VOLUME OUTPUT FROM THE STANDARD RUN OF CHAPTER 4 IS ALSO SHOWN. THE TOP GRAPH SHOWS THE AIR TEMPERATURE DEPRESSION INPUT AND THE MEAN PRECIPITATION RATE OUTPUT.
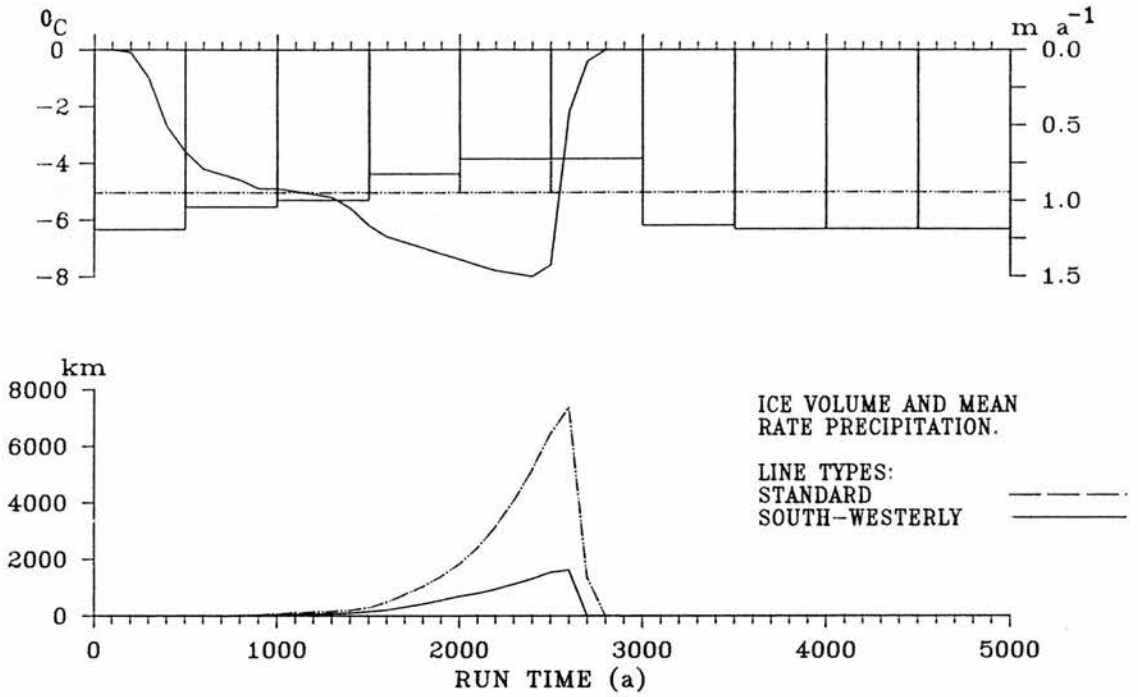
FIGURE 5.26 THE PREDICTION OF THE COUPLED MODEL FOR ICE SHEET THICKNESS
AT 2.6 KA. WHEN A SOUTH—WESTERLY WIND DIRECTION IS EMPLOYED.
THIS REPRESENTS THE MAXIMUM ICE SHEET ATTAINED IN THE THE
RUN.
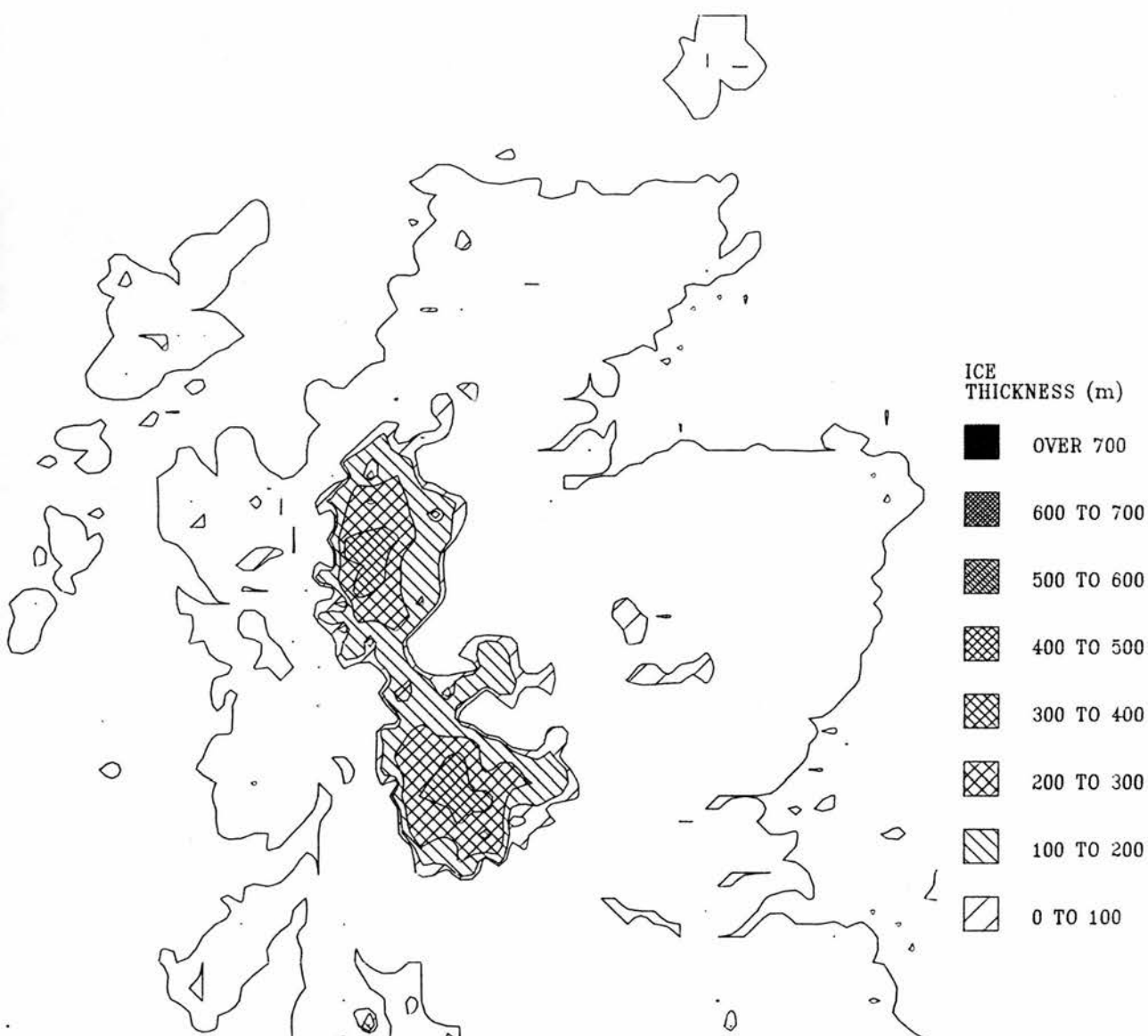
FIGURE 5.27 THE PREDICTION OF THE COUPLED MODEL FOR ANNUAL PRECIPITATION
RATE AT 2.6 KA WHEN A SOUTH-WESTERLY WIND DIRECTION IS
EMPLOYED.

PRECIPITATION
(m/a)

OVER 2.25

2.00 TO 2.25

1.75 TO 2.00

1.50 TO 1.75

1.25 TO 1.50

1.00 TO 1.25

0.75 TO 1.00

UNDER 0.75
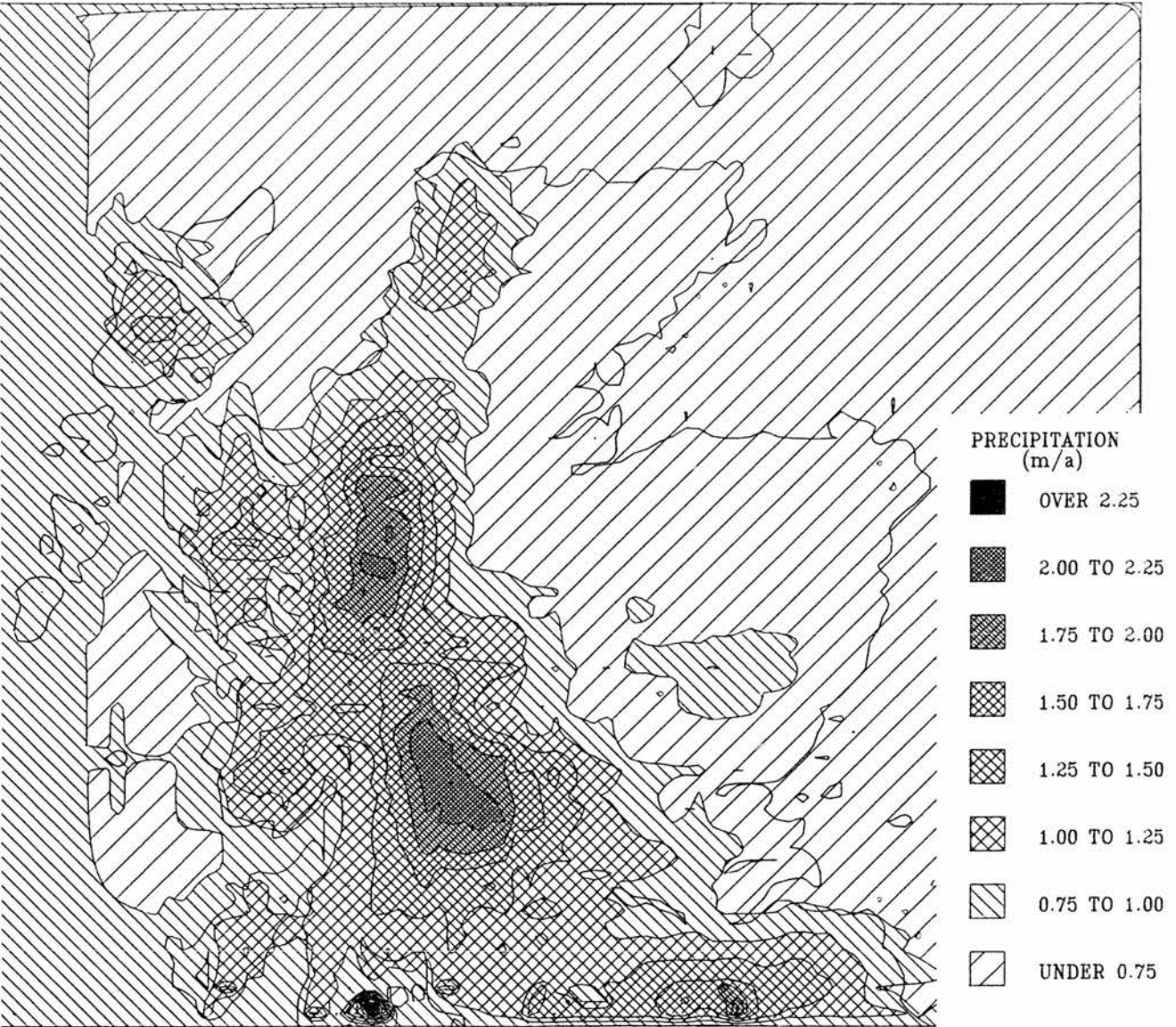
FIGURE 5.28 THE SENSITIVITY ANALYSIS OUTPUT PRODUCED BY THE COUPLED MODEL
WITH A WESTERLY WIND DIRECTION. ICE SHEET VOLUME AND MEAN
PRECIPITATION RATE ARE SHOWN FOR THE USUAL STANDARD RUN AND FOR
RUNS IN WHICH THE SATURATED ATMOSPHERIC MOISTURE CONTENT WAS
INCREASED AND DECREASED BY 50 %.
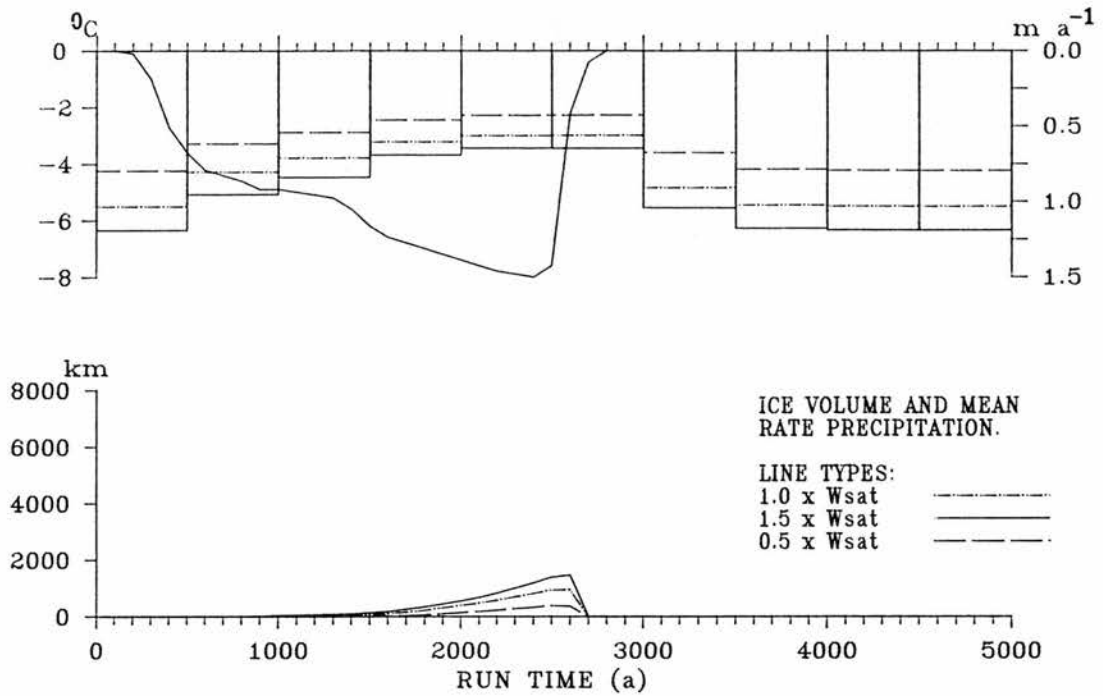
FIGURE 5.29 THE SENSITIVITY ANALYSIS OUTPUT PRODUCED BY THE COUPLED MODEL
WITH A WESTERLY WIND DIRECTION. ICE SHEET VOLUME AND MEAN
PRECIPITATION RATE ARE SHOWN FOR THE USUAL STANDARD RUN AND FOR
RUNS IN WHICH THE BOUNDARY MOISTURE CONDITIONS WERE INCREASED
AND DECREASED BY 50 %.

363
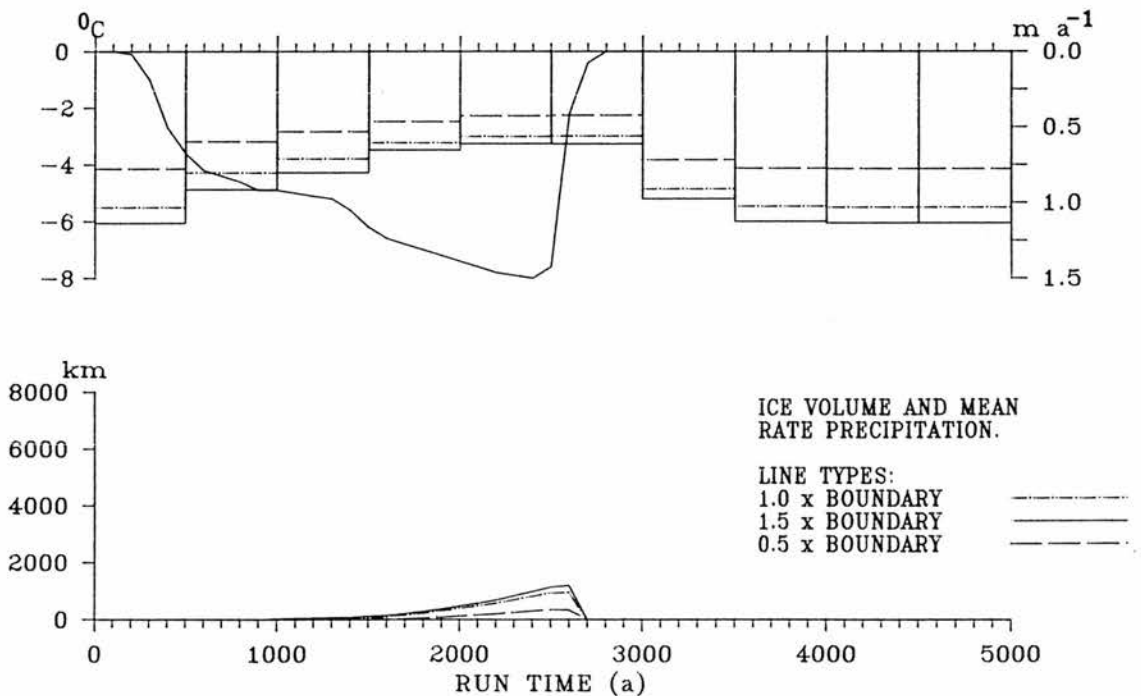
FIGURE 5.30 THE SENSITIVITY ANALYSIS OUTPUT PRODUCED BY THE COUPLED MODEL
WITH A SOUTH−WESTERLY WIND DIRECTION. ICE SHEET VOLUME AND MEAN
PRECIPITATION RATE ARE SHOWN FOR THE USUAL STANDARD RUN AND FOR
RUNS IN WHICH THE SATURATED ATMOSPHERIC MOISTURE CONTENT WAS
INCREASED AND DECREASED BY 50 %.

ICE VOLUME AND MEAN
RATE PRECIPITATION.

LINE TYPES:
1.0 x Wsat
1.5 x Wsat
0.5 x Wsat
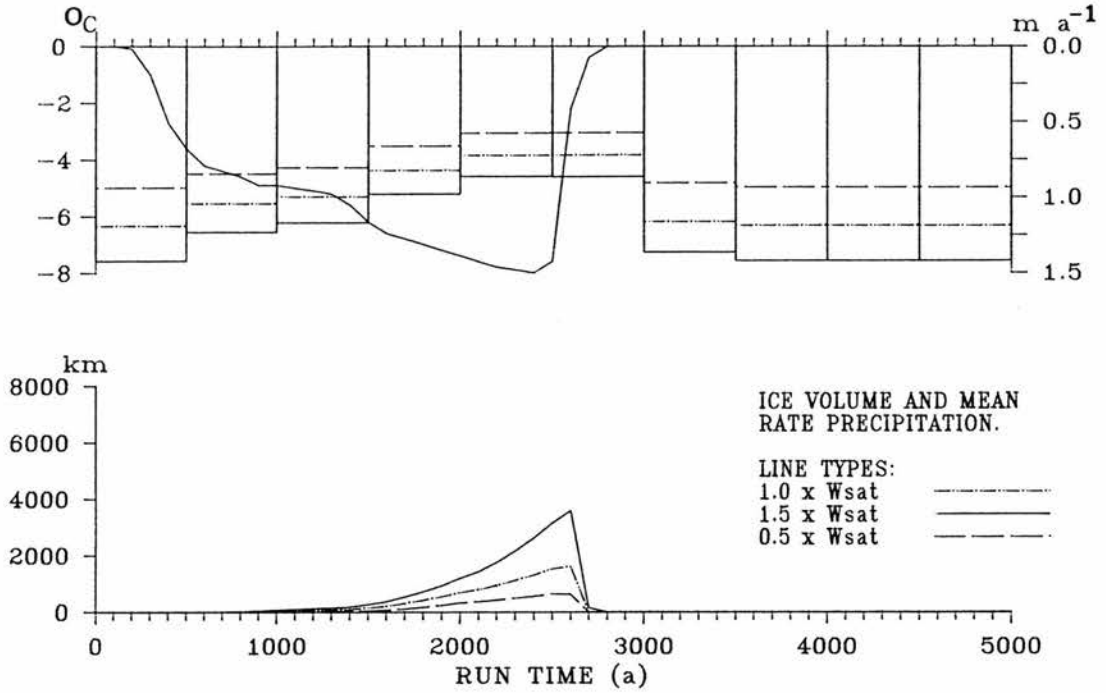
FIGURE 5.31 THE SENSITIVITY ANALYSIS OUTPUT PRODUCED BY THE COUPLED MODEL
WITH A SOUTH−WESTERLY WIND DIRECTION. ICE SHEET VOLUME AND MEAN
PRECIPITATION RATE ARE SHOWN FOR THE USUAL STANDARD RUN AND FOR
RUNS IN WHICH THE BOUNDARY MOISTURE CONDITIONS WERE INCREASED
AND DECREASED BY 50 %.

ICE VOLUME AND MEAN
RATE PRECIPITATION.

LINE TYPES:
1.0 x BOUNDARY
1.5 x BOUNDARY
0.5 x BOUNDARY
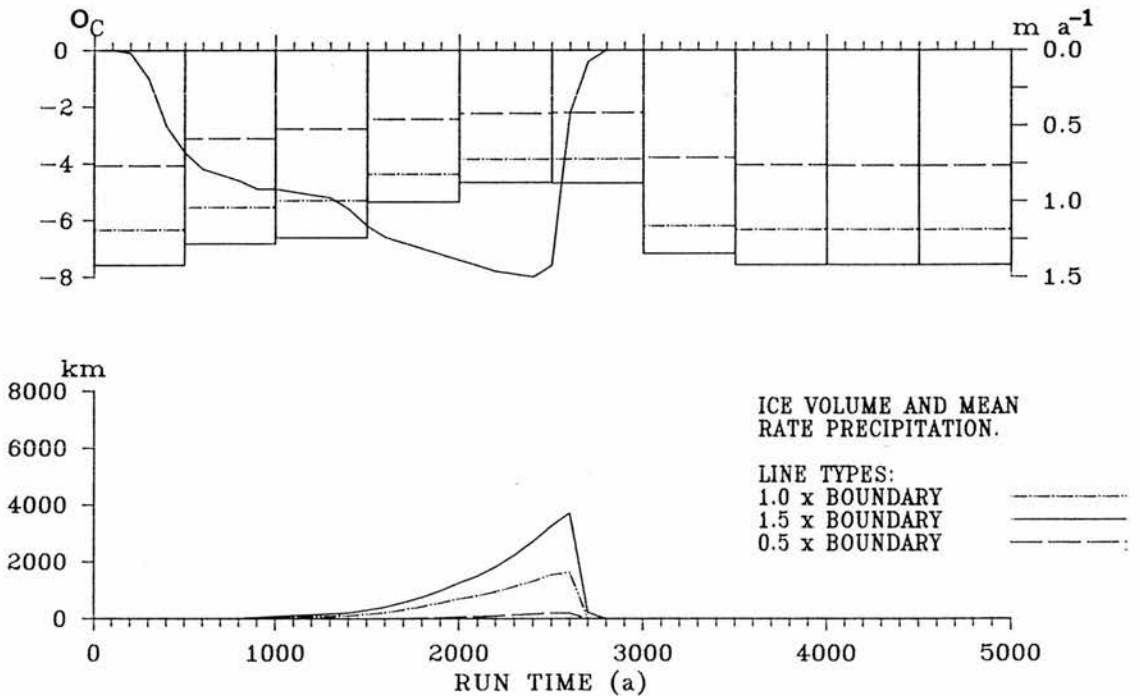
FIGURE 5.32 THE OUTPUT PRODUCED BY THE COUPLED MODEL WITH A WESTERLY WIND DIRECTION. ICE SHEET VOLUME AND MEAN PRECIPITATION RATE ARE SHOWN FOR THE USUAL STANDARD RUN AND FOR A RUN IN WHICH THE PRECIPITATION RATE AT 1.0 KA WAS DOUBLED.
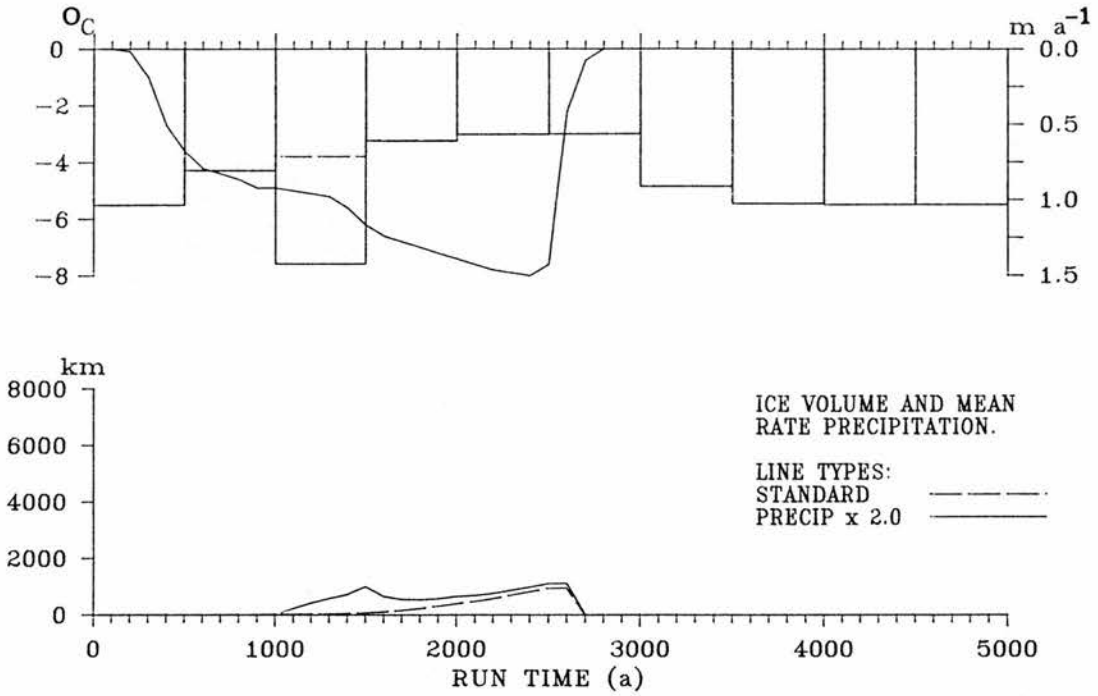
FIGURE 5.33 THE OUTPUT PRODUCED BY THE COUPLED MODEL WITH A SOUTH-WESTERLY WIND DIRECTION. ICE SHEET VOLUME AND MEAN PRECIPITATION RATE ARE SHOWN FOR THE USUAL STANDARD RUN AND FOR A RUN IN WHICH THE PRECIPITATION RATE AT 1.0 KA WAS DOUBLED.
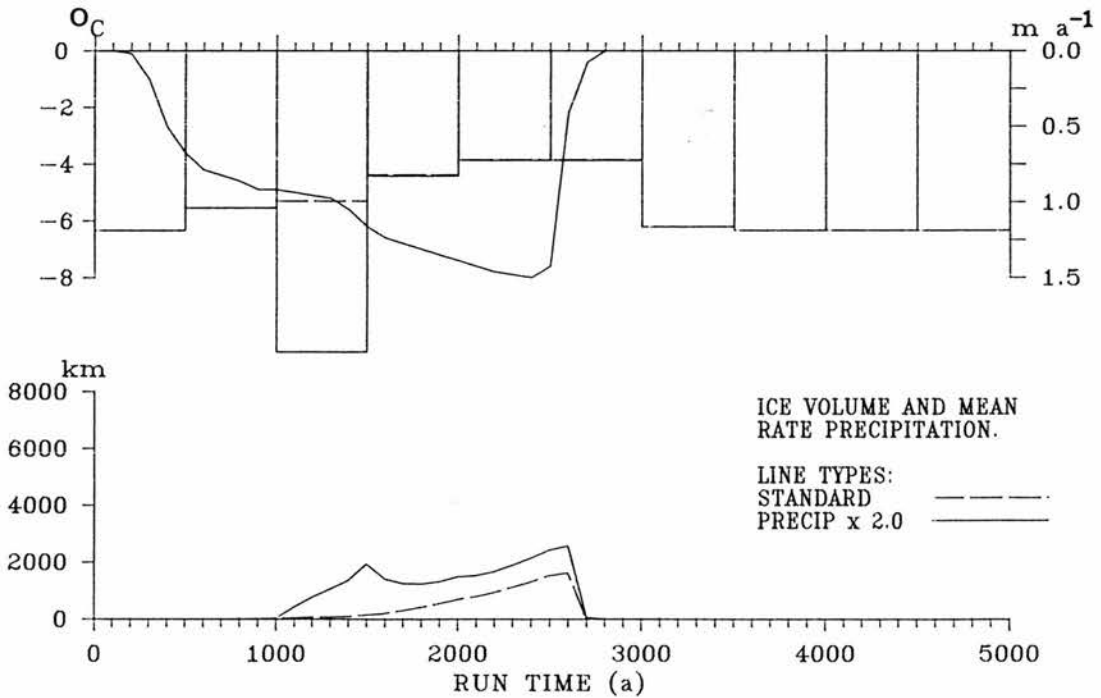
FIGURE 5.34 LINES OF EQUAL ABLATION PLOTTED AS A FUNCTION OF SURFACE
ELEVATION AND IMPOSED JULY TEMPERATURE DEPRESSION. ABLATION
IS SHOWN FROM 0.5 TO 6.0 M/A IN STEPS OF 0.5.
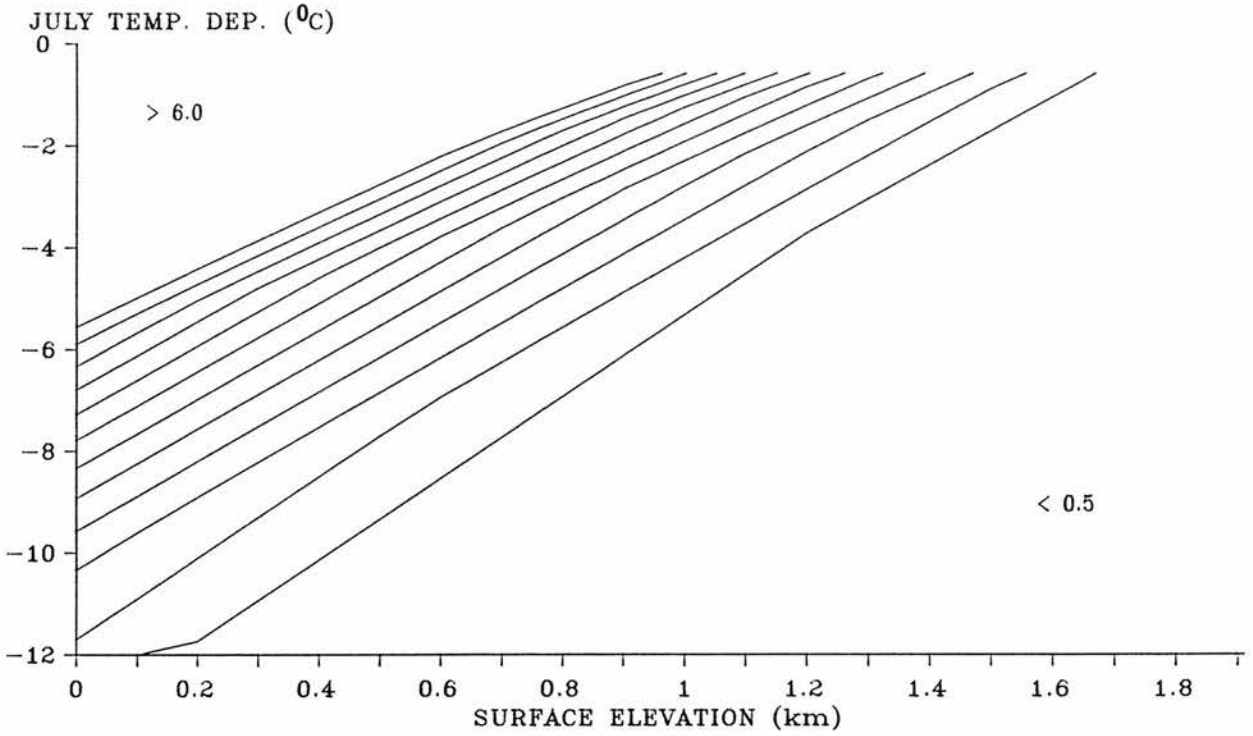
FIGURE 5.35 LINES OF EQUAL EFFECTIVENESS AS A FUNCTION OF SURFACE
ELEVATION AND IMPOSED JULY TEMPERATURE DEPRESSION.
EFFECTIVENESS IS SHOWN FROM 0.2 TO 1.0 IN STEPS OF 0.1.
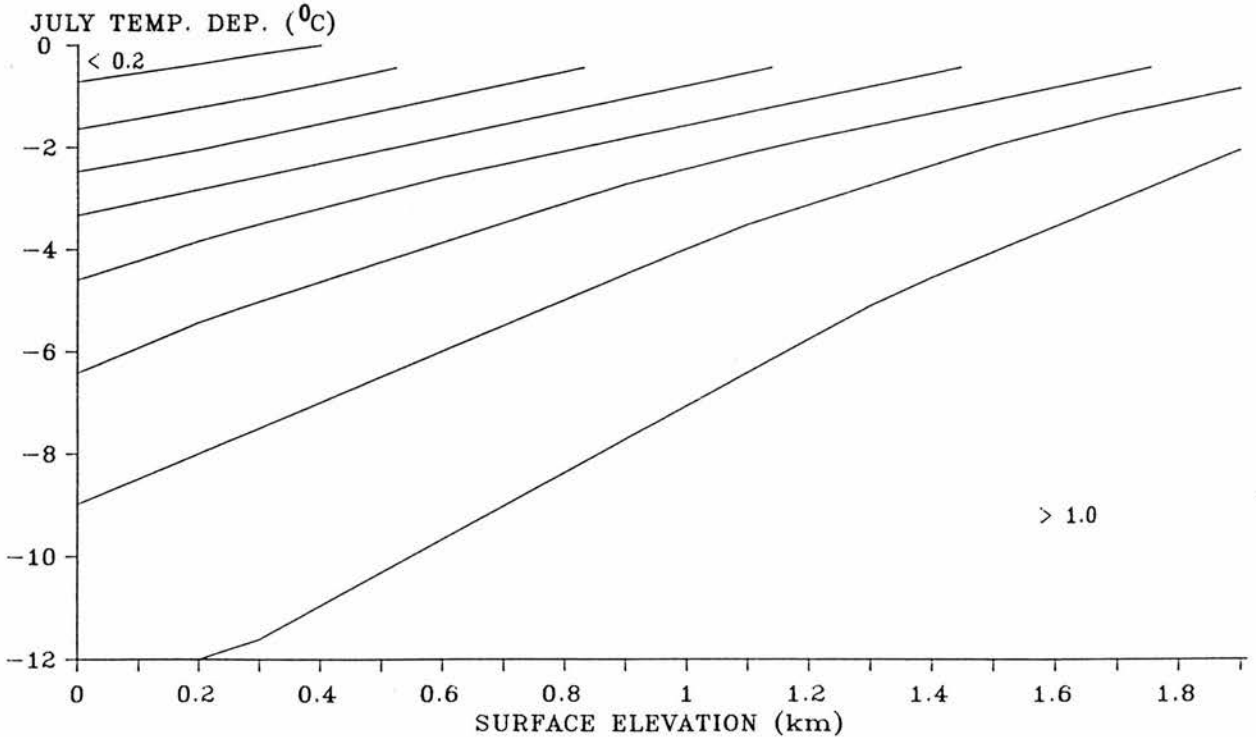
FIGURE 5.36 NET MASS BALANCE SHOWN AS A FUNCTION OF SURFACE ELEVATION,
TEMPERATURE DEPRESSION AND LATITUDE.
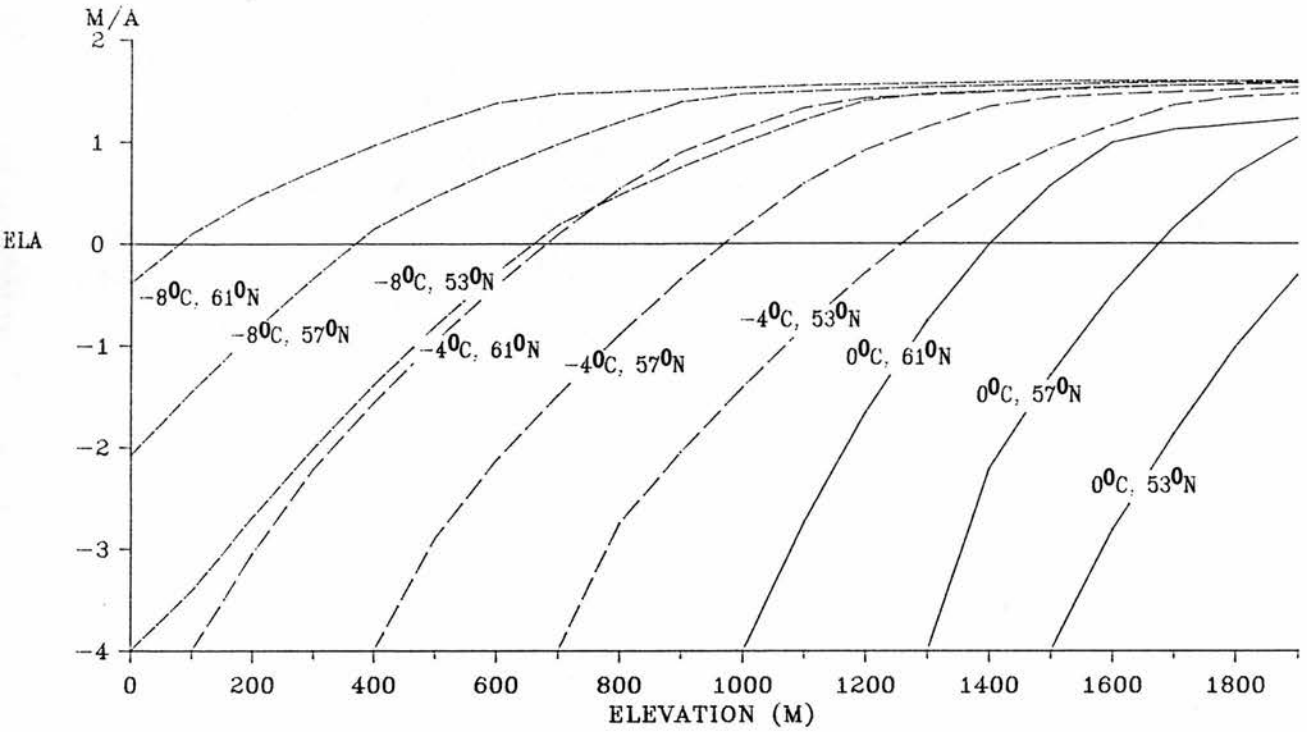
FIGURE 5.37 NET MASS BALANCE SHOWN AS A FUNCTION OF SURFACE ELEVATION,
TEMPERATURE DEPRESSION AND PRECIPITATION RATE.
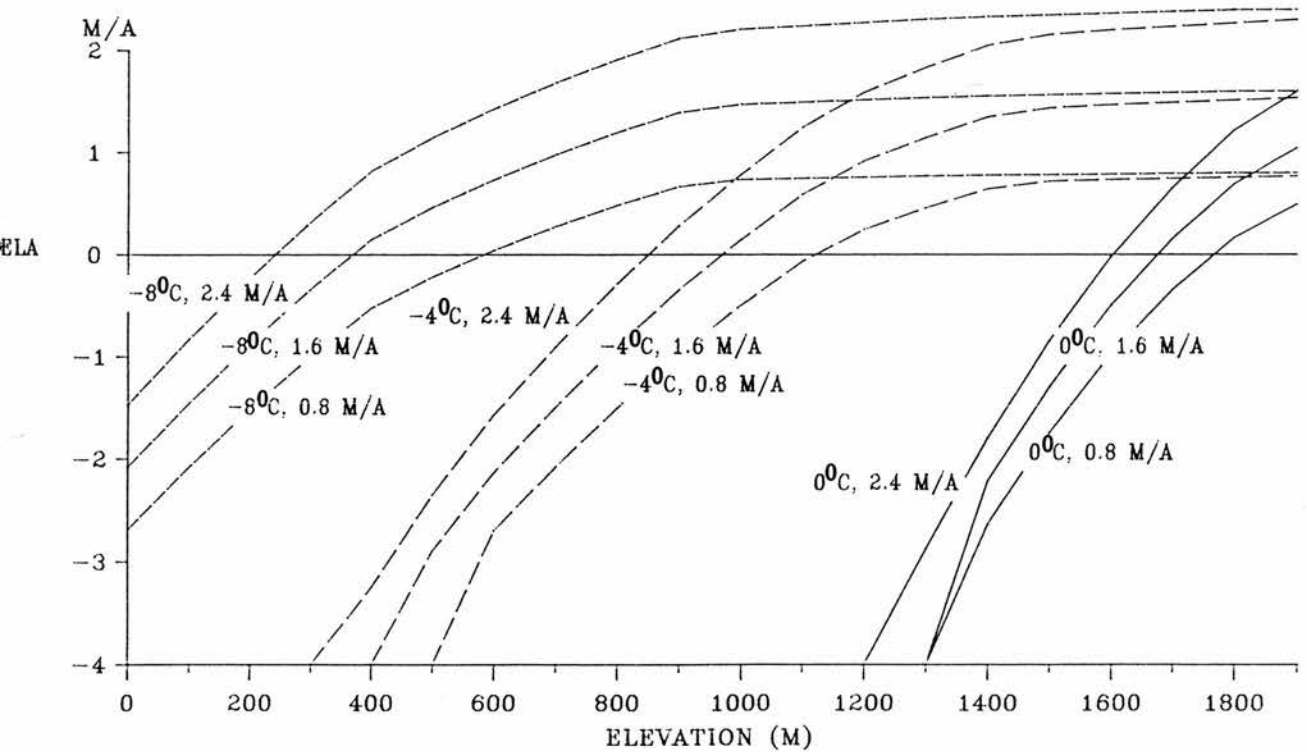
FIGURE 5.38 THE EXTENT OF AREAS WITH POSITIVE A NET MASS BALANCE FOR VARYING TEMPERATURE DEPRESSIONS. RESULTS ARE SHOWN TEMPERATURE DEPRESSIONS OF −4.0, −6.0 AND −8.0°C. IN ALL CASES THE MAXIMUM BEDROCK TOPOGRAPHY WAS USED.
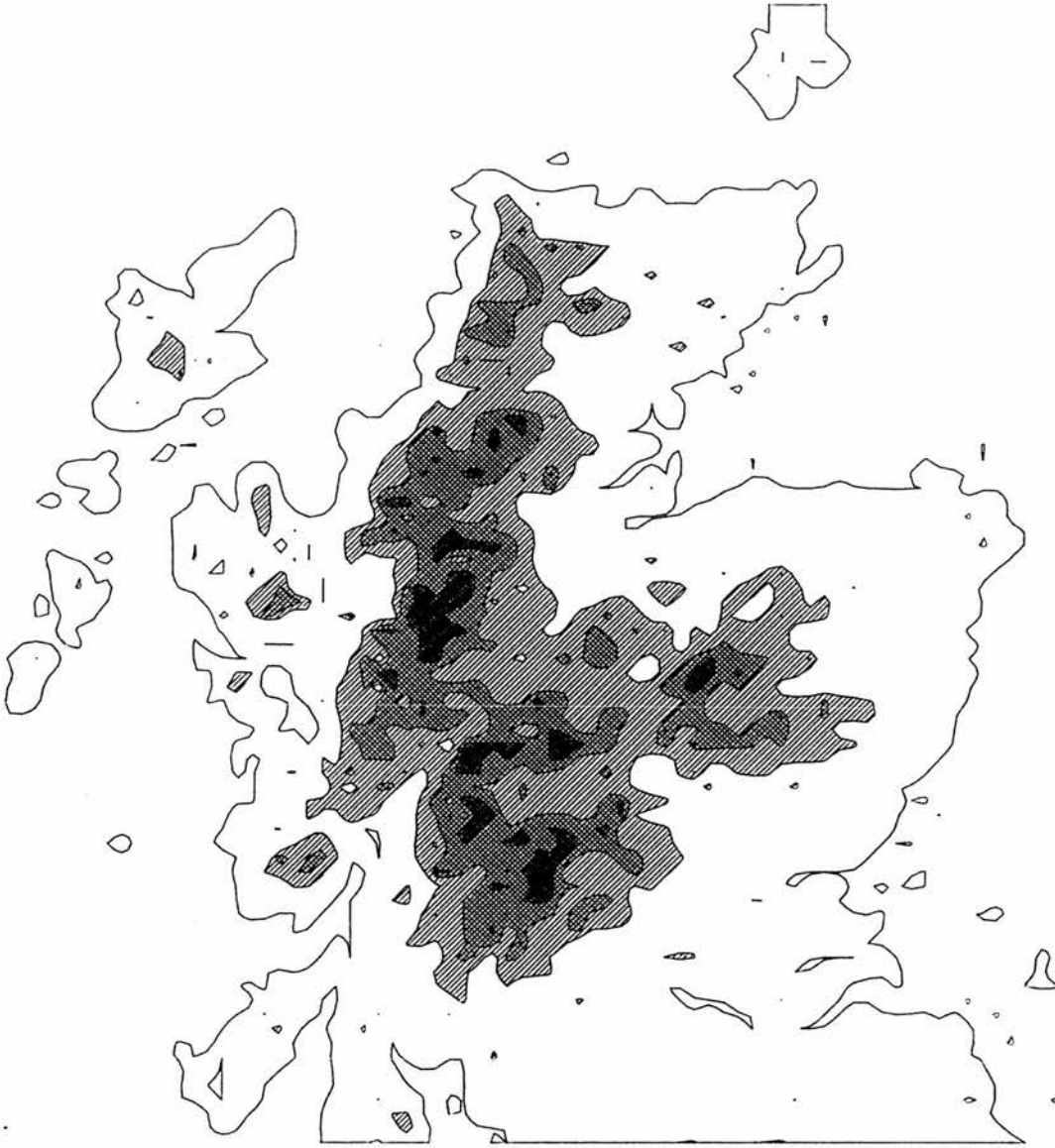
AREA HAS A POSITIVE NET MASS BALANCE
WHEN TEMPERATURE DEPRESSION IS:

■ IN EXCESS OF 4.0 DEGREES C

▨ IN EXCESS OF 6.0 DEGREES C

▨ IN EXCESS OF 8.0 DEGREES C

FIGURE 5.39 A COMPARISON OF THE OUTPUT PRODUCED BY MODELS USING A WESTERLY
WIND DIRECTION. ICE SHEET VOLUME AND MEAN PRECIPITATION RATE
ARE SHOWN FOR THE STANDARD CONSTANT–PRECIPITATION MODEL OF
CHAPTER 4, AND FOR THE COUPLED MODEL USING THE OLD AND THE NEW
METHODS OF DETERMINING ABLATION AND EFFECTIVENESS.
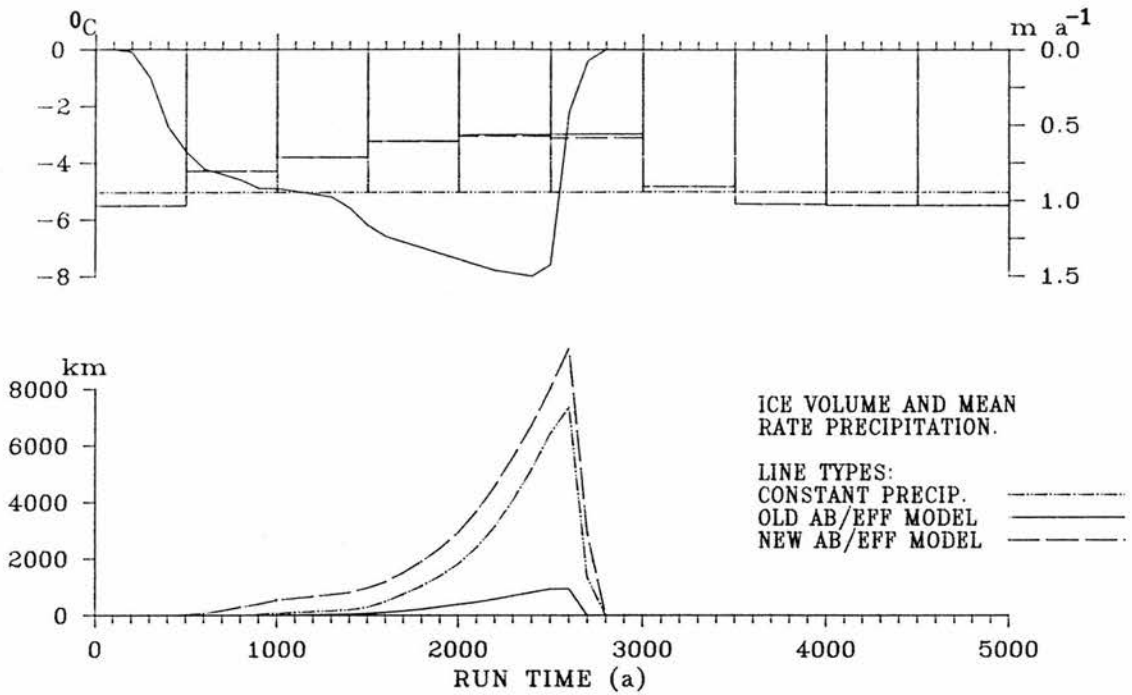
FIGURE 5.40 A COMPARISON OF THE OUTPUT PRODUCED BY MODELS USING A SOUTH–
WESTERLY WIND DIRECTION. ICE SHEET VOLUME AND MEAN PRECIPITATION
RATE ARE SHOWN FOR THE STANDARD CONSTANT–PRECIPITATION MODEL
OF CHAPTER 4, AND FOR THE COUPLED MODEL USING THE OLD AND THE
NEW METHODS OF DETERMINING ABLATION AND EFFECTIVENESS.
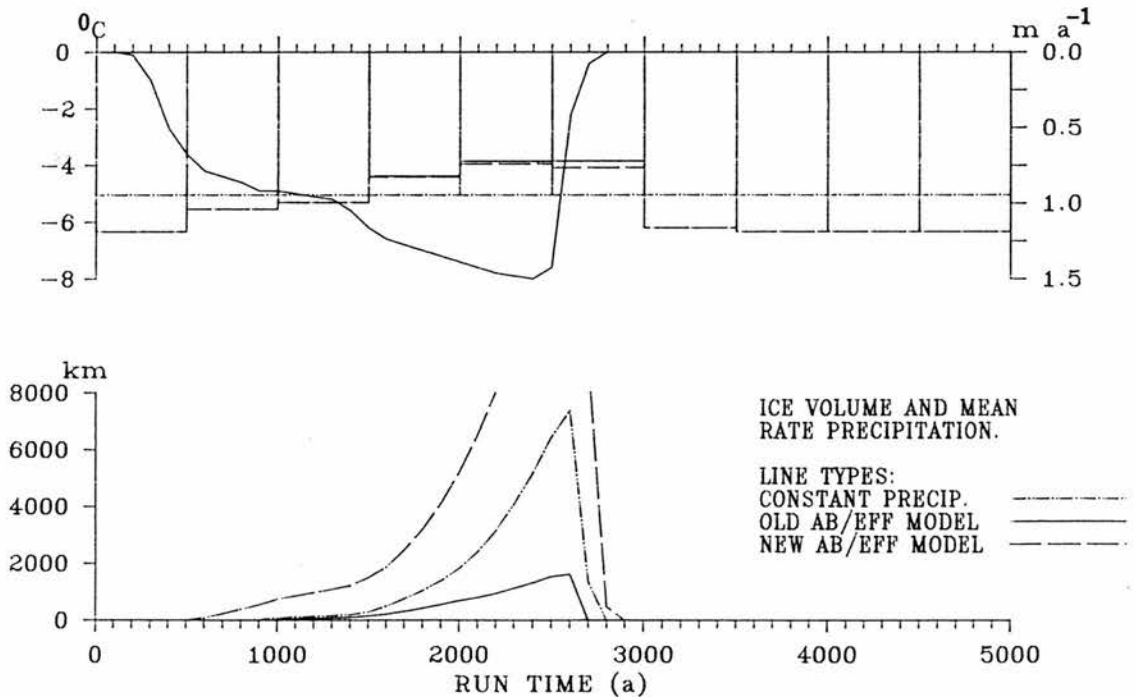
PART THREE : IMPLICATIONS AND CONCLUSIONS.

CHAPTER SIX : IMPLICATIONS AND CONCLUSIONS.

(6.1) SUMMARY OF THE RESEARCH.

(6.1.1) A DESCRIPTION OF THE MODEL.

The research reported in this thesis is concerned with the construction of a general ice sheet model and its application in two case studies. The case studies are the Antarctic Peninsula ice sheet during the last 40.0 ka BP and the Scottish ice sheet of the Loch Lomond stadial centred around 10.0 ka BP. In these case studies the ice sheet model is alternatively coupled to a model of the isostatic response of bedrock and to a model of atmospheric moisture and precipitation.

The Loch Lomond stadial case study investigates the growth and decay of a small land-based ice sheet. The high spatial resolution of this case study means that the results obtained can be used to investigate the mechanisms operating during the initiation of continental-scale ice sheets. The focus of this research is the response of the ice sheet to atmospheric changes, in particular to changes in air temperature and precipitation.

The Antarctic Peninsula case study is concerned with the growth and decay of a large marine-based ice sheet. It contrasts with the Loch Lomond stadial case study

because it deals with a far larger ice sheet which reaches a maximum volume that is approximately 100 times the volume of the Loch Lomond's maximum. Another contrast between the two ice sheets is that the Antarctic Peninsula ice sheet responded to oceanic change. In particular, it responded to changes in sea level and sea water temperature, the latter affecting the rate at which ice melts from the underside of floating ice shelves.

The ice sheet model itself has two important characteristics. First, it is time dependent and can be used to trace the response of an ice sheet to atmospheric and oceanic changes through time. This feature is important because it allows estimates of growth and decay rates to be made; it also allows the likelihood of an ice sheet reaching a long-term equilibrium to be assessed. Second, it is spatial and can be used to study the changing spatial locations of features such as ice divides, domes, streams and margins. This is important because the majority of glacial geomorphological evidence reflects the position of these features and it is important to understand whether this evidence relates to permanent or transient locations. The twin characteristics of time dependence and spatial perspective lead to a distinctively geographical mode of enquiry, which is in contrast to the steady state and flowline assumptions normally used in the modelling of

372

former ice sheets.

*The model has two further advantages. First, it relies
wholly on assumptions about the processes occurring in an
ice sheet system. This concentration on the modelling of
process means that independent field data can be used to
test the model. This field data concerns the glacial
geomorphology of the case study areas and can give
estimates of former ice sheet extent, thickness, flow
direction and isostatic uplift. The majority of this
evidence relates to glacial maxima, but estimates of the
ice sheet's life span and its changing dynamics can also
be made. Comparison of the model's predictions with field
estimates allows the identification of the strengths and
weaknesses of the model. A mismatch between prediction
and field estimate indicates areas of the model that need
to be re-cast. Also, the predictions can be used as a
basis to plan future field work. This is particularly
important in areas, such as the Antarctic Peninsula,
where field evidence is scarce.*

*A second important component of the research is the
identification of the key variables influencing the
behaviour of the model. If the model survives tests
against field estimates then ice sheet dynamics can be
investigated using the twin techniques of experimentation
and sensitivity analysis. Areas of the model that are*

identified as being particularly sensitive may either reflect a true real world importance of a set of processes or may be artifacts of the model used. The selection between these two alternatives can be made by further, more detailed modelling of the sensitive areas. This type of analysis is pursued in the Loch Lomond stadial case study where ablation and snow accumulation were investigated in depth.

(6.1.2) PREDICTIONS OF ICE SHEET BEHAVIOUR.

The Antarctic Peninsula case study focused on the effects of the growth and decay of a large offshore ice dome. Although, the time series of sea level and marine basal melt used to drive this model are continuous and vary only gradually, the output for ice sheet volume varies dramatically. Long periods of steady state are separated by brief transition periods. This implies that the ice sheet system contains mechanisms that can buffer the ice sheet against changes in forcing until a threshold is crossed. Once a threshold has been crossed the ice sheet responds rapidly until another threshold is reached. The interaction of sea level, calving, ice flow and marine bathymetry introduces thresholds in ice sheet behaviour and implies that ice sheet response often lags changes in the driving variables.

The growth and decay of the Bellinghausen Sea ice dome has major implications for the ice flow regime in the rest of the ice sheet. In particular, ice flow directions and magnitudes over Alexander Island vary dramatically through time. At the glacial maximum ice from Palmer Land flows directly West over the southern part of the Island, while ice flow subsequent to the decay of the ice dome is southerly and radiates from an independent Alexander Island ice dome. In contrast North Alexander Island experiences persistent ice stream flow northwards along George VI Sound throughout the whole of the glacial cycle. This contrast illustrates the degree of spatial and temporal disparity that can occur within a single ice mass.

This disparity is also a feature of the rates of ice sheet retreat consequent on sea level rise and marine basal melt increase. These rates vary from a rapid continuous retreat in the Bellinghausen Sea area to a slow erratic decay pattern to the West of Alexander Island. This contrast is explained by the contrasting nature of the bathymetry in the two areas. The Bellinghausen Sea forms a deep continuous trough which has no potentially stabilizing bedrock rises. While the area to the West of Alexander Island forms a shallow shelf which experiences isostatic uplift in response to ice sheet decay. This uplift slows further retreat in the

area.

*The behaviour of the Loch Lomond ice sheet is even
more dynamic. An exponential phase of ice sheet growth is
caused by the gradual decrease of air temperature and the
effects of feedback within the ice sheet model. The
latter causes ice thickness change to be amplified as a
result of the coupling of surface elevation to net mass
balance and ice thickness. A steep rise of air
temperature after 10.0 ka BP causes rapid ice sheet decay
via down-wasting over virtually all of the surface of the
ice sheet. The brief phase of ice sheet maximum does not,
therefore, represent a period of steady state but is
merely a turn-around between phases of ice sheet growth
and decay.*

*The above discussion on the behaviour of the Loch
Lomond ice sheet concentrates on ice sheet volume output.
The comparison of this volume output with the changing
distributions of ice sheet thickness and extent raises
two further important points. First, a contrast can be
drawn between ice volume increase that arises through the
accumulation of snow on upland surfaces and the
accumulation of snow on ice surfaces occupying bedrock
basins below the Equilibrium Line Altitude. The former
accounts for ice volume increase on mountain tops during
the initial phases of glaciation, where the radial*

376

outflow of ice means that substantial thicknesses of ice do not develop. The latter situation relies on ice flow from adjacent highlands, which increases surface elevations and initiates local snow accumulation, and accounts for most ice volume growth.

The second feature revealed by a comparison of ice volume and extent output are the contrasting dynamics of different areas of the ice sheet during growth. Air temperature depression remains relatively constant for several hundred years around 10.0 ka BP. During this period ice sheet extent remains stationary, while the total ice volume increases by 16 %. Thickness increases in the ice sheet interior do not lead to an expansion of the ice sheet's extent. This implies that the margins and the interior of the ice sheet are partially de-coupled and respond to the constant air temperature depression differently. This behaviour is most noticeable in the vicinity of the mountainous rim of the Rannoch Moor, which restricts ice flow from the interior.

Both of these mechanisms lead to a mismatch between changes in volume and changes in extent, which implies that reconstructions based on steady state assumptions, or on the assumption of a fixed relationship between extent and volume, may be invalid.

(6.2) IMPLICATIONS.

(6.2.1) IMPLICATIONS OF MODEL TESTING.

When applied to a case study the general ice sheet model can be used to make specific predictions about ice sheet form and behaviour. These predictions can then be tested using field estimates from the case study areas, if they are available.

The testing of the Antarctic Peninsula model was limited to four specific predictions because field data from the area is sparse. The tests used in the case study are: the changing patterns of ice flow over Alexander Island; the timing of ice dome decay; the isostatic uplift consequent to this decay; and the morphology of the present day ice sheet. Two main mismatches between model predictions and field estimates were identified. These mismatches illustrate alternative uses of the testing procedure in ice sheet modelling.

The first mismatch concerns the predicted changes in ice flow direction and intensity over Alexander Island during the decay of the Bellinghausen Sea ice dome. The majority of the field evidence in the area has been interpreted as representing glacial maximum conditions at 18.0 ka BP. This evidence supports the existence of former Bellinghausen Sea ice dome. Evidence relating to relative sea level changes also implies the existence of

this ice dome. However little data exists that can be used to test the model's predictions of the consequences of the decay of this ice dome. The model is useful in pointing to locations suitable for the testing of these predictions. In particular it is possible to produce a series of scenarios for specific nunataks at specific locations. Field data collection at these sites can thus be more focused because it aims to test the predictions of the model.

The second mismatch concerns the over-prediction of the present day ice cover in George VI Sound. Two explanations are advanced to account for this mismatch. The first is that isostasy is under-estimated in the model and that this leads to an under-estimate of marine decay. The second explanation is that the spatial resolution of the model is insufficient to capture the calving and grounding line dynamics of the area. Results from a sensitivity analysis favour the second hypothesis. The original mismatch between field evidence and model prediction is therefore useful in the identification of limitations within the model.

The testing of the Loch Lomond ice sheet model was restricted to predictions of maximum ice sheet extent, ice thickness, ice sheet life span and the nature of decay. In general the predictions of extent and thickness

379

agree with field estimates, although the extent of ice in the North-West Highlands is somewhat over-predicted. However, the non-equilibrium nature of the predicted ice sheet maximum and the contrasts between ice sheet volume growth and areal expansion have serious implications for the use of Loch Lomond glaciers as palaeo-climate indicators. This is because reconstructions often assume both a steady state and a fixed relationship between accumulation area and ablation area. Future work in the area may therefore need to assess these implications.

A major difficulty in the testing of the model is the lack of adequate field data relating to times other than the glacial maximum. This means that the model's predictions can only be tested for one specific time. In the case of the Loch Lomond stadial testing relies on the maximum ice sheet extent and thickness, while, in the Antarctic Peninsula case study the testing is only for flow directions during the glacial maximum. The degree to which the model can be constrained is therefore limited. For example, the predicted dynamics of the Loch Lomond ice sheet's growth cannot be tested using the presently available field data. Thus it could not, for instance, be favoured over a model predicting a long-term equilibrium ice sheet. It is therefore important that future field data collection should attempt to collect estimates of ice sheet form and behaviour at a variety of

times, because this allows model testing to become more critical. The collection of data relating to a variety of ice sheet properties would also be helpful because this also increases the number of independent tests that can be made.

(6.2.2) IMPLICATIONS FROM MODEL EXPERIMENTS.

The model can be used to isolate the important factors influencing ice sheet behaviour. This is done by repeating the standard model run using a variety of alternative parameter values and model inputs. If these alternative runs show dramatic differences compared to the standard run then the particular section of the model being analysed is important in determining overall model behaviour. Whether this reflects a corresponding real world importance can be determined by modelling the sensitive section of the model in greater detail.

Sensitivity analysis of the Antarctic Peninsula model reveals that surface accumulation and basal melting are particularly important in determining overall model behaviour. The former is important because there is a distinct threshold accumulation rate below which marine ice domes do not develop. Similarly basal melting determines whether or not such an ice dome decays from its maximum extent.

Several other areas of the model are found to influence the detailed growth and decay of the ice sheet. These include the spatial distribution of topography within the case study area, the rate of the bedrock's isostatic response and the parameterization of ice flow within the model. In addition, it was found that both of driving variables (sea level and basal melting) are important in determining the rate of ice sheet growth and decay.

Loch Lomond ice sheet experiments using a constant air temperature depression indicate that the range of altitude within an area determines whether a particular air temperature depression results in a local steady state ice mass or a large expanding ice mass. The geographical distribution of topography is also important in determining the transition between these two modes of behaviour. In particular, contrasts between 'ridge' and 'basin' topographies are important. Ice masses developed on ridges have a relatively uniform response to air temperature changes because increased ice accumulation is balanced by increased down-glacier ice flow and increased ablation at lower altitudes. In contrast, ice masses developed over basin topography are not buffered by ice flow to the same extent. This is because the basin has a limited capacity to ablate incoming ice, if this limit is exceeded, the convergence of incoming glaciers leads to

increased surface elevation which, if it exceeds the local Equilibrium Line Altitude, initiates local ice accumulation.

The Loch Lomond stadial model was found to extremely sensitive to the variation of accumulation and ablation rates. However, the variation of modelled ice flow had very little effect on the ice sheet's overall behaviour. For this reason a more detailed model of the Loch Lomond stadial's climate was developed. This alternative model had two components. First, it used a model based on the continuity equation for atmospheric moisture to investigate the effects of local air temperature changes and North Atlantic polar front migration on Scottish precipitation during the Loch Lomond stadial. Second, it incorporated an alternative method of specifying ablation and effectiveness. The aim was to investigate whether more detailed modelling altered the behaviour of the ice sheet model significantly.

Results from this new model indicate that the incorporation of precipitation and ablation into the model is crucial in determining ice sheet growth and decay. The original Loch Lomond stadial case study used a constant precipitation distribution and its predictions agree with field evidence. However, when the ice sheet model is coupled to the atmospheric moisture model,

reduced precipitation leads to a significant under-prediction of ice sheet size. Several explanations for this mismatch are investigated. Explanations involving the inaccuracy of the atmospheric moisture model and the inheritance of pre-existing ice are rejected. A third explanation involves the accuracy of the ablation and effectiveness estimates in the model.

A new ablation/effectiveness model is developed, the predictions of which agree with field interpretations. This implies that the Loch Lomond model is so sensitive to the climatic assumptions used that an alteration of the representation of climate can significantly alter the predictions of the model. This sensitivity is likely to reflect the real world importance of climate because this behaviour persists through several different versions of the model. The dynamics associated with models that produce realistic ice sheet volumes are similar. In addition, the nature of ice sheet growth and retreat in these runs is the same. This increases confidence in the predictions of the original model outlined above.

The coupled atmospheric moisture - ice sheet model is also used to investigate the effects of alternative wind directions on ice sheet growth during the Loch Lomond stadial. Two alternative wind directions are modelled. First, a westerly airflow is used, which is equivalent to

*present day conditions. Second, a south-westerly wind
direction is used, which Sissons (1979b) postulates as
the predominate airflow during the Loch Lomond stadial.
Results from the model favour the use of a south-westerly
airflow because this leads to a geographical ice extent
which is in closer agreement with field estimates. In
particular, the south-westerly airflow model predicts
relatively more ice around Rannoch Moor and relatively
less ice over the North-West Highlands. This result can
be interpreted as either a change in the predominate wind
direction or a change in the direction of the snow-
bearing winds during Loch Lomond times. The model uses
annual mean quantities and cannot, therefore, separate
predominate and snow-bearing winds. This implies that the
temporal resolution of the model is insufficient and that
the disaggregation of annual and seasonal weather
patterns may be important in the modelling of the Loch
Lomond stadial's climate.*

(6.3) CONCLUSIONS.

*The two case studies represent alternative stages of
ice sheet evolution. The Loch Lomond stadial case study
represents the initial phases of ice sheet growth and can
be used to investigate the type of dynamics associated
with ice sheet initiation. The Antarctic Peninsula case
study represents a broader study of continental ice sheet
growth and decay.*

The results from the two case studies have both similarities and contrasts. There is a contrast in the nature of their growth and decay. The Loch Lomond stadial ice sheet grows rapidly in an unconstrained fashion. Growth is related to the interaction of climate and topography. Two types of behaviour are possible. First, small highland ice masses develop in response to small air temperature depressions and can reach equilibrium because ice accumulated at higher altitudes can be lost at lower altitudes via ablation. A second type of behaviour is associated with larger air temperature depressions when ablation cannot cope with ice flow from high altitude areas. Ice sheet growth is unconstrained until other larger scale processes become important such as the latitudinal variation of net mass balance and marine loss. The former occurs when the ice sheet is large enough to carry ice over large distances and balance ice accumulation in the North by ice ablation in the South.

The marine loss mechanism can constrain ice sheet behaviour over smaller distances and is investigated in the Antarctic Peninsula case study. The Antarctic Peninsula case study contrasts with the Loch Lomond stadial case study because the ice sheet is both larger and longer lived, and involves interaction with the ocean. Ice sheet behaviour is constrained by marine ice

*losses and several steady state forms develop. This
contrasts with the non-equilibrium behaviour of the Loch
Lomond ice sheet. Although the interaction of the ice
sheet and the ocean can lead to a time independent ice
sheet equilibrium,changes of sea level and marine basal
melting lead to ice sheet response that is often both
rapid and complex.*

*Despite these contrasts, the two case study ice sheets
display two major similarities. These are associated with
the importance of topography and climate in determining
ice sheet behaviour. In the case of the Loch Lomond
stadial, ice sheet behaviour is determined by the the
topography of Scotland. Both the range of altitude within
the area and geographical distribution of topography
determine the nature of ice sheet growth.*

*The Antarctic Peninsula ice sheet is also heavily
influenced by the distribution of topography. Both ice
sheet growth and decay are interrupted by thresholds
partially controlled by the bathymetry of the area. For
instance, the spatial distribution of ice sheet growth
has a longitudinal asymmetry. This asymmetry is explained
by the different types of topography to the West and to
the East of the ice sheet seeding area. The influence of
topography on ice sheet decay has already been discussed.
An important conclusion from this section is that the*

spatial resolution of the study (25 km) may not be sufficient to capture the calving and grounding line dynamics of George VI Sound, where an oceanic trough is immediately adjacent to mountainous massifs.

The second similarity between the two case studies is associated with climate. Climate is the major influence on the form and behaviour of the Loch Lomond ice sheet. Its role in the Antarctic Peninsula case study is less dominant. However changes in net mass balance are critical in determining whether the initially land-based ice sheet can expand offshore and form a marine-based ice dome.

LIST OF REFERENCES.

Andrews J. T. and Mahaffy M. A. W. (1976)
Growth rate of the Laurentide ice sheet and sea level
lowering. Quaternary Research 6, 167-83.

Atkinson B. W. and Smithson P.A. (1972)
An investigation into meso-scale precipitation
distributions in a warm sector depression. Quaterly
Journal of the Meteorological Society 98, 353-48.

Atkinson B. W. and Smithson P.A. (1974)
Meso-scale circulations and rainfall patterns in an
occluding depression. Quaterly Journal of the
Meteorological Society 100, 3-22.

Atkinson T. C., Biffa K. R., Coope G. R., Joachim M. J.
and Perry D. W. (1985)
Climatic calibration of Coleoptern data. in Berglund B.
E. (ed) Handbook of Holocene Palaeoecology and
Palaeohydrology. John Wiley and Son, London, 851-8.

Barry R. G. (1981)
Mountain Weather and Climate. Methuen and Company
Limited, London.

Barry R. G. and Chorley R. J. (1982)
Atmosphere, Weather and Climate. Fourth edition. Methuen
and Company Limited, London.

Bentley C. R. (1983)
The West Antarctic ice sheet: diagnosis and prognosis. in
Proceedings of the carbon dioxide research Conference:
carbon dioxide, science and concensus (Berkeley Springs,
West Virginia, September 19-23 1982). IV, 3-50.

Bentley C. R. and Jezek K. C. (1981)
RIS, RISP and RIGGS: post-IGY glaciological
investigations of the Ross ice shelf in the US programme.
Journal of the Royal Society of New Zealand 11, 355-72.

Berger A. L. (1978)
Long-term variations of caloric insolation resulting from
the Earth's orbital elements. Quaternary Research 9, 139-
67.

Birchfield G. E., Weertman J. and Lunde A. T. (1981)
A paleoclimate model of Northern hemisphere ice sheets.
Quaternary Research 15, 126-42.

Birks H. H. and Mathewes R. W. (1978)
Studies in the vegetational history of Scotland V. Late Devensian and early Flandrian pollen and macrofossil stratigraphy at Abernethy forest, Inverness-shire. New Phytology 80, 455-84.

Bishop J. F. and Walton J. L. W. (1981)
Bottom melting under George VI ice shelf Antarctica. Journal of Glaciology 27, 429-47.

Bloom A. L., Broecker W. S. and Chappell J. M. A., Matthews R. K. and Messolella K. J. (1974)
Quaternary sea level fluctuations on a tectonic coast: new $^{230}TH/^{234}U$ dates from the Huon Peninsula, New Guinea. Quaternary Research 14, 185-205.

Boulton G. S. and Jones A. S. (1979)
Stability of temperate ice caps and ice sheets on beds of deformable sediment. Journal of Glaciology 24, 29-43.

Boyle E. A. and Keigwin L. D. (1987)
North Atlantic circulation during the last 20,000 years linked to high-latitude surface temperature. Nature 330, 35-40.

Braithwaite R. J. (1981)
On glacier energy balance, ablation and air temperature. Journal of Glaciology 27, 381-91.

Braithwaite R. J. (1984)
Calculation of degree-days for glacier-climate research. Zeitschrift fur Gletscherkunde und Glazialgeologie 20, 1-8.

Braithwaite R. J. and Olesen O. B. (1984)
Ice ablation in West Greenland in relation to air temperature and global radiation. Zeitschrift fur gletscherkunde und glazialgeologie 20, 155-68.

Braithwaite R. J. and Thomsen H. H. (1984)
Runoff conditions at Kuussuup Tasia, Christianshab, estimated by modelling. Gronlands Geologiske Undersogelse, Gletscher-hydrologiske meddeleelser Nr. 84/2.

Broecker W. S., Andree M., Wolfli W., Oeschger H., Bonani G., Kennett J. and Peteet D. (1988)
The chronology of the last deglaciation: implications to the cause of the Younger Dryas event. Paleoceanography 3, 1-19.

Brotchie J. F. and Silvester R. (1969)
On crustal flexure. Journal of Geophysical Research 74, 5240-52.

Brown C. S., Meier M. F. and Post A. (1982)
Calving speed of Alaska tidewater glaciers, with application to Columbia glacier. Geological Survey Professional Paper 1258-C.

Buckland P. C. and Coope G. R. (1985)
A bibliography and literature review of Quaternary entomology. Department of Geography, University of Birmingham. Working Paper Series Number 20.

Budd W. F. (1966)
The dynamics of the Amery ice shelf. Journal of Glaciology 6, 335-58.

Budd W. F. (1970a)
The longditudinal stress and strain-rate gradients in ice masses. Journal of Glaciology 9, 19-28.

Budd W. F. (1970b)
Ice flow over bedrock perturbations. Journal of Glaciology 9, 29-48.

Budd W. F. (1981)
The importance of ice sheets in long term changes of climate and sea level. in Sea level, ice and climatic change (Proceedings of the Canberra symposium) I.A.S.H. Publication Number 131, 141-7.

Budd W. F. and Allison I. F. (1975)
An empirical scheme for estimating the dynamics of unmeasured glaciers. in Snow and Ice (Proceedings of the Moscow symposium) I.A.S.H. Publication Number 104, 246-56.

Budd W. F. and Jenssen D. (1975)
Numerical modelling of glacier systems. in Snow and Ice (Proceedings of the Moscow symposium) I.A.S.H. Publication Number 104, 257-91.

Budd W. F. and Smith I. N. (1981)
The growth and retreat of ice sheets in response to orbital radiation changes. in Sea level, ice and climatic change (Proceedings of the Canberra symposium) I.A.S.H. Publication Number 131, 369-409.

Budd W. F. and Smith I. N. (1982)
Large scale numerical modelling of the Antarctic ice sheet. Annals of Glaciology 3, 42-9.

Budd W. F. and Smith I. N. (1985)
The state of balance of the Antarctic ice sheet: an updated assessment 1984. in *Glaciers, ice sheets and sea level: effect of a CO2-induced climatic change. Report of a workshop held in Seattle, Washington September 13-15 1984.* 172-7.

Budd W. F., Jenssen D. and Radok U. (1971)
Derived physical characteristics of the Antarctic ice sheet. *University of Melbourne, Meteorlogical Department, Publication Number 18.*

Budd W. F., Keage P. L. and Blundy N. A. (1979)
Empirical studies of ice sliding. *Journal of Glaciology 23,* 157-70.

Budd W. F., Jenssen D. and Smith I. N. (1984)
A three dimensional time-dependent model of the West Antarctic ice sheet. *Annals of Glaciology 5,* 29-36.

Budd W. F., Jenssen D. and McInnes B. J. (1985)
Numerical modelling of ice stream flow with sliding. in Jacka T. H. (ed) *Australian Glaciological Research 1982-83, A.N.A.R.E. Notes,* Antarctic Division, Hobart, 130-137.

Chandler T. S. and Gregory S. (1976)
The climate of the British Isles. Longman Group Limited, New York.

Clapperton C. M. and Sugden D. E. (1982)
Late Quaternary glacial history of George VI Sound area, West Antarctica. *Quaternary Research 18,* 243-67.

Clapperton C. M. and Sugden D. E. (1983)
Geomorphology of the Ablation Point Massif, Alexander Island, Antarctica. *Boreas 12,* 125-35.

CLIMAP Project Members (1981)
Seasonal reconstruction of the earth's surface at the last glacial maximum. *Geological Society of America Map and Chart series, MC-36.*

Cooke D. W. and Hays J. D. (1978)
Estimates of Antarctic Ocean seasonal sea ice cover during glacial intervals. in *Proceedings of the Third symposium on Antarctic geology and Geophysics, Madison, August 1977,* 112-48.

Coope G. R. (1975)
Climatic fluctuations in Northwest Europe since the last interglacial, indicated by fossil assemblages of Coleoptera. in Wright A. E. and Moseley F. (eds) Ice Ages: Ancient and Modern. Seel House Press, Liverpool, 153-68.

Coope G. R. (1977)
Fossil Coleoptera assemblages as sensitive indicators of climatic changes during the Devensian (last) cold stage. Philosophical Transactions of the Royal Society of London, Series B 280, 313-40.

Coope G. R. (1979)
Late Cenozoic fossil Coleoptera: evolution, biogeography and ecology. Annual Review of Ecology and Systematics 10, 247-67.

Coope G. R., Morgan A. and Osborne P. J. (1971)
Fossil Coleoptera as indicators of climatic fluctuations during the last glaciation in Britain. Palaeogeography, Palaeoclimatology, Palaeoecology 10, 87-101.

Corps of Engineers (1956)
Snow Hydrology. North Pacific Division, Corps of Engineers, United States Army, Oregon.

Doake C. S. M. (1985)
Antarctic mass balance: glaciological evidence from Antarctic Peninsula and Weddell Sea sectors. in Glaciers, icesheets and sea level: effect of a CO_2-induced climatic change. Report of a workshop held in Seattle, Washington September 13-15 1984, 197-209.

Duplessy J. -C. (1978)
Isotope studies. in Gribbin J. (ed) Climatic Change. Cambridge University Press, 46-67.

Emiliani C. (1955)
Pliestocene temperatures. Journal of Geology 63, 538-78.

Fastook J. L. (1985)
Ice shelves and ice streams: three modelling experiments. in Glaciers, icesheets and sea level: effect of a CO2-induced climatic change. Report of a workshop held in Seattle, Washington September 13-15 1984, 279-300.

Fastook J. L. and Schmidt W. (1982)
Finite-element analysis of calving from ice fronts. Annals of Glaciology 3, 103-6.

Glen J.W. (1955)
The creep of polycrystalline ice. Proceedings of the Royal Society of London, Series A 228, 519-38.

Gray J. M. and Brooks C. L. (1972)
The Loch Lomond Readvance moraines of Mull and Menteith.
Scottish Journal of Geology 8, 95-103.

Green F. H. W. and Harding R. J. (1980)
Altitudinal gradients of soil temperatures in Europe.
Transactions of the Institute of British Geographers 5,
243-54.

Haurwitz B. (1941)
Dynamic Meteorology. McGraw-Hill Book Company, New York.

Hays J. D. (1978)
A review of the late Quaternary climatic history of
Antarctic seas. in van Zinderen Bakker E. M. (ed)
Antarctic glacial history and world palaeoenvironments.
A. A. Balkema, Rotterdam, the Netherlands, 57-72.

Hughes T. J. (1984)
Review of 'Theoretical Glaciology: material science of
ice and the mechanics of glaciers and ice sheets. by
Hutter K.'. *Journal of Glaciology 30*, 254-5.

Hughes T. J. (1987)
Deluge II and the continent of doom: rising sea level and
collapsing Antarctic ice sheet. *Boreas 16*, 89-100.

Hutter K. (1981)
The effect of longditudinal strain on the shear stress of
an ice-sheet. In defence of using stetched coordinates.
Journal of Glaciology 27, 39-56.

Imbrie J and Imbrie J. Z. (1980)
Modeling of the climatic response to orbital variations.
Nature 207, 943-53.

Jenssen D. (1977)
A three dimensional polar ice-sheet model. *Journal of
Glaciology 18*, 373-89.

Johannsen T. W. (1970)
The climate of Scandinavia. in Wallen C. C. (ed) *World
Survey of Climatology Volume 5: Climates of northern and
western Europe.* Elsevier Publication Company, Amsterdam,
the Netherlands, 23-81.

Keen R. A. (1984)
Statistical-dynamical model of accumulation on the
Greenland ice sheet. *Annals of Glaciology 5*, 69-74.

Kellaway G. P. (1949)
Map Projections. Second Edition. Methuen, London.

Kellogg T. B. (1975)
Late Quaternary climatic changes in the Norwegian and Greenland Seas. in Weller G. and Bowling S. A. (eds) Climate of the Arctic, 24th Alaska Science Conference, 215-33.

Kellogg W. W. (1975)
Climatic feedback mechanisms involving the polar regions. in Weller G. and Bowling S. A. (eds) Climate of the Arctic, 24th Alaska Science Conference, 111-6.

Kirkby M.J., Naden P.S., Burt T. P. and Butcher D. P. (1987)
Computer Simulation in Physical Geography. John Wiley and sons Limited, Chicester, U. K.

Kollmeyer R. C. (1980)
West Greenland outlet glaciers: an inventory of the major ice berg producers. in World glacier inventory, Proceedings of the Riederald workshop, September 1978. I.A.S.H. Publication Number 126, 57-64.

Larsen E., Eide F., Longva O. and Mangerud J. (1984)
Allerod-younger Dryas climatic inferences from the cirque glaciers and vegetational developments in the Nordfjord area, western Norway. Alpine and Arctic Research 16, 137-60.

Lauscher F. (1976)
Methoden zur weltklimatologie der hydrometeore. der anteil des festen niederschlags am gesamtniederschlag. Arch. Met. Geophys. Biokl. 24, 129-76.

Lian M. S. and Cess R. D. (1977)
Energy balance climate models: a reappraisal of ice-albedo feedback. Journal of Atmospheric Sciences 34, 1058-78.

Lliboutry L. (1968)
General theory of subglacial cavitation and sliding of temperate glaciers. Journal of Glaciology 7, 21-58.

Lowe J J. and Walker M. J. C. (1976)
Radiocarbon dates and the deglaciation of Rannoch Moor, Scotland. Nature 246, 632-3.

Lowe J J. and Walker M. J. C. (1980)
Problems associated with radiocarbon dating the close of the Lateglacial period in the Rannoch Moor area, Scotland. in Lowe J. J., Gray J. M. and Robinson J. E. (eds) Studies in the Lateglacial of North-West Europe. Pergamon Press, Oxford, 123-67.

Lowe J J. and Walker M. J. C. (1984)
Reconstructing Quaternary Environments. Longman Group
Limited, Harlow, U. K.

MacAyeal D. R. (1984)
Potential effect of a CO_2 warming on sub-ice-shelf
circulation and basal melting. in Environment of West
Antarctica: potential CO2-induced changes. Report of a
workshop held in Madison, Wisconsin 5-7 July 1983.
National Academic Press, Washington D.C., 212-21.

Mahaffy M. A. W. (1976)
A numerical three dimensional ice flow model. Journal of
Geophysical Research 81, 1059-66.

Manabe S. and Broccoli R. D. (1985)
The influence of continental ice on the climate of an ice
age. Journal of Geophysical Research 90, 2167-79.

Manley G. (1970)
The climate of the British Isles. in Wallen C. C. (ed)
World Survey of Climatology Volume 5: Climates of
northern and western Europe. Elsevier Publication
Company, Amsterdam, the Netherlands, 81-135.

McInnes B. J. and Budd W. F. (1984)
A cross-sectional model for West Antarctica. Annals of
Glaciology 5, 95-99.

McIntyre A., Kipp N, Be A. W. H., Crowley T. Gardner J.
V., Prell J. V. and Ruddiman W. F. (1976)
Glacial North Atlantic 18,00 years ago: a CLIMAP
reconstruction. in Cline R. M. and Hays J. D. (eds)
Investigation of late Quaternary paleo-oceanography and
paleo-climatology, Geological Society of America Memoir
145, Geological Survey of America, Boulder, 43-76.

McIntyre N. F. (1985)
The dynamics of ice-sheet outlets. Journal of Glaciology
31, 99-107.

Meier M. F., Tangborn W. V., Mayo L.R. and Post A. (1971)
Combined ice and water balances of Gulkana and Wolverine
glaciers, Alaska, and South Cascade glacier, Washington,
1965 and 1966 Hydrological years. United States
Geological Survey Professional Paper 715-A.

Meteorological Office (1968)
Monthly and annual averages of rainfall for the United
Kingdom of Great Britain and Northern Ireland for the W.
M. O. period 1931-60. Meteorological Office Hydrological
Memoir Number 37, Bracknell, U. K.

Mix A. C. and Ruddiman W. F. (1984)
Oxygen isotope analyses and Pleistocene ice volumes.
Quaternary Research 21, 1-20.

Mock S. J. and Weeks W. F. (1966)
The distribution of 10 meter snow temperatures on the
Greenland ice sheet. Journal of Glaciology 6, 23-41.

Morland L. W. and Johnson I. R. (1980)
Steady motion of ice sheets. Journal of Glaciology 15,
229-46.

Morland L. W. and Smith G. D. (1984)
Influence of non-uniform temperature distribution on the
steady motion of ice-sheets. Journal of Fluid Mechanics
140, 113-33.

Muszinski I. and Birchfield G. E. (1987)
Coupled marine ice-stream-ice-shelf model. Journal of
Glaciology 33, 3-15.

Nye J. F. (1952)
The mechanics of glacier flow. Journal of Glaciology 2,
82-93.

Nye J. F. (1957)
The distribution of stress and velocity in glaciers and
ice sheets. Proceedings of the Royal Society of London,
Series A 239, 113-33.

Nye J. F. (1959)
The motion of ice sheets and glaciers. Journal of
Glaciology 3, 493-507.

Oerlemans J. (1980)
Continental ice sheets and the planetary radiation
budget. Quaternary Research 14, 349-59.

Oerlemans J. (1981)
Modeling of Pleistocene European ice sheets: some
experiments with simple mass-balance parameterizations.
Quaternary Research 15, 77-85.

Oerlemans J. (1982)
Glacial cycles and ice-sheet modelling. Climatic Change
4, 353-74.

Oerlemans J. and van der Veen C. J. (1984)
Ice sheets and climate. D. Reidel Publishing Company,
Dordrecht, the Netherlands.

Paterson W. S. B. (1981)
The physics of glaciers. Second edition, Pergamon Press
Limited, Oxford.

Peacock J. D. (1970)
Some aspects of the glacial geology of West Inverness-shire. *Bulletin of the Geological Society of Great Britain 33*, 43-56.

Peacock J. D. (1971)
Marine shell radiocarbon dates and the chronology of deglaciation in western Scotland. *Nature 230*, 43-5.

Pollard D. (1978)
An investigation of the astronomical theory of the ice ages using a simple climate-icesheet model. *Nature 272*, 233-5.

Potter J. R., Paren J. G. and Loynes J. (1984)
Glaciological and oceanographic calculations of the mass balance and isotope ratio of a melting ice shelf. *Journal of Glaciology 30*, 161-70.

Putnins P. (1970)
The climate of Greenland. in Orvig S. (ed) *World survey of climatology: climates of the polar regions*, Elsevier Publishing Company, Amsterdam. the Netherlands, 3-129.

Reed R. K. and Elliot W. P. (1979)
New precipitation maps for the North Atlantic and North Pacific oceans. *Journal of Geophysical Research 84*, 7839-46.

Reeh N. (1968)
On the calving of ice from floating glaciers and ice shelves. *Journal of Glaciology 7*, 215-32.

Reeh N. (1985)
Greenland ice-sheet mass balances and sea-level change. in *Glaciers, icesheets and sea level: effect of a CO_2-induced climatic change. Report of a workshop held in Seattle, Washington September 13-15 1984*. 155-71.

Reynolds J. M. (1981)
Lakes on George VI ice shelf, Antarctica. *Polar Record 20*, 425-32.

Rind D., Peteet D., Broecker W., McIntyre A. and Ruddiman W. (1986)
The impact of cold Atlantic sea surface temperatures on climate: implications for the Younger Dryas cooling (11-10 k). *Climate Dynamics 1*, 3-33.

Ruddiman W. F. and McIntyre A (1981a)
The mode and mechanism of the last deglaciation: oceanic evidence. *Quaternary Research 16*, 125-34.

Ruddiman W. F. and McIntyre A (1981b)
The North Atlantic during the last glaciation.
Palaeogeography, Paleoaclimatology, Palaeoecology 35,
145-214.

Ruddiman W. F., Sancetta C. D. and McIntyre A (1977)
Glacial/interglacial response rate of subpolar North
Atlantic waters to climatic change: the record in oceanic
sediments. Philosophical Transactions of the Royal
Society of London, Series B 280, 119-42.

Sanberg J. A. M. and Oerlemans J. (1983)
Modelling of Pleistocene European ice sheets: the effect
of upslope precipitation. Geologie en Mijnbouw 62, 267-
73.

Sawyer J. S. (1956)
The physical and dynamical problems of orographic rain.
Weather 11, 375-81.

Schwerdtfeger W. (1968)
New data on the winter radiation balance at the South
Pole. Antarctic Journal 3, 193-4.

Schwerdtfeger W. (1970)
The climate of the Antarctic. in Orvig S. (ed) World
Survey of Climatology Volume 14: Climates of the Polar
Regions. Elsevier Publication Company, Amsterdam, The
Netherlands, 257-320.

Shackleton N. J. (1987)
Oxygen isotopes, ice volume and sea level. Quaternary
Science Reviews 6, 183-90.

Shackleton N. J. and Opdyke N. D. (1973)
Oxygen isotope and stratigraphy of equatorial Pacific
core V28-238: oxygen isotope temperatures and ice volumes
on a 10^5 and 10^6 yr time scale. Quaternary Research 3,
39-55.

Sissons J. B. (1967)
Glacial stages and radiocarbon dates in Scotland.
Scottish Journal of Geology 3, 375-81.

Sissons J. B. (1972)
The last glaciers in part of the South-East Grampians.
Scottish Geographical Magazine 88, 168-81.

Sissons J. B. (1974)
The Quaternary in Scotland: a review. Scottish Journal of
Geology 10, 311-37.

Sissons J. B. (1976)
The geomorphology of the British Isles: Scotland.
Methuen, London.

Sissons J. B. (1977)
The Loch Lomond readvance in the northern mainland of
Scotland. in Gray J. M. and Lowe J. J. (eds) *Studies in
the Scottish Lateglacial environment.* Pergamon Press,
Oxford, 45-59.

Sissons J. B. (1979a)
Palaeoclimatic inferences from former glaciers in
Scotland and the Lake District. *Nature 278*, 518-21.

Sissons J. B. (1979b)
The Loch Lomond stadial in the British Isles. *Nature 280,*
199-203.

Sissons J. B. (1980)
Palaeoclimatic inferences from Loch Lomond advance
glaciers. in *Lowe J. J., Gray J. M. and Robinson J. E.
(eds) Studies in the Lateglacial of North-West Europe.*
Pergamon Press, Oxford, 31-43.

Sissons J. B. (1983)
Shorelines and isostasy in Scotland. in Smith D. E. and
Dawson A. G. (eds) *Shorelines and Isostasy.* Academic
Press, London, 209-226.

Sissons J. B. and Grant A. J. H. (1972)
The last glaciers in the Loch nagar area, Aberdeenshire.
Scottish Journal of Geology 8, 85-93.

Sissons J. B. and Sutherland D. G. (1976)
Climatic inferences from former glaciers in the South-
East Grampian Highlands, Scotland. *Journal of Glaciology
17*, 325-45.

Sugden D. E. (1970)
Landforms of deglaciation in the Cairngorm Mountains.
Transactions of the Institute of British Geographers 45,
79-92.

Sugden D. E. (1977)
Reconstruction of the morphology, dynamics and thermal
characteristics of the Laurentide ice sheet at its
maximum. *Arctic and Alpine Research 9*, 21-47.

Sugden D. E. and Clapperton C. M. (1980)
West Antarctic ice sheet fluctuations in the Antarctic
Peninsula area. *Nature 286*, 378-81.

Sutherland D. G. (1981)
The raised shorelines and deglaciation of the Loch Long/Loch Fyne area, western Scotland. Unpublished Ph. D. thesis, University of Edinburgh.

Thomas R. H. (1985)
Responses of the polar ice sheets to climatic warming. in *Glaciers, icesheets and sea level: effect of a CO_2-induced climatic change. Report of a workshop held in Seattle, Washington September 13-15 1984*. 301-16.

Thorp P. W. (1981)
A trimline method for defining the upper limit of Loch Lomond advance glaciers: examples from the Loch Leven and Glen Coe areas. *Scottish Journal of Geology 17*, 49-64.

Tibaldi S. (1986)
Envelope orography and maintenance of the quasi-stationary circulation in the E.C.M.W.F. global models. *Advanced Geophysics 29*, 339-74.

Tucker G. B. (1961)
Precipitation over the North Atlantic Ocean. *Quaterly Journal of the Royal Meteorological Society 87*, 147-58.

Tucker G. B. and Barry R. G. (1984)
Climate of the North Atlantic Ocean. in van Loon H. (ed) *World Survey of Climatology Volume 15, Climates of the Oceans*. Elsevier Science Publications, Amsterdam, 50-87.

Turcotte D. L. and Schubert G. (1982)
Geodynamics: applications of continuum physics to geological problems. John Wiley and Sons Incorporated, Toronto.

Vernekar A. D. (1972)
Long term variations of incoming solar radiation. *Meteorological Monographs Volume 12*, American Meteorological Society, Boston.

Walcott R. I. (1970a)
Flexural rigidity, thickness and viscosity of the lithosphere. *Journal of Geophysical Research 75*, 3941-54.

Walcott R. I. (1970b)
Isostatic response to loading of the crust in Canada. *Canadian Journal of Earth Sciences 7*, 716-27.

Walcott R. I. (1973)
Structure of the earth from glacio-isostatic rebound. *Annual Review of Earth and Planetary Science 1*, 15-37.

Walker M. J. C. and Lowe J. J. (1979)
Postglacial environmental history of Rannoch Moor,
Scotland. II. Pollen diagrams and radiocarbon dates from
the Rannoch Station and Corrour areas. Journal of
Biogeography 6, 349-62.

Weertman J. (1957)
Deformation of floating ice shelves. Journal of
Glaciology 3, 38-42.

Weertman J. (1964)
The theory of glacier sliding. Journal of Glaciology 5,
287-303.

Weertman J. (1973)
Creep of ice. in Whalley E., Jones S. J. and Gold L. W.
(eds) Physics and Chemistry of Ice. Royal Society of
Canada, Ottawa, Canada. 320-337.

Williams R. B. G. (1975)
The British climate during the last glaciation: an
interpretation based on periglacial phenomena. in Wright
A. E. and Moseley F. (eds) Ice Ages: Ancient and Modern.
Seel House Press, Liverpool 95-110.

Williams L. (1979)
An energy model of the potential glacierization of
Northern Canada. Arctic and Alpine Research 11, 443-56.

Young N. W. (1981)
Responses of ice sheets to environmental change. in Sea
level, ice and climatic change (Proceedings of the
Canberra symposium) I.A.S.H. Publication Number 131, 331-
360.

Zubenok L. I. and Strokina L. A. (1963)
Evaporation from the Earth's surface. Tr. Gl. Geofiz.
Obs. 139, 93-107.

Appendix I : The relationship between July and annual air temperature depressions.

This appendix outlines the relationship between July air temperature depression and annual temperature depression. The relationship is used in the model to link the July air temperature depression forcing function (sub-section 2.2.1) to the effectiveness calculation (2.3.1). It is need because air temperatures in Britain during the Loch Lomond stadial experienced an increase in continentality as well as a general depression.

The relationship used in the model is derived in the following manner:

(i)   the annual air temperature cycle is represented by a cosine function.

(ii)   the offset and the amplitude of the cosine function are assigned values for both the present day and for the Loch Lomond stadial using data from Williams (1975).

(iii)   the offset and amplitude of a general cosine curve are substituted by linear relationships to July air temperature depression using the curves of part (ii).

(iv)   the general cosine curve is then integrated to obtain mean annual temperature as a function of July air temperature depression.

(v)   this relationship can then be used to find annual temperature depressions from the present day value of 10.0 ^{o}C. These depressions are 2.57 times greater than the equivalent July air temperature depression.

Appendix II : *The derivation of an equation predicting effectiveness.*

This appendix outlines the derivation of the effectiveness relationship used in the model. Effectiveness is the fraction of total annual precipitation which falls as snow. It is not a commonly measured meteorological variable and therefore has to be estimated from the recorded number days of days on which snow was observed to fall.

Data was used from 21 meteorological stations in the U. K. and Scandinavia (Chandler and Gregory 1976, Manley 1970 and Johannssen 1970). The data was for monthly mean measurements and consisted of the number of days with recorded snowfall during the month, the total monthly precipitation and the total annual precipitation.

An estimate of the amount of snowfall falling in a given month can be obtained by multiplying the total monthly precipitation by the number of days with observed snowfall, and then dividing by the total number of days in the month. This was done for each month at each station. The annual amount of snowfall at each station was then found by summing the estimates for individual months, and the effectiveness found by dividing this annual total by the annual total precipitation.

This method is fairly coarse, however it does make the best use of the poor snowfall data available and avoids any bias caused seasonal changes in precipitation rates.

The 21 estimates of snowfall effectiveness where then regressed against the altitude and latitude of the meteorological stations to obtain a predictive equation. The regression analysis achieved a high percentage of variation explained, which varied from 57.9 to 90.3 % R^2.

This relationship is used in the overall ice sheet model. It incorporates imposed annual air temperature depressions (see Appendix I) as equivalent changes in the altitude of annual isotherms using a lapse rate of 6.5 $^{\circ}$C km^{-1}.

$$\frac{\partial Z}{\partial t} = b - \nabla(\overline{U} \cdot Z) \tag{2.1}$$

$$b = P \cdot Eff - Ab \tag{2.2}$$

$$Ab = 10^{(E_o - E)/1 \cdot 2} \tag{2.3}$$

$$E_0 = 6 \cdot 85 - 0 \cdot 085\phi + \Delta E_J \tag{2.4}$$

$$Eff = -0 \cdot 698 + 0 \cdot 014\phi + 0 \cdot 224(E - \Delta E_A) \tag{2.5}$$

$$P_0 = 0 \cdot 8 + 1 \cdot 8E \tag{2.6}$$

$$P = \begin{cases} P_0 & \text{if } E \leq 2 \\ P_0/2^{(E-2)} & \text{if } E > 2 \text{ and } B \leq 2 \\ P_0/2^Z & \text{if } E > 2 \text{ and } B > 2 \end{cases} \tag{2.7}$$

$$B = B_{mean} + a(B_{max} - B_{mean}) \tag{2.8}$$

$$E = \max(B, B_{mean} + Z) \tag{2.9}$$

$$Z > \frac{\rho_w}{\rho_i}(-B) \tag{2.10}$$

$$E = \left(1 \cdot 0 - \frac{\rho_i}{\rho_w}\right)Z \tag{2.11}$$

$$V_c = 27 \cdot 1(-B) \tag{2.12}$$

$$C = \frac{mZ}{\Delta x}\min(V_c, V_{c\,max}) \tag{2.13}$$

$$B^* = \frac{1}{16}(Z_{10} + 2Z_5 + Z) \tag{2.14}$$

$$L = Z\frac{\rho_i}{\rho_m} \tag{2.15}$$

$$L = (B - B_0) \frac{\rho_w}{\rho_m} \qquad (2.16)$$

$$\frac{\partial B}{\partial t} = D_a \nabla^2 (B_0 - B + L) \qquad (2.17)$$

$$\frac{\partial \sigma_{xx}}{\partial x} + \frac{\partial \tau_{xy}}{\partial y} + \frac{\partial \tau_{xz}}{\partial z} = 0$$
$$(2.18)$$

$$\frac{\partial \sigma_{yy}}{\partial y} + \frac{\partial \tau_{yx}}{\partial x} + \frac{\partial \tau_{yz}}{\partial z} = 0$$

$$\frac{\partial \sigma_{zz}}{\partial z} + \frac{\partial \tau_{xz}}{\partial x} + \frac{\partial \tau_{zy}}{\partial y} = -\rho_i g$$

$$\tau_{xz} = \rho_i g \alpha_x (E - z)$$
$$(2.19)$$
$$\tau_{yz} = \rho_i g \alpha_y (E - z)$$

$$\tau_b = \rho_i g Z \alpha \qquad (2.20)$$

$$\alpha^2 = \alpha_x^2 + \alpha_y^2 \qquad (2.21)$$

$$\tau_b = \rho_i g Z \alpha + 2G - T$$
$$(2.22)$$
$$\dot{\epsilon}_{xz} = A \tau^{n-1} \tau_{xz}$$

$$\dot{\epsilon}_{yz} = A \tau^{n-1} \tau_{yz}$$
$$(2.23)$$

$$\dot{\epsilon}_{xz} = \frac{1}{2} \left(\frac{\partial U_y}{\partial z} + \frac{\partial U_z}{\partial y} \right)$$

$$\dot{\epsilon}_{yz} = \frac{1}{2} \left(\frac{\partial U_x}{\partial z} + \frac{\partial U_z}{\partial x} \right)$$
$$(2.24)$$

$$\bar{U}_x = \frac{2A(\rho_i g)^n}{n+2} |\alpha|^{n-1} \alpha_x Z^{n+1}$$

$$\bar{U}_y = \frac{2A(\rho_i g)^n}{n+2} |\alpha|^{n-1} \alpha_y Z^{n+1} \qquad (2.25)$$

$$\bar{U}_x = \bar{U}_{x0} + \triangle X \cdot \epsilon_s \qquad (2.26)$$

$$Z^* = Z - \frac{\rho_w}{\rho_i}(-B) \qquad (2.27)$$

$$U_s = K_2 \frac{\tau_b}{Z^{*2}} \qquad (2.28)$$

$$\frac{\partial F}{\partial x} \implies \frac{F_{i+1} - F_{i-1}}{\triangle X} \qquad (2.29)$$

$$\frac{\partial^2 F}{\partial x^2} \implies \frac{F_{i+1} - F_i + F_{i-2}}{(\triangle X)^2} \qquad (2.30)$$

$$\frac{\partial F}{\partial t} = G \implies F_{t+1} = F_t + \triangle t \cdot G \qquad (2.31)$$

$$\triangle t_{max} = \frac{(\triangle X)^2_{|\alpha'|}}{2U'Z'n} \qquad (2.32)$$

$$z^+_{i,j} = \frac{1}{16}\left(Z_{i+2,j} + Z_{i-2,j} + 10Z_{i,j} - 4\left(Z_{i+1,j} + Z_{i-1,j}\right)\right)$$

$$Z_{i,j} = \frac{1}{16}\left(Z^+_{i,j+2} + Z^+_{i,j-2} + 10Z^+_{i,j} - 4\left(Z^+_{i,j+1} + Z^+_{i,j-1}\right)\right) \qquad (2.33)$$

$$b = 1.88 + 0.21E - 0.12\theta + 0.10\phi \qquad (3.1)$$

$$B_0 = Z\frac{\rho_i}{\rho_m} + B \qquad (3.2)$$

$$b = 1.88 + 0.21E + 0.10\phi \qquad (3.3)$$

$$\frac{\partial W}{\partial t} = \frac{W_{sat} - W}{T_*} - W(f_0 + f_1 S) - U.\nabla W + D_W.\nabla^2 W \qquad (5.1)$$

$$e = 6.1 \times 10^{(aT/T+b)} \qquad (5.2)$$

$$\chi = \frac{217\,e}{273 + T} \qquad (5.3)$$

$$S = \max(0.0, (B_i - B_{i-1})/\triangle X) \qquad (5.4)$$

$$T_a = -4.19 + 1.26 T_w \qquad (5.5)$$

$$S_i = \max\left(0.0, (B_i - (\sum_{k=i}^{i-n} B_k)/n)/\triangle X_n\right) \qquad (5.6)$$

$$S_{i,j} = \max\left(0.0, (B_{i,j} - (\sum_{k=i,m=j}^{i-n,j-n} B_{k,m})/n)/\triangle X_n\right) \qquad (5.7)$$

$$\frac{\partial W}{\partial x} \approx \frac{W_w - W_{i-1}}{\triangle X_a} \;,\; \frac{\partial W}{\partial x} \approx \frac{W_{i+1} - W_e}{\triangle X_a} \qquad (5.8)$$

$$G.F.I. = \sum_{i=1,j=1}^{n,m} \left(P_{i,j}^{stan} - P_{i,j}^{sens}\right) \qquad (5.9)$$

$$T_m = Off - Amp.\cos\left(\frac{\pi n}{6}\right) \qquad (5.10)$$

$$Off = 10.0 + 2.57\triangle T_J - 0.38(\phi - 53.17) - 6.5E \qquad (5.11)$$

$$Amp = 7.0 - 1.57\triangle T_J - 0.25(\phi - 50.5) - 2.0E \qquad (5.12)$$

$$\frac{dT}{dE} = \frac{\partial T}{\partial E} + \frac{\partial T}{\partial x}.\frac{\partial E}{\partial X} \qquad (5.13)$$

$$Eff_m = 0.50 - 0.05 T_m \qquad (5.14)$$

$$S_m = 1.74 + 0.50 T_m + 0.03 T_m^2 \qquad (5.15)$$

408

$$Ab_m = \max(0.0, -0.36 + 0.54S_m) \qquad (5.16)$$

$$b = P \cdot Eff - Ab \qquad (5.17)$$

a	envelope topography constant, constant in saturation vapour pressure equation
A	Arrhenius constant used the flow law
Ab	annual ablation rate
Ab_m	monthly ablation rate
b	annual net mass balance, constant in saturation vapour pressure equation
B	bedrock surface elevation
B_0	relaxed bedrock surface elevation
B_{max}	maximum bedrock surface elevation
B_{mean}	mean bedrock surface elevation
B^*	isostatic bedrock deflection
C	flux of ice lost via calving (as an equivalent ice thickness)
D_a	diffusivity of the asthenosphere
D_w	diffusivity of water vapour in the atmosphere
E	surface elevation
E_0	altitude of the 1 m a^{-1} ablation isopleth
Eff	annual effectiveness, the fraction of total precipitation falling as snow
Eff_m	monthly effectiveness
e	saturation vapour pressure
f_0	parameter relating rainfall to water vapour content
f_1	parameter relating orographic rainfall to upwind surface slope
g	gravitational constant
G	additional term used in the determination of basal shear stress

K_2	constant ice sliding law
L	equilibrium isostatic depression under present ice cover
m	multiplier in the calving equation
n	power constant in the flow law, month number in the annual air temperature equation
Off	offset of annual temperature curve
P	annual precipitation rate
P_0	present day annual precipitation rate
S	upwind ground suface slope
S_m	sum of day degrees above $0.0\ ^\circ C$ per month
t	time
T	additional term used in the determination of basal shear stress, air temperature
T_a	sea level air temperature
T_m	monthly air temperature
T_w	sea surface temperature
T^*	time scale of evaporation
U	ice velocity by deformation in the subscripted direction, horizontal wind speed
$\bar{U}$	vertically averaged horizontal ice velocity
U_s	sliding velocity
U_{x0}	vertically averaged horizontal velocity of incoming ice
V_c	calving velocity
$V_{c\ max}$	maximum calving velocity constraint
W	atmospheric moisture content
W_{sat}	saturated atmospheric moisture content

z	ice thickness
z_5	ice thickness 5.0 ka previous
z_{10}	ice thickness 10.0 ka previous
z^*	effective ice thickness, a measure of normal load on the bed
z^+	intermediate ice thickness used in the smoothing operation
x,y,z	coordinate system subscripts
α	surface slope, overall and in the subscripted direction
χ	saturated moisture content
ΔE_A	imposed shift in annual air temeperature isopleths
ΔE_J	imposed shift in July air temperature isopleths
Δt	time step
Δt_{max}	maximum stable time step size
ΔT_J	imposed July air temperature depression
Δx	grid spacing
ϵ	strain rate in the subscripted plane
ϵ_s	constant ice shelf strain rate
ρ_i	density of ice
ρ_m	density of bedrock mantle
ρ_w	density of water
ϕ	latitude
σ	normal stress in the subscripted plane
τ	shear stress in the subcripted plane
τ_b	basal shear stress
θ	longitude